Aus dem Biomedizinischen Centrum

der Ludwig-Maximilians-Universität München

Lehrstuhl für Molekularbiologie

Vorstand: Prof. Dr. rer. nat. Peter B. Becker

Roles of nucleosome remodeling factors ACF1 and Domino during *Drosophila melanogaster* oogenesis

Dissertation

Zum Erwerb des Doktorgrades der Naturwissenschaften

An der Medizinischen Fakultät der

Ludwig-Maximilians-Universität München

vorgelegt von

Kenneth Börner

aus Dresden

Jahr 2016

Mit Genehmigung der Medizinischen Fakultät

der Ludwig-Maximilians-Universität München

Betreuer:	Prof. Dr. rer. nat. Peter. B. Becker
Zweitgutachter:	Prof. Dr. Andreas Ladurner
Dekan:	Prof. Dr. dent. Reinhard Hickel
Tag der mündlichen Prüfung:	25.01.2017

Eidesstattliche Versicherung

Börner, Kenneth

Ich erkläre hiermit an Eides statt,

dass ich die vorliegende Dissertation mit dem Thema

“Roles of nucleosome remodeling factors ACF1 and Domino during *Drosophila melanogaster* oogenesis”

selbständig verfasst, mich außer der angegebenen keiner weiteren Hilfsmittel bedient und alle Erkenntnisse, die aus dem Schrifttum ganz oder annähernd übernommen sind, als solche kenntlich gemacht und nach ihrer Herkunft unter Bezeichnung der Fundstelle einzeln nachgewiesen habe.

Ich erkläre des Weiteren, dass die hier vorgelegte Dissertation nicht in gleicher oder in ähnlicher Form bei einer anderen Stelle zur Erlangung eines akademischen Grades eingereicht wurde.

_____ _____

Ort, Datum Unterschrift Doktorandin/Doktorand

Für meine Familie und Freunde

‚With great power must also come --- great responsibility‘

Benjamin Parker, August 1962

Preface

Two original research papers on the functions of nucleosome remodeling factors during *D. melanogaster* oogenesis are presented in this cumulative thesis. Each research article contains the respective reference list and supplementary information. Furthermore, unpublished work on the interaction of two nucleosome remodeling factors is presented in ‘Results’ including ‘Material and Methods’. Additional references from the chapters ‘Introduction’ and ‘Results’ are cited at the end of this thesis. My contributions to the research articles are listed at the beginning of each research article as well as in the enclosed ‘Declaration of contributions’.

I. Table of contents

II. Abbreviations

aa	amino acid
ACDC	ACF1-Domino containing complex
ACF1	ATP-utilizing chromatin assembly and remodeling factor 1
ADP	adenosine diphosphate
ANP32E	acidic nuclear phosphoprotein 32 kDa E
ARP	actin-related protein
ATM	ataxia telangiectasia mutated protein
ATP	adenosine triphosphate
ATPase	adenosine triphosphatase
ATR	ataxia telangiectasia and Rad3-related protein
BAF53	BRG-associated factor 53
BAZ	bromodomain adjacent to a zinc finger
Bic-D	Bicaudal-D
BMP	bone morphogenic protein
Bromo	bromodomain
BSA	bovine serum albumin
Cas-3	activated Caspase-3
CHD	chromodomains, helicase, DNA-binding domain
CHRAC	chromatin accessibility complex
CtBp	C-terminal-binding protein
CTCF	corrected total cell fluorescence
ctl	control
DAPI	4',6-diamidino-2-phenylindole
DDT	DNA-binding homeobox-containing proteins and the different transcription and chromatin remodeling factors in which they are found
DNA-PK	DNA-dependent protein kinase
DNase I	Deoxyribonuclease I
DTT	Dithiothreitol
DOA1	Domino-A peptide 1 antibody
DOB1	Domino-B peptide 1 antibody
DOB2	Domino-B peptide 2 antibody

DOM	Domino
DSB	double-strand DNA break
EDTA	Ethylendiamintetraacetate
Egl	Egalitarian
EGTA	Ethylenglycol-bis(2-aminoethyl)-N,N,N’,N’-tetraacetic acid
elav	embryonic lethal abnormal visual protein
E(Pc)	enhancer of Polycomb
Esa1	essential Sas family acetyltransferase 1
FasIII	Fasciclin III
FISH	fluorescence *in situ* hybridization
fos	fosmid
Gal4	galactose-responsive transcription factor GAL4
GFP	green fluorescence protein
GSC	germline stem cell
γH2A.V	phosphorylated H2A.V
H2A.V	histone H2A variant
HA	hemagglutinin
HEPES	N-(2-Hydroxyethyl)piperazine-H’-2-ethanesulfonic acid
HP1	heterochromatin protein 1
HSA	helicase-SANT-associated
HSP70	heat shock protein 70 kDa
HTP-C	histone H2A phosphatase complex
HTS	hu-li tai shao
IF	immunofluorescence
IFM	immunofluorescence microscopy
IgG	immunoglobulin G
ING3	inhibitor of growth 3
INO80	inositol-requiring protein 80
IP	immunoprecipitation
ISWI	imitation switch
kDa	kilodalton
MAT	maternal tubulin
MBS	metabisulfite

MRG15	mortality factor 4 related gene 15
MRGBP	MRG15 binding protein
MTD	maternal triple driver
NAP-1	nucleosome assembly protein
NuA4	Nucleosome acetyltransferase of histone H4
NDS	normal donkey serum
NoRC	nucleolar remodeling factor
NURF	nucleosome remodeling factor
p400	E1A-associated protein p400
PBS	phosphate buffered saline
PCR	polymerase chain reaction
PEG	polyethylene glycol
PFA	Paraformaldehyde
PHD	plant homeodomain
PGC	primordial germ cell
PMSF	Phenylmethanesulfonyl fluoride
PP2A	protein phosphatase 2
PRC1	Polycomb repressor complex 1
PRC2	Polycomb repressor complex 2
PTM	post-translational modification
PVDF	Polyvinylidene Fluoride
RNAi	RNA interference
RNAse H	Ribonuclease H
RSF	remodeling and spacing factor
S2	*Drosophila* Schneider cells
SANT	SWI3– ADA2–N-CoR–TFIIIB
SD	standard deviation
SDS-PAGE	sodium dodecyl sulfate-polyacrylamide gel electrophoresis
Sf21	*Spodoptera frugiperda 21*
shRNA	short hairpin RNA
SLIDE	SANT-like ISWI domain
SN	supernatant
SNF2H	sucrose nonfermenting-2 homolog

SNF2L	sucrose nonfermenting-2 like
SSC	somatic stem cell
SRCAP	Snf2-related CBP activator protein
SWI/SNF	switch/sucrose non-fermentable
SWR1	Swi2/Snf2-related 1
TCS	tissue culture supernatant
TIP60	Tat-interactive protein 60 kDa
tj	traffic jam
ToRC	toutatis-containing remodeling factor
TRRAP	transformation/transcription domain associated protein
TSS	transcription start site
UAS	upstream activating sequence
UTR	untranslated region
WAC	WSTF, ACF1, cbp146
WB	Western blot
WT	wild type

III. List of publications

Kenneth Börner, Dhawal Jain, Paula Vazquez-Pianzola, Sandra Vengadasalam, Natascha Steffen, Dmitry V. Fyodorov, Pavel Tomancak, Alexander Konev, Beat Suter and Peter B. Becker (2016). *A role for tuned levels of nucleosome remodeler subunit ACF1 during Drosophila oogenesis.* Developmental Biology, Volume 411, Issue 2, 15 March 2016, Pages 217-230, doi:10.1016/j.ydbio.2016.01.039

Kenneth Börner and Peter B. Becker (2016). *Splice variants of the SWR1-type nucleosome remodeling factor Domino have distinct functions during Drosophila melanogaster oogenesis.* Development 143(17), Pages 3154-3167, 1 September 2016, doi: 10.1242/dev.139634.

IV. Declaration of contributions

Declaration of contributions to 'A role for tuned levels of nucleosome remodeler subunit ACF1 during *Drosophila* oogenesis'

This study was conceived by Dhawal Jain, Peter B. Becker and myself. I performed all experiments with the following exceptions: *Acf1*^{7} fly line was made by Alexander Konev and Dmitry V. Fyodorov; *Acf1* and *Chrac-16* fosmid fly lines were made by Dhawal Jain in collaboration with Pavel Tomancak; Western blot (Fig. S5H) and mRNA quantification (Fig. S9) were done by Dhawal Jain; RNA *in situ* hybridization was done by Paula Vazquez-Pianzola under supervision of Beat Suter (Figs. 1F, G; 4E, G; S1A-D) and preliminary experiments (Figs. 1,2 and 4) were done by Sandra Vengadasalam and Natascha Steffen. I prepared all figures and wrote the manuscript together with Peter B. Becker. All coauthors edited the manuscript prior to submission.

Declaration of contributions to 'Splice variants of the SWR1-type nucleosome remodeling factor Domino have distinct functions during *Drosophila melanogaster* oogenesis'

This study was conceived by Peter B. Becker and myself. I performed all experiments, prepared all figures and wrote the manuscript together with Peter B. Becker.

1 Introduction

1.1 Chromatin dynamics during development

Development of higher multicellular organisms from the totipotent zygote to more specialized tissues and organs is reflected at the level of single cells with the selective usage of the genetic information. An important principle underlying this selectivity is that the genetic information is rendered inaccessible by histone and non-histone proteins within a highly organized and compacted chromatin structure. The utilization of the genetic information requires regulated access to the underlying DNA sequence for regulatory factors and complex machineries not only to adopt to developmental, but also to metabolic and environmental cues. The concerted actions of regulatory factors, that initiate differential expression patterns during development, are interconnected with local and global alterations in chromatin structure. These adoptions in cellular programs may be propagated throughout development stages by maintenance of heritable chromatin features, while chromatin plasticity is maintained in some pluripotent cell lineages. Detailed knowledge about chromatin features and plasticity is required to understand the complex network of developmental stimuli and programs that give rise to the fascinating diversity of life on earth. The hierarchical levels of chromatin structure, starting with the basic unit of the nucleosome to chromosomes, are briefly discussed in the next chapter.

1.2 Nucleosome and chromatin structure

Nucleosomes are the fundamental repeating unit of packaging DNA in eukaryotic cells. In this unit, 147 bp of DNA are wrapped in ~1.65 left-handed superhelical turns around a histone octamer (Fig. 1.1) (1). This core nucleosomal particle consists of two copies each of the histone proteins H2A, H2B, H3 and H4 (Fig. 1.1). Histones are small, basic and conserved proteins that contain a bipartite structure, the histone core and the histone tails. The histone core shows a structured ‘histone fold’ motif, containing three α-helices connected by two loops, to facilitate dimerization within the octamer. Additionally, histones contain at the N-terminus unstructured and flexible tails (Fig. 1.1), which constitute important intra- and internucleosomal interaction surfaces for higher-order chromatin structure (2,3). Several direct contacts between the DNA and the histone proteins as well as hydrogen bonds mediate stable wrapping of the DNA around the histone octamer (1,4), but this nucleosomal organization also hinders the accessibility for sequence-specific binding factors. Nucleosomal

core particles are connected via free linker DNA to form long arrays of nucleosomes, the primary structure of chromatin, visualized as the ‘beads-on-a-string’ structure in microscopy.

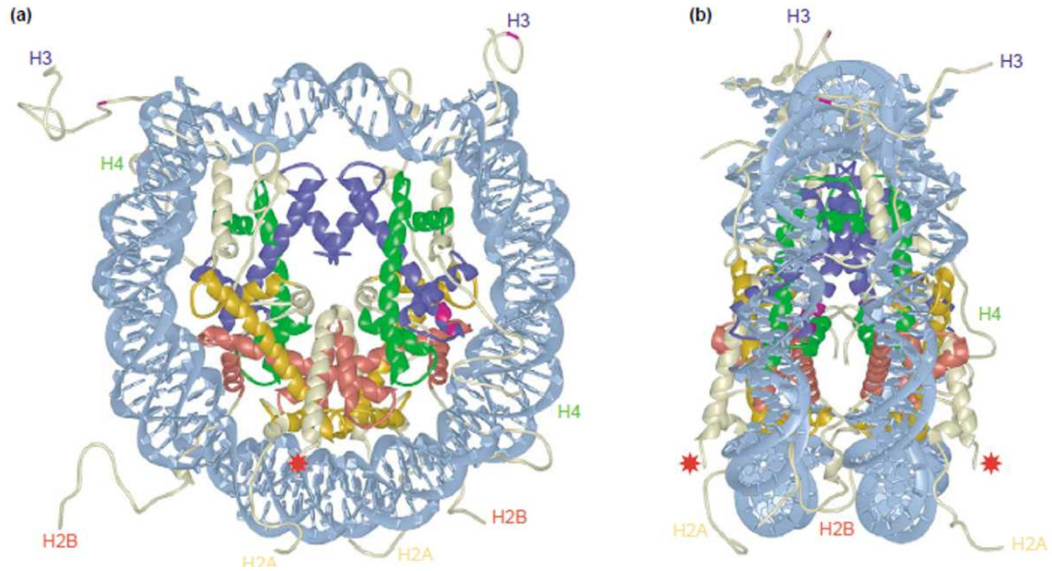

Figure 1.1. Overall structure of the nucleosome core particle. **(A)** Front view of the nucleosome. Viewed down the superhelical axis. H2A, H2B, H3, and H4 are colored in yellow, red, blue, and green respectively. Histone tails and extensions are shown in white and DNA in light blue. **(B)** Side view of the nucleosome (obtained by 90° rotation). Adapted from Luger (2003), Current Opinion in Genetics and Development (5). Reprinted with permission of Elsevier.

The composition of nucleosomes may be varied, for example by posttranslational modifications (PTMs) or incorporation of non-canonical histone variants, both topics are discussed in more detail below. While the first level of compaction with the formation of the ‘10 nm fiber’ already achieves a ~5 fold compaction (Fig. 1.2), other levels of compaction are necessary and observed *in vitro* and *in situ*. The long standing theory of a secondary level of compaction, the ’30 nm fiber’, is still a matter of debate (Fig. 1.2) (6) and conclusive *in vivo* evidence for the existence is still missing (7–9). Recent models rather suggest an irregular and highly dynamic 10 nm chromatin structure in which nucleosomes interact and interdigitate extensively with close-by nucleosomes and nucleosomal fibers contributing to most of the interphase and mitotic chromosome structure (Fig. 1.2) (9–11).

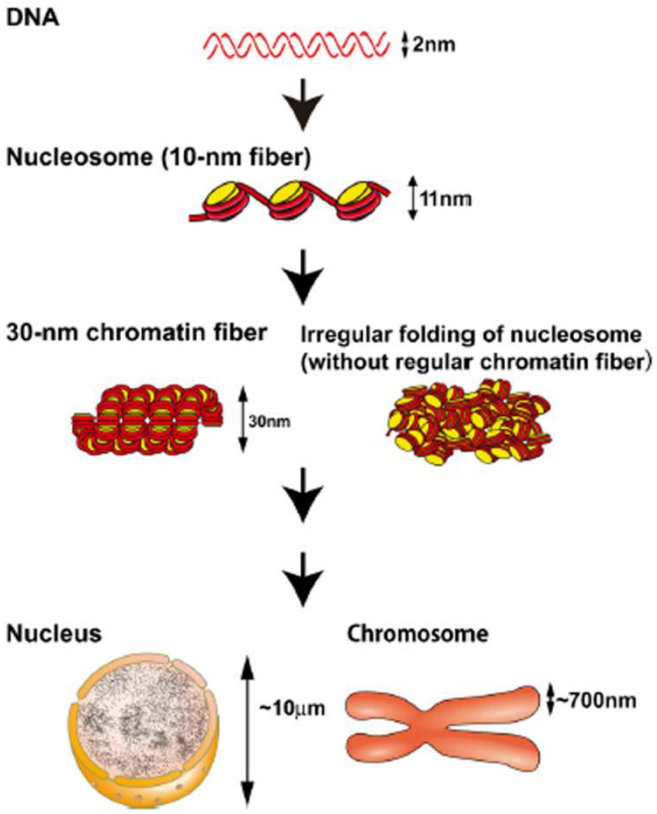

Figure 1.2. Models of higher-order chromatin structure *in vivo*. Old and novel views of chromatin structure. A 2 nm DNA molecule is wrapped around a histone octamer to form a nucleosome with a diameter of 11 nm. It had been assumed for a long time that nucleosomes fold into 30 nm chromatin fibers (left side) and subsequently into higher order chromatin structures of interphase nuclei or mitotic chromosomes. Recent hypothesis argue for the formation of irregularly folded nucleosome fibers (right side). Adapted from Maeshima et al. (2014), Chromosoma (11).

1.3 Regulation of chromatin dynamics

The development of a highly organized chromatin structure as a mean of packaging and protecting the genetic information seems at the first glance as an insuperable obstacle for regulatory factors that need to access specific DNA sites dynamically upon differential stimuli. To this end, several strategies evolved to efficiently modulate the transition of chromatin states such as DNA methylation, PTMs, association of non-coding RNAs and the binding of architectural binding proteins (12–15) among other mechanisms. Two particular important mechanisms, namely nucleosome remodeling factors and histone variants, are in focus of this thesis and discussed in more detail below.

1.3.1 Nucleosome remodeling factors – sculptors of the chromatin landscape

Nucleosome remodeling factors (also referred to as 'chromatin remodeling factors' or shortened 'remodelers') are enzymes that use the energy freed by ATP-hydrolysis to alter the interactions between nucleosomal DNA and histone octamers. Nucleosome remodeling factors are highly abundant, conserved from yeast to humans and reside commonly in multisubunit complexes, termed nucleosome remodeling complexes (16). The central factor of a nucleosome remodeling complex is a 'motor' ATPase belonging to the large SNF2 family of helicase-related proteins which can be grouped into at least 23 subfamilies depending on their sequence similarities and domain organization (17,18). Mechanistic details of remodeling reactions come only from a small number of selected enzymes and models are a matter of recent debate (19). In the prevailing model, the ATPase domain engages in defined contacts with nucleosomal DNA and histone octamers and the translocation of the ATPase domain leads to displacement of DNA segments from the histone surfaces (18). It becomes more evident that individual remodeling mechanisms may differ depending on enzyme architecture and arrangements of DNA-histone substrates (20). Most insights about nucleosome remodeling come from studies of the four major subfamilies of ATPases, SWI/SNF, ISWI, CHD and INO80, which share a bipartite ATPase domain but differ in their combination of flanking domains (18,21) (Fig. 1.3). Those domains may contribute to DNA-protein or protein-protein interactions and some domains are implicated in binding of PTMs. In this thesis, a particular emphasis is on the two subfamilies represented by the ATPases ISWI and INO80, their domain structures and functions (refer to chapter 1.3.1.1 and 1.3.1.2).

The action of remodeling enzymes may translate into different physiological outcomes: nucleosome repositioning along the DNA (sliding), disassembly of nucleosomes (eviction) and incorporation of histone variants (histone exchange) (Fig. 1.4A). Nucleosome sliding or eviction may generate access to DNA sequences, a fundamental process for regulating gene expression, while histone variants endow chromatin locally with specialized functions. Furthermore, nucleosome remodeling factors can also facilitate nucleosome assembly in cooperation with histone chaperones (Fig. 1.4B) or adjust the linker length between neighboring nucleosome to achieve evenly spaced nucleosomal arrays (nucleosome spacing) (Fig. 1.4C). It is thought that regularly spaced nucleosomes facilitate the formation and integrity of higher-order chromatin structure (22) and thereby influence all aspects of chromosome biology.

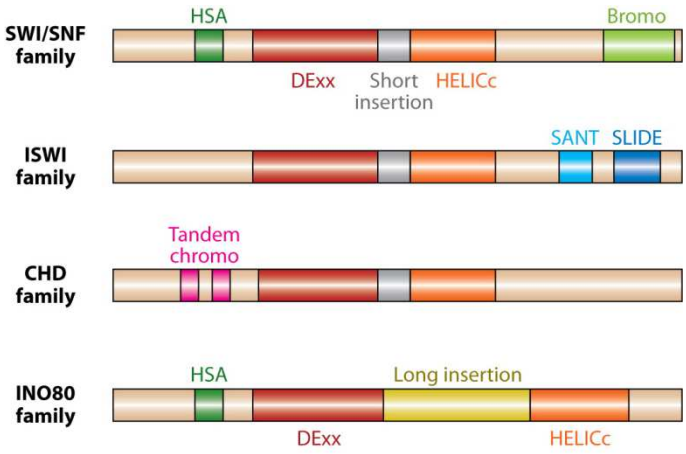

Figure 1.3. The four major nucleosome remodeling enzymes. SWI2/SNF2-family ATPases contain a characteristic ATPase domain with two parts: DExx (red) and HELICc (orange) domain. Notably, remodelers of the INO80 family share a long insertion within the ATPase domain (yellow rectangle), while the other families only show a short insertion (grey rectangle). Different remodeler families are further characterized by the unique combination of flanking domains: Bromodomain (light green) and HSA domain (dark green) for SWI/SNF family, SANT-SLIDE module (blue) for ISWI family, tandem chromodomains (magenta) for the CHD family, and HSA domain (dark green) for the INO80 family. This work focuses mainly on ATPases of the ISWI and INO80 family. Adapted from Clapier and Cairns (2009), Annual Review of Biochemistry (16).

Hence, it is of fundamental interest to understand how different remodelers achieve different remodeling outcomes in response to a variety of stimuli. It became more evident during the last decade that nucleosome remodeling factors are regulated at many different levels, ranging from tissue-specific expression and association of accessory subunits, PTMs and binding of small molecules to autoregulation and feedback mechanisms (20) (Fig. 1.5). In fact, all these mechanisms are of general importance since mutations and misregulation of nucleosome remodeling factors can turn healthy cells into cancerous cells (16,23,24). The next two chapters focus on the regulation of the remodeler ATPases ISWI and INO80, in particular how accessory subunits and alternatively splicing affect their functions, respectively.

.

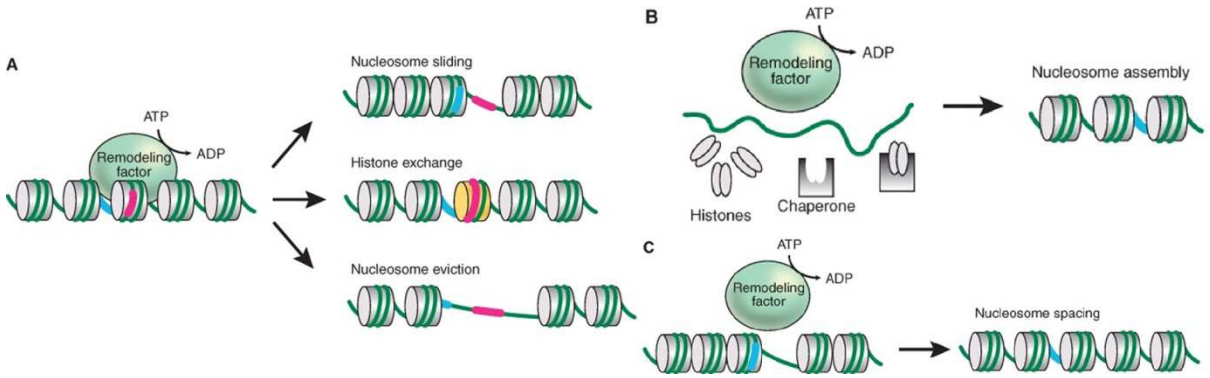

Figure 1.4. Physiological outcomes of ATP-dependent nucleosome remodeling. **(A)** Possible outcomes of the ATP-dependent nucleosome remodeling reactions are shown: translational movement of a nucleosome (nucleosome sliding) to regulate excess to DNA sequences, exchange of canonical histone with histone variant (histone exchange) and disassembly of a nucleosome (nucleosome eviction). **(B)** Nucleosome remodeling factors may also facilitate nucleosome assembly in cooperation with histone chaperones (nucleosome assembly). **(C)** Nucleosome remodeling factors may adjust the linker length between neighboring nucleosomes to achieve evenly spaced nucleosomal arrays (nucleosome spacing). Adapted from Becker and Workman (2013), Cold Spring Harbor Perspectives in Biology (20).

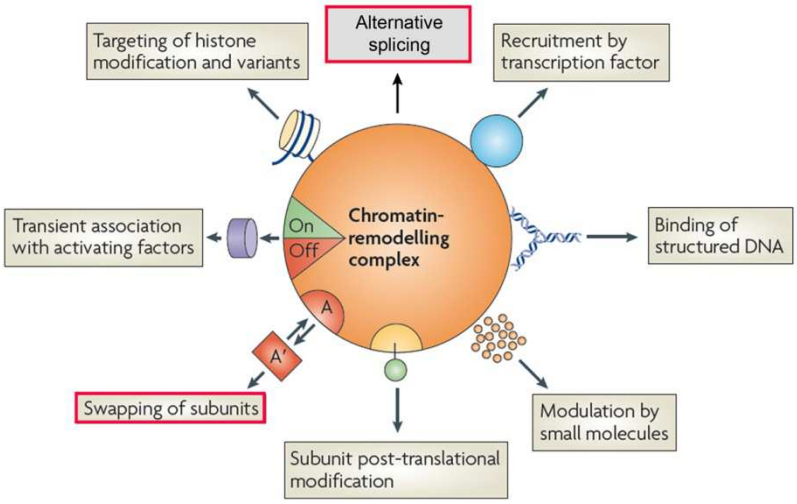

Figure 1.5. Regulation of nucleosome remodeling factors. At least eight distinct mechanisms in combination can regulate a single nucleosome remodeling complex. Alternative splicing and swapping of subunits (red rectangles) are of particular interest for this thesis and explained in detail in the text. Recruitment to specific target genes may be achieved by binding to transcription factors, structured DNA, histone variants or post-translationally modified histones. Small molecules, transient interactions with specific subunits or posttranslational modifications may modulate the activity of the complex. Adapted from Morrison and Shen (2009), Nature reviews Molecular cell biology (25). Reprinted with permission of Nature Publishing Group.

1.3.1.1 ISWI family of nucleosome remodeling complexes

ISWI (Imitation Switch) nucleosome remodeling complexes are conserved in function and composition throughout evolution (26) and in higher eukaryotes, the 'motor' ATPase ISWI, is an essential factor (27). ISWI-containing complexes induce nucleosome sliding along DNA (Fig. 1.4A) and thus enable structural adjustments of chromatin required to utilize the genome and to maintain its integrity (16,19,28). Consequently, ISWI complexes are involved in many fundamental functions ranging from DNA replication and repair to transcriptional regulation and maintenance of chromosome structure (29). The diversity of the functions of the ISWI ATPase can be explained, at least to some extent, by the fact that ISWI resides in several different complexes (Fig. 1.6).

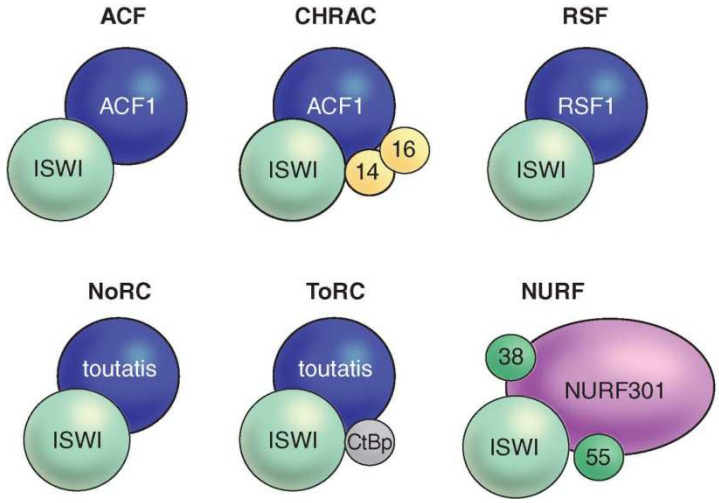

Figure 1.6. The ISWI ATPase resides in several nucleosome remodeling factors. Schematic representation of known ISWI-containing remodeling complexes in *D. melanogaster* is shown. The functions of ACF, CHRAC, RSF, and NURF are described in the text with particular focus on ACF and CHRAC. In flies, ISWI also interacts with the mammalian counterpart of Tip5, toutatis, in NoRC and with CtBp in ToRC, both likely to be involved in transcription regulation and nucleosome assembly outside of the nucleolus. It is likely that further ISWI assemblies will be discovered in flies since more complexes have been already identified in mammals. Adapted from Becker and Workman (2013), Cold Spring Harbor Perspectives in Biology (20).

To date, in *D. melanogaster* the best-studied ISWI complexes are the ACF (ATP-utilizing chromatin assembly and remodeling factor), CHRAC (Chromatin Accessibility complex) and NURF (nucleosome remodeling factor) complexes (Fig. 1.6) (20). ACF and CHRAC contain the large signature subunit ACF1, whereas CHRAC features two additional small histone fold-like proteins, CHRAC-14 and CHRAC-16 (Fig. 1.6) (30,31), which are thought to act as DNA chaperones (32). RSF (remodeling and spacing factor), ACF and CHRAC are considered to use their nucleosome remodeling activity to close gaps in nucleosomal arrays

during chromatin assembly or after disruption, and thus improve the stability and the folding of the chromatin fiber (Fig. 1.2) (31,33–36). On the other hand, ISWI-containing NURF, NoRC (nucleolar remodeling factor) and ToRC (toutatis-containing remodeling factor) are prominently involved in transcription activation by interaction with transcription factors (Fig. 1.5) (37–39). Furthermore, most organisms such as *S. cerevisiae* and humans employ several ISWI homologous, while *D. melanogaster* only has a single ISWI enzyme (29). This makes the ISWI enzyme from flies particular interesting for functional studies *in vivo*. So far, most knowledge of ISWI functions come from mechanistic studies *in vitro* using isolated remodelers from different model organisms.

In general, ISWI enzymes are characterized by a C-terminal module containing three motifs, namely HAND, SANT and SLIDE (Fig. 1.3) (40). These domains are involved in DNA and histone octamer binding to stimulate the ATPase activity of ISWI enzymes (40–42). Mechanistic studies clearly document that ISWI enzymes catalyze the repositioning of nucleosomes along the DNA in *cis* without nucleosome disruption, a mechanism termed nucleosome sliding (Fig 1.4A) (43). A positive correlation between the linker length of nucleosomes and ISWI ATPase and sliding activity has been observed in several species (19,44,45). Importantly, the isolated ISWI enzyme introduces spacing and regularity of nucleosomal arrays (Fig. 1.4C) (41). Unexpectedly, the sliding activity of ISWI is inherent to the core ATPase domain indicating that accessory domains and subunits evolved to optimize catalysis and modulate the remodeling outcome (Fig. 1.5) (19,42). An impressive example comes from a recent study that identified two short regulatory domains, AutoN and NegC, in ISWI (46). AutoN inhibits ATP hydrolysis and NegC inhibits the coupling of ATP hydrolysis with nucleosome remodeling (46). An integrated view implies that nucleosomal epitopes, in particular the H4 tail, trigger conformational changes to regulate remodeling activity of the ISWI ATPase (47). Not only features of canonical histones, but also histone variants, such as H2A.Z, seem to modulate remodeling reactions of ISWI remodelers (48), a topic of particular interest in the chapters below.

Besides nucleosome sliding, ISWI complexes also facilitate chromatin assembly in cooperation with the histone chaperone NAP-1 *in vitro* (Fig. 1.4B) (31,36,38,41), transform histone-DNA intermediates into nucleosomes (49,50) and move chromatosomes, nucleosomal arrays containing linker histone H1, *in vitro* (51,52). These mechanisms are thought to be crucial for modulating the integrity, regularity and spacing of nucleosomal arrays, thereby laying the foundation for the formation of higher-order chromatin structures (20,22). However, the underlying mechanisms are still under investigation and several layers of

regulation are assumed to play crucial roles in integrating ISWI activity into yet poorly understood physiological contexts (47).

The obligatory complex formation of the ISWI ATPase with other accessory subunits *in vivo* (Fig. 1.6) may be the most intriguing observation for ISWI remodelers. In this regard, fine-tuning and recruitment of ISWI activity *in vivo* by accessory subunits is thought to be a fundamental principle (Fig. 1.5) (47). Therefore, the emphasis of this thesis is on the characterization of the accessory subunit ACF1 and its function throughout development. ACF1, the signature subunit of ISWI-containing ACF and CHRAC, harbors in its N-terminus WAC, DDT and BAZ1/2 domains, whereas the C-terminus contains a PHD1/2-bromodomain module (Fig. 3.3). CHRAC-14/16 interaction is mediated via the N-terminus of ACF1, which enhances remodeling activity of CHRAC (32). On the other hand, ISWI binding is mediated via DDT and BAZ1/2 domains in ACF1 (53). The PHD-bromodomain module shows affinity towards unmodified histones (53), representing a possible recruitment scenario for ACF/CHRAC to chromatin. However, physiological targets are still unknown and under investigation (54).

Recently, an elegant biochemical study highlights the contribution of ACF1 in sensing the linker length of nucleosomes (55). In this model, the N-terminal domain of ACF1 and the H4 tail compete for binding with regulatory domains of ISWI depending on linker length to modulate nucleosome spacing by ACF (55). Yet, physiological roles for individual protein domains in targeting have not been addressed in detail. Unfortunately, ACF and RSF could not be trapped via formaldehyde crosslinking at regulatory sites of the genome (54) illustrating challenges in defining targeting mechanisms *in vivo*.

So far, physiological roles for ACF and CHRAC are poorly understood, but biochemical assays suggest very similar remodeling reactions (32). Whether ACF and CHRAC are separate entities is still unclear. In *D. melanogaster*, the combined functions of these two related complexes have been analyzed to some extent by characterization of loss-of-function mutation of the *Acf1* gene in the $Acf1^{1}$ and $Acf1^{2}$ alleles (33,56). Notably, loss of ACF1 in embryos reduces the regularity of nucleosome arrays, leads to defects in chromatin-mediated repression processes such as heterochromatin formation and polycomb silencing and replication defects (33,56). As a consequence, loss of ACF1 results in delayed development and ‘semi-lethality’ during larvae-pupae transition (33). The observation of chromatin defects at all developmental stages suggests a rather general role for ACF1-containing complexes in chromatin assembly and maintenance of chromatin structure (52,56). Indeed, variegated

phenotypes for H2A.V incorporation and heterochromatin formation had been observed before in *Acf1* mutants embryos (56). To date, comprehensive analysis is still missing to state the physiological relevance of these alterations. Alternatively, variegated and moderate phenotypes in *Acf1* mutant animals may also be explained by the fact that the highly related and redundant remodeler RSF-1 fulfills similar functions (34).

In contrast to these global defects, ACF1 expression is only high in early stages of embryogenesis, a developmental time of fast replication cycles and massive chromatin assembly, and then fades in most of the cells (56). Likewise, human ACF1 facilitates replication through heterochromatin (57), but recently roles in signaling and repair of dsDNA breaks have been described as well (58,59). Remarkably, levels of ACF1 expression are kept prominently high only in undifferentiated neuroblasts and primordial germ cells (PGCs), latter ones are precursors of the adult germline (56). This finding led to the speculation that high levels of ACF1 are a hallmark of unstructured, plastic chromatin in undifferentiated cells prior to developmental epigenome diversification (52). Yet, it remains elusive how ACF1 enrichment in undifferentiated cells is achieved mechanistically. Nucleosome remodeling factors are thought to play important roles during germline differentiation by contributing to chromatin plasticity and diversification (52,60,61).

Indeed, previous studies suggest essential roles for ISWI-containing remodelers in germline development (62–64). In this regard, the hyperdynamic state of chromatin in stem cells (65,66) may be modulated by nucleosome remodeling factors such as ISWI (62), although mechanistic insights are lacking. A single study suggests that cell cycle and self-renewal of germline stem cells is controlled via the co-transcriptional function of NURF on BMP signaling pathways (63). However, evidence for the functional relevance of chromatin assembly factors such as ACF/CHRAC for germline differentiation are still missing. Therefore, functions of ACF/CHRAC in germline development have been addressed in this thesis and more details are discussed below.

1.3.1.2 INO80 family of nucleosome remodeling complexes

In remarkable contrast to other SWI/SNF2 family members (Fig. 1.3), remodeling factors of the conserved INO80/SWR1 subfamily (referred to as SWR1-type) have evolved a long spacer region between the two lobes of the ATPase domain that enables unique regulation mechanisms (Fig. 1.3) (25). Nucleosome remodeling complexes of the SWR1-type family have been identified as transcriptional regulators in many organisms ranging from INO80 and SWR1 in *S. cerevisiae*, INO80 and Domino in *D. melanogaster* to INO80, SRCAP and p400 in mammals (25). The functional diversity of SWR1-type remodeling complexes not only as transcriptional regulators, but also as modulators of genome stability pathways such as cell cycle control, DNA replication and chromosome segregation is reflected at the level of complex formation (67). In contrast to the functional monomer CHD1 or the prototypic 4-subunit nucleosome slider CHRAC, SWR1-type complexes contain up to 15 subunits in complex assemblies with a size of ~1.5 MDa (Fig. 1.7) (67).

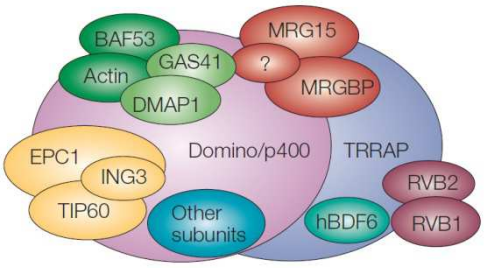

Figure 1.7. Composition of the human TIP60 complex. SWR1-like remodelers reside in large multi-subunit complexes that are conserved from yeast to humans. The ATPase subunit in the human TIP60 complex and in the fly DOM/TIP60 complex is p400 and Domino, respectively. TIP60 in flies and humans is the counterpart of the yeast acetyltransferase Esa1 in the NuA4 complex. Other homologues are also shared between yeast NuA4, fly DOM/TIP60 and human TIP60 complex such as TRRAP, EPC1, ING3, MRG15 and MRGBP. TIP60 complexes share actin and the Arp4-like protein BAF53. Human TIP60 contains the helicases Rvb1 and Rvb2, which are the counterparts of reptin and pontin in flies. Adapted from van Attikum and Gasser (2005), Nature reviews Molecular cell biology (68). Reprinted with permission of Nature Publishing Group.

Notably, some essential subunits build up the catalytic core including the remodeling ATPase itself, RuvB-like helicases and actin-related protein subunits (Fig. 1.7), whereas the other subunits have distinct functions in particular processes mostly to facilitate the association of unique chromatin substrates with the remodeling complex (25). The spacer region in the ATPase domain of SWR1-type remodelers (Fig. 1.3) interacts with the RuvB-like helicases (69,70), an essential submodule to facilitate the migration of DNA strand-exchange structures (71). On the other hand, the N-terminal HSA domain as a prominent feature of

SWR1-type remodelers (Fig. 1.3) recruits a submodule containing actin and ARPs (Fig. 1.7) (72). SWR1-type remodelers are widely thought to catalyze the sliding of nucleosomes to affect transcriptional regulation (Fig. 1.4A) (73,74), which is at least similar to the functional outcome of ISWI remodeler reactions. On the other hand, SWR1-type remodelers are uniquely allocated to exchange canonical histone H2A-H2B dimers with H2A histone variants (Fig. 1.4A) (25). H2A histone variants are discussed in detail below and characteristics and functions of SWR1-type remodeler are of further interest in this chapter.

Mechanistic details for replacement of H2A-H2B dimers with H2A variants come from extensive studies of the yeast SWR1 complex, which incorporates H2A.Z at promotors in a step-wise manner (75–77). Different studies in higher eukaryotes showed that the SWR1-type enzymes, p400 and SRCAP, harbor histone replacement functions *in vitro* and *in vivo* as well (74,78–80). However, very little is known about the reverse reaction, the eviction of H2A.Z-containing nucleosomes for H2A-H2B dimers. In yeast, there is isolated evidence that the genome-wide distribution of H2A.Z appears to be established by the antagonistic functions of SWR1 and INO80 remodeling complexes, where INO80 replaces H2A.Z-H2B with H2A-H2B dimers (81). It is still under investigation if INO80 complexes play similar roles in higher eukaryotes (82). Recently, the vertebrate-specific histone chaperone ANP32E has been identified as part of a TIP60/p400 complex, which facilitates the eviction of H2A.Z-H2B dimers from chromatin (83). The dynamic nature of H2A variant exchange remains an intriguing topic to understand how local and specialized chromatin structures modulate chromosome biology.

In line with some evidence from studies in yeast supporting histone H2A variant removal, in *D. melanogaster* a TIP60 nucleosome remodeling complex (Fig. 1.7) is involved in removal of the histone H2A variant H2A.V (79). In contrast to other higher eukaryotes, the fly genome only contains a single SWR1-like gene: *domino* (*dom*) (84). Moreover, alternative splicing (Fig. 1.5) of the *dom* transcript produces two major isoforms, *dom-A* and *dom-B*, which differ in their C-termini (Fig. 1.8) (84). These unique characteristics make the fly SWR1-type remodeler DOM a fascinating molecule to study histone variant biology. Therefore, functions of DOM in histone variant H2A.V exchange have been addressed in this thesis and more details are discussed below.

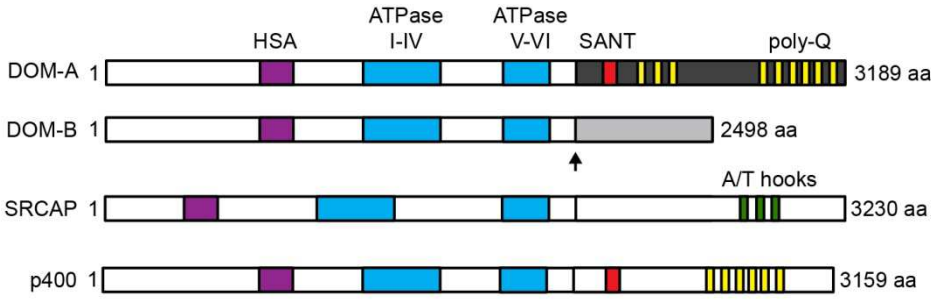

Figure 1.8. Splice variants of the SWR1-type remodeler Domino. Schematic representations of *D. melanogaster* Domino (DOM) isoforms and mammalian SRCAP and p400 are shown (85). Arrow indicates different C-terminal regions in DOM-A (dark gray) and DOM-B (light gray). Purple, blue, red, yellow and green rectangles represent HSA domain, ATPase domains, SANT domain, poly-Q stretches and A/T hooks, respectively.

dom has been originally identified and characterized as required for cell proliferation and viability, homeotic gene regulation and Notch signaling (84–91). *dom* is essential for fly development (84) indicated by the observation that *dom* mutants die during pupariation (84,92). Remarkably, an impressive example of functional conservation of SWR1-like remodelers comes from a genetic study showing a partial rescue of *dom* mutant lethality by complementation with the orthologous human *SRCAP* gene (Fig. 1.8) (85). Previous studies did not address distinct functions of the two DOM isoforms. Furthermore, it is likely that observed *dom* mutant phenotypes can be explained by improper regulation of the histone variant H2A.V, but experimental proof is lacking.

In terms of protein domain architecture, the longer DOM-A isoform features several poly-glutamine (poly-Q) stretches and a SANT domain. SANT is thought to function as histone-tail interaction module that couples binding to enzyme catalysis (93), whereas poly-Q stretches are widely found in transcriptional regulators to modulate protein interactions (Fig. 1.8) (94). In contrast, the shorter DOM-B C-terminus is largely unstructured (Fig. 1.8) (84,85). Early studies have suggested distinct functions since both DOM isoforms showed different expression patterns. DOM-B is rather ubiquitously expressed and DOM-A is found only in the embryonic nervous system, larval salivary glands and S2 tissues culture cells (84,85,95).

Progress has been made towards the identification and characterization of SWR1-type remodeling complexes in yeast (67) and other species, but only very little is known about DOM-containing complexes in flies. DOM-A has been purified from S2 cells as part of a 16-subunit assembly containing the acetyltransferase TIP60, apparently combining features of

the yeast SWR1 remodeling and NuA4 acetyltransferase complexes (Fig. 1.7) (79). Similarly, our knowledge about H2A.V exchange by DOM *in vivo* is anecdotal. It has been suggested that DOM is involved in H2A.V exchange in the context of the DNA damage response (79). Under these conditions, a TIP60/DOM-A complex acetylates γ-H2A.V at lysine 5 to facilitate exchange of γ-H2A.V by unmodified H2A.V (79). In a reverse reaction, DOM is involved in H2A.V incorporation at the *E2f* and *Hsp70* promotor (87,96). It has been proposed that H2A.V must be evenly distributed in the genome, yet specifically targeted to promotor to fulfill all its diverse functions. This is likely to be achieved by several distinct mechanisms of DOM remodeling that are described in more detail below.

1.3.2 Histone variants – determinants of chromatin diversity and plasticity

Canonical histones may be exchanged by non-allelic histone variants that differ in their sequence. In contrast to canonical histones, which function in genome packaging and gene regulation, histone variants have diverse roles in many processes ranging from DNA repair, meiotic recombination, chromosome segregation, transcription initiation and elongation, sex chromosome condensation to sperm chromatin compaction (97). Most variants are polyadenylated, can contain introns and are expressed independently throughout the cell cycle, all features distinct from canonical histones (98). Histone variants alter the nucleosome structure and dynamics contributing to genome-wide chromatin complexity and plasticity that reflects their diverse biological roles in developmental processes (99). Eukaryotic cells acquired many histone variants during a long evolutionary history with some ‘universal’ variants found in nearly all eukaryotes, reflecting their ancient functions in contrast to specialized functions of some lineage-specific variants (97). The special constraints of nucleosomal protein-protein and DNA-protein interactions offered different potentials to evolve structural diversification of histone variants (97,100). On the one hand, the H4 family of proteins is one of the most slowly evolving in eukaryotes (100), whereas the H2A family contains a plethora of variants. Among the ‘universal’ variants are the H3 variants, centromeric histone variant H3 and the H2A variants H2A.Z and H2A.X. The position of the H2A-H2B dimers on the ‘edges’ of the canonical octamer made H2A histone variants a favorable target to regulate DNA-protein interactions (99). For this thesis, the histone variants H2A.Z and H2A.X are of interest with an emphasis on the single H2A histone variant, H2A.V, in *D. melanogaster*.

1.3.2.1 H2A.Z – a universal histone variant implicated in chromatin responsiveness?

The almost universal variant H2A.Z diverged from other H2As before the diversification of modern eukaryotes sharing ~60% identity with canonical H2A, but ~80% identity between most organisms (101). This suggests that H2A.Z fulfills unique functions. Indeed, H2A.Z is essential in many organisms with the exception of *S. cerevisiae* and *Schizosaccharomyces pombe* (102–104). Essential functions of H2A.Z are located in the C-terminus (105) which differs most from H2A in respect to length and sequence together with the L1 region and the acidic patch of the 'docking domain' (Fig. 1.9) (99). These differences affect H2A-H2B dimer or H1 interaction as well as nucleosome stability (99), although the overall nucleosome structure is very similar to the canonical one (1,106).

H2A.Z nucleosomes are found enriched at gene promotors where they localize to both sides of a nucleosome-depleted region (101,107–111) to promote efficient recruitment and release of RNA polymerase II (112,113). As an architectural element of promotors H2A.Z fulfills apparently contradictory roles in gene activation and repression. However, H2A.Z is also found at other regulatory regions like enhancers and insulators as well as heterochromatin (101). In this respect, H2A.Z regulates nucleosome mobility, positioning and dynamics which may alter binding of transcriptional activators and repressors or other DNA-binding proteins. Consequently, this influences many biological processes including DNA repair, heterochromatin, boundary element and chromatin fiber formation, suppression of antisense RNAs, embryonic stem cell differentiation, chromosome segregation and mitosis (97,99,101). The diversity of biological processes affected by H2A.Z might be also explained by PTMs (114), H1 linker histone binding (115), HP1 interaction (116), effects on nucleosome remodeling complexes (48) or nucleosome composition (97).

Apparently, conflicting results on transcriptional regulation may be explained by acetylation and monoubiquitylation. Multiple lysine residues in the N-terminus of H2A.Z can be acetylated which alters the nucleosome structure acting as a gene-regulation switch (114). On the other hand, H2A.Z seems a crucial target of monoubiquitin-mediated silencing by Polycomb repressor complex 1 (PRC1) (117), although recent work in *D. melanogaster* indicates monoubiquitin-independent PRC1 silencing of target genes (118). Notably, H2A.Z incorporation into chromatin alters secondary and tertiary structure by interaction of the extended acidic patch of H2A.Z with the H4 tail (99). This leads to compensation of the chromatin fibre in which single nucleosomes are thought to bind less efficiently with H1 linker histone (115). In contrast, HP1 binding is enhanced in H2A.Z containing nucleosomes

in comparison to H2A that may facilitate the formation of higher-order chromatin (116). Furthermore, activity of human ISWI family remodeler, SNF2H and SNF2L, is stimulated by the acidic patch of H2A.Z nucleosomes (48). Yet, is still unclear whether ISWI remodelers affect H2A.Z distribution on a global scale.

Unexpectedly, not only homotypic nucleosomes containing two H2A.Z-H2B dimers, but also heterotypic nucleosomes with H2A.Z-H2B and H2A-H2B dimer were found *in vitro* and *in vivo* (75,111,119,120). It was thought that due to differences in the L1 interaction surface of H2A and H2A.Z, heterotypic nucleosomes would be destabilized. However, heterotypic H2A.Z nucleosomes are the majority in human HeLa cells (120). Interestingly, although homotypic H2A.Z nucleosomes seem to be more stable intrinsically than heterotypic or H2A-containing nucleosomes *in vitro* (114), higher turnover rates for H2A.Z nucleosomes were detected *in vivo* (101). Even more, nucleosome containing H2A.Z-H3.3 dimers seem to be very unstable (121,122). However, the influence of H2A.Z on nucleosome stability is still a matter of debate and conclusions are hampered due to many technical differences in the experimental setups (99).

Intriguingly, the non-uniform distribution of H2A.Z nucleosomes throughout the genome might be caused by several non-mutually exclusive mechanisms (99). Site-specific H2A.Z incorporation can be achieved by targeting factors of the SWR1-type family of nucleosome remodeling complexes. Alternatively, H2A.Z may be randomly incorporated genome-wide and afterwards removed from non-target sites by active mechanisms. Thirdly, intrinsic features of homo-, heterotypic and canonical nucleosomes may lead to differential stabilities that contribute to particular localization patterns. More details are discussed in the previous chapter 1.3.1.2 and addressed in results 3.2.

1.3.2.2 H2A.X – an ancient DNA damage sensor poised for chromatin remodeling?

The almost universal H2A.X variant is very similar to the canonical H2A in the ‘core’, but contains a C-terminal motif Ser-Gln-(Glu/Asp)-φ (φ hydrophobic residue). This serine can be phosphorylated (γH2A.X) (123,124) by phosphoinositide 3-kinase-like kinases such as ATM, ATR and DNA-PK upon dsDNA break (125,126). Phosphorylation of H2A.X appears at sites of dsDNA break repair either if DNA is damaged or broken in the context of physiological processes including meiotic recombination, V(D)J splicing and class switch recombination (127). This argues for γH2A.X being a universal response to dsDNA break repair (127). Strikingly, apart from the C-terminus, human H2A and H2A.X differ only by four amino acids which are found in the N-terminal tail, L1 loop and C-terminal docking domain.

Remarkably, some organisms, such as *S. cerevisiae* and the protozoan *Giardia lamblia,* do not contain canonical H2A, but rely solely on the H2A.X variant containing the SQ(E/D)φ motif (97). In *D. melanogaster* a similar motif (SQAY) is present in the only H2A.Z-like histone variant, namely H2A.V. Surprisingly, H2A.X seems to be dispensable since some organisms such as *Caenorhabditis elegans* and some protists lack H2A.X (97). It has been suggested that universal H2A.X is ancestral and preceded canonical H2A in evolutionary history (97). This notion is further supported by the fact that H2A.X exhibits features of replication-independent histone variant genes and replication-dependent canonical histone genes such as 3' mRNA stem loop structures and non-polyadenylated mRNA (128,129).

In response to dsDNA break (DSB) repair, H2A.X is phosphorylated most rapidly and accumulates around damage sites generating γH2A.X foci (123,124). It is estimated that each γH2A.X focus corresponds to one DSB with ~2000 γH2A.X molecules (123,127). γH2A.X foci contain DNA up to 50 kb away from of the DSB in *S. cerevisiae* (130) and up to several Mb in mammals (124). It is thought that γH2A.X foci are involved in amplifying DSB repair signaling to arrest the cell cycle and prevent cells from entering mitosis (127). H2A.X mutant mice show severe phenotypes such as radiation sensitivity, male infertility and genomic instability (131). γH2A.X may function as a scaffold in helping to recruit and retain DSB signaling and repair proteins (127,132). Alternatively, γH2A.X may contribute to DSB repair by altering the chromatin structure surrounding the dsDNA break. In this case, it has been suggested that γH2A.X promotes chromatin remodeling by retention of histone modifying enzymes and nucleosome remodeling factors at the repair site (97,99,127).

It is still not fully understood how γH2A.X is removed from chromatin. Firstly, γH2A.X could be directly dephosphorylated at chromatin. Alternatively, modified H2A.X is removed from chromatin and subsequently dephosphorylated or degraded. In *S. cerevisiae,* a histone H2A phosphatase complex, HTP-C, dephosphorylates γH2A.X apparently only after removal from chromatin and thereby regulates DSB repair checkpoint (133,134). On the other hand, human PP2A accumulates in γH2A.X foci by direct binding of γH2A.X on chromatin suggesting an *in situ* dephosphorylation in higher eukaryotes (127). Even other mechanisms have been proposed for flies in which γH2A.V is actively removed for unmodified H2A.V by a DOM/TIP60 complex (79,96). However, these findings still lack further validation *in vivo* and are addressed in results 3.2.

It becomes more evident that γH2A.X might also fulfill functions outside of the DSB repair pathway. For example, γH2A.X is required for inactivation of the male X chromosome in

meiosis (135), meiotic silencing of unpaired chromatin (136) and has undefined cell-cycle regulated roles in DSB-independent foci (127). Since the C-terminus of H2A/H2A.X is located at a strategic position in the nucleosome, it not surprising that H2A.X and γH2A.X may regulate nucleosome stabilization and thereby chromatin fibre formation (97,99,127), although this is still a matter of debate. A common denominator of these roles of γH2A.X might be to facilitate chromatin remodeling by altering directly the local chromatin structure and by acting as a scaffold for chromatin modifying enzymes.

1.3.2.3 H2A.V – the all-in-one H2A histone variant in *D. melanogaster*

In *D. melanogaster*, structural features of the two 'universal' H2A histone variants, H2A.Z and H2A.X, are combined into the single, non-allelic H2A histone variant, H2A.V, making this a unique model system for H2A variant biology. H2A.V shows differences to canonical H2A along the entire sequence that accumulate in the N-terminal tail, the L1 loop and C-terminal docking domain and tail (Fig. 1.9) (28).

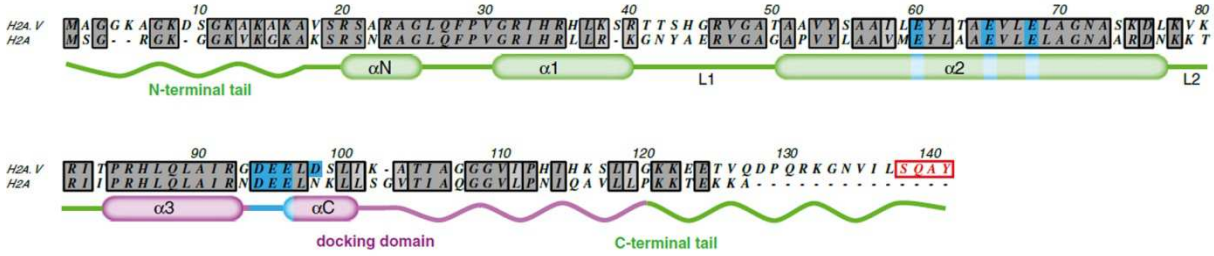

Figure 1.9. Sequence features of histone H2A variant H2A.V. Sequence alignment between H2A.V and canonical H2A of *Drosophila melanogaster* is shown. Indicated are secondary structure features: the N- and C-terminal unstructured 'tails', the three histone fold helices (α1–α3) separated by loops L1 and L2, the N- and C- terminal helices (αN and αC), the acidic patch residues of the docking domain (blue) and the SQ[E/D]φ-like motif at the C-terminus of H2A.V (red). Adopted from Baldi and Becker (2013), Chromosoma (28). Reprinted with permission from Springer.

H2A.V is essential for fly development and fertility (103) and homozygous mutants die as third instar larvae (103,105). However, it is still unknown how improper H2A.V regulation affects fertility. H2A.V is ubiquitously expressed with highest levels in embryos until 10 h of development, possibly reflecting early needs for H2A.V during fastest nuclei division and chromatin assembly (28). Furthermore, H2A.V is maternally contributed as mRNA into the developing oocyte, while additional mechanisms of maternal contribution at the protein level have been suggested (137).

According to sequence similarities, H2A.V belongs to the H2A.Z family (Fig. 1.9) (28). In the N-terminal tail of H2A.V, an additional lysine at position 5 can be acetylated by TIP60 in

context of the DNA damage response (79), whereas a serine at position 2, a conserved phosphorylation site in other species, is missing (Fig. 1.9). Notably, H2A.V mutants can only be partially complemented with a H2A.V lacking the N-terminal tail (105). Similarly, the C-terminal docking domain, which has one more acidic amino acid in the acidic patch (Fig. 1.9), is also essential for fly development (105).

At the global level, H2A.V is found with decreasing amplitudes at phased nucleosomes close to transcription start sites (TSS) of active promotors (138), similarly to H2A.Z profiles in yeast. However, there are some characteristic differences: H2A.V is limited to phased nucleosome downstream of the TSS, +1 nucleosomes with H2A.V do not occupy the TSS and nucleosomal arrays show a longer spacing of 175 bp (138). Occupancy of homotypic H2A.V nucleosomes close to the TSS positively correlate with transcriptional levels (111,138). It is thought that less stable H2A.V/H3.3 nucleosomes may facilitate the transition of RNA polymerase from initiation into elongation (28).

In remarkable contrast to other species, H2A.V in *D. melanogaster* seems to be involved not only in gene activation, but also in the establishment of repressive chromatin structures such as heterochromatin and polycomb-mediated silencing (28). Surprisingly, H2A.V seems to function upstream of H3K9 methylation and HP1 recruitment in heterochromatin formation (139). Only the nucleosome remodeling factors ACF/CHRAC can be placed further upstream of these events, since their loss not only affects H3K9 and HP1, but also leads to variegated H2A.V incorporation (56). H2A.V-containing nucleosomes could be more prone to form chromatin fibers, a possible prerequisite for heterochromatin formation. Yet, it still remains unclear whether ISWI-containing ACF/CHRAC are required for global H2A.V incorporation, while SWR1-type factors such as DOM are more likely to fulfill this task.

In addition to all H2A.Z-related features, H2A.V seems to fulfill further tasks since it contains the conserved SQ(E/D)φ motif, a particular feature of H2A.X variants, which can be phosphorylated upon DNA damage. Indeed, a serine at position 137 in H2A.V gets phosphorylated by ATM/ATR kinases during an early event of DSB recognition and repair (137,140). However, lethality of H2A.V mutants can be rescued by an H2A.V lacking the C-terminal phosphorylation motif indicating that phosphorylation is not absolutely required for DNA damage response (105). During meiotic recombination, a process with naturally occurring DSBs, H2A.V gets phosphorylated by ATM kinase as well (137). How the DNA damage signal is cancelled remains a matter of recent debate and most likely involves a catalyzed reaction by a DOM/TIP60 complex (79). In general, the mechanisms of H2A.V

placement and removal are only poorly understood and, therefore, in focus of this thesis with more details discussed in chapters 1.3.1.2, 1.4 and 3.2.

1.4 *Drosophila* oogenesis – a prominent model system for chromatin biology

During development of sexually reproducing organisms, highly specialized haploid cells, gametes, are produced by germline cell stem cells (GSC) in a complex differentiation process that requires finely tuned transcription programs and chromatin reorganization. *D. melanogaster* oogenesis provides a prominent model system to study germline and somatic stem cell self-renewal and differentiation in the context of egg chamber maturation (64,141,142). Therefore, *D. melanogaster* oogenesis was used to study nucleosome remodeling factors ACF/CHRAC and DOM in context of cell differentiation and chromatin diversification.

In general, egg formation starts in the germarium, the anterior tip of the tubular ovariole structure, in which 2-3 GSCs reside in a somatic niche (Fig. 1.10). Stem cells feature less compacted chromatin in a hyperdynamic state that contributes to maintenance of pluripotency (65,66). Activity of GSCs is controlled extrinsically by cell-cell signaling and cell-cell contacts and by intrinsic stem cell programs, chromatin structure, transcription and splicing (141). GSCs divide asymmetrically to self renew and produce a daughter cystoblast (Fig. 1.10) (143). Next, four rounds of mitosis with incomplete cytokinesis result in an interconnecting 16-cell-cyst that travels towards the posterior end of the germarium (Fig. 1.10). Along the way, two of the sixteen cells get specified as pro-oocytes with enrichment of oocyte determinants and the initiation of meiosis (Fig. 1.10) (144,145). Oocyte determinants may be asymmetrically localized in prospective oocytes as mRNAs by the RNA-binding machinery (146,147). Pro-oocytes are not yet fully committed because these cells can still revert fate. At this point, programmed DSBs during meiotic recombination are marked by phosphorylation of H2A.V (γH2A.V) in region 2 of the germarium (148). One of these two cells gets specified as the oocyte by yet unknown mechanisms while the other 15 germline cells adopt a nurse cell fate (Fig. 1.10) (149). These latter ones change their cell cycle program to endoreplication which leads to a highly polyploid genome with many naturally occurring DSBs and γH2A.V foci. In parallel, somatic stem cells (SSC) in region 2 of the germarium self renew and produce somatic follicle cells, which encapsulate 16-cell-cysts at the posterior end of region 3 (Fig. 1.10) (143). At this point, γH2A.V foci disappear in germline cysts since recombination events are completed (148) and individual egg chambers bud off the germarium. This encapsulation process is coordinated by a plethora of signaling

pathways and produces with high accuracy egg chambers with 15 nurse cells and a single oocyte at the posterior end (Fig. 1.10).

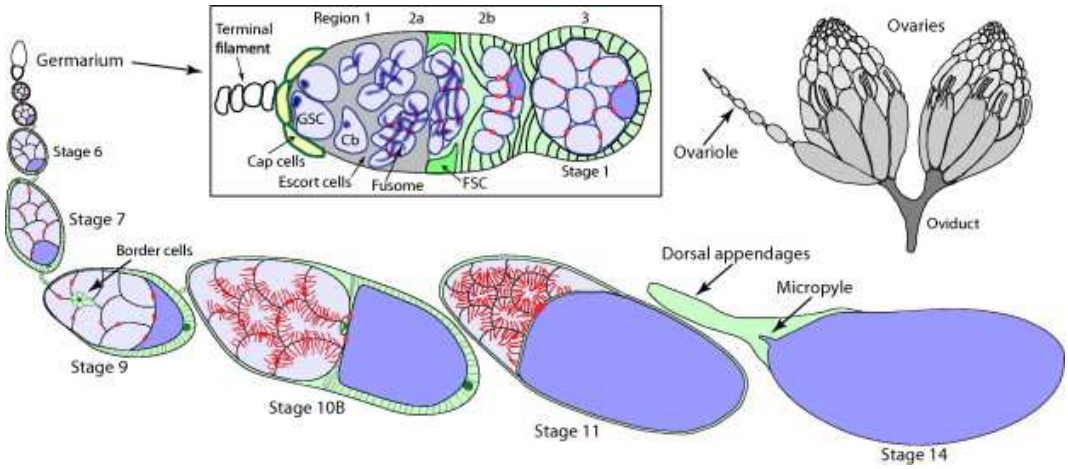

Figure 1.10. Overview of *D. melanogaster* oogenesis. *D. melanogaster* females have a pair of ovaries (top right), each of which consists of ~15 ovarioles. In general, oogenesis runs through 14 stages of development and begins in the germarium (center box). There, germline and somatic stem cells (GSC and FSC, respectively) divide continuously to support the formation of new egg chambers. Germline cysts move from anterior (stage 1) to posterior end of the germarium (stage 3). Cap cells (yellow), terminal filament cells (white), somatic follicle cells (green), nurse cells (light purple), oocytes (dark purple) and ring canals and nurse cell F-actin bundles (red) are shown. Adopted from Hudson and Cooley (2014), Methods (142). Reprinted with permission from Elsevier.

Afterwards, oogenesis and egg chamber maturation continue through 14 stages of development in which aberrations can be easily scored (Fig. 1.10) (142). Progression into meiosis and oocyte maturation requires extensive genome reorganization to achieve a highly compacted oocyte genome, the so-called karyosome, which is in a mostly transcriptional inactive state (150). Unfavorable environmental conditions such as starving or intrinsic features such as ‘low quality’ oocytes might facilitate abortion of egg chambers during stage 8 by a yet unknown check point mechanism (151–153). Maternal contribution of RNAs and proteins is achieved by an active transport mechanism from the 15 interconnected nurse cells to the oocyte during later stages of egg chamber development. Furthermore, the landscape of histone modifications and variants changes throughout gamete production while their impact on transcriptional programs and functional roles remain largely unclear (61).

Given the widespread requirement for chromatin plasticity during development (52,60,61) it is not surprising that nucleosome remodeling factors besides other chromatin modifying enzymes such as histone methyltransferases (154–156), histone demethylases (157,158) and

PRC2 (159) have been found important for oogenesis. Nucleosome remodeling factor may affect higher-order chromatin structure, local placement of histone variants or alternatively help to establish and maintain cell type-specific expression patterns as cotranscriptional regulators (52). Remarkably, the nucleosome remodeling ATPases ISWI, Brahma and DOM are required for self-renewal of GSCs and SSCs, respectively (27,62,64,160,161), possibly due to their effects on transcription programs.

Nucleosome remodeling complexes are recruited to target genes via sequence-specific transcription factors to promote or block transcriptional initiation or elongation by movement, assembly or disassembly of nucleosomes (52). For example, ISWI as part of the NURF nucleosome remodeling complex controls GSC fate and division via a functional link to the steroid hormone ecdysone in BMP signaling and transcriptional regulation of differentiation programs (160). Studies from the conserved wingless/Wnt signaling even suggest an antagonism between the two different nucleosome remodeling complexes, NURF and ACF (162,163), which illustrates on the importance of the regulated targeting of these two complexes. In general, one important principle to regulate complex assembly and function is the developmental or cell type-specific expression of subunits (Fig. 1.5) (52).

Indeed, the ACF signature subunit ACF1 is expressed prominently high in primordial germ cells (56) suggesting unknown functions of chromatin assembly factor ACF/CHRAC in generation of gonads. However, it is unclear whether high levels of ACF1 are maintained in adult germline cells and how loss of ACF1 affects fertility and oocyte development. It is assumed that ACF has distinct roles in comparison to NURF as cotranscriptional regulator in germline cells. It also remains to be shown to which extent ACF1 functions in context of a CHRAC *in vivo*. Therefore, work in this thesis focuses on the characterization of the role of ACF1 in ACF/CHRAC during *D. melanogaster* oogenesis and describes developmentally associated phenotypes in germline and somatic cells by altering ACF1 levels.

Additionally, self renewal and differentiation programs during oogenesis may be controlled by the local placement of histone variants which affect genome organization, gene expression, cell division and DNA repair. H2A.V is ubiquitously expressed during oogenesis (137) and H2A.V mutant flies are sterile (103). Yet, why loss of H2A.V causes sterility is still unclear. A major role for DOM in H2A.V incorporation is assumed, but not well documented *in vivo.* Oogenesis in adult flies is strongly perturbed in *dom* mutant alleles, that affect both *dom* splice variants, causing complete sterility (84). Another principle to regulate functions of nucleosome remodeling factors may be alternative splicing of subunits, possibly in a

developmental or cell type-specific manner (Fig. 1.5) (52). Notably, both DOM splice variants, DOM-A and DOM-B, are important for GSC and SSC self-renewal as well as cystoblast differentiation (62,64). The mechanisms of DOM function in these processes are unclear, but involvement of H2A.V exchange has been suggested. For example, *dom* mutant GSC clones in *D. melanogaster* testes show a modestly decreased H2A.V signal (164). Furthermore, H2A.V and γH2A.V are not detectable in mutant germline clones for MRG15, a DOM-A/TIP60 complex subunit (137). However, direct evidence for a role of DOM – and specific roles for each isoform – in H2A.V incorporation during oogenesis is lacking. Therefore, work in this thesis focuses on characterization of the roles of DOM isoforms during *D. melanogaster* oogenesis and describes non-redundant requirement for both DOM isoforms in several cell differentiation programs and for H2A.V exchange.

1.5 Aims of this thesis

Mechanistic details of nucleosome remodeling reactions come from isolated factors comprising different organisms and are a matter of recent investigations, while the physiological roles of individual remodeling factors are still largely unclear.

Not only detailed knowledge of the transcriptional landscape, but also about the interconnected local and global changes in chromatin are required to understand developmental networks and processes. In recent years, nucleosome remodeling enzymes have been identified as essential factors of germline development, although their functional contributions remain elusive. Therefore, one aim of my work was to use the prominent model system of *D. melanogaster* oogenesis to study the functions of two important nucleosome remodeling factors *in vivo*.

ACF/CHRAC are general nucleosome sliding factors that improve the regularity and integrity of the chromatin fiber to facilitate the formation of repressive chromatin. Expression of the signature subunit ACF1 is restricted during embryonic development, but remains high in precursors of germline cells. This suggests an unexpected role of this general remodeler in the specific process of germline development. We now established novel genetic tools such as a loss-of-function *Acf1* mutant allele and transgenic flies expressing tagged ACF1 to study the fate of ACF1 during oogenesis (results 3.1). Our aim was to describe ACF1 localization and developmentally associated phenotypes in germline and somatic cells. Furthermore, we strive to dissect the contributions of distinct domains in ACF1 to specific oogenesis phenotypes. Finally, we addressed whether ACF1 functions in ACF or CHRAC *in vivo* uncovering that fine-tuned levels of ACF/CHRAC are required for proper development of eggs.

The SWR1-type nucleosome remodeling factor Domino (Dom) is thought to replace histone H2A by the variant H2A.V to endow chromatin locally with specialized functionality. However, a major role for DOM and its two splice variants, DOM-A and DOM-B, in H2A.V incorporation is assumed, but not well understood *in vivo*. Loss of both DOM isoforms causes defects in oogenesis making this an interesting process to address their specialized functions *in vivo* (results 3.2). Therefore, we generated transgenic flies expressing tagged Domino isoforms to characterize systematically *dom* mutant phenotypes as well as DOM expression and localization. Moreover, we established a cell type-specific knockdown approach in different developmental processes to assess non-redundant functions of DOM-A and DOM-B in germline and soma for egg production. Finally, we made further use of this system to

dissect how DOM isoforms are involved in incorporation and removal of H2A.V and γH2A.V during different developmental processes of oogenesis.

Lastly, recent unpublished data from our lab suggests a direct interaction of ACF1 with DOM-B in a novel assembly called ACF1-DOM containing (ACDC) complex. To test this more directly, we made use of recombinantly expressed DOM-B and ACF1 to verify the physical interaction of these distinct nucleosome remodeling factors with affinity chromatography (results 3.3). We wished to identify interaction domains on both proteins and clarify whether the 'motor' ATPase ISWI may be part of an ACDC complex. Finally, we produced recombinant DOM-A protein as well as isoform-specific antibodies to address whether ACF1 interaction is restricted only to the DOM-B isoform as previous studies suggested.

2 Summary

The organization of eukaryotic genomes into nucleosomes and chromatin not only provides means for packaging and protection, but also offers potential to modulate access of regulatory factors to specific DNA sequences, which may be occluded by histones and non-histone proteins. To this end, conserved ATP-dependent nucleosome remodeling factors evolved to alter histone-DNA interactions in response to intrinsic and extrinsic stimuli. These remodeling reactions may - depending on the enzyme and its accessory subunits - lead to the sliding of histone octamers along the DNA or the alteration of the histone composition through incorporation of variants. Mechanistic details of nucleosome remodeling are currently under investigation, while many essential roles in physiological contexts are still poorly understood. In this work, the prominent model system of *Drosophila melanogaster* oogenesis was used to study the roles of two distinct nucleosome remodeling factors ACF1 and Domino *in vivo*.

ACF1 is the signature subunit of the prototypic nucleosome sliding complexes ACF and CHRAC. These complexes use the activity of the ISWI ATPase to improve the regularity and integrity of the chromatin fiber, which may facilitate the formation of repressive chromatin. During embryonic development ACF1 expression becomes highly enriched in germline precursors, suggesting unexpected roles in these cells. We now showed that the cell type-specific expression of ACF1 in germline stem cells and oocytes is accomplished by a corresponding enrichment of its mRNA through dedicated machinery. Loss of ACF1 in the novel $Acf1^{7}$ allele or mild overexpression of ACF1 and CHRAC-16 by additional gene copies led to apoptotic egg chambers. Additionally, a rare 16-cell cyst packaging phenotype with two functional oocytes was observed in the previously known $Acf1^{1}$ allele. These defects were induced by the expression of a PHD-bromodomain module from the C-terminus of ACF1, suggesting competitive interactions with yet unknown target molecules. In summary, finely tuned ACF1 levels are required for proper oogenesis.

Loss of the SWR1-type remodeling factor Domino (Dom) causes female sterility, a defect possibly caused by misregulation of the histone H2A variant H2A.V. This variant fulfills functions of mammalian H2A.Z and H2A.X in transcriptional regulation and DNA damage response. However, clear evidence for an involvement of DOM in H2A.V exchange is still missing. We now established a cell type-specific knockdown approach to show that the two DOM splice variants, DOM-A and DOM-B, have non-redundant functions in germline and soma for egg formation, similar to H2A.V. Notably, DOM-B promotes global H2A.V incorporation into chromatin of germline and somatic cells of the germarium. In contrast,

H2A.V incorporation in endoreplicating nurse cells is independent of DOM, while a DOM-A/TIP60 complex is involved in eviction of H2A.V at later stages. In summary, the two DOM isoforms have distinct functions in cell type-specific development and H2A.V exchange.

Lastly, following earlier circumstantial and unpublished evidence for an interaction between the ACF and DOM/TIP60 remodeling complexes during early embryogenesis we tested for direct binding of recombinant ACF1 to DOM *in vitro*. The observation of direct, physical interactions between ACF1 and DOM is in line with the idea of a larger assembly combining two nucleosome remodeling enzymes with different remodeling outcomes. Such a scenario may exemplify a novel layer of regulating nucleosome remodeling reactions.

Zusammenfassung

Nukleosomen, die Grundeinheit eukaryotischer Genome, werden über hierarchische Ebenen zu höheren Chromatinstrukturen organisiert. Diese Strukturen bewerkstelligen nicht nur die kompakte Verpackung und den Schutz der DNA, sondern bieten auch vielfältige Möglichkeiten, um den Zugang von regulatorischen Faktoren zu spezifischen DNA-Sequenzen zu kontrollieren, die ansonsten von Histon- oder Nicht-Histon-Proteinen gebunden sind. Mit der Evolution komplexer Chromatin-Strukturen ging die Entwicklung von ATP-abhängigen *Remodeling*-Faktoren einher, die die Nukleosomenstruktur durch Anpassung der Histon-DNA Bindungen in Abhängigkeit von internen und externen Signalen verändern. *Remodeling* Reaktionen können je nach Enzym und damit assoziierten Untereinheiten zum Beispiel dazu führen, dass Nukleosomen entlang der DNA verschoben oder die Zusammensetzung von Histonen in Nukleosomen geändert werden. Die genauen Mechanismen dieser Reaktionen sind Bestandteil aktueller Forschungsarbeiten. Allerdings sind die meisten physiologischen Aufgaben von *Remodeling* Faktoren in Zellen und Geweben nur teilweise verstanden. Im Rahmen dieser Arbeit wurde das etablierte Modellsystem der Eizellentwicklung von *Drosophila melanogaster* genutzt, um die Funktionen der beiden unterschiedlichen *Remodeling* Faktoren ACF1 und Domino zu untersuchen.

Das ACF1 Protein ist die Signaturkomponente von ACF und CHRAC Komplexen, die als Musterbeispiele für das Verschieben von Nukleosomen dienen. Diese Komplexe nutzen die ATP-verbrauchende DNA Translokaseaktivität des Enzyms ISWI, um die Regelmäßigkeit und Integrität der Chromatinfaser zu verbessern, was möglicherweise zur Bildung von repressiven Chromatinstrukturen beiträgt. Die Expression von ACF1 wird im Laufe der Embryonalentwicklung auf die Vorläuferzellen der Keimbahn beschränkt, ein Hinweis auf noch unbekannte Funktionen in diesen Zellen. Die vorliegende Arbeit zeigt, dass ACF1 verstärkt sowohl in den Stammzellen der Keimbahn als auch in den sich daraus entwickelnden Eizellen vorkommt. Die Anreicherung des Proteins wird bereits auf der Ebene der mRNA Moleküle mittels bekannter RNA Transportsysteme erreicht. Der Verlust von ACF1 durch eine neue Nullmutation (*Acf1*^{7}) führt zu defekten Eikammern. Solche Defekte entstehen auch, wenn die Proteine ACF1 und CHRAC-16 mittels zusätzlicher Genkopien in geringfügig erhöhter Menge hergestellt werden. Desweiteren führt eine bereits bekannte Genmutation in *Acf1* (*Acf1*^{1}) zu einem seltenen Zell-Verpackungsdefekt. Hierbei werden anstelle einer Eizelle zwei funktionelle Eizellen in eine Eikammer verpackt. Dieser Defekt wird durch die ektopische Expression des ACF1 C-Terminus verursacht, der charakteristische Proteindomänen (PHD-Bromodomäne) aufweist, was zur Behinderung anderer, noch

unbekannter Zielmoleküle führen kann. Zusammenfassend zeigt diese Arbeit, dass fein regulierte Mengen des *Remodeling* Faktors ACF1 wichtig sind für dessen Funktion während der Eizellentwicklung.

Weibliche Sterilität wird auch durch den Verlust anderer *Remodeling* Faktoren verursacht. Defekte in Domino (Dom), einem Protein aus der Familie der SWR1-ähnlichen Enzyme, führen wahrscheinlich durch die fehlerhafte Regulation der Histon-Variante H2A.V zu Sterilität. Dieses Histon übernimmt die Aufgaben der Varianten H2A.Z and H2A.X in Mammalia bezüglich der Regulation der Transkription sowie der Reparatur von DNA-Doppelstrangbrüchen. Allerdings steht der eindeutige Nachweis einer Beteiligung von DOM am Ein- und Ausbau von H2A.V ins Chromatin noch aus. In der vorliegende Arbeit werden die beiden Spleißvarianten des *Remodeling* Faktors, DOM-A und DOM-B, individuell in verschiedenen Zelltypen ausgeschaltet. Beide DOM Isoformen sowie die Histon-Variante H2A.V sind für die Funktionen von Keimbahn- und Somazellen während der Oogenese notwendig. Hierbei ist DOM-B für den überweigenden Teil des H2A.V Einbaus ins Chromatin von Keimbahn- und Somazellen verantwortlich. Im Gegensatz dazu erfolgt der Einbau von H2A.V ins Chromatin spezifischer Zellen der Eizell-Versorgung (*nurse cells*) durch einen noch unbekannten DOM-unabhängigen Mechanismus. Interessanterweise wird der Ausbau von H2A.V aus dem Chromatin von Keimbahnzellen in einem späteren Entwicklungsstadium durch einen DOM-A/TIP60 Komplex unterstützt. Diese Ergebnisse belegen die Notwendigkeit der beiden Isoformen des *Remodeling* Faktors Domino sowohl für die Zelltyp-spezifische Entwicklung als auch für den Ein- und Ausbau der Histon-Variante H2A.V.

Abschließend wurden biochemische Studien zur wechselseitigen Bindung von rekombinanten ACF1 und DOM durchgeführt. Das Ergebnis unterstützt Hinweise früherer Arbeiten aus der Gruppe, die auf die Existenz eines bisher nicht charakterisierten Komplexes aus ACF und DOM/TIP60 in der frühembryonalen Entwicklung schließen. Weiterführende Arbeiten werden zeigen, ob es sich bei der Kombination dieser beiden unterschiedlichen *Remodeling* Faktoren womöglich um eine neue Ebene der Regulation und Kooperation von *Remodeling* Reaktionen handelt.

3 Results

3.1 A role for tuned levels of nucleosome remodeler subunit ACF1 during *Drosophila* oogenesis

A role for tuned levels of nucleosome remodeler subunit ACF1 during *Drosophila* oogenesis

Kenneth Börner[1], Dhawal Jain[1], Paula Vazquez-Pianzola[2], Sandra Vengadasalam[1], Natascha Steffen[1], Dmitry V. Fyodorov[3], Pavel Tomancak[4], Alexander Konev[5], Beat Suter[2] and Peter B. Becker[1]

[1]Biomedical Center and Center for Integrated Protein Science Munich, Ludwig-Maximilians-University, Munich, Germany

[2]Institute of Cell Biology, University of Bern, 3012 Bern, Switzerland

[3]Albert Einstein College of Medicine, Cell Biology, Bronx, NY 10461, USA

[4]Max Planck Institute of Molecular Cell Biology and Genetics, D-01307 Dresden, Germany

[5]Department of Radiation and Molecular Biophysics, St. Petersburg Nuclear Physics Institute, Gatchina 188300, Russia

Published in Developmental Biology, Volume 411, Issue 2, 15 March 2016, Pages 217-230.

doi:10.1016/j.ydbio.2016.01.039

Declaration of contributions to 'A role for tuned levels of nucleosome remodeler subunit ACF1 during *Drosophila* oogenesis'

This study was conceived by Dhawal Jain, Peter B. Becker and myself. I performed all experiments with the following exceptions: *Acf1*^{7} fly line was made by Alexander Konev and Dmitry V. Fyodorov; *Acf1* and *Chrac16* fosmid fly lines were made by Dhawal Jain in collaboration with Pavel Tomancak; Western blot (Fig. S5H) and mRNA quantification (Fig. S9) were done by Dhawal Jain; RNA *in situ* hybridization was done by Paula Vazquez-Pianzola under supervision of Beat Suter (Figs. 1F, G; 4E, G; S1A-D) and preliminary experiments (Figs. 1,2 and 4) were done by Sandra Vengadasalam and Natascha Steffen. I prepared all figures and wrote the manuscript together with Peter B. Becker. All coauthors edited the manuscript prior to submission.

Developmental Biology 411 (2016) 217–230

Contents lists available at ScienceDirect

Developmental Biology

journal homepage: www.elsevier.com/locate/developmentalbiology

A role for tuned levels of nucleosome remodeler subunit ACF1 during *Drosophila* oogenesis

Kenneth Börner [a], Dhawal Jain [a], Paula Vazquez-Pianzola [b], Sandra Vengadasalam [a], Natascha Steffen [a], Dmitry V. Fyodorov [c], Pavel Tomancak [d], Alexander Konev [e], Beat Suter [b], Peter B. Becker [a,*]

[a] Biomedical Center and Center for Integrated Protein Science Munich, Ludwig-Maximilians-University, Munich, Germany
[b] Institute of Cell Biology, University of Bern, 3012 Bern, Switzerland
[c] Albert Einstein College of Medicine, Cell Biology, Bronx, NY 10461, USA
[d] Max Planck Institute of Molecular Cell Biology and Genetics, D-01307 Dresden, Germany
[e] Department of Radiation and Molecular Biophysics, St. Petersburg Nuclear Physics Institute, Gatchina 188300, Russia

ARTICLE INFO

Article history:
Received 15 September 2015
Received in revised form
11 December 2015
Accepted 31 January 2016
Available online 2 February 2016

Keywords:
Nucleosome remodeling
ISWI ATPase
Germarium
PHD finger
Bromodomain

ABSTRACT

The Chromatin Accessibility Complex (CHRAC) consists of the ATPase ISWI, the large ACF1 subunit and a pair of small histone-like proteins, CHRAC-14/16. CHRAC is a prototypical nucleosome sliding factor that mobilizes nucleosomes to improve the regularity and integrity of the chromatin fiber. This may facilitate the formation of repressive chromatin. Expression of the signature subunit ACF1 is restricted during embryonic development, but remains high in primordial germ cells. Therefore, we explored roles for ACF1 during *Drosophila* oogenesis. ACF1 is expressed in somatic and germline cells, with notable enrichment in germline stem cells and oocytes. The asymmetrical localization of ACF1 to these cells depends on the transport of the *Acf1* mRNA by the Bicaudal-D/Egalitarian complex. Loss of ACF1 function in the novel $Acf1^{7}$ allele leads to defective egg chambers and their elimination through apoptosis. In addition, we find a variety of unusual 16-cell cyst packaging phenotypes in the previously known $Acf1^{1}$ allele, with a striking prevalence of egg chambers with two functional oocytes at opposite poles. Surprisingly, we found that the $Acf1^{1}$ deletion – despite disruption of the *Acf1* reading frame – expresses low levels of a PHD-bromodomain module from the C-terminus of ACF1 that becomes enriched in oocytes. Expression of this module from the *Acf1* genomic locus leads to packaging defects in the absence of functional ACF1, suggesting competitive interactions with unknown target molecules. Remarkably, a two-fold overexpression of CHRAC (ACF1 and CHRAC-16) leads to increased apoptosis and packaging defects. Evidently, finely tuned CHRAC levels are required for proper oogenesis.

1. Introduction

The ATPase Imitation Switch (ISWI) is the catalytic core of nucleosome remodeling factors that induce nucleosome sliding on DNA and thus enable structural adjustments of chromatin required to utilize the genome and to maintain its integrity (Baldi and Becker, 2013; Clapier and Cairns, 2009; Mueller-Planitz et al., 2013). Among the six ISWI complexes currently known in *Drosophila melanogaster*, NURF, NoRC and ToRC are prominently involved in transcription activation (Alkhatib and Landry, 2011; Emelyanov et al., 2012; Vanolst et al., 2005). RSF, ACF and CHRAC on the other hand, are thought to use their nucleosome remodeling activity to close gaps in nucleosomal arrays during chromatin assembly or after disruption, and thus improve the stability and the folding of the chromatin fiber (Fyodorov et al., 2004; Hanai et al., 2008; Ito et al., 1997; Racki et al., 2009; Varga-Weisz et al., 1997). Yeast CHRAC, the Isw2 complex, slides nucleosomes to restrict nucleosome-free regions and represses cryptic transcription that would otherwise originate within these gaps (Whitehouse et al., 2007; Yadon et al., 2010). ACF and CHRAC are highly related complexes. Both are composed of ISWI and the larger signature subunit ACF1, but CHRAC contains two small histone-fold subunits CHRAC-14 and CHRAC-16 in addition (Corona et al., 2000; Ito et al., 1999). *In vitro*, both factors catalyze similar nucleosome sliding reactions (Hartlepp et al., 2005).

* Correspondence to: Ludwig-Maximilians-University, Biomedical Center, Molecular Biology Division, Großhaderner Strasse 9, 82152 Munich, Germany,
Tel.: +49 89 2180 75 428; fax: +49 89 2180 75 425.
E-mail address: pbecker@med.uni-muenchen.de (P.B. Becker).

http://dx.doi.org/10.1016/j.ydbio.2016.01.039
0012-1606/

Physiological roles for CHRAC and ACF are poorly understood. To some extent the combined functions of these two related complexes have been assessed by characterization of a loss-of-function mutation of the *Acf1* gene in the *Acf1*^{1} and *Acf1*^{2} alleles (Chioda et al., 2010; Fyodorov et al., 2004). These studies showed that loss of ACF1 in *Drosophila* embryos reduces the regularity of nucleosome arrays and leads to defects in chromatin-mediated repression processes, such as heterochromatin formation and polycomb silencing. ACF1-deficient embryos also show replication defects indicated by shortened S phases (Fyodorov et al., 2004). Altogether, loss of ACF1 results in 'semi-lethality' during larvae-pupae transition and delayed development (Fyodorov et al., 2004).

Acf1 mutant animals show chromatin defects at all developmental stages. Remarkably however, ACF1 is expressed prominently only in undifferentiated cells, which led to the speculation that high levels of ACF1 are a hallmark of unstructured, plastic chromatin in undifferentiated cells prior to developmental epigenome diversification (Chioda et al., 2010). During embryogenesis ACF1 expression fades in most cells and only remains high in neuroblasts and primordial germ cells (PGCs) (Chioda et al., 2010). PGCs are the precursors of the adult germline. However, it is unknown whether high levels of ACF1 are also retained in adult germline tissues. We now have studied the fate of ACF1 in *Drosophila* oogenesis and describe developmentally associated phenotypes in germline and somatic cells by altering ACF1 levels.

Drosophila oogenesis is particularly suited to study germline stem cell (GSC) and somatic stem cell (SSC) renewal, oocyte determination and specification as well as egg formation and maturation. The formation and maturation of eggs occurs in tubular ovarioles. Their most anterior end bears a structure called germarium with 2–3 GSCs in their niche. GSCs divide asymmetrically to produce another stem cell and a daughter cystoblast. Next, cystoblasts undergo four mitotic divisions with incomplete cytokinesis to form an interconnected 16-cell cyst. Importantly, one particular cell is determined to become the oocyte while the remaining 15 cells transform into polyploid nurse cells as cysts travel to the posterior end of the germarium. Thereafter, somatic follicle cells encapsulate and package 16-cell cysts, which bud off as individual egg chambers. Further, egg chamber maturation runs through different developmental stages in which aberrations can be easily scored due to the stereotype positions and appearance of the oocyte and the 15 nurse cells in each egg chamber (Hudson and Cooley, 2014).

Given the widespread requirement for chromatin plasticity during development (Chioda and Becker, 2010; Ho and Crabtree, 2010), it is not surprising that nucleosome remodeling factors have been found important for oogenesis. The nucleosome remodeling ATPases ISWI, Brahma and Domino have been shown to be required for self-renewal of GSCs and SSCs, respectively (Ables and Drummond-Barbosa, 2010; Deuring et al., 2000; He et al., 2014; Xi and Xie, 2005; Yan et al., 2014), conceivably due to their effects on transcription programs.

We now found that ACF1 is expressed in most somatic and germline cells of the female reproductive system with particular high levels in GSCs and oocytes. *Acf1* mRNA enrichment in prospective oocytes is accomplished by the Bicaudal-D/Egalitarian RNA transport machinery. ACF1 is required for proper oogenesis since its loss in a novel, true loss-of-function mutant, *Acf1*^{7}, or through RNA interference leads to increased numbers of defective egg chambers. Notably, the well-studied *Acf1*^{1} allele gives rise to compound egg chamber phenotypes. This allele had hitherto been thought to represent a clear loss-of-function mutation. We now found that this allele still expresses a PHD-Bromo domain module from the ACF1 C-terminus that interferes with 16-cell cyst encapsulation. Remarkably, altering ACF/CHRAC levels by additional gene copies of *Acf1* and *Chrac-16* also interferes with egg chamber maturation. Evidently, finely tuned CHRAC levels are required for proper oogenesis.

2. Materials and methods

2.1. Drosophila strains and genetics

Oregon-R and *w1118* were used as wild type controls. *Acf1* alleles *Acf1*^{1} and *Acf1*^{2} were described earlier (Fyodorov et al., 2004). In this study the *Acf1*^{7} allele was generated by imprecise excision of the *P{EP}Acf1*^{EP1181} P-element previously used to isolate the *Acf1*^{1} allele. A total of 198 excision events were analyzed by PCR across the *Acf1* locus. Resulting deletions were analyzed by PCR with Acf1-F and Acf1-R primers that flank the insertion site followed by sequencing with Acf1-seq primer (Table S1). The *Acf1*^{7} allele carries a 3098 bp deletion (3R:31,794,683–31,797,780) that spans the first intron starting from the *P{EP}Acf1*^{EP1181} insertion site and a part of the third exon of the *Acf1* gene. A 34 bp sequence (CATGATGAAATATCTGAAATATCAATGAAATGTC) of unknown origin was inserted into this region. *Acf1* deficiency (#26539, *w[1118]; Df (3R)BSC687/TM6C, Sb[1] cu[1]*) and *Chrac-16*^{G659} (#33532, *w[*] P{w[+mC]=EP}Chrac-16[G659]*) were obtained from Bloomington Drosophila Stock Center (BDSC), USA.

The *Acf1* fosmid variants are based on the fosmid library clone pflyfos021945 and the *Chrac-16* fosmid on pflyfos016131. The genomic region of *Acf1* and *Chrac-16* were modified by recombineering in *Escherichia coli* using the pRedFLP4 recombination technology (Ejsmont et al., 2009). All oligonucleotides and oligonucleotide combinations are listed in Supplementary material (Tables S1 and S2). *Acf1*-GFP fosmid (*Acf1-fos*) codes for full-length ACF1 (1-1476 aa) with a C-terminal 2xTY1-EGFP-3xFLAG-tag. *Acf1-N*-GFP fosmid (*Acf1-N-fos*) codes for ACF1 lacking the C-terminal PHD1, PHD2 and bromodomain (1-1055 aa) with a C-terminal 2xTY1-EGFP-3xFLAG-tag. *Acf1-C*-GFP fosmid (*Acf1-C-fos*) codes only for the C-terminal part of ACF1 (1022-1476 aa) with an N-terminal 2xTY1-EGFP-3xFLAG-tag. *Chrac-16*-mCherry fosmid (*Chrac-16-fos*) codes for full-length CHRAC-16 (1-140 aa) with an N-terminal 2xTY1-mCherry-3xFLAG-tag. A detailed description of the protocol can be obtained from the authors. All *Acf1* and *Chrac-16* fosmid variants were verified by sequencing before injection into *D. melanogaster*. Transgenic flies were made by phiC31 integrase-mediated site-specific integration into attP landing sites (Genetic Services, Inc., USA). *Acf1* fosmid constructs were integrated on the second chromosome into attP40 landing site and *Chrac-16* fosmid construct on the third chromosome into attP2 landing site. Fosmid constructs contain a *dsRed* cassette driven by 3xP3 promoter to select for transformants.

The following homozygous fly lines containing fosmid constructs were obtained by appropriate crosses: *Acf1-fos*, *Acf1-N-fos*, *Acf1-C-fos*, *Acf1-fos*; *Acf1*^{1}, *Acf1-N-fos*; *Acf1*^{1}, *Acf1-C-fos*; *Acf1*^{1}, *Acf1-fos*; *Acf1*^{7}, *Acf1-N-fos*; *Acf1*^{7}, *Acf1-C-fos*; *Acf1*^{7}, *Chrac-16-fos*, *Acf1-fos*; *Chrac-16-fos*, *Acf1-N-fos*; *Chrac-16-fos*, *Acf1-C-fos*; *Chrac-16-fos*.

Short hairpin RNA constructs for *UAS-shAcf1* (JF01298, attP2, Val1; GL00124, attP40, Val22), *UAS-shIswi* (HMS00628, attP40, Val20) and *UAS-shChrac-16* (HMC02362, attP2, Val20) were obtained from the TRiP at Harvard Medical School, Boston, USA. *UAS-shEGFP* (#41557, attP40 Val22), *MTD-Gal4* (#31777) and *matα4-Gal4* (#7063) were obtained from BDSC, USA. *c587-Gal4* and *traffic jam-Gal4* were kind gifts of Allan C. Spradling (Carnegie Institution for Science, USA) and Jean-René Huynh (Institut Curie, France), respectively. *UAS-shRNA* males were crossed with *Gal4* driver virgins at 29°C and 5-7 day old F1 females were used for analysis. For a germline-specific reduction of ISWI in adult ovaries *UAS-shIswi* males were crossed with *MTD-Gal4* driver females at 18 °C. F1 females were kept at 29 °C for 3 days and used for further analysis.

Generation of *Bic-D*^{mom} flies was done as previously described (Swan and Suter, 1996; Vazquez-Pianzola et al., 2014). Briefly, *Df (2L)Exel7068/SM6B;hs-Bic-D* flies were crossed to *Bic-D*^{r5}*/SM1* flies. The progeny of this cross was heat shocked twice per day for 2 h at 37 °C until they reached adulthood. Adults were heat shocked at least for one day before stopping the treatment to shut off Bic-D expression.

All fly stocks were kept at 25 °C and ovaries of 5–7 day old females were used for analysis. Individual egg chambers of stage 3–10 were scored for morphological defects from three biological replicates. Mean values in % with SD were calculated for apoptotic and packaging phenotypes.

2.2. Egg laying assay

Female virgins for *Acf1*^{1}, *Acf1*^{7}, *Acf1-fos*; *Acf1*^{1}, *Acf1-fos*; *Acf1*^{7} and *w1118* were collected for 2–3 days at 25 °C. Six females of each genotype were mated with six *w1118* males in vials with yeast paste for 2 days. Females were put in individual vials for 24 h without males and laid eggs were counted. The egg laying capacity was determined as the number of laid eggs per female and day. The data of six females was averaged and mean values with SD from three biological replicates were calculated.

2.3. In situ hybridization to whole mount ovaries

Linearized EST LD32807 (Berkley Drosophila Genome Project, BDGP, USA) containing the *Acf1* cDNA and pBS-Bic-D-short were used as templates to generate digoxigenin-labeled and FiTC labeled RNA antisense probes, respectively. *In situ* hybridizations were performed as described (Vazquez-Pianzola et al., 2014).

2.4. Immunological techniques and microscopy

Immunofluorescence microscopy was performed using standard procedures with the following primary antibodies: rat α-ACF1 8E3 [1:2, (Chioda et al., 2010)], mouse α-Orb 6H4 and 4H8 [1:60, Developmental Studies Hybridoma Bank (DHSB), USA], mouse α-Fasciclin III 7G10 (1:100, DHSB), mouse α-HtsRC (1:20, DHSB), mouse α-UNC93-5.2.1 (γH2A.V, 1:1000, DHSB), rabbit α-Vasa (1:100, Santa Cruz Biotechnology), rabbit α-cleaved Caspase-3 (1:100, Cell Signaling Technology, USA) and rabbit α-GFP TP401 (1:500, Acris Antibodies, Germany). F-actin was visualized with Rhodamine-conjugated phalloidin (1:500, Invitrogen). DAPI (0.1 mg/ml, 1:500) or Hoechst (2 μg/ml) was used to stain DNA. The following secondary antibodies from Jackson Immuno Research laboratories were used: Donkey α-mouse Cy3 (1:250), Donkey α-mouse Alexa488 (1:300), Donkey α-rat Alexa488 (1:300) and Donkey α-rabbit Alexa488 (1:300). GFP and mCherry fluorescence in flies expressing recombineered fosmid constructs were detected without secondary antibodies in unfixed ovaries, which were stained with DAPI for 10 minutes and washed twice with PBS for 2 min. Imaging was performed with a Leica TCS SP5 II confocal microscope. Images were processed using ImageJ (NIH, USA) and Adobe Photoshop.

2.5. Western blot

For ovary samples, 12 pairs of ovaries were dissected and homogenized in 1 × Laemmli buffer with a pestle and incubated at 95 °C for 5 min. For embryo samples, nuclear extracts were made from 0–12 hour old embryos (Kunert and Brehm, 2008). Western blot was performed using standard procedures with the following antibodies: rat α-ACF1 8E3 [1:20, (Chioda et al., 2010)], rabbit α-ISWI (1:1000, kind gift from J. Tamkun), mouse α-Lamin T40 (1:2000, kind gift from H. Saumweber). For LI-COR Odyssey system detection, goat α-rat IgG 800CW, goat α-mouse IgG 680RD and goat α-rabbit IgG 800CW (1:10000, LI-COR Biosciences) were used as secondary antibodies.

2.6. RNA quantification from ovary tissues via real-time PCR

Ovary tissues of wild type, *Acf1*^{1} and *Acf1*^{7} flies were collected in PBS at 4 °C, quickly transferred to Trizol reagent (Qiazol, Qiagen) and frozen at −80 °C. The tissues were then homogenized using electric pestle in a low-binding Eppendorf tube. Next steps were done following the manufacturer's recommendations. Total RNA was extracted using RNeasy Mini kit (Qiagen). On-column DNase digestion was performed using RNase free DNase (Qiagen) to digest genomic DNA. RNA was quantified with a Nanodrop device (Thermo Scientific) and aliquots were frozen at −80 °C. cDNA was prepared using SuperScript® III First-Strand Synthesis System (Life technologies). RNase-H (NEB) was used to digest RNA-DNA hybrids. cDNA was subsequently quantified with Fast SYBR-Green (Applied Biosystems) on LightCycler 480 system (Roche). All oligonucleotides are listed in Supplementary material (Table S3).

3. Results

3.1. ACF1 is enriched in cells of the female germline

Monoclonal antibody 8E3 reacts specifically with ACF1 as demonstrated by lack of immunofluorescence staining of *Acf1* mutant embryos and absence of the ACF1 Western blot signal upon probing mutant embryo extracts (Chioda et al., 2010). Using this antibody we previously showed that ACF1 expression is strongly reduced during embryogenesis but persists in primordial germ cells (Chioda et al., 2010). Probing ovarioles from wild type flies we found by immunofluorescence microscopy (IFM) that ACF1 was expressed in most somatic and germline cells of the germarium and the maturing egg chambers (Fig. 1A). Comparison of the fluorescence intensity showed that ACF1 was considerably enriched in the GSCs and possibly the first cystoblast descendant (Fig. 1B, C) with a notable absence in the somatic filament cells, cap cells and anterior escort cells that contribute to forming the stem cell niche (Fig. 1B, C). In contrast to somatic niche cells, ACF1 was expressed in somatic posterior escort cells and all stages of follicle cell development (Fig. 1B, D and E). Further, prominent enrichment of ACF1 staining was seen in the oocyte in stage one 16-cell cysts, soon after the oocyte becomes determined (Fig. 1D). The enrichment of ACF1 in the oocyte nucleus versus the nuclei of polytenic nurse cells continued to be striking in all later egg chambers (Fig. 1A, E). ACF1 was present, but not particularly enriched on the karyosome, and strongly accumulated in the oocyte nucleoplasm (Fig. S1E). The 8E3 antibody provides a novel tool for staining the GSCs and oocytes in the female germline of *Drosophila*.

A common mechanism for asymmetric localization of proteins in prospective oocytes is the transport and localization of their respective mRNAs through an RNA-binding machinery organized by Bicaudal-D (Bic-D) and Egalitarian (Egl) (Claußen and Suter, 2005; Vazquez-Pianzola and Suter, 2012). Indeed, we found by fluorescence in situ hybridization (FISH) that *Acf1* mRNA, like its protein product, localized to the prospective oocyte from early stages on (Fig. 1F). The mRNA was present in the nurse and follicle cell cytoplasm and enriched at the posterior cortex of the oocyte cytoplasm from stage 1 of oogenesis onwards and then relocalized to the anterior cortex by stage 8 (Fig. S1A–D), like many of the Bic-D/Egl targets. A similar localization pattern was previously observed for *Iswi* mRNA (Jambor et al., 2015). To test whether *Acf1* mRNA transport to the oocyte depends on the Bic-D/Egl

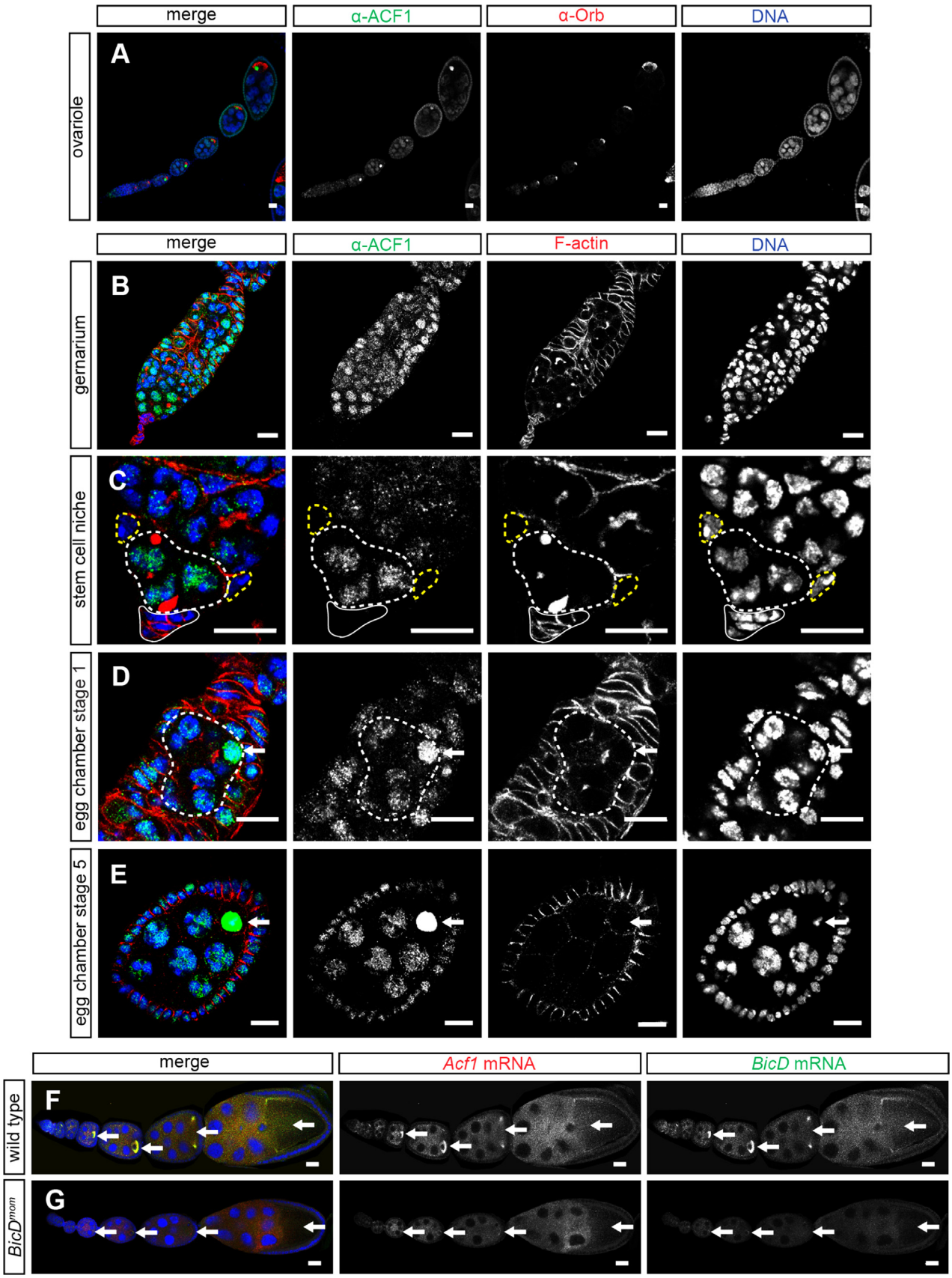

Fig. 1. ACF1 enrichment in germline cells of *Drosophila* ovarioles. (A–E) Immunofluorescence images of different oogenesis stages in wild type. (A) Ovariole with staining of ACF1 (green), Orb (red) and DNA (blue) is shown. (B) Germarium, (C) stem cell niche with cap cells (solid line), germline stem cells (GSCs, white dashed line) and anterior escort cells (yellow dashed line), (D) egg chamber stage 1 (dashed line) and (E) egg chamber stage 5 with staining of ACF1 (green), F-actin (red) and DNA (blue) are shown. Arrows indicate oocyte nuclei. Scale bar: 10 μm. (F-G) *In situ* hybridization with staining of *Acf1* mRNA (red), *BicD* mRNA (green) and DNA (blue) is shown for the following genotypes: (F) wild type and (G) *Bic-D*^{mom}. Arrows indicate oocyte nuclei. Scale bar: 20 μm.

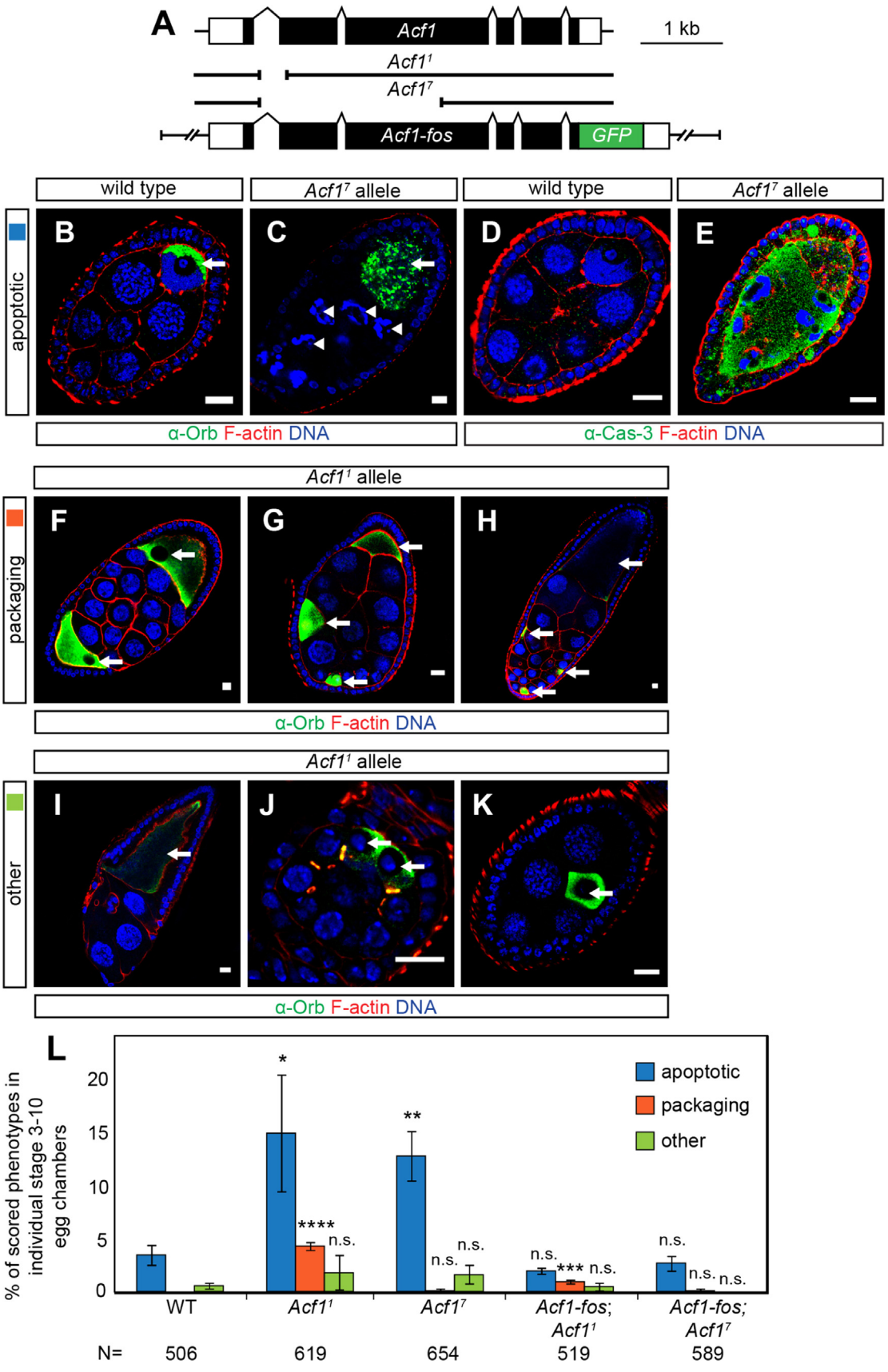

Fig. 2. *Acf1* alleles give rise to oogenesis phenotypes. (A) Schematic representation of the *Acf1* gene, *Acf1*^{1} and *Acf1*^{7} genomic deletions and the *Acf1* fosmid construct. White and black rectangles represent untranslated and translated exons, respectively. Green rectangle shows inserted 2xTY1-GFP-3xFLAG-tag. (B–E) Immunofluorescence images of apoptotic phenotype. Representative egg chambers of the *Acf1*^{7} allele with staining of (B, C) Orb (green), F-actin (red) and DNA (blue) and (D, E) cleaved Caspase-3 (green), F-actin (red) and DNA (blue) are shown for wild type and the *Acf1*^{7} allele. Arrows indicate oocyte nuclei. Arrowheads indicate nurse cell nuclei. Scale bar: 10 μm. (F-H) Immunofluorescence images of packaging phenotypes. Representative egg chambers of the *Acf1*^{1} allele with staining of Orb (green), F-actin (red) and DNA (blue) are shown for the *Acf1*^{1} allele. Egg chambers with additional cysts and two (F), three (G) and four oocytes (H) are shown. (I–K) Immunofluorescence images of other phenotypes. Egg chambers with one oocyte and seven nurse cells (I), two adjacent oocytes (J) and delocalized oocyte (K) are shown. Arrows indicate oocyte nuclei. Scale bar: 10 μm. (K) Quantification of apoptotic, packaging and other phenotypes. The data show mean values in percent with SD of three biological replicates. N represents the total number of scored egg chambers stage 3–10. Two-tailed Student's *t*-test was used in comparison to wild type. * represents a p-value of <0.05, ** <0.01, *** <0.001 and **** <0.0001. n.s. represents not significant.

localization machinery, we depleted the germline of Bic-D protein after oocyte determination using *Bic-D*^{mom} flies (Swan and Suter, 1996; Vazquez-Pianzola et al., 2014). The *Bic-D*^{mom} tool involves rescuing the *Bic-D*^{null} phenotype by adding a copy of *Bic-D* under an inducible heat shock promoter. Once the oocyte determination phenotype had been rescued, induction of *Bic-D* expression was stopped. Around 4 days later these ovaries contained mid-oogenesis egg chambers lacking *Bic-D* mRNA (Fig. 1G) and protein (Vazquez-Pianzola et al., 2014). We found the oocyte enrichment of the *Acf1* mRNA severely impaired in these egg chambers (Fig. 1G) indicating that *Acf1* is a novel target of the RNA transport machinery.

3.2. Egg chamber formation and maturation phenotypes associated with Acf1 alleles

To explore potential roles for ACF in oogenesis, we analyzed ovarioles from two *Acf1* homozygous mutant fly lines. The *Acf1*^{1} allele had been considered a null allele (Fyodorov et al., 2004). It is characterized by a short deletion of parts of the first intron and second exon (Fig. 2A), which disrupts the reading frame. We also characterized a novel allele, *Acf1*^{7}, which bears a larger deletion of 3098 bp in the *Acf1* coding sequence (Fig. 2A; see Section 2) generated by imprecise excision of *P{EP}Acf1*^{EP1181} P-element.

We analyzed ovarioles of wild type, *Acf1*^{1} and *Acf1*^{7} flies by staining the cytoplasmic oocyte marker Orb, along with DNA and F-actin. Orb marks the single oocyte at the posterior end of wild type 16-cell cysts. We scored individual egg chambers stage 3–10 and found two distinct categories of morphological abnormalities. The largest fraction (*Acf1*^{1}: 16%; *Acf1*^{7}: 13%; apoptotic defects, Fig. 2L) consisted of egg chambers in the process of decay in which oocyte and nurse cells appeared in various stages of apoptosis (Fig. 2B and C) as verified by staining for activated caspase-3 (Fig. 2D and E). Interestingly, the increased number of apoptotic cysts only appeared from stage 7 or 8 onwards (Fig. S2A–D) while oogenesis appeared normal in the germarium (Fig. S2E–G). In theory, ACF1 loss could affect chromosome maturation and morphology, which might be identified as defects in oocyte nuclei condensation and nurse cell polyteny. However, such chromatin derangements were not scored (Fig. S2H–K). Staining with the DNA double strand break marker γH2A.V might reveal even subtle chromatin defects if they predispose *Acf1* chromosomes to DNA damage. However, we did not detect any major difference in γH2A.V staining patterns or intensities between wild type and *Acf1*^{7} ovarioles (Fig. S2L–U).

More interestingly, a significant number of about 5% of all egg chambers in *Acf1*^{1} showed various deficiencies in 16-cell cyst packaging (packaging defects; Fig. 2L). The most striking packaging phenotype, which was often observed, revealed two oocytes at the opposite poles of the egg chamber (Fig. 2F), which is reminiscent of compound egg chamber phenotypes reported in other studies (Besse et al., 2002; Hawkins et al., 1996; Jackson and Blochlinger, 1997; McGregor et al., 2002; Urwyler et al., 2012). Both oocytes appeared equivalent as they were positive for Orb (Fig. 2F), showed correctly positioned nuclei in close proximity to epithelial follicle and nurse cells (Fig. 2F) and contained four ring canals (Fig. S3A–D). Other variations of compound egg chamber phenotypes were also observable, such as three or four oocytes at opposing positions with nurse cells of different size and ploidy (Fig. 2G, H). Similar packaging phenotypes were also seen analyzing the *Acf1*^{2} deletion allele (data not shown), which had been generated independently from the *Acf1*^{1} allele by imprecise excision of a different P-element (Fyodorov et al., 2004). Compound egg chambers were observed at all stages of maturation, including the earliest egg chamber stage 1 (Fig. S3F). In principle, such an arrangement may come about if two adjacent germline cysts are packaged together into one egg chamber by somatic follicle cells. Indeed, in many cases more than one cyst was encapsulated by follicle cells in *Acf1*^{1} (Fig. S3E, F). Furthermore, only *Acf1*^{1} but not *Acf1*^{7} germaria showed additional FasIII-positive stalk-like structures and egg chambers with additional, wrongly positioned polar cells (Fig. S3G–L). Surprisingly however, compound eggs were never scored in *Acf1*^{7} (Fig. 2L). We hypothesize that the two *Acf1* alleles are not equivalent: some aspects of *Acf1*^{1} appear to lead to packaging phenotypes that are not characteristic of *Acf1*^{7}.

In a third category, about 2% of all egg chambers in *Acf1*^{1} and *Acf1*^{7} showed a wide variety of abnormalities such as egg chambers with one oocyte and seven nurse cells (Fig. 2I), two adjacent oocytes (Fig. 2J) and centralized oocytes (Fig. 2K). However, the penetrance of these other abnormalities in *Acf1*^{1} and *Acf1*^{7} was not significantly different from wild type and therefore excluded from further analysis (Fig. 2L).

We next focused on the analysis of apoptotic and packaging phenotypes in ovariole structures to better understand the effect of *Acf1* alleles on *Drosophila* oogenesis and fertility. We found defective ovarioles significantly increased in both *Acf1* alleles in comparison to wild type (wild type: 12%, *Acf1*^{1}: 32%, *Acf1*^{7}: 20%; Fig. S4A). It is thought that apoptotic egg chambers at the posterior end of an ovariole can interrupt egg production in individual ovarioles or throughout the entire ovary (Thomson et al., 2010), which should lead to a decreased number of laid eggs in both *Acf1* alleles. In fact, apoptotic egg chambers were found almost exclusively to be the most posterior egg chamber (*Acf1*^{1}: 20/21 , *Acf1*^{7}: 38/38; Fig. S2B, C) and females of both *Acf1* alleles showed a significant reduction in egg laying to less than 85% in comparison to wild type (Fig. S4C). In summary, both *Acf1* alleles show defective egg chambers and compromise female fertility.

To verify that the observed oogenesis phenotypes are due to mutations in the *Acf1* gene locus we crossed the *Acf1*^{1} and *Acf1*^{7} alleles to an *Acf1* deficiency. Indeed, this confirmed the penetrance of apoptotic and packaging phenotypes in both *Acf1* alleles (Fig. S4B). We further validated the observed phenotypes by generating a transgene expressing GFP-tagged *Acf1* from a recombined fosmid (*Acf1-fos*) using the flyfosmid recombineering technique (Ejsmont et al., 2009). This way, we obtained a fly line expressing GFP-tagged ACF1 from its chromosomal regulatory context (Fig. 2A). *Acf1-fos* was integrated into the attP40 landing site on the 2nd chromosome by PhiC31-mediated recombination and used to complement the *Acf1* alleles. We found GFP-tagged ACF1 expressed in ovarioles by Western blot (Fig. S5A). In comparison to the two specific ACF1 signals detected in wild type, we found the expected higher molecular weight band only in ACF1-GFP complemented flies. The lower ACF1-specific band, which was present in wild type and ACF1-GFP complemented flies, most likely represents C-terminally truncated ACF1. We also confirmed that ACF1-GFP localized to GSCs, oocytes, follicle and nurse cells by IFM using a GFP antibody (Fig. S5B–G). Importantly, expression of an ACF1-GFP transgene fully rescued all apoptotic defects in *Acf1*^{1} and *Acf1*^{7} allele and packaging defects were ameliorated in *Acf1*^{1} (Fig. 2L).

3.3. ACF1 depletion in early phases of oogenesis manifests itself in later egg chamber phenotypes

To better understand the consequences of loss of ACF function for oogenesis, we depleted ACF1 and its partner ISWI by cell type-specific RNA interference (RNAi) using the Gal4/UAS system (Ni et al., 2011). ACF expression was interfered with by expressing small hairpin (sh) RNAs directed against *Acf1* or *Iswi* mRNA under the control of UAS system. Expression was driven in the germline cells by using *MTD* or *matα4* (Yan et al., 2014) and in the somatic cells by *c587* (Eliazer et al., 2011; Kai and Spradling, 2003) or *traffic*

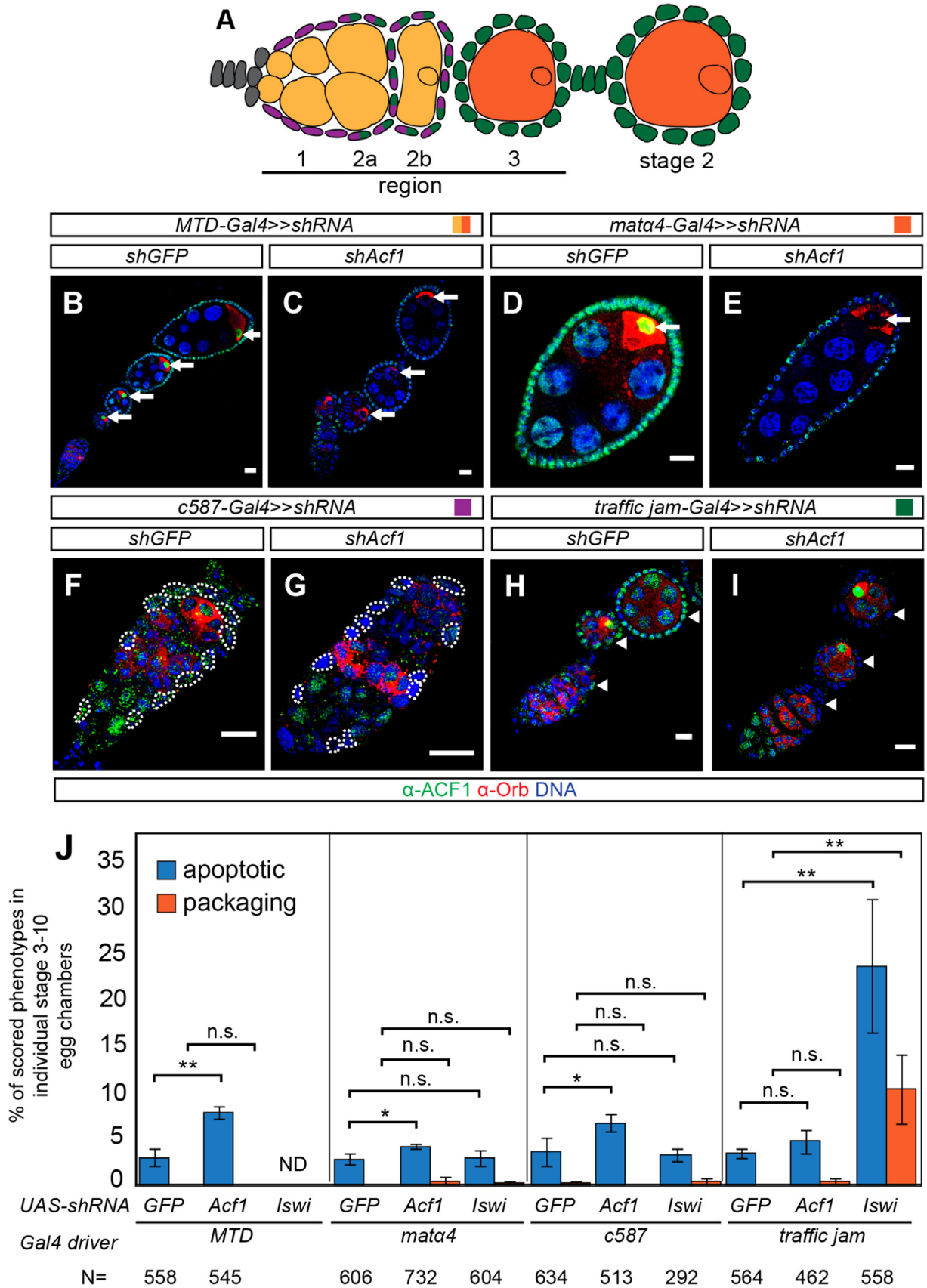

Fig. 3. Cell type-specific RNAi-mediated knockdown of ACF subunits in oogenesis causes apoptotic and packaging phenotypes. (A) Schematic drawing of early *Drosophila* oogenesis. Color code for cell type-specific expression pattern of different driver lines: *MTD-Gal4* (germline cells; light and dark orange), *matα4-Gal4* (germline cells stage 1 onwards, dark orange), *c587-Gal4* (somatic escort and early follicle cells, purple) and *traffic jam-Gal4* (somatic follicle cells, green). (B–I) Immunofluorescence images showing cell type-specific ACF1 knockdown in oogenesis. Germarium, ovariole or egg chamber with staining of ACF1 (green), Orb (red) and DNA (blue) are shown for: (B) *UAS-shGFP < < MTD-Gal4* (C), *UAS-shAcf1 < < MTD-Gal4* (D) *UAS-shGFP < < matα4-Gal4*, (E) *UAS-shAcf1 < < matα4-Gal4*, (F) *UAS-shGFP < < c587-Gal4*, (G) *UAS-shAcf1 < < c587-Gal4*, (H) *UAS-shGFP < < traffic jam-Gal4* and (G) *UAS-shGFP < < traffic jam-Gal4.* Arrows indicate oocyte nuclei. White dashed lines indicate escort cells. Color-coded square represents specific cell-type expression pattern in Fig. 3A. Scale bar: 10 μm. (J) Quantification of apoptotic and packaging phenotypes. The data show mean values in percent with SD of three biological replicates. *N* represents the total number of scored egg chambers stage 3–10. All analyzed ovary samples of *shIswi* with *MTD-Gal4* ($n=14$) showed an agametic phenotype but detailed oogenesis phenotypes were not determined (ND) further. Two-tailed Student's *t*-test was used. * represents a *p*-Value of <0.05 and ** <0.01. n.s. represents not significant.

jam Gal4 drivers (Olivieri et al., 2010) (Fig. 3A). As a control for non-specific effects we expressed shRNA directed against an irrelevant *GFP* sequence with the same drivers. This did not affect ACF1 levels (Fig. 3B, D, F and H) and led to a low rate of apoptotic egg chambers (Fig. 3J) similar to wild type flies (Fig. 2L).

MTD-directed knockdown of ACF1 expression in germline cells (Fig. 3C; Fig. S6A and B) increased the number of apoptotic egg chambers from stage 7 or 8 onwards to about 8% (Fig. 3J; Fig. S6E, F). However, *matα4*-mediated knockdown showed a small, statistically significant increase in apoptotic phenotype of unclear physiological relevance (4%, Fig. 3J). Under this circumstance ACF1 was virtually absent from germline cells but still detectable on follicle cells from stage 2 egg chambers onwards (Fig. 3E; Fig. S6C, D). Similarly, removal of ACF1 from follicle cells but not from germline cells with *traffic jam-Gal4* (Fig. 3I; Fig. S7C, D) did not have an effect (Fig. 3J). In contrast, ACF1 depletion in somatic escort and early follicle cells with *c587-Gal4* (Fig. 3G; Fig. S7A, B) caused a modest, two-fold increase in apoptotic egg chambers from stage 7 or 8 onwards (7%; Fig. 3J; Fig. S7E, F). The penetrance of apoptotic phenotypes scored upon early germline and soma knockdown of ACF1 could sum up to the observed apoptotic phenotypes in the $Acf1^1$ and $Acf1^7$ allele (Fig. 2L). Remarkably, we did not observe any packaging defects of the kind scored with the $Acf1^1$ allele (Fig. 3J).

Interfering with the expression of the ATPase ISWI through similar crosses might more generally reveal the cell type-specific importance of ISWI complexes for oogenesis. As expected, ablation of ISWI in early germline cells with *MTD-Gal4* yielded an agametic phenotype with characteristically small ovaries and defects in early oogenesis (data not shown; Fig. 3J) (Ables and Drummond-Barbosa, 2010; Xi and Xie, 2005; Yan et al., 2014). Interestingly, knockdown with *matα4-Gal4* did not cause any pronounced phenotype (Fig. 3J), arguing for a requirement for ISWI complexes primarily in early phases of cyst formation. To circumvent the requirement for ISWI function in early germline development we repeated the cross of *MTD-Gal4* with *shIswi* at 18 °C and put F1 offspring females to 29 °C for three days. We reasoned that a reduction of IWSI in adult germline cells should increase the penetrance of apoptotic egg chambers at least to levels comparable to a germline-specific *Acf1* knockdown. Indeed, an ISWI reduction in adult germline cells revealed an increased number of apoptotic egg chambers (64%, Fig. S8A) and induced packaging defects (14%, Fig. S8B). This further indicates that a loss of ACF1 function compromises oogenesis as part of the ISWI-containing ACF complex. However, the penetrance of apoptotic egg chambers was considerably higher suggesting a contribution of other ISWI-containing remodeling complexes.

Next, we focused on the phenotypical analysis of ISWI reduction in all stages of follicle cell development using the *traffic jam-Gal4* driver, which led to strongly increased numbers of apoptotic egg chambers (25%; Fig. 3J), induced a considerable number of packaging defects (11%; Fig. 3J), and yielded a 'dumpless' phenotype with short eggs (58%; Fig. S8K). Surprisingly, some of these packaging defects were reminiscent of $Acf1^1$ allele phenotypes, including compound egg chambers (Fig. S8C). However, even more complex packaging phenotypes with three and more oocytes in non-opposing positions were frequently scored (Fig. S8D). In contrast to $Acf1^1$ phenotypes, ISWI ablation in follicle cells gave rise to many egg chambers with abnormal cell numbers ranging from only one to eight cells (Fig. S8E, F and I). These egg chambers had fewer ring canal connections (Fig. S8F) and were already observed in region 2a/b of the germarium (Fig. S8G, I). This could argue for a soma-dependent early germline defect in cell proliferation. Furthermore, we also found gaps in the follicle cell epithelium (Fig. S8I) and additional stalk-like structures (Fig. S8J) that could lead to packaging defects (Fig. S8H). In contrast, reduction of ISWI in somatic escort and early follicle cells in the germarium via *c587-Gal4* showed no phenotype (Fig. 3J). So far, ISWI function has not been considered critical in follicle cell development (Xi and Xie, 2005).

3.4. Germline-specific enrichment of an ACF1 remnant from the $Acf1^1$ allele

The RNA interference phenotype resembled the phenotype of the $Acf1^7$ allele. We therefore considered that $Acf1^1$ may not be a true 'null' allele. Since the *Acf1* promoter and first exon are intact in the *Acf1* alleles (Fig. 2A) it is likely that mRNA is transcribed. Indeed, we found some *Acf1* gene sequences transcribed in ovaries from the $Acf1^1$ and $Acf1^7$ alleles, however with lower levels in comparison to wild type (Fig. S9A). We speculated that a small C-terminal fragment of ACF1 may be translated from an internal methionine in the $Acf1^1$ but not in the $Acf1^7$ allele. This was addressed using the monoclonal 8E3 antibody that recognizes an epitope in the ACF1 C-terminus (aa 1064-1476; data not shown). As expected, this antibody did not detect the two specific ACF1 bands by Western blot analysis of ovary extract from either of the two mutants (Fig. 4A). Despite all efforts, a low molecular weight band specific for the ACF1 C-Terminus was not detectable in $Acf1^1$ and $Acf1^7$ ovary extracts (data not shown). Remarkably, however, the ACF1 antibody yielded a robust immunofluorescence signal in oocyte nuclei of $Acf1^1$ mutant egg chambers, including the two oocytes of compound egg chambers (Fig. 4B, C). In contrast, ACF1 C-terminal immunoreactivity was absent in $Acf1^7$ egg chambers (Fig. 4B, D). Any stable 3′ parts of *Acf1* mRNA transcribed from the $Acf1^1$ allele are expected to be processed by the RNA transport machinery, since the 3′ UTR remains intact. Indeed, we found *Acf1*-derived mRNA localized and enriched in the oocyte only in $Acf1^1$ and $Acf1^2$ mutant egg chambers, including both oocytes of compound egg chambers (Fig. 4F, data not shown), but not in the $Acf1^7$ allele (Fig. 4G). We conclude that $Acf1^1$ is not a 'null' allele, but rather expresses a portion of the ACF1 C-terminus that enriches in germline cells. It is, therefore, possible that packaging phenotypes are due to the presence of an out-of-context ACF1 fragment.

3.5. Ectopic expression of the ACF1 C-terminus leads to compound egg chamber phenotypes

The comparison of the effects of $Acf1^1$ and $Acf1^7$ alleles on oogenesis and the detection of *Acf1* mRNA and protein only in $Acf1^1$ led to the hypothesis that the former allele produces a C-terminal ACF1 fragment. The ACF1 C-terminus bears two prominent PHD fingers and a bromodomain, for which no target is known. Conceivably, expressing this module may interfere with critical functions by competing with other, yet unknown factors for shared interaction sites. In order to test this hypothesis more directly, we used transgenic fly lines containing fosmids which express GFP-tagged *Acf1-N* and *Acf1-C* termini (*Acf1-N-fos*, *Acf1-C-fos*, Fig. 5A). The N-terminal ACF1 fragment (ACF1-N) contains the domains required to interact with ISWI (Eberharter et al., 2004) and the CHRAC-14/16 heterodimer (Hartlepp et al., 2005), but lacks the PHD-bromo module (Fig. 5B). Conversely, the C-terminal ACF1 fragment (ACF1-C) lacks the ISWI interaction surface, but contains the PHD-bromo module (Fig. 5B). *Acf1-N-fos* and *Acf1-C-fos* were made by flyfosmid recombineering technique and integrated on the 2nd chromosome at the same site as the fosmid expressing full-length ACF1-GFP. Interestingly, ACF1-N was not specifically enriched in the oocyte (Fig. 5D). However, ACF1-C was not only expressed in follicle and nurse cells but also enriched in oocyte nuclei (Fig. 5E), in agreement with the earlier results of RNA FISH in $Acf1^1$ mutant ovarioles (Fig. 4F).

Acf1-N-fos and *Acf1-C-fos* were tested in the background of wild

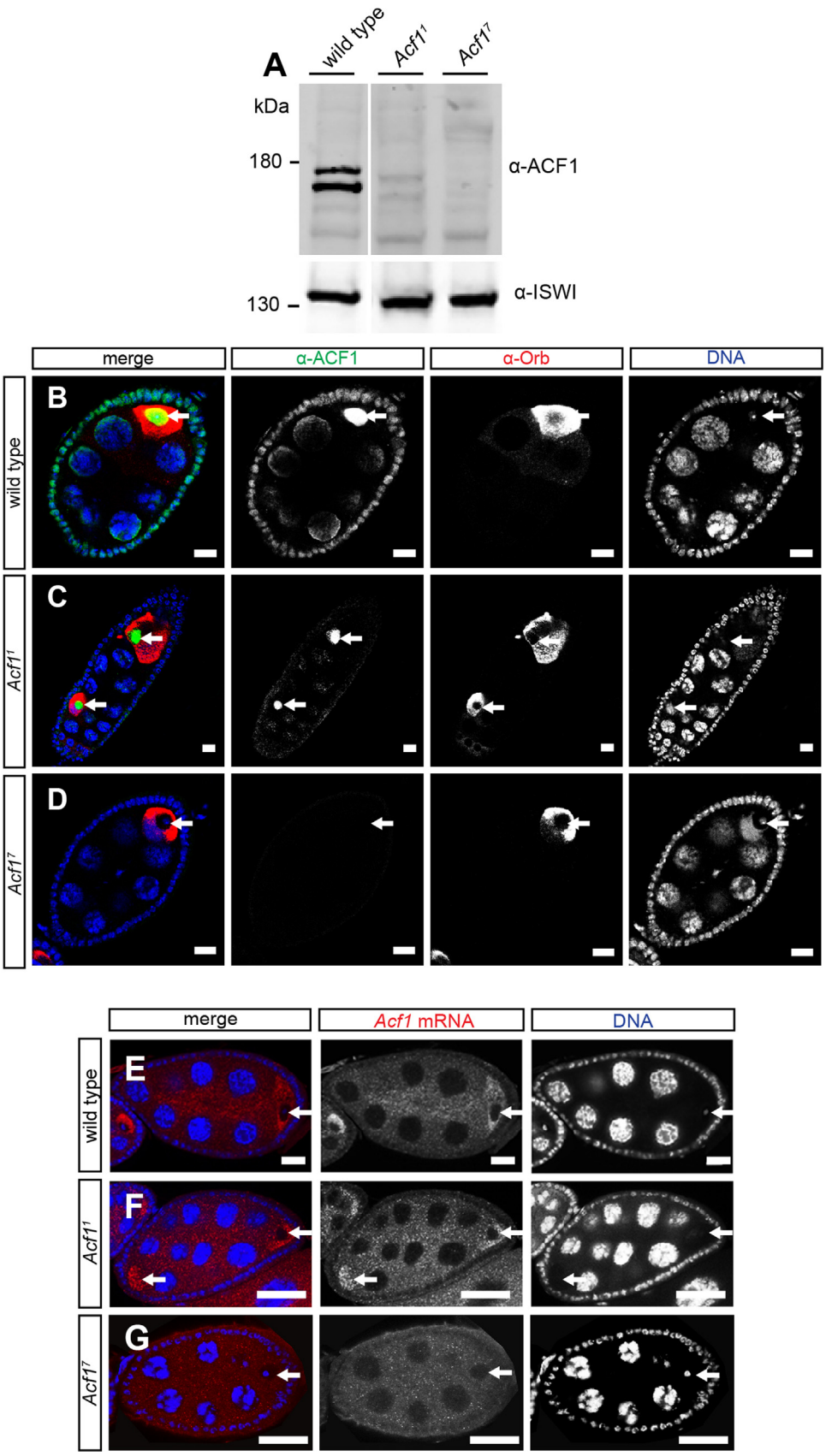

Fig. 4. Germline-specific enrichment of the ACF1 C-terminus from the *Acf1*^{1} allele. (A) Western blot from ovaries probed with α-ACF1 8E3 is shown for the following homozygous genotypes: wild type, *Acf1*^{1} and *Acf1*^{7}. ISWI signal served as a loading control. (B–D) Immunofluorescence images of egg chambers with staining of ACF1 (green), Orb (red) and DNA (blue) are shown for the following homozygous genotypes: (B) wild type, (C) *Acf1*^{1} and (D) *Acf1*^{7}. Arrows indicate oocyte nuclei. Scale bar: 10 μm. (E–G) *In situ* hybridization with staining of *Acf1* mRNA (red) und DNA (blue) is shown for the following homozygous genotypes: (E) wild type, (F) *Acf1*^{1} and (G) *Acf1*^{7}. Arrow indicates oocyte. Scale bar: 20 μm.

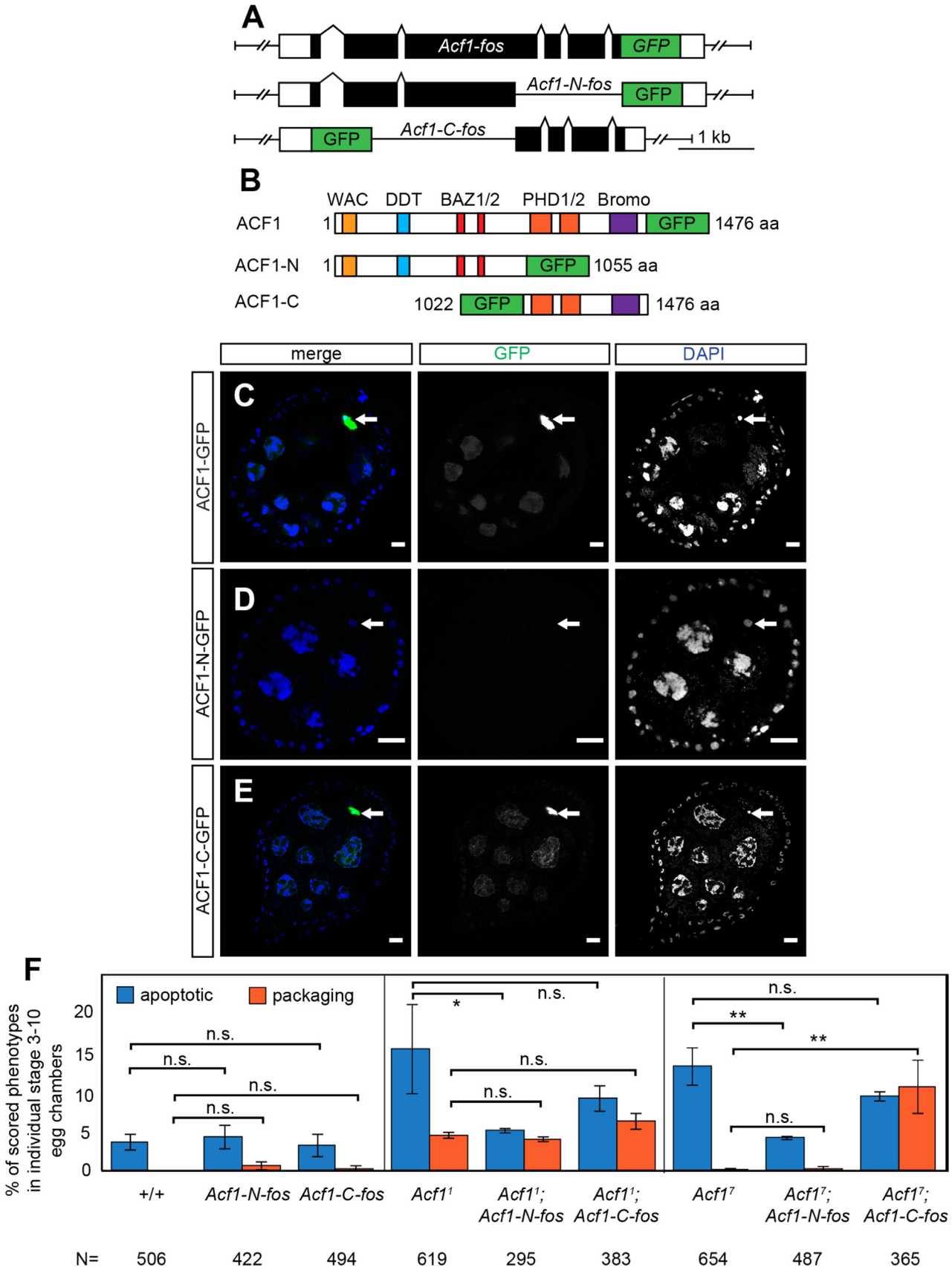

Fig. 5. Ectopic expression of the ACF1 C-terminus leads to compound egg chamber phenotypes. (A) Schematic representation of the *Acf1-C* and *Acf1-N* fosmid constructs. White and black rectangles represent untranslated and translated exons, respectively. Green rectangles show inserted 2xTY1-GFP-3xFLAG-tag. (B) Schematic representation of domain structure of ACF1-C and ACF1-N. Green rectangles show inserted 2xTY1-GFP-3xFLAG-tag. (C–E) Live cell fluorescence images of egg chambers from fly lines expressing tagged *ACF1-GFP* constructs showing GFP (green) and DNA (blue) signal. (A) ACF1-GFP, (B) ACF1-N-GFP and (C) ACF1-C-GFP are shown. Arrows indicate oocyte nuclei. Scale bar: 10 μm. (F) Quantification of apoptotic and packaging phenotypes. The data show mean values in percent with SD of three biological replicates. *N* represents the total number of scored egg chambers stage 3–10. Two-tailed Student's *t*-test was used. * represents a *p*-Value of <0.05 and ** <0.01. n.s. represents not significant.

type, *Acf1*^{1} and *Acf1*^{7} alleles for oogenesis phenotypes and particularly for the occurrence of packaging defects. Neither ACF1-N nor ACF1-C had a dominant negative effect, since neither of them showed increased apoptotic phenotypes in wild type background (Fig. 5F). Curiously, the presence of ACF1-N reduced the occurrence of apoptotic egg chambers in both *Acf1* alleles to wild type levels (*Acf1*^{1}: 2%; *Acf1*^{7}: 1%; Fig. 5F). However, ACF1-N did not ameliorate packaging phenotypes in *Acf1*^{1} (4%, Fig. 5F). The ACF1 N-terminus, containing the CHRAC-16 and ISWI interaction domains, was sufficient to rescue the apoptotic phenotype, conceivably as part of ACF/CHRAC complexes. We repeated cell-type specific RNAi for CHRAC-16 and used an insertion mutant allele, *P{EP}Chrac-16*^{G659}, to test for the contribution of CHRAC-16 to ACF/CHRAC phenotypes. In brief, we did not observe apoptotic phenotypes with CHRAC-16 RNAi or *Chrac-16*^{G659} (Fig. S10A, B) supporting a more prominent role of ACF1 during oogenesis than for CHRAC-16.

The ACF1 C-terminus did not rescue apoptotic phenotypes as expected (Fig. 5F). Strikingly, however, the presence of ACF1-C in *Acf1*^{7} induced packaging defects, including compound egg chambers (10%; Fig. 5F). In conclusion, ACF1-N, containing CHRAC and ISWI interaction domains, is sufficient to rescue the apoptotic phenotype in *Acf1* alleles, while ACF1-C, containing a PHD-bromo module, induces packaging defects only in the absence of full-length ACF1.

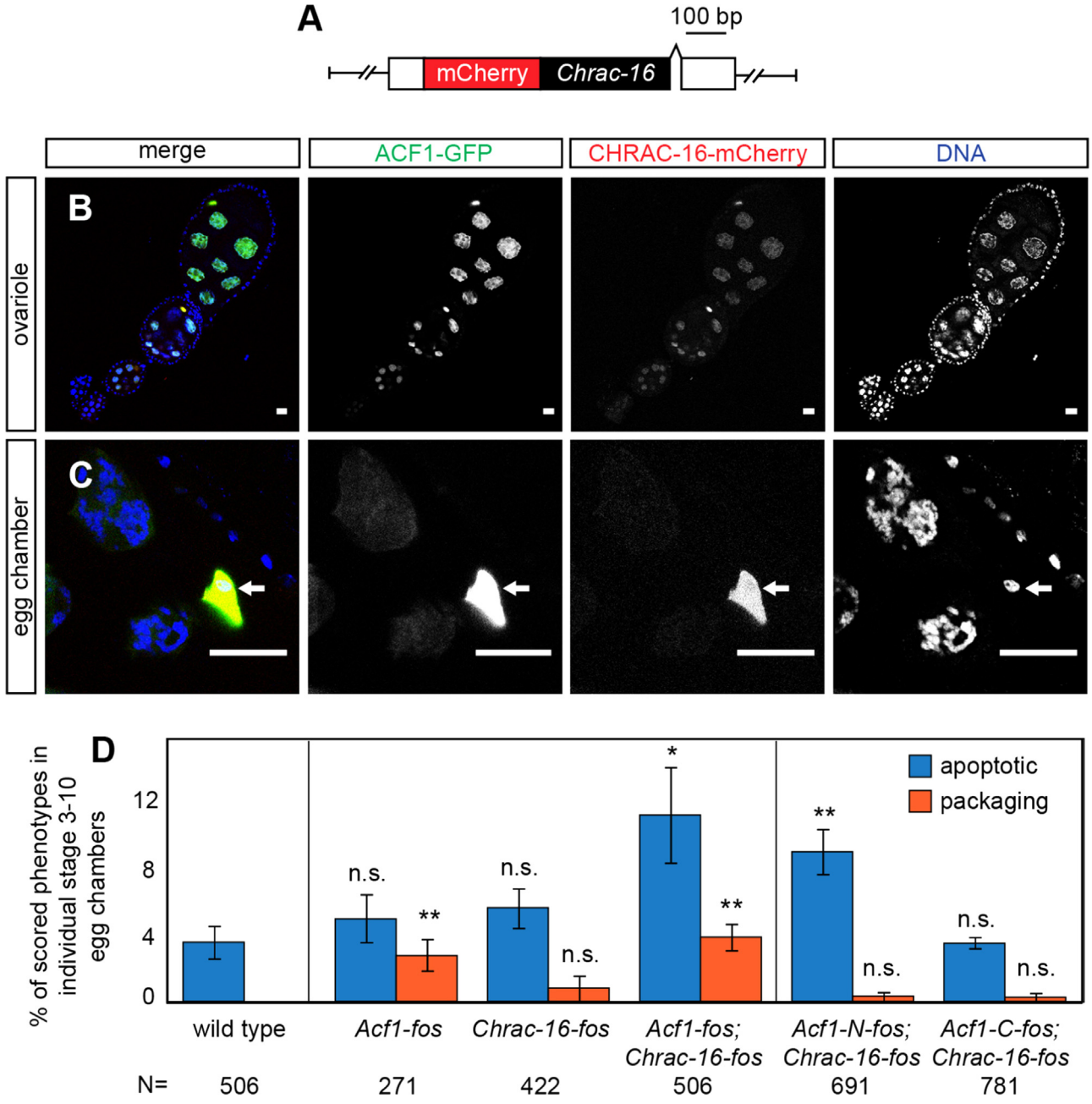

Fig. 6. Tuned ACF1 and CHRAC levels are critical for oogenesis. (A) Schematic representation of the *Chrac-16* fosmid construct. White and black rectangles represent untranslated and translated exons, respectively. Red rectangle shows inserted 2xTY1-mCherry-3xFLAG-tag. (C, D) Live cell fluorescence images of fly line expressing tagged ACF1-GFP and CHRAC-16-mCherry with GFP (green), mCherry (red) and DNA signal (blue) are shown. Arrows indicate oocyte nuclei. Scale bar: 10 μm. (E) Quantification of apoptotic and packaging phenotypes. The data show mean values in percent with SD of three biological replicates. *N* represents the total number of scored egg chambers stage 3–10. Two-tailed Student's *t*-test was used in comparison to wild type. * represents a *p*-Value of <0.05 and ** <0.01. n.s. represents not significant.

3.6. Tuned ACF1 and CHRAC-16 levels are critical for oogenesis

The results from the expression of ACF1 fragments suggest that packaging phenotypes may arise from competitive interactions of isolated domains with yet undefined targets. Conceivably, such untargeted interactions may interfere with other remodeling processes. We wondered whether such competition might also happen if full-length ACF1 or the small CHRAC-16 signature subunit of CHRAC was overexpressed. However, it is only poorly understood whether ACF1 functions in ACF or CHRAC *in vivo*. Despite all efforts, we were unable to raise a specific CHRAC-16 antibody suitable for IFM. Therefore, we generated a fly line bearing a fosmid expressing mCherry-tagged CHRAC-16 from its native genomic context (*Chrac-16-fos*, Fig. 6A) to study the localization of CHRAC complex in oogenesis. We detected both ACF1-GFP and CHRAC-16-mCherry signals in nurse cells and oocytes of all stages (Fig. 6B and C). This finding suggests that the four-subunit CHRAC complex localizes to the female germline.

To test for competitive interactions of excess full-length ACF1, we analyzed the ovarioles of flies bearing two copies of the ectopic, tagged *Acf1* gene locus in addition to endogenous *Acf1* genes. Indeed, these flies expressed approximately a double dose of ACF1 analyzed by quantitative Western blotting (2.6 fold; Fig. S5E). Remarkably, increased ACF1 levels led to a low, yet statistically significant number of packaging defects (3%; Fig. 6D), including compound egg chambers.

Moreover, homozygous *Acf1-fos*; *Chrac-16-fos* flies carrying four copies of *Acf1* and *Chrac-16* genes showed an increased number of apoptotic egg chambers (12%; Fig. 6D) with packaging defects similar to *Acf1-fos* (4%; Fig. 6D). However, no further increase in apoptosis was observed with additional copies of either *Acf1* or *Chrac-16-fosmid* (Fig. 6D). This finding suggests that excess CHRAC interferes with proper oogenesis. This hypothesis was further addressed by combination of *Chrac-16-fosmid* with *Acf1-N* or *Acf1-C-fosmid*. Indeed, increased apoptotic defects were only observed in combination of *ACF1-N-fos* with *Chrac-16-fos* (9%; Fig. 6D) but not with *ACF1-C-fos* which lacks the CHRAC-16 interaction domain (3%; Fig. 6D). We conclude that combining elevated levels of ACF1 and CHRAC-16 poses a risk for oogenesis failure.

Our data suggest that the $Acf1^{7}$ allele represents a true loss-of-function phenotype, best described as a variegated failure to assemble viable egg chambers. Failed attempts are removed through apoptosis. Expression of the N-terminal portion of ACF1 rescues this phenotype. By contrast, the interesting packaging defects found in $Acf1^{1}$ alleles are presumably due to interference of an out-of-context ACF1 interaction module. In support of this conclusion, we found that expression of ACF1-C in an $Acf1^{7}$ background induces packaging phenotypes, including compound egg chambers. Remarkably, a mild overexpression of CHRAC leads to increased apoptotic and packaging defects. Indicating that, finely tuned CHRAC levels are required for proper oogenesis.

4. Discussion

The highly related nucleosome remodeling complexes ACF and CHRAC are prototypic nucleosome sliding factors. Their biochemical activities are very similar and their physiological functions thought to be highly related. The available information suggests that these factors do not contribute to regulating gene expression, but fulfill more general tasks in the assembly and maintenance of properly packaged chromatin fibers with regular nucleosome spacing. Their high and global expression during early embryogenesis may be rationalized by a presumed need for such activity during times of extremely rapid replication cycles. Human ACF1 (and by inference the remodelers hACF and hCHRAC) facilitates replication through heterochromatin (Collins et al., 2002), but recently roles in the signaling and repair of DNA breaks have been described as well (Lan et al., 2010; Sánchez-Molina et al., 2011). An analogous function for the *Drosophila* factors, which may also be beneficial during early embryonic development, has not been reported yet.

With these considerations in mind we were surprised by the rather specific enrichment of ACF1 in the *Drosophila* germline. We had suggested earlier that high levels of ACF1 may indicate a state of chromatin plasticity that is characteristic of undifferentiated cells (Chioda et al., 2010). However, our new finding that ACF1 is expressed in differentiated follicle and nurse cells do not support this hypothesis. The specific enrichment of ACF1 in GSCs and prospective oocytes by the Bicaudal-D/Egalitarian RNA transport machinery suggests specific functions of the remodeler during oogenesis. However, specific ACF1 enrichment in the oocyte nucleoplasm could also hint to requirements of ACF1 in early processes of embryo development (Chioda et al., 2010; Fyodorov et al., 2004).

We analyzed two independent *Acf1* mutant alleles to explore the consequences of ACF1 loss on oogenesis. Both mutants showed an increased level of apoptotic egg chambers from stage 7 or 8 onwards. Similar abortions of egg chambers were also scored if ACF1 had been ablated in either germline or somatic cells, provided that the knockdown was induced early. The abortion of eggs might be promoted by external cues, such as unfavorable environmental conditions or intrinsic factors, such as 'low quality' oocytes (Jenkins et al., 2013; McCall, 2004; Thomson et al., 2010). Following the latter idea, loss of ACF1 remodeling activity might lead to the accumulation of multiple subtle changes in chromatin structure and function that collectively may compromise the execution of gene expression or cell cycle programs critical to the complex oogenesis process.

While we cannot exclude a role for ACF/CHRAC in transcription control, we do not favor such a scenario. Preliminary transcriptome profiling of $Acf1^{7}$ mutant embryos does not suggest systematic and direct effects of ACF1 on transcription. Furthermore, ACF1 cannot be trapped by formaldehyde crosslinking at regulatory regions (Jain et al., 2015).

The ACF1 loss-of-function phenotype was neither explained by replication defects that may lead to asynchrony of 16-cell cyst formation or reduced nurse cell polyploidy nor by defects in the resolution of meiotic recombination. Such perturbations of the integrity of the chromatin fiber would be detectable by enhanced γH2A.V staining, which was not observed. The modesty of the failure rate might be explained by functional redundancy, for example with RSF, an ISWI-containing remodeling complex predicted to have very similar functions to ACF/CHRAC (Baldi and Becker, 2013; Loyola et al., 2001; Lusser et al., 2005; Torigoe et al., 2011).

Our findings that depletion of ISWI in early germline cells causes an agametic phenotype and that ISWI functions outside of the germarium are not required for further oocyte differentiation is in agreement with previous observations (Xi and Xie, 2005; Yan et al., 2014). A requirement for the ISWI-containing remodeler NURF for GSC fate and activity had already been described, but this can be explained by the known role of NURF as (co-) regulator of transcription programs (Ables and Drummond-Barbosa, 2010; Xi and Xie, 2005). Besides, ISWI depletion in follicle cells causes a variety of severe packaging defects arguing for a role of ISWI remodeling activity in somatic cells, which had not been considered so far (Xi and Xie, 2005).

Remarkably, we also found a range of interesting 16-cell cyst packaging defects in the related, but independent, $Acf1^{1}$ and $Acf1^{2}$ alleles. These alleles had been assumed loss-of-function alleles, because the small deletions disrupt the reading frame and no

protein is detectable by Western blotting or IFM in mutant embryos. The packaging defects manifested themselves as a variety of compound egg chambers containing more than one 16-cell cyst and often with oocytes prominently placed at opposite poles. This rare phenotype had been described only in a few mutants of different signaling pathways (Besse et al., 2002; Hawkins et al., 1996; Jackson and Blochlinger, 1997; McGregor et al., 2002; Urwyler et al., 2012) and Polycomb genes (Narbonne et al., 2004). The fact that we observe surplus stalk-like structures and polar cells suggests that the morphogenetic abnormalities are due to encapsulation defects.

The depletion of ACF1 by RNAi as well as the true loss-of-function mutation in the *Acf1*^{7} allele never yielded packaging defects. This argues against *Acf1*^{1} being a null allele, reiterating earlier concerns (Ables and Drummond-Barbosa, 2010). Our finding of a cell-specific expression of a C-terminal ACF1 fragment containing a prominent PHD-bromo module now provides a molecular explanation for the phenomenon. Indeed, the ectopic expression of this module induced packaging phenotypes in the absence of functional ACF1, suggesting competitive interactions with yet unknown target molecules. Our novel finding that depletion of ISWI in somatic cells also leads to a variety of packaging phenotypes, including compound egg chambers similar to the ones scored in the *Acf1*^{1} allele may indicate an interference of the out-of-context ACF1 C-terminus with the function of another ISWI remodeling complex.

Tagging the signature subunit of CHRAC, CHRAC-16, for the first time allowed monitoring its expression *in vivo*. The colocalisation of CHRAC-16 and ACF1 in prospective oocytes and nurse cells suggests a function for CHRAC (as opposed to just ACF) during oogenesis. This notion receives support from the finding that mild combined overexpression of ACF1 and CHRAC-16 generated apoptotic and packaging phenotypes. This leads to the surprising conclusion that proper oogenesis requires that CHRAC levels are finely adjusted within a two-fold range. Whether excess CHRAC interferes with functions of other chromatin regulators by competition with shared targets remains an interesting question and challenge for future research.

Author contributions

KB, DJ, PVP, SV, NS, AK performed experiments; DVF, PT, AK, BS, PBB developed concepts and approaches; KB, PVP, BS, PBB analyzed data; KB, PBB prepared the manuscript; all authors edited the manuscript prior to submission.

Acknowledgments

Stocks obtained from the Bloomington *Drosophila* Stock Center (NIH P40OD018537) were used in this study. We thank the TRiP at Harvard Medical School (NIH/NIGMS R01-GM084947) for providing transgenic RNAi fly lines. The monoclonal antibodies Orb 4H8 and 6H4 were developed by Paul Schedl, 7G10 anti-Fasciclin III was developed by Corey Goodman, HtsRC was developed by Lynn Cooley and UNC93-5.2.1 was developed by R. Scott Hawley. They were obtained from the Developmental Studies Hybridoma Bank, created by the NICHD of the NIH and maintained at The University of Iowa, Department of Biology, Iowa City, IA 52242.

We thank Drs. S. Mietzsch, G. Reuter, N.R. Matias and J.R. Huynh for stimulating discussions and advice. We thank B. Schaller, D. Beuchle and Y. Ilina for technical help. M. Chioda participated in the early phase of the project. This work was supported by the Deutsche Forschungsgemeinschaft through Grants Be1140/7-1 and SFB1064/A01 (PBB), by the Swiss National Science Foundation through Grant 31003A 153280 (BS) and by the Russian Ministry of Science and Education through Grants RF 8131 06.08.2012 and RFBR 15-04-99583 (AK).

Appendix A. Supplementary material

Supplementary data associated with this article can be found in the online version at http://dx.doi.org/10.1016/j.ydbio.2016.01.039.

References

Ables, E.T., Drummond-Barbosa, D., 2010. The steroid hormone ecdysone functions with intrinsic chromatin remodeling factors to control female germline stem cells in Drosophila. Cell Stem Cell 7, 581–592. http://dx.doi.org/10.1016/j.stem.2010.10.001.

Alkhatib, S.G., Landry, J.W., 2011. The nucleosome remodeling factor. FEBS Lett. 585, 3197–3207. http://dx.doi.org/10.1016/j.febslet.2011.09.003.

Baldi, S., Becker, P.B., 2013. The variant histone H2A.V of Drosophila-three roles, two guises. Chromosoma 122, 245–258. http://dx.doi.org/10.1007/s00412-013-0409-x.

Besse, F., Busson, D., Pret, A.-M., 2002. Fused-dependent Hedgehog signal transduction is required for somatic cell differentiation during Drosophila egg chamber formation. Development 129, 4111–4124.

Chioda, M., Becker, P.B., 2010. Soft skills turned into hard facts: nucleosome remodelling at developmental switches. Heredity 105, 71–79. http://dx.doi.org/10.1038/hdy.2010.34.

Chioda, M., Vengadasalam, S., Kremmer, E., Eberharter, A., Becker, P.B., 2010. Developmental role for ACF1-containing nucleosome remodellers in chromatin organisation. Development 137, 3513–3522. http://dx.doi.org/10.1242/dev.048405.

Clapier, C.R., Cairns, B.R., 2009. The biology of chromatin remodeling complexes. Annu. Rev. Biochem. 78, 273–304. http://dx.doi.org/10.1146/annurev.biochem.77.062706.153223.

Claußen, M., Suter, B., 2005. BicD-dependent localization processes: from Drosophilia development to human cell biology. Ann. Anat. 187, 539–553. http://dx.doi.org/10.1016/j.aanat.2005.07.004.

Collins, N., Poot, R. a, Kukimoto, I., García-Jiménez, C., Dellaire, G., Varga-Weisz, P.D., 2002. An ACF1-ISWI chromatin-remodeling complex is required for DNA replication through heterochromatin. Nat. Genet. 32, 627–632. http://dx.doi.org/10.1038/ng1046.

Corona, D.F., Eberharter, a, Budde, a, Deuring, R., Ferrari, S., Varga-Weisz, P., Wilm, M., Tamkun, J., Becker, P.B., 2000. Two histone fold proteins, CHRAC-14 and CHRAC-16, are developmentally regulated subunits of chromatin accessibility complex (CHRAC). EMBO J. 19, 3049–3059. http://dx.doi.org/10.1093/emboj/19.12.3049.

Deuring, R., Fanti, L., Armstrong, J.A., Sarte, M., Papoulas, O., Prestel, M., Daubresse, G., Verardo, M., Moseley, S.L., Berloco, M., Tsukiyama, T., Wu, C., Pimpinelli, S., Tamkun, J.W., Sapienza, L., Moro, P.A., Genetica, I., 2000. The ISWI chromatin-remodeling protein is required for gene expression and the maintenance of higher order chromatin structure in vivo. Mol. Cell 5, 355–365.

Eberharter, A., Vetter, I., Ferreira, R., Becker, P.B., 2004. ACF1 improves the effectiveness of nucleosome mobilization by ISWI through PHD-histone contacts. EMBO J. 23, 4029–4039. http://dx.doi.org/10.1038/sj.emboj.7600382.

Ejsmont, R.K., Sarov, M., Winkler, S., Lipinski, K. a, Tomancak, P., 2009. A toolkit for high-throughput, cross-species gene engineering in Drosophila. Nat. Methods 6, 435–437. http://dx.doi.org/10.1038/nmeth.1334.

Eliazer, S., Shalaby, N.A., Buszczak, M., 2011. causes stem cell tumors in the Drosophila ovary 2011. doi:10.1073/pnas.1015874108/-/DCSupplemental.www.pnas.org/cgi/doi/10.1073/pnas.1015874108.

Emelyanov, A.V., Vershilova, E., Ignatyeva, M. a, Pokrovsky, D.K., Lu, X., Konev, A.Y., Fyodorov, D.V., 2012. Genes Dev. 26, 603–614. http://dx.doi.org/10.1101/gad.180604.111.

Fyodorov, D.V., Blower, M.D., Karpen, G.H., Kadonaga, J.T., 2004. Acf1 confers unique activities to ACF / CHRAC and promotes the formation rather than disruption of chromatin in vivo. Genes Dev. 18, 170–183. http://dx.doi.org/10.1101/gad.1139604.

Hanai, K., Furuhashi, H., Yamamoto, T., Akasaka, K., Hirose, S., 2008. RSF governs silent chromatin formation via histone H2Av replacement. PLoS Genet. 4, e1000011. http://dx.doi.org/10.1371/journal.pgen.1000011.

Hartlepp, K.F., Fernández-Tornero, C., Eberharter, A., Grüne, T., Müller, C.W., Becker, P.B., 2005. The histone fold subunits of Drosophila CHRAC facilitate nucleosome sliding through dynamic DNA interactions. Mol. Cell. Biol. 25, 9886–9896. http://dx.doi.org/10.1128/MCB.25.22.9886.

Hawkins, N.C., Thorpe, J., Schüpbach, T., 1996. Encore, a gene required for the regulation of germ line mitosis and oocyte differentiation during Drosophila oogenesis. Development 122, 281–290.

He, J., Xuan, T., Xin, T., An, H., Wang, J., Zhao, G., Li, M., 2014. Evidence for chromatin-remodeling complex PBAP- controlled maintenance of the drosophila

ovarian germline stem cells. PLoS One, 9. http://dx.doi.org/10.1371/journal.pone.0103473.
Ho, L., Crabtree, G.R., 2010. Chromatin remodelling during development. Nature 463, 474–484. http://dx.doi.org/10.1038/nature08911.
Hudson, A.M., Cooley, L., 2014. Methods for studying oogenesis. Methods 68, 207–217. http://dx.doi.org/10.1016/j.ymeth.2014.01.005.
Ito, T., Bulger, M., Pazin, M.J., Kobayashi, R., Kadonaga, J.T., 1997. ACF, an ISWI-containing and ATP-utilizing chromatin assembly and remodeling factor. Cell 90, 145–155.
Ito, T., Levenstein, M.E., Fyodorov, D.V., Kutach, A.K., Kobayashi, R., Kadonaga, J.T., 1999. assembly ACF consists of two subunits , Acf1 and ISWI , that function cooperatively in the ATP-dependent catalysis of chromatin assembly. Genes Dev.
Jackson, S.M., Blochlinger, K., 1997. cut interacts with Notch and protein kinase A to regulate egg chamber formation and to maintain germline cyst integrity during Drosophila oogenesis. Development 124, 3663–3672.
Jain, D., Baldi, S., Zabel, a, Straub, T., Becker, P.B., 2015. Active promoters give rise to false positive "Phantom Peaks" in ChIP-seq experiments. Nucleic Acids Res., 1–10. http://dx.doi.org/10.1093/nar/gkv637.
Jambor, H., Surendranath, V., Kalinka, A.T., Mejstrik, P., Saalfeld, S., Tomancak, P., 2015. Systematic imaging reveals features and changing localization of mRNAs in *Drosophila* development. Elife 4, 1–22. http://dx.doi.org/10.7554/eLife.05003.
Jenkins, V.K., Timmons, A.K., McCall, K., 2013. Diversity of cell death pathways: Insight from the fly ovary. Trends Cell Biol. 23, 567–574. http://dx.doi.org/10.1016/j.tcb.2013.07.005.
Kai, T., Spradling, A., 2003. An empty Drosophila stem cell niche reactivates the proliferation of ectopic cells. Proc. Natl. Acad. Sci. U.S.A. 100, 4633–4638. http://dx.doi.org/10.1073/pnas.0830856100.
Lan, L., Ui, A., Nakajima, S., Hatakeyama, K., Hoshi, M., Watanabe, R., Janicki, S.M., Ogiwara, H., Kohno, T., Kanno, S.I., Yasui, A., 2010. The ACF1 complex is required for dna double-strand break repair in human cells. Mol. Cell 40, 976–987. http://dx.doi.org/10.1016/j.molcel.2010.12.003.
Loyola, A., LeRoy, G., Wang, Y.H., Reinberg, D., 2001. Reconstitution of recombinant chromatin establishes a requirement for histone-tail modifications during chromatin assembly and transcription. Genes Dev. 15, 2837–2851. http://dx.doi.org/10.1101/gad.937401.
Lusser, A., Urwin, D.L., Kadonaga, J.T., 2005. Distinct activities of CHD1 and ACF in ATP-dependent chromatin assembly. Nat. Struct. Mol. Biol. 12, 160–166. http://dx.doi.org/10.1038/nsmb884.
McCall, K., 2004. Eggs over easy: cell death in the Drosophila ovary. Dev. Biol. 274, 3–14. http://dx.doi.org/10.1016/j.ydbio.2004.07.017.
McGregor, J.R., Xi, R., Harrison, D., 2002. Development 129, 705–717.
Mueller-Planitz, F., Klinker, H., Becker, P.B., 2013. Nucleosome sliding mechanisms: new twists in a looped history. Nat. Struct. Mol. Biol. 20, 1026–1032. http://dx.doi.org/10.1038/nsmb.2648.
Narbonne, K., Besse, F., Brissard-Zahraoui, J., Pret, A.-M., Busson, D., 2004. polyhomeotic is required for somatic cell proliferation and differentiation during ovarian follicle formation in Drosophila. Development 131, 1389–1400. http://dx.doi.org/10.1242/dev.01003.
Ni, J.-Q., Zhou, R., Czech, B., Liu, L.-P., Holderbaum, L., Yang-Zhou, D., Shim, H.-S., Tao, R., Handler, D., Karpowicz, P., Binari, R., Booker, M., Brennecke, J., 2011. Nat. Methods 8, 405–407. http://dx.doi.org/10.1038/nmeth.1592.
Olivieri, D., Sykora, M.M., Sachidanandam, R., Mechtler, K., Brennecke, J., 2010. An in vivo RNAi assay identifies major genetic and cellular requirements for primary piRNA biogenesis in Drosophila. EMBO J. 29, 3301–3317. http://dx.doi.org/10.1038/emboj.2010.212.
Racki, L.R., Yang, J.G., Naber, N., Partensky, P.D., Acevedo, A., Purcell, T.J., Cooke, R., Cheng, Y., Narlikar, G.J., 2009. The chromatin remodeller ACF acts as a dimeric motor to space nucleosomes. Nature 462, 1016–1021. http://dx.doi.org/10.1038/nature08621.
Sánchez-Molina, S., Mortusewicz, O., Bieber, B., Auer, S., Eckey, M., Leonhardt, H., 2011. Nucleic Acids Res. 39, 8445–8456. http://dx.doi.org/10.1093/nar/gkr435.
Swan, A., Suter, B., 1996. Role of Bicaudal-D in patterning the Drosophila egg chamber in mid-oogenesis. Development 122, 3577–3586.
Thomson, T.C., Fitzpatrick, K.E., Johnson, J., 2010. Intrinsic and extrinsic mechanisms of oocyte loss. Mol. Hum. Reprod. 16, 916–927. http://dx.doi.org/10.1093/molehr/gaq066.
Torigoe, S.E., Urwin, D.L., Ishii, H., Smith, D.E., Kadonaga, J.T., 2011. Identification of a rapidly formed nonnucleosomal histone-DNA intermediate that is converted into chromatin by ACF. Mol. Cell 43, 638–648. http://dx.doi.org/10.1016/j.molcel.2011.07.017.
Urwyler, O., Cortinas-Elizondo, F., Suter, B., 2012. Drosophila sosie functions with H-Spectrin and actin organizers in cell migration, epithelial morphogenesis and cortical stability. Biol. Open 1, 994–1005. http://dx.doi.org/10.1242/bio.20122154.
Vanolst, L., Fromental-Ramain, C., Ramain, P., 2005. Toutatis, a TIP5-related protein, positively regulates Pannier function during Drosophila neural development. Development 132, 4327–4338. http://dx.doi.org/10.1242/dev.02014.
Varga-Weisz, P.D., Wilm, M., Bonte, E., Dumas, K., Mann, M., Becker, P.B., 1997. Chromatin-remodelling factor CHRAC contains the ATPases ISWI and topoisomerase II. Nature 388, 598–602.
Vazquez-Pianzola, P., Adam, J., Haldemann, D., Hain, D., Urlaub, H., Suter, B., 2014. Clathrin heavy chain plays multiple roles in polarizing the Drosophila oocyte downstream of Bic-D. Development 141, 1915–1926. http://dx.doi.org/10.1242/dev.099432.
Vazquez-Pianzola, P., Suter, B., 2012. Conservation of the RNA transport machineries and their coupling to translation control across eukaryotes. Comp. Funct. Genom., 2012. http://dx.doi.org/10.1155/2012/287852.
Whitehouse, I., Rando, O.J., Delrow, J., Tsukiyama, T., 2007. Chromatin remodelling at promoters suppresses antisense transcription. Nature 450, 1031–1035. http://dx.doi.org/10.1038/nature06391.
Xi, R., Xie, T., 2005. Stem cell self-renewal controlled by chromatin remodeling factors. Science 310, 1487–1489. http://dx.doi.org/10.1126/science.1120140.
Yadon, A.N., Van de Mark, D., Basom, R., Delrow, J., Whitehouse, I., Tsukiyama, T., 2010. Chromatin remodeling around nucleosome-free regions leads to repression of noncoding RNA transcription. Mol. Cell. Biol. 30, 5110–5122. http://dx.doi.org/10.1128/MCB.00602-10.
Yan, D., Neumüller, R. a, Buckner, M., Ayers, K., Li, H., Hu, Y., Yang-Zhou, D., Pan, L., Wang, X., Kelley, C., Vinayagam, A., Binari, R., Randklev, S., Perkins, L. a, Xie, T., Cooley, L., Perrimon, N., 2014. A regulatory network of Drosophila germline stem cell self-renewal. Dev. Cell 28, 459–473. http://dx.doi.org/10.1016/j.devcel.2014.01.020.

3.1.1 Supplementary information

A role for tuned levels of nucleosome remodeler subunit ACF1 during *Drosophila* oogenesis

Börner et al.

Published in Developmental Biology, Volume 411, Issue 2, 15 March 2016, Pages 217-230.

doi:10.1016/j.ydbio.2016.01.039

Supplementary material

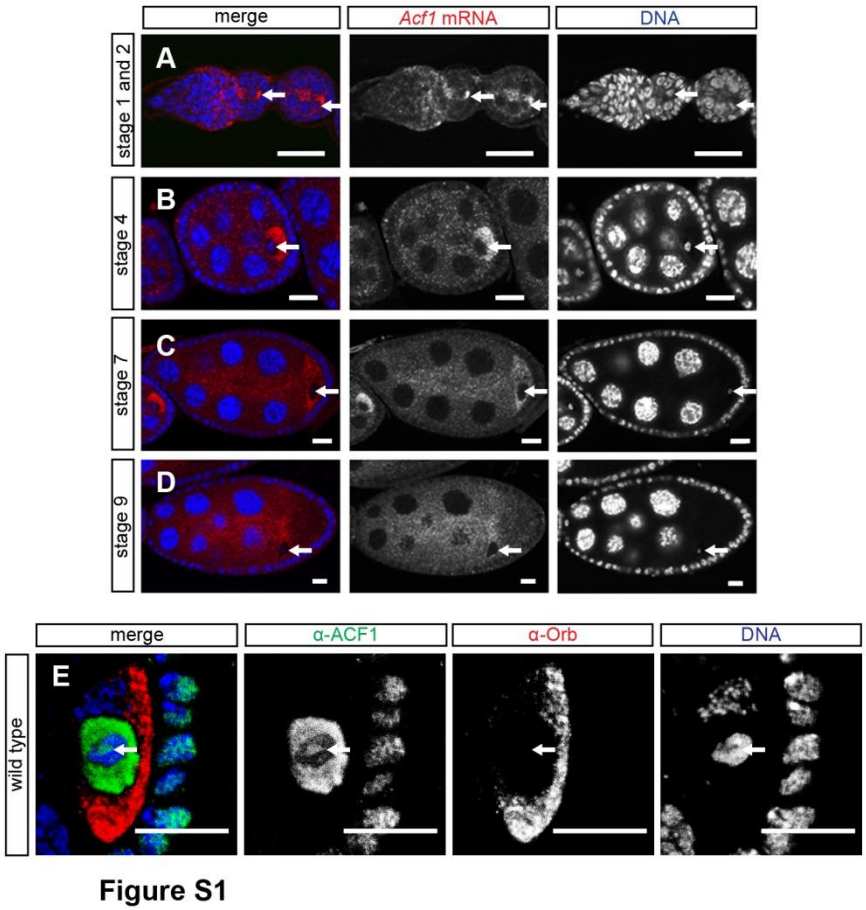

Figure S1

Figure S1. *Acf1* mRNA expression and ACF1 protein localization in *Drosophila* ovarioles.

(A-D) *In situ* hybridization of different oogenesis stages in wild type with staining of *Acf1* mRNA (red) and DNA (blue) is shown. Arrows indicate oocyte nuclei. Scale bar: 20 µm. (E) Immunofluorescence images of oocyte and follicle cells of wild type stage 6 egg chamber with staining of ACF1 (green), Orb (red) and DNA (blue) is shown. Arrows indicate oocyte nuclei. Scale bar: 10 µm.

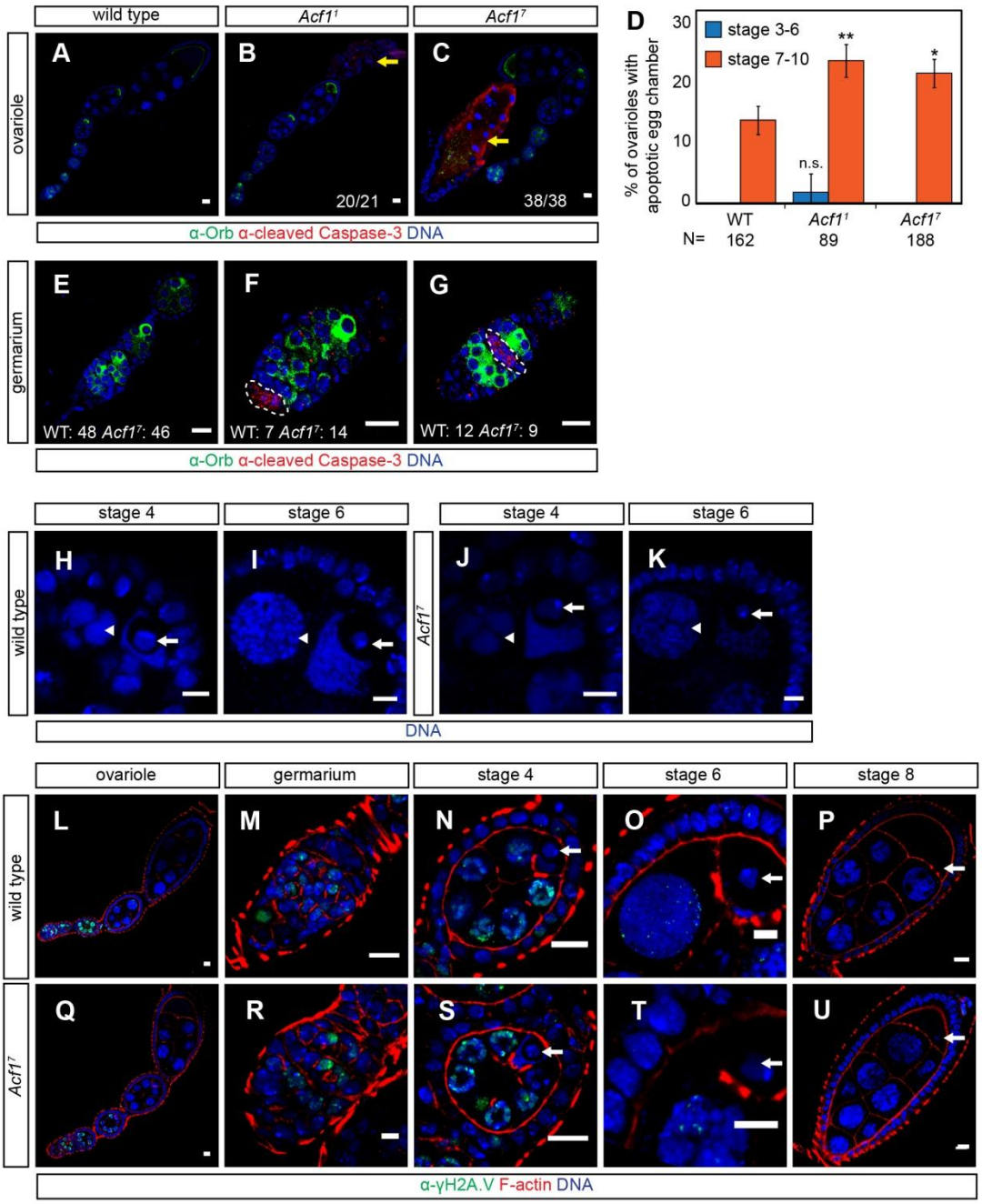

Figure S2

Figure S2. *Acf1*^{7} allele does not affect chromatin morphology or γH2A.V localization.

(A-C) Immunofluorescence images of apoptotic phenotype. Representative ovarioles of (A) wild type, (B) *Acf1*^{1} and (C) *Acf1*^{7} allele with staining of cleaved Caspase-3 (green), Orb (red) and DNA (blue) are shown. Yellow arrows indicate apoptotic egg chamber. Number of scored ovarioles with apoptotic egg chamber at most posterior position in comparison to total number of counted ovarioles is indicated in Fig. S2B, C. Scale bar: 10 µm. (D) Quantification of apoptotic egg chambers in egg chamber stage 3-6 and 7-10. The data show mean values in percent with SD of three biological replicates. N represents the total number of scored ovarioles. Two-tailed Student's t-test was used in comparison to wild type. * represents a p-value of <0.05 and ** <0.01. n.s. represents not significant. (E-G) Immunofluorescence images of apoptotic cysts in different regions of the germarium. Representative germaria with staining of Orb (green), cleaved Caspase-3 (red) and DNA (blue) are shown. Total number of scored phenotypes is shown for wild type (WT) and the *Acf1*^{7} allele (*Acf1*^{7}). Scale bar: 10

μm. (H-K) Immunofluorescence images of oocyte and nurse cell nuclei. Egg chamber stage 4 and 6 for wild type and *Acf1*^{7} with staining of DNA (blue) are shown. Arrows indicate oocyte nuclei. Arrowheads indicate nurse cell nuclei. Scale bar: 10 μm. (L-U) Immunofluorescence images of γH2A.V localization in representative ovarioles. (L-P) Wild type and (Q-U) *Acf1*^{7} with staining of γH2A.V (green), F-actin (red) and DNA (blue) are shown. Arrows indicate oocyte nuclei. Arrowheads indicate nurse cell nuclei. Scale bar: 10 μm.

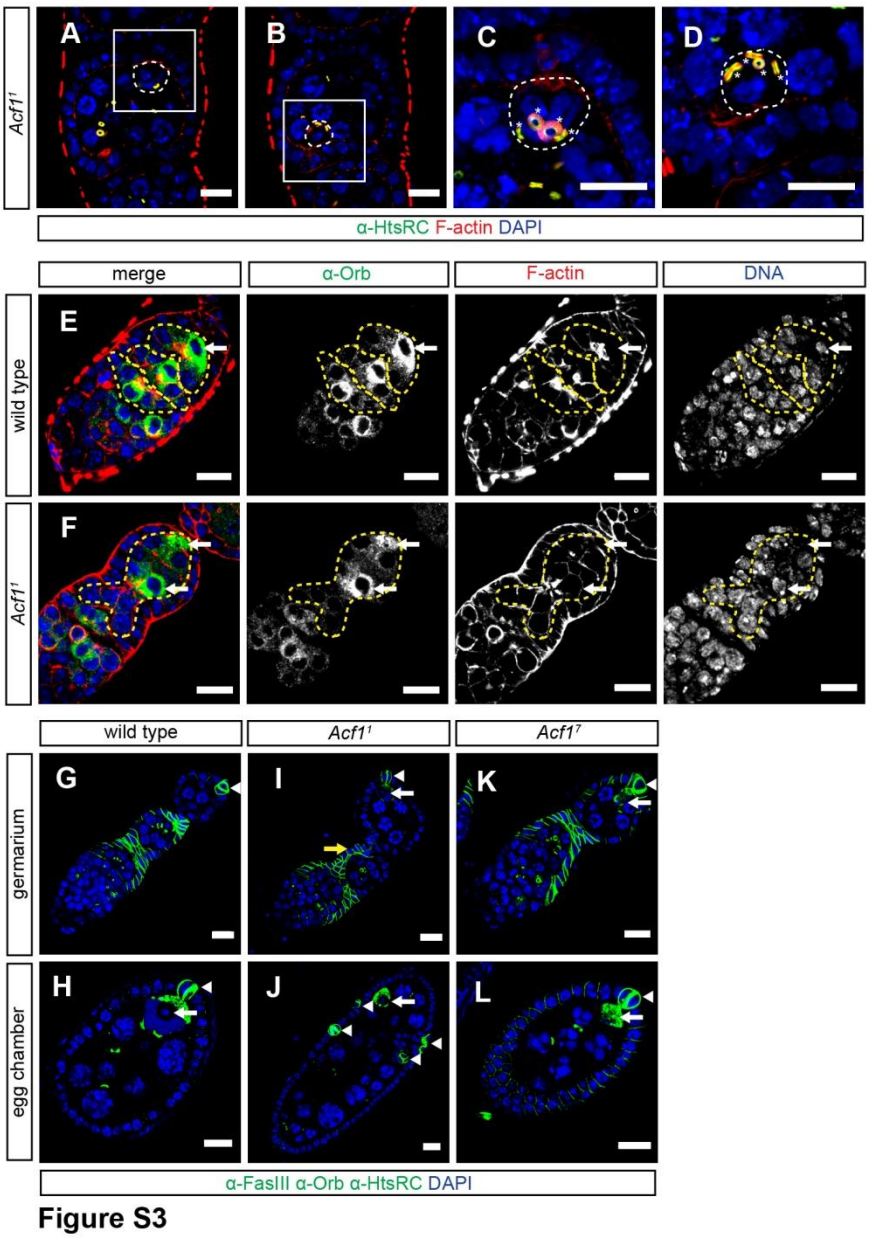

Figure S3

Figure S3. Compound egg chamber phenotypes associated with *Acf1*^{1} allele are due to encapsulation defects.

(A-D) Immunofluorescence images of packaging phenotype. (A, B) Two sections of a representative *Acf1*^{1} egg chamber with staining of HtsRC (green), F-actin (red) and DNA (blue) are shown. White square indicates zoom in Fig. S2C and D. (C-D) Images show zoom with projections of five 1 µm z-stack sections. White dashed line indicates oocyte nuclei. Asterisks indicate ring canals. Scale bar: 10 µm. (E-F) Immunofluorescence images of packaging phenotype. Germarium of wild type and *Acf1*^{1} with staining of Orb (green), F-actin (red) and DNA (blue) are shown. Yellow dashed lines indicate cysts. Arrows indicate oocyte nuclei. Scale bar: 5 µm. (G-L) Immunofluorescence images of packaging phenotypes with staining of FasIII, Orb and HtsRC (green) and DNA (blue) are shown for the following homozygous phenotypes: (G-H) wild type, (I-J) *Acf1*^{1} and (K-L) *Acf1*^{7} allele. White arrows indicate oocyte nuclei. Yellow arrows indicate stalk-like structures. Arrowheads indicate polar cells. Scale bar: 10 µm.

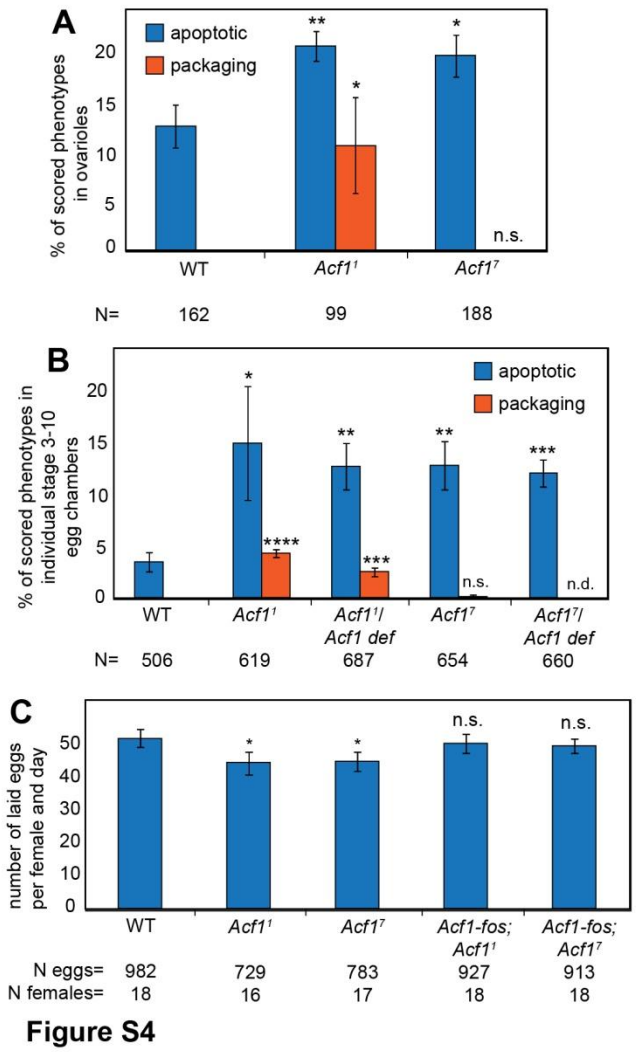

Figure S4

Figure S4. *Acf1* alleles show increased ovariole phenotypes and reduced egg laying capacity.

(A) Quantification of apoptotic and packaging phenotypes in ovarioles. The data show mean values in percent with SD of three biological replicates. N represents the total number of scored ovarioles. Two-tailed Student's t-test was used in comparison to wild type. * represents a p-value of <0.05 and ** <0.01. n.s. represents not significant. (B) *Acf1*^{1} and *Acf1*^{7} alleles combined with an *Acf1* deficiency show apoptotic and packaging phenotypes. The data show mean values in percent with SD of three biological replicates. N represents the total number of scored ovarioles. Two-tailed Student's t-test was used in comparison to wild type. * represents a p-value of <0.05, ** <0.01, ***<0.001 and ****<0.0001. n.s. represents not significant and n.d. not determined. (C) Quantification of egg laying capacity. The date show mean values of laid eggs per female and day with SD of three biological replicates. N eggs represents the total number of scored eggs and N females the total number of analyzed females. Two-tailed Student's t-test was used in comparison to wild type. * represents a p-value of <0.05 and n.s. not significant.

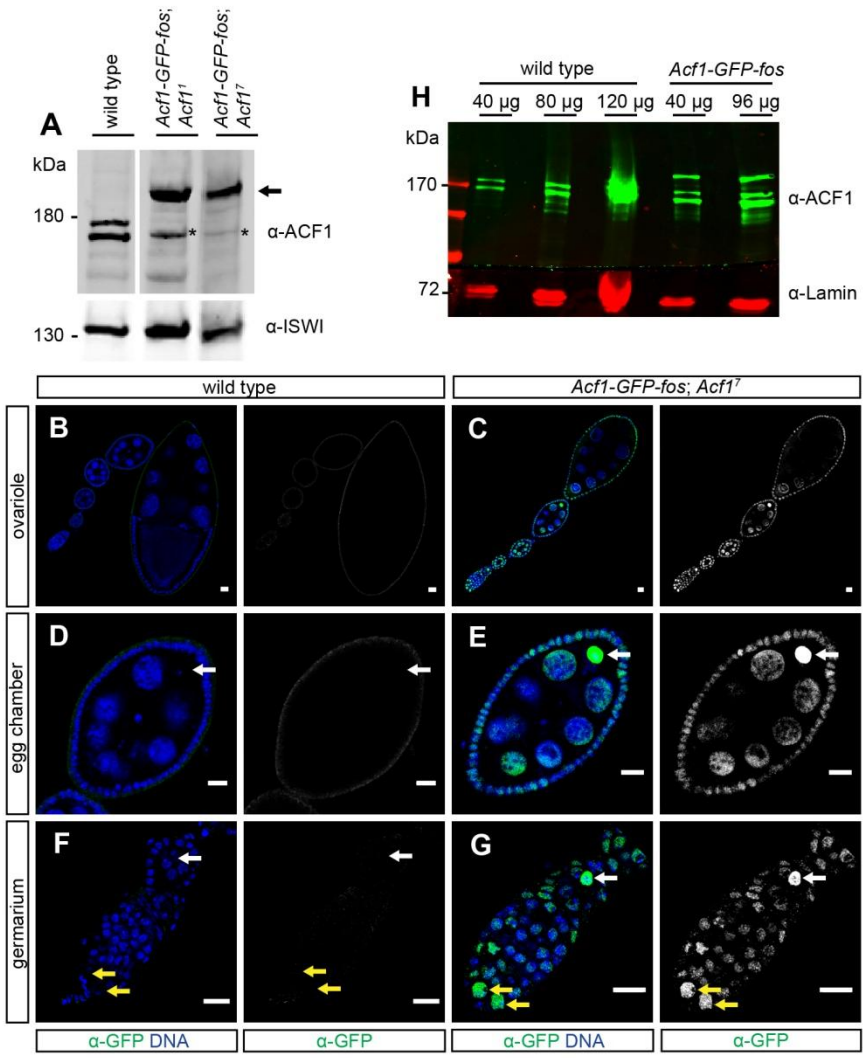

Figure S5

Figure S5. Characterization of *Acf1* fosmid.

(A) Western blot with ovary extract probed with α-ACF1 8E3 is shown for the following homozygous genotypes: wild type, *Acf1-GFP-fos*; *Acf1*^{1} and *Acf1-GFP-fos; Acf1*^{7}. ISWI signal served as a loading control. Arrow indicates ACF1-GFP. Asterisks indicate C-terminal truncated ACF1-GFP. (B-G) Immunofluorescence images of different oogenesis stages with staining of GFP (green) and DNA (blue) are shown for the following homozygous genotypes: (B, D and F) wild type and (C, E and G) *Acf1-GFP-fos*; *Acf1*^{7}. White arrows indicate oocyte nuclei. Yellow arrows indicate GSCs. Scale bar: 10 µm. (H) Quantitative Western blot for fly line expressing GFP-tagged ACF1. Nuclear extracts of 0-12 hour old embryos from wild type and *Acf1*-GFP fosmid flies were probed with α-ACF1 and α-Lamin. Three protein concentrations from wild type and two from *Acf1*-GFP fosmid extracts are shown. In total, four protein concentrations from two biological replicates were used for linear regression analysis. ACF1 protein levels were on average 2.6 fold upregulated in *Acf1*-GFP fosmid flies compared to wild type flies.

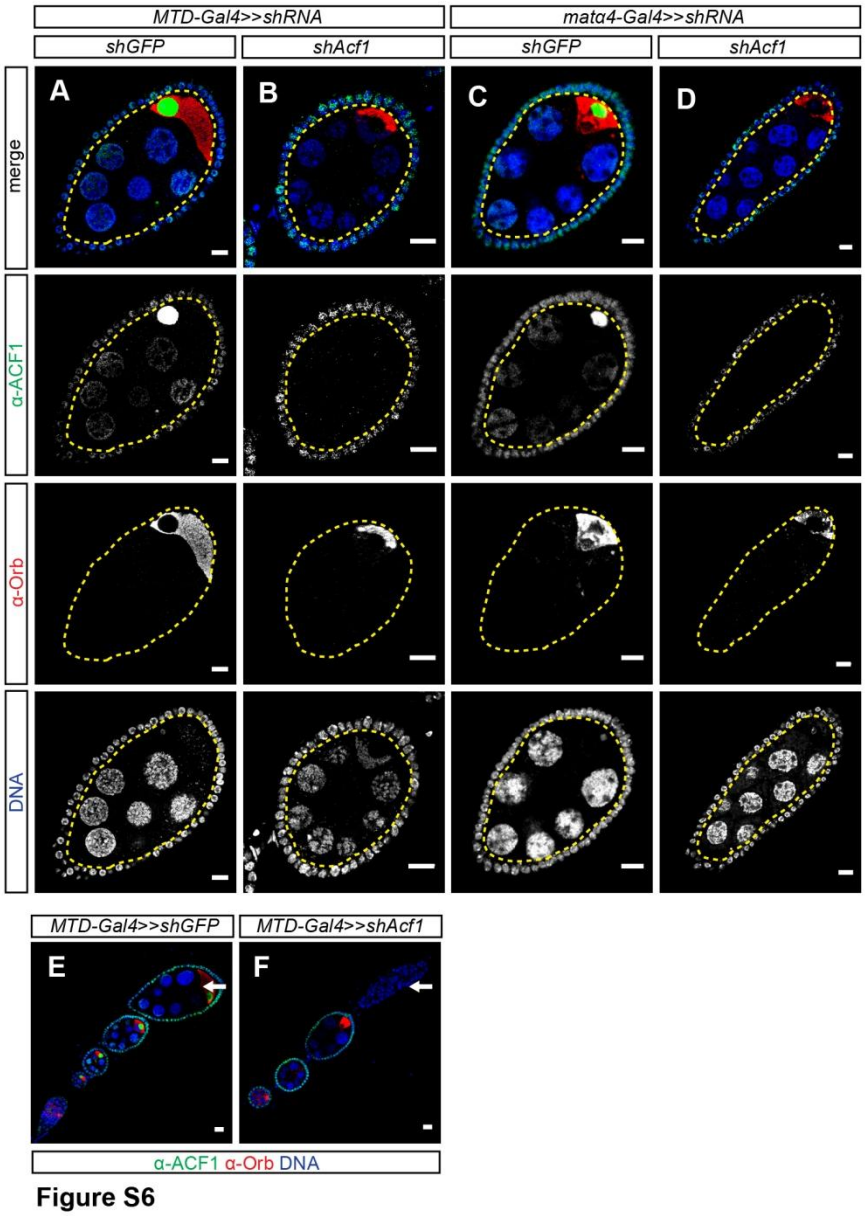

Figure S6

Figure S6. Verification of ACF1 knockdown in germline cells.

(A-E) Immunofluorescence images showing cell type-specific ACF1 knockdown in germline cells. Egg chamber with staining of ACF1 (green), Orb (red) and DNA (blue) are shown for: (A) *UAS-shGFP<<MTD-Gal4* (B), *UAS-shAcf1<<MTD-Gal4* (C) *UAS-shGFP<<matα4-Gal4* and (D) *UAS-shAcf1<<matα4-Gal4*, (E) *UAS-shGFP<<MTD-Gal4* and (F) *UAS-shAcf1<<MTD*-Gal4. Yellow dashed line indicates germline cells. White arrow indicates apoptotic egg chamber. Scale bar: 10 μm.

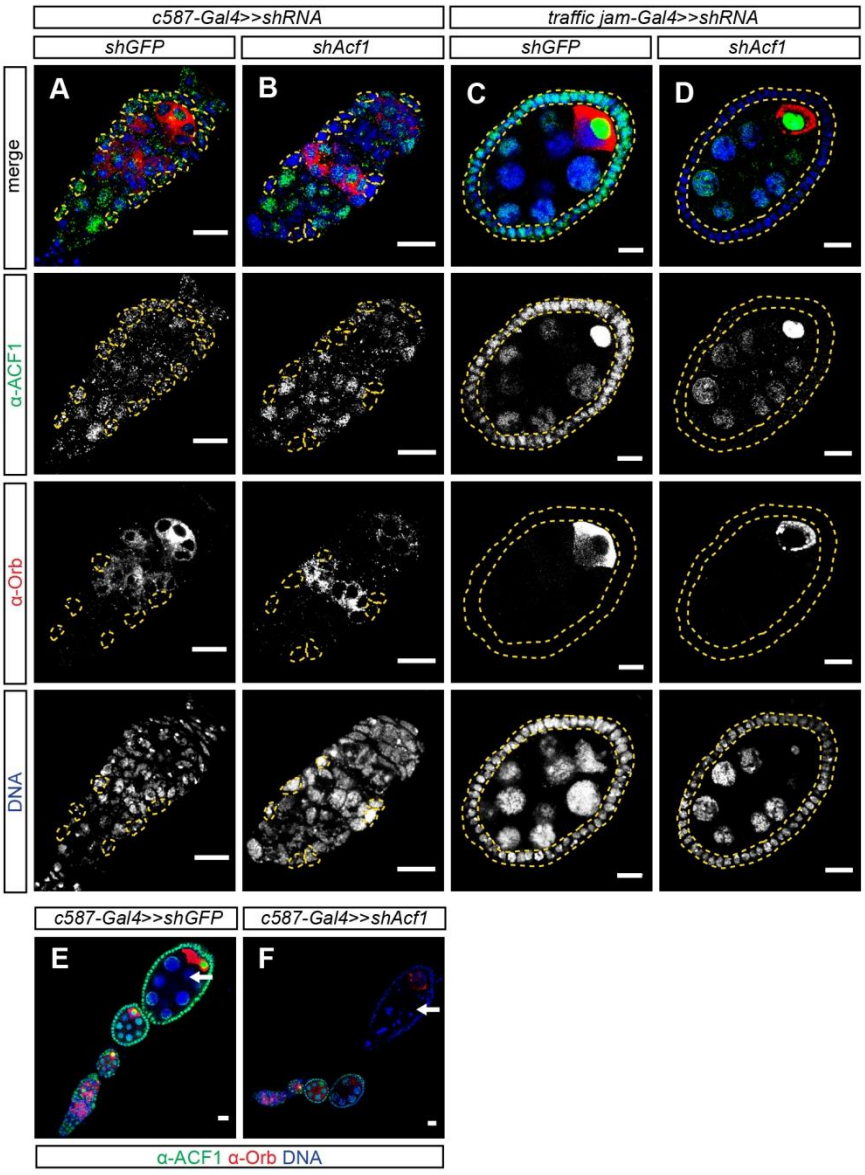

Figure S7

Figure S7. Verification of ACF1 knockdown in somatic cells.

(A-D) Immunofluorescence images showing cell type-specific ACF1 knockdown in somatic cells. Egg chamber with staining of ACF1 (green), Orb (red) and DNA (blue) are shown for: (A) *UAS-shGFP<<c587-Gal4* (B) *UAS-shAcf1<<c587-Gal4* (C) *UAS-shGFP<<traffic jam-Gal4* and (D) *UAS-shGFP<<traffic jam-Gal4*, (E) *UAS-shGFP<<c587-Gal4* and (F) *UAS-shAcf1<<c587-Gal4.* Yellow dashed line indicates somatic cells. White arrow indicates apoptotic egg chamber. Scale bar: 10 μm.

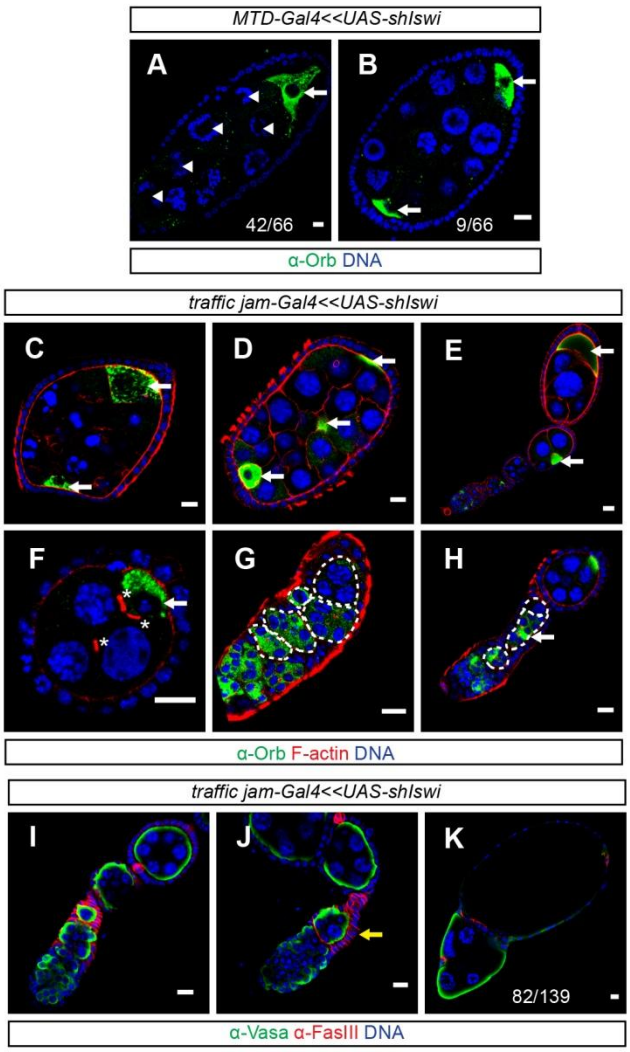

Figure S8. ISWI reduction in germline and somatic cells leads to oogenesis phenotypes.

(A-B) Immunofluorescence images of oogenesis phenotypes upon germline-specific ISWI reduction in adult ovaries. *UAS-shIswi* males were crossed with *MTD-Gal4* driver females at 18°C. F1 females were kept at 29°C for 3 days and used for analysis. Egg chambers with staining of Orb (green) and DNA (blue) are shown for (A) apoptotic and (B) packaging phenotype. Number of scored egg chamber phenotypes in comparison to total number of counted egg chambers is indicated in Fig. S8A, B. (C-K) Immunofluorescence images of packaging phenotypes in *traffic jam-Gal4<<UAS-shIswi* females. (C-H) Germarium, ovariole or egg chamber with staining of Orb (green), F-actin (red) and DNA (blue) are shown. (I-K) Ovariole or egg chamber with staining of Vasa (green), FasIII (red) and DNA (blue) are shown. White arrows indicate oocyte nuclei. White arrowheads indicate nurse cell nuclei. Yellow arrows indicate stalk-like structures. Asterisks indicate ring canals. White dashed lines indicate cysts. Number of scored dumpless eggs in comparison to total number of counted eggs is indicated in Fig. S8K. Scale bar: 10 μm.

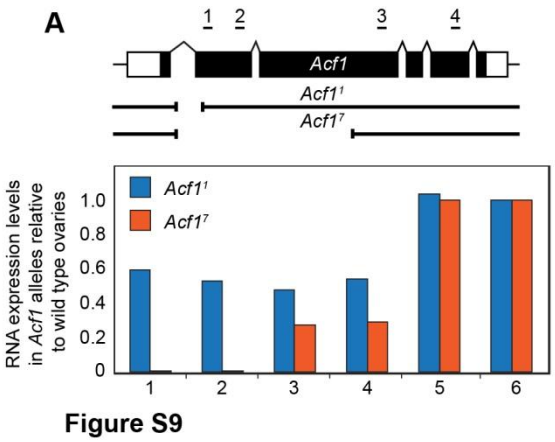

Figure S9. Quantification of *Acf1* RNA expression in ovaries of *Acf1* alleles.

(A) Relative expression levels of *Acf1* RNA from ovary extracts of the $Acf1^{1}$ and $Acf1^{7}$ alleles were quantified by real-time PCR. Schematic representation of the *Acf1* gene and $Acf1^{1}$ and $Acf1^{7}$ genomic deletions are shown. White and black rectangles represent untranslated and translated exons, respectively. Black lines indicate the following amplicons: 1 WAC domain, 2 DDT domain, 3 PHD1 domain, 4 Bromo domain (1-4 span *Acf1* gene locus), 5 Iswi and 6 MBD-R2 (unrelated control locus, normalized to 1). Expression levels from wild type ovaries were set to 1 and relative mean values of two biological replicates are shown.

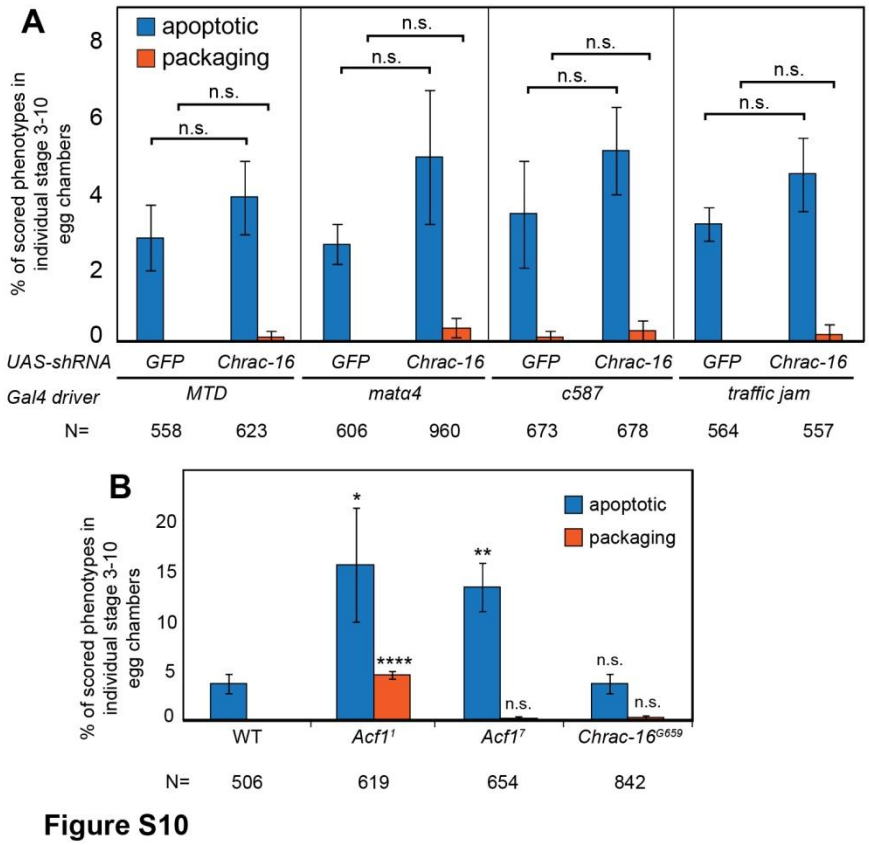

Figure S10

Figure S10. Loss-of-function analysis of CHRAC-16 in oogenesis.

(A) Quantification of apoptotic and packaging phenotypes upon cell type-specific reduction of CHRAC-16. *UAS-shChrac-16* males were crossed with *MTD-Gal4*, *matα4-Gal4*, *c587-Gal4* and *traffic jam-Gal4* females and ovary samples of F1 females were analyzed. The data show mean values in percent with SD of three biological replicates. N represents the total number of scored egg chambers stage 3-10. Two-tailed Student's t-test was used. n.s. represents not significant. (B) Quantification of apoptotic and packaging phenotypes from ovaries of homozygous *P{EP}Chrac-16^{G659}* females. For comparison, the data of wild type, *Acf1^{1}* and *Acf1^{7}* allele are shown from Fig. 2K. The data show mean values in percent with SD of three biological replicates. N represents the total number of scored egg chambers stage 3-10. Two-tailed Student's t-test was used. n.s. represents not significant.

Oligonucleotide	Sequence
Acf1-Rec-N-F	gccatttaaacttaaggacattcaagagcaaaaggaaaacaccaaacatggaagtgcataccaatcaggac
Acf1-Rec-N-R	ttcttgccctccttctgattcaggtcgaatccttcccgcttgcaaatgggcttgtcgtcgtcatccttgta
Acf1-Rec-C-F	tgcagctaccgtttaggcctagcgatatgaacggggaagtcaaagcttgcgaagtgcataccaatcaggac
Acf1-Rec-C-R	gtagactaactaatttacacgatagctggtggagatcagcgtccggctcacttgtcgtcgtcatccttgta
Acf1-Rec-ΔC-F	gctttgctcaagtctttctgcacctaaacatcttgcacgactgtattcaggaagtgcataccaatcaggac
CHRAC16-Rec-N-F	ccaaaaaaattcccaagccatagtttgcttgggaattaagtaaacaaatggaagtgcataccaatcaggac
CHRAC16-Rec-N-R	gtttccgcggtcggtggacgctccacgggtggttggctccttggttcgcccttgtcgtcgtcatccttgta
Acf1-F	actcgtctgccaactgcgtgt
Acf1-R	ctcctcatcgtcgctgtctg
Acf1-seq	aggtcttctgctgctacatc

Table S1

Table S1. Sequences of oligonucleotides used in this study.

	Forward oligonucleotide	Reverse oligonucleotide	tag
Acf1-GFP fosmid	Acf1-Rec-C-F	Acf1-Rec-C-R	C-terminal 2xTY1-EGFP-3xFLAG
Acf1-C-GFP fosmid	Acf1-Rec-ΔC-F	Acf1-Rec-C-R	N-terminal 2xTY1-EGFP-3xFLAG
Acf1-N-GFP fosmid	Acf1-Rec-N-F	Acf1-Rec-N-R	C-terminal 2xTY1-EGFP-3xFLAG
CHRAC16-mCherry fosmid	CHRAC16-Rec-N-F	CHRAC16-Rec-N-R	N-terminal 2xTY1-mCherry-3xFLAG

Table S2

Table S2. Oligonucleotide combinations used in this study.

Number	Amplicon	Forward oligonucleotide	Reverse oligonucleotide
1	ACF1-WAC	gatagtggccaagtttctgc	tccaacttgacacccaacac
2	ACF1-DDT	gatgacacgtgcactgactg	gatcgaaaacagtgccaagc
3	ACF1-PHD1	gcaggcgacaaagaagaaac	catcctcatcggtcatatcg
4	ACF1-Bromo	gcagatcatgaagcacaagg	tgatggtagtcgggaacctc
5	ISWI	ctctcacagggtttcactgc	cgtccttggcaatgttgtc
6	MBD2	ccacggaggaaggtaaaaca	agtccctgagggttcctttg

Table S3

Table S3. Real-time PCR amplicons used in this study.

3.2 Splice variants of the SWR1-type nucleosome remodeling factor Domino have distinct functions during *Drosophila melanogaster* oogenesis

Splice variants of the SWR1-type nucleosome remodeling factor Domino have distinct functions during *Drosophila melanogaster* oogenesis

Kenneth Börner and Peter B. Becker

Biomedical Center and Center for Integrated Protein Science Munich, Ludwig-Maximilians-University, Munich, Germany

Published in Development 143(17), Pages 3154-3167, 1 September 2016.

doi: 10.1242/dev.139634

Declaration of contributions to 'Splice variants of the SWR1-type nucleosome remodeling factor Domino have distinct functions during *Drosophila melanogaster* oogenesis'

This study was conceived by Peter B. Becker and myself. I performed all experiments, prepared all figures and wrote together with Peter B. Becker the manuscript.

© 2016. Published by The Company of Biologists Ltd | Development (2016) 143, 3154-3167 doi:10.1242/dev.139634

RESEARCH ARTICLE

Splice variants of the SWR1-type nucleosome remodeling factor Domino have distinct functions during *Drosophila melanogaster* oogenesis

Kenneth Börner and Peter B. Becker*

ABSTRACT

SWR1-type nucleosome remodeling factors replace histone H2A by variants to endow chromatin locally with specialized functionality. In *Drosophila melanogaster* a single H2A variant, H2A.V, combines functions of mammalian H2A.Z and H2A.X in transcription regulation and the DNA damage response. A major role in H2A.V incorporation for the only SWR1-like enzyme in flies, Domino, is assumed but not well documented *in vivo*. It is also unclear whether the two alternatively spliced isoforms, DOM-A and DOM-B, have redundant or specialized functions. Loss of both DOM isoforms compromises oogenesis, causing female sterility. We systematically explored roles of the two DOM isoforms during oogenesis using a cell type-specific knockdown approach. Despite their ubiquitous expression, DOM-A and DOM-B have non-redundant functions in germline and soma for egg formation. We show that chromatin incorporation of H2A.V in germline and somatic cells depends on DOM-B, whereas global incorporation in endoreplicating germline nurse cells appears to be independent of DOM. By contrast, DOM-A promotes the removal of H2A.V from stage 5 nurse cells. Remarkably, therefore, the two DOM isoforms have distinct functions in cell type-specific development and H2A.V exchange.

KEY WORDS: Chromatin, Remodeling, Histone variants, H2A.Z, H2A.X, HIS2AV, Germline

INTRODUCTION

The local replacement of nucleosomal histone H2A by variants is an evolutionarily conserved principle that endows chromatin with structural and functional diversity (Bönisch and Hake, 2012; Talbert and Henikoff, 2010). Two H2A variants can be considered as universal since they are found in all eukaryotes: H2A.Z and H2A.X. Currently, H2A.X is best known for the role of its phosphorylated form in DNA damage signaling. H2A.Z most likely has a role in regulating transcription, as it marks the nucleosomes next to promoters. Curiously, *Drosophila melanogaster* only has a single H2A variant, H2A.V, which combines the functions of H2A.Z and H2A.X as an architectural element downstream of active promoters, in heterochromatin organization and, in its phosphorylated form (γH2A.V), in the DNA damage response (Baldi and Becker, 2013).

H2A variants are incorporated by evolutionarily conserved SWR1-like remodeling enzymes, which use the energy freed by ATP hydrolysis to disrupt canonical nucleosomes. SWR1 enzymes share an N-terminal HSA domain and a spacer region that splits the conserved ATPase domain, enabling unique regulation mechanisms (Morrison and Shen, 2009). Mammals utilize two SWR1-like enzymes: p400 (or Ep400) and SRCAP (Cai et al., 2005; Eissenberg et al., 2005; Jin et al., 2005; Ruhl et al., 2006). By contrast, the *D. melanogaster* genome only contains a single SWR1-like enzyme gene: *domino* (*dom*) (Ruhf et al., 2001). Alternative splicing of the *dom* transcript produces two major isoforms, DOM-A and DOM-B (Ruhf et al., 2001), which differ in their C-termini. The DOM-A isoform features poly-glutamine (poly-Q) stretches and a SANT domain, whereas the DOM-B C-terminus is largely unstructured (Eissenberg et al., 2005; Ruhf et al., 2001). Early reports found DOM-B to be rather ubiquitously expressed, but DOM-A was detected only in the embryonic nervous system, larval salivary glands and S2 cells (Eissenberg et al., 2005; Messina et al., 2014; Ruhf et al., 2001), suggesting distinct functions for the two isoforms.

SWR1-like remodelers typically reside in multi-subunit complexes (Morrison and Shen, 2009), but little is known about DOM-containing complexes. DOM-A has been purified from S2 cells as part of a 16-subunit assembly that also contains the acetyltransferase TIP60, apparently combining features of the yeast SWR1 remodeling and NuA4 acetyltransferase complexes (Kusch et al., 2004). Likewise, our understanding of the roles of DOM enzymes in H2A.V exchange *in vivo* is anecdotal. DOM has been linked to H2A.V incorporation at the *E2f* promotor (Lu et al., 2007). It has also been suggested that H2A.V exchange requires prior acetylation by TIP60 (Kusch et al., 2004, 2014).

Previous genetic analyses characterized *dom* as required for cell proliferation and viability, homeotic gene regulation and Notch signaling (Eissenberg et al., 2005; Ellis et al., 2015; Gause et al., 2006; Kwon et al., 2013; Lu et al., 2007; Ruhf et al., 2001; Sadasivam and Huang, 2016; Walker et al., 2011), but did not attempt to resolve distinct functions of the two isoforms. *dom* is essential for fly development (Ruhf et al., 2001) and *dom* mutants die during pupariation (Braun et al., 1998; Ruhf et al., 2001). Furthermore, oogenesis in adult flies is strongly perturbed, causing sterility (Ruhf et al., 2001).

D. melanogaster oogenesis provides an excellent opportunity to study self-renewal and differentiation of germline and somatic stem cells (GSCs and SSCs, respectively) in the context of egg chamber morphogenesis (Hudson and Cooley, 2014; Ting, 2013; Yan et al., 2014). The formation of eggs starts in the germarium at the anteriormost end of an ovariole. There, two to three GSCs divide asymmetrically to self-renew and shed a daughter cystoblast. This cell initiates four mitotic divisions with incomplete cytokinesis to form an interconnected 16-cell cyst. One particular cell of a cyst is determined to become the oocyte and the remaining 15 cells

Biomedical Center and Center for Integrated Protein Science Munich, Ludwig-Maximilians-University, Großhaderner Strasse 9, 82152 Munich, Germany.

*Author for correspondence (pbecker@med.uni-muenchen.de)

P.B.B., 0000-0001-7186-0372

Received 11 May 2016; Accepted 21 July 2016

Development (2016) 143, 3154-3167 doi:10.1242/dev.139634

transform into polyploid nurse cells by endoreplication. In parallel, SSCs produce somatic follicle cells, which encapsulate cysts to form individual egg chambers. Oogenesis further runs through 14 stages of egg chamber development to produce a functional egg.

It is not surprising that nucleosome remodeling factors have been found to be important for oogenesis given the widespread requirement for chromatin plasticity during development (Chioda and Becker, 2010; Ho and Crabtree, 2010; Iovino, 2014). Interestingly, an RNA interference (RNAi) screen identified DOM as important for GSC self-renewal and cystoblast differentiation (Yan et al., 2014). DOM function is also essential for SSC self-renewal (Xi and Xie, 2005). The mechanisms of DOM function in these processes are unclear, but involvement of H2A.V exchange has been suggested. H2A.V signals show a modest decrease in *dom* mutant GSC clones in *D. melanogaster* testes (Morillo Prado et al., 2013) and are not detectable in mutant germline clones for MRG15, a DOM-A/TIP60 complex subunit (Joyce et al., 2011). Yet, direct evidence for a role of DOM – and specific roles for each isoform – in H2A.V incorporation during oogenesis is lacking.

We used a cell type-specific RNAi approach to dissect the functions of DOM-A and DOM-B during *D. melanogaster* oogenesis. Our analysis suggests non-redundant requirements for both DOM isoforms in several cell differentiation programs and for H2A.V exchange.

RESULTS

Expression of both DOM splice variants in *D. melanogaster* ovarioles

DOM is ubiquitously expressed in the female germline of *D. melanogaster* ovarioles (Yan et al., 2014), but other studies suggest expression of only DOM-B in soma and germline cells (Ruhf et al., 2001; Xi and Xie, 2005). Owing to the lack of specific DOM-A and DOM-B antibodies for immunofluorescence microscopy we generated transgenes expressing GFP-3×FLAG-tagged DOM from a recombined fosmid using the flyfosmid recombineering technique (Ejsmont et al., 2009). This way, we obtained fly lines expressing N-terminally tagged DOM (*GFP-dom*) and C-terminally tagged DOM-A (*dom-A-GFP*) and DOM-B (*dom-B-GFP*) from its chromosomal regulatory context (Fig. 1A,B). The latter two constructs express one tagged isoform, while the other is untagged. As a control, we replaced the *dom* locus with the GFP-3×FLAG cassette (Δ*dom-GFP*) (Fig. 1B).

We complemented lethality and sterility of two *dom* alleles to assess the functionality of the *dom* transgenes. Viable homozygous dom^1 or dom^9 fly lines were obtained by complementation with the *dom* transgenes (Fig. S1A). By contrast, the Δ*dom-GFP* transgene did not rescue pupal lethality in the dom^1 allele and compromised viability in the dom^9 allele (Fig. S1A). Furthermore, a characteristic larval phenotype of dom^1 mutants (Braun et al., 1998; Ruhf et al., 2001) was completely rescued by the *dom* transgenes (Fig. S1B,C). Importantly, egg laying capacity was restored to wild-type levels in homozygous dom^9 females complemented with the *dom* transgenes, but not by the Δ*dom-GFP* transgene (Fig. 1C). Our analysis provides the first comprehensive validation of *dom* allele phenotypes using complementation with *dom* transgenes.

Western blotting using the FLAG antibody showed expression of *dom* transgenes in ovaries (Fig. 1D) and larval brains (Fig. S1D) (Ruhf et al., 2001). We confirmed the ubiquitous expression of DOM-B in germline and somatic cells of ovarioles with the GFP antibody (Fig. 1F) (Ruhf et al., 2001; Xi and Xie, 2005). The specificity of antibody was confirmed as wild-type ovarioles showed only background staining (Fig. 1H). Interestingly, we also observed expression of DOM-A in germline and somatic cells of ovarioles (Fig. 1E). Both DOM isoforms were present in GSCs, cystoblasts, SSCs and follicle cells, with enrichment in oocyte nuclei in comparison to nurse cells (Fig. 1E,F). Nuclear localization was not due to the GFP tag since GFP expressed from the Δ*dom-GFP* transgene showed only cytoplasmic signal (Fig. 1G). In summary, DOM-A and DOM-B are expressed in germline and somatic cells during oogenesis.

Cell type-specific knockdown of DOM-A and DOM-B reveals requirements during fly development

To dissect the cell type-specific requirements for DOM-A and DOM-B we induced RNAi by expressing small hairpin (sh) RNA directed against *dom* under the control of the Gal4/UAS system (Ni et al., 2011). We also generated transgenic flies expressing shRNA directed selectively against each individual DOM isoform and compared the resulting phenotypes with corresponding depletions of H2A.V and TIP60. *GFP* shRNA served as a control for non-specific effects.

The effect of ubiquitous depletion of DOM should resemble the lethal phenotype of the dom^1 allele (Ruhf et al., 2001). Indeed, we observed pupal lethality upon expression of *dom-1* shRNA with an *actin-Gal4* driver, whereas siblings lacking the driver were not affected (Fig. 2A). Remarkably, individual depletion of DOM-A or DOM-B led to pupal lethality, indicating essential functions for each isoform during fly development (Fig. 2A).

DOM and other TIP60 complex subunits are well known as positive regulators of Notch signaling in wing formation (Eissenberg et al., 2005; Ellis et al., 2015; Gause et al., 2006; Kwon et al., 2013). We also scored typical Notch phenotypes, such as defective wing margins and wing nicks, with high penetrance upon expression of two *dom* shRNAs from the *C96-Gal4* driver (Fig. S2). Interestingly, the two DOM isoforms appear to have distinct functions in wing development since *dom-A* shRNA led to wing margin phenotypes with high penetrance, whereas *dom-B* shRNA had only minor effects (Fig. S2).

To document the efficiency and specificity of RNAi depletion we raised monoclonal antibodies against peptides of DOM-A (DOA1) and DOM-B (DOB2) for western blot detection. No DOM signals were detected in larval brain extracts with DOA1 and DOB2 antibodies upon *dom-1* shRNA depletion driven by *elav-Gal4* (Fig. 2B). Furthermore, signals for multiple DOM-A bands and DOM-B were strongly reduced upon depletion with *dom-A* and *dom-B* shRNAs, respectively (Fig. 2B). Multiple DOM-A bands have been reported previously (Kusch et al., 2004; Ruhf et al., 2001) and might reflect additional minor DOM-A isoforms or low-level degradation. As a control, levels of the SWI2/SNF2 ATPase ISWI were unaltered (Fig. 2B).

Despite all efforts, the monoclonal DOM-A and DOM-B antibodies could not be used for immunofluorescence microscopy applications. Alternatively, we combined GFP-tagged *dom* transgenes with shRNA constructs expressed from the *traffic jam-Gal4* driver, which is specifically expressed in somatic follicle cells but not in germline nurse cells (Olivieri et al., 2010). As a control, we detected the *dom* transgenes in follicle and nurse cells using the GFP antibody (Fig. 2C,I). We did not detect GFP signal in follicle cell nuclei upon *dom-1*, *dom-A* and *dom-B* shRNA depletion in the respective *GFP-dom*, *dom-A-GFP* and *dom-B-GFP* transgenes (Fig. 2D,E,G,I). However, GFP signal was detected in nurse cell nuclei of the same egg chambers (Fig. 2D,E,G). Importantly, DOM-A or DOM-B depletion did not affect the localization and levels of the other isoform (Fig. 2F,H,I and Fig. S3), arguing for an

Development (2016) 143, 3154-3167 doi:10.1242/dev.139634

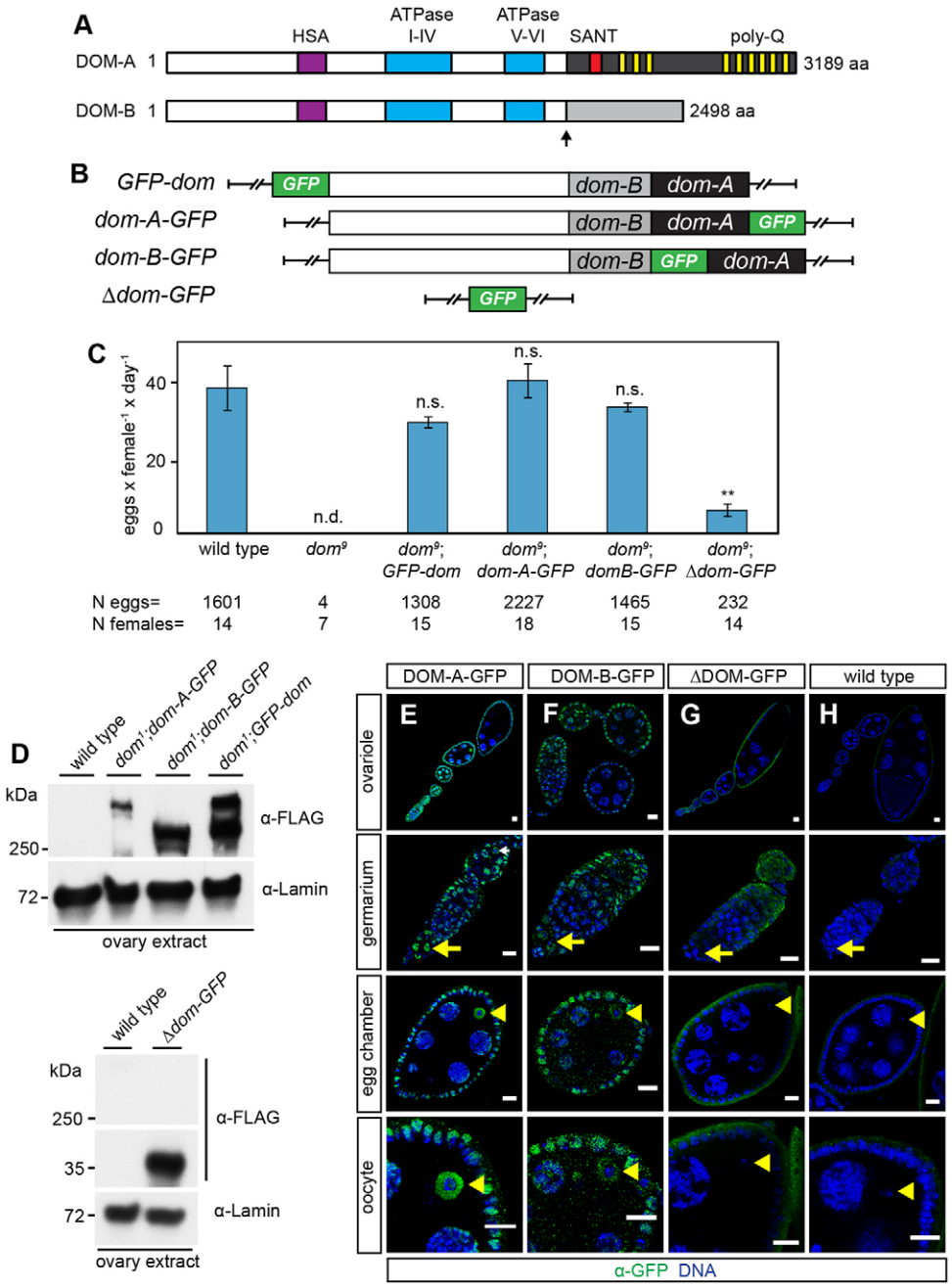

Fig. 1. Ubiquitous expression of DOM-A and DOM-B in *D. melanogaster* ovarioles. (A) Schematic representation of DOM isoforms. Arrow indicates the different C-terminal regions in DOM-A (dark gray) and DOM-B (light gray). Purple, blue, red and yellow rectangles represent HSA, ATPase, SANT and poly-Q domains, respectively. (B) Schematic representation of the *dom* fosmid constructs. White, dark gray and light gray rectangles represent the 5′ genomic region of *dom* and splice variant of *dom-A* or *dom-B*, respectively. Green rectangle indicates the inserted 2×TY1-sGFP-3×FLAG tag. (C) Complementation of the dom^{9} allele with *dom* transgenes rescues the sterility phenotype. Quantification of egg laying capacity is shown. The data show mean values of eggs laid per female per day with s.d. of three biological replicates. *N* eggs represents the total number of scored eggs and *N* females the total number of analyzed females. $^{**}P<0.01$; n.s., not significant. Two-tailed Student's *t*-test compared with wild type. n.d., not determined. (D) Western blot from ovaries probed with anti-FLAG is shown for the following homozygous genotypes: wild type, dom^{1};*dom-A*, dom^{1};*dom-B*, dom^{1};*GFP-dom*. Lamin signal served as a loading control. (E-H) Immunofluorescence images of different oogenesis stages with staining of GFP (green) and DNA (blue) for the following homozygous genotypes: (E) *dom-A-GFP*, (F) *dom-B-GFP*, (G) Δ*dom-GFP* fosmid and (H) wild type. Arrows and arrowheads indicate germline stem cells (GSCs) and oocyte nuclei, respectively. Scale bars: 10 µm.

independent localization of the two DOM isoforms. Furthermore, TIP60 depletion did not affect DOM-A or DOM-B localization (Fig. S4). We conclude that shRNAs against *dom*, *dom-A* and *dom-B* specifically and efficiently deplete their corresponding target protein.

Loss of DOM-A in germline cells leads to early cystoblast defects, while loss of DOM-B generates defective late egg chambers

Previous analysis could not reveal the specific contributions of DOM-A and DOM-B function to germline development (Ruhf et al., 2001; Yan et al., 2014). We confirmed the importance of DOM for fertility by scoring the egg laying capacity of F1 females from crosses of different *dom* shRNAs with the germline-specific *MTD-Gal4* driver (Fig. 3A) (Yan et al., 2014). We found the egg laying capacity strongly impaired upon separate depletion of DOM isoforms, an effect that was similar if the H2A.V variant was depleted (Fig. 3B,C). *Tip60* shRNAs showed moderately decreased egg laying capacity (Fig. 3C).

We stained ovaries of knockdown animals for the germline-specific cytoplasm marker Vasa and the follicle cell-specific adhesion molecule Fasciclin III (Fig. 3D-I). As expected, depletion with *dom-1* shRNA led to an agametic phenotype with characteristic small ovaries and defects in cyst differentiation in the germarium (Fig. 3E) (Yan et al., 2014). The effects of depleting DOM-A and H2A.V resembled this phenotype (Fig. 3F,H). By contrast, germline development in the germarium appeared normal upon DOM-B and TIP60 depletion (Fig. 3G,I), but many defective late egg chambers were observed (Fig. 3G,I). We conclude that the two DOM isoforms are both required for proper oogenesis, but that

Development (2016) 143, 3154-3167 doi:10.1242/dev.139634

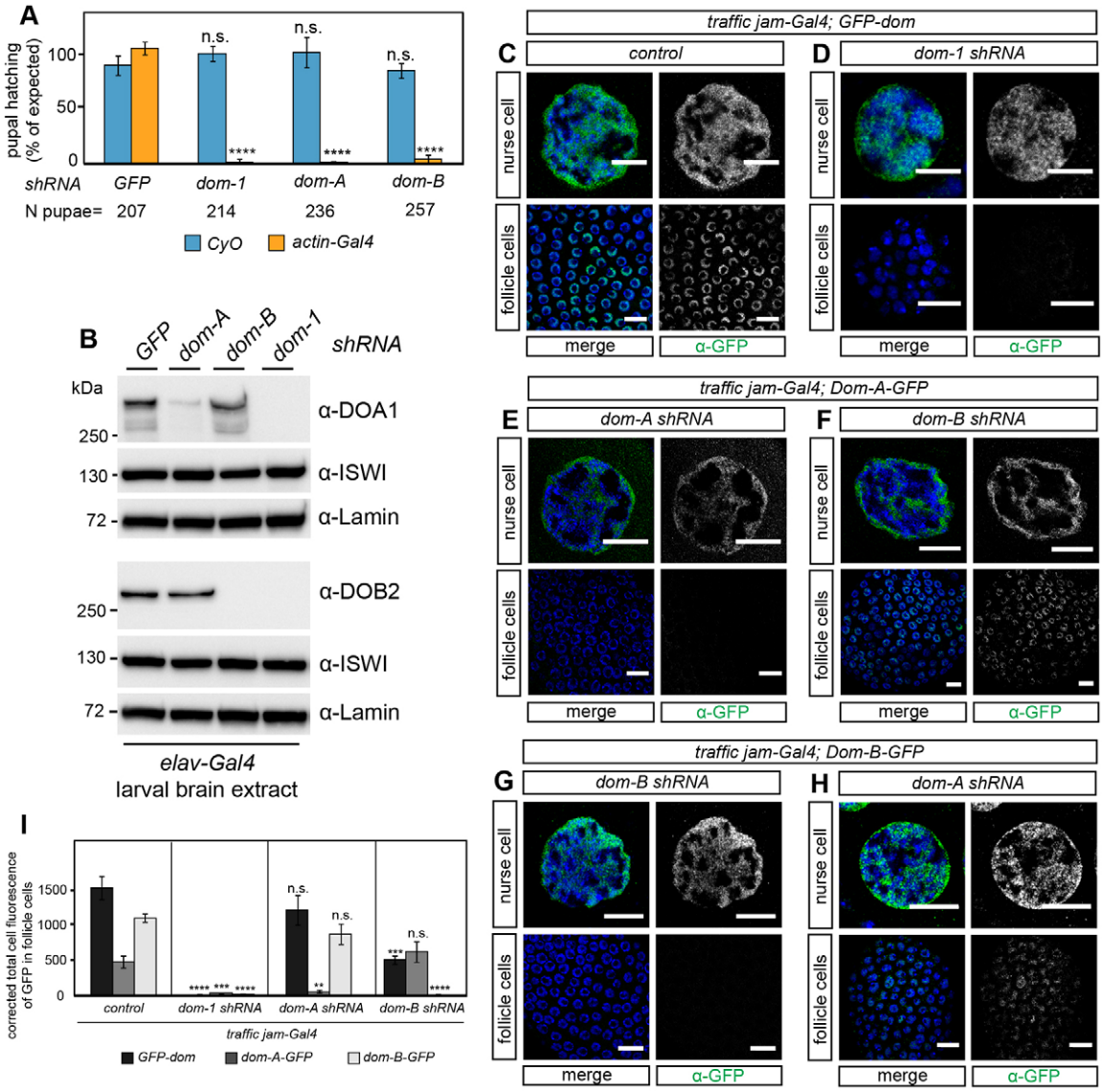

Fig. 2. Cell type-specific knockdown of DOM-A and DOM-B reveals requirements during fly development. (A) DOM-A and DOM-B are essential during fly development. *UAS-shRNA* males for *GFP*, *dom-1*, *dom-A* and *dom-B* were crossed with *actin-Gal4*/*CyO* driver females. Pupal hatching was determined as the observed to expected frequency of *CyO* and *actin-Gal4* F1 offspring. The data show mean values of percentage with s.d. from three biological replicates. *N* pupae represents the total number of pupae scored. Two-tailed Student's *t*-test for comparison of *CyO* or *actin-Gal4* siblings with *GFP* shRNA. (B) Validation of specificity for *dom-A* and *dom-B* shRNA knockdowns. *UAS-shRNA* males for *GFP*, *dom-1*, *dom-A* and *dom-B* were crossed with *elav-Gal4* females. F1 offspring larval brains are probed with DOA1 and DOB2 antibodies in western blot. Lamin and ISWI signals provided controls. (C-H) Validation of specificity of *dom-A* and *dom-B* shRNA knockdowns using transgenic *dom* fosmids. GFP-tagged *dom* transgenes are combined with *dom-1*, *dom-A* and *dom-B* shRNA constructs and the somatic follicle cell-specific driver *traffic jam-Gal4*. Representative immunofluorescence images of nurse and follicle cells with staining of GFP (green) and DNA (blue) are shown. Scale bars: 10 µm. See also Fig. S2. (I) Quantification of GFP signals in follicle cells of egg chambers. Corrected total cell fluorescence of GFP was calculated for ten follicle cells. Mean values with s.d. of three biological replicates are shown. Two-tailed Student's *t*-test for comparison of *dom-1*, *dom-A* or *dom-B* shRNA with control. ***P*<0.01, ****P*<0.001, *****P*<0.0001; n.s., not significant.

they differ in their requirements: DOM-A is essential for early germline development, whereas DOM-B is crucial for egg chamber development at later stages of oogenesis.

Loss of DOM-A or DOM-B in germline cells outside of the germarium leads to a 'dumpless' egg phenotype

DOM-B was required in germline cells for proper egg chamber development. The abundant defects in the germarium upon DOM-A depletion precluded the assessment of a similar role during later stages of oogenesis. Therefore, we combined the *matα4-Gal4* driver, which is specifically expressed in the germline from stage 1 egg chambers onwards (Fig. 4A) (Yan et al., 2014), with different *dom*, *H2A.V* and *Tip60* shRNAs and stained for Vasa and the cytoplasmic oocyte marker ORB. Notably, *matα4-Gal4*-directed knockdown did not affect the development of germarium and ovariole, but resulted in defective late egg chambers with short eggs and non-fragmented nurse cells characteristic of the 'dumpless' egg phenotype (Fig. 4B-G). Interestingly, individual loss of either DOM isoform or TIP60 led to 'dumpless' eggs comparable to DOM or H2A.V depletion (Fig. 4H,I) and accordingly to significantly reduced egg laying (Fig. 4J,K). We conclude that both DOM isoforms are required in germline cells outside of the germarium for egg chamber formation.

Development (2016) 143, 3154-3167 doi:10.1242/dev.139634

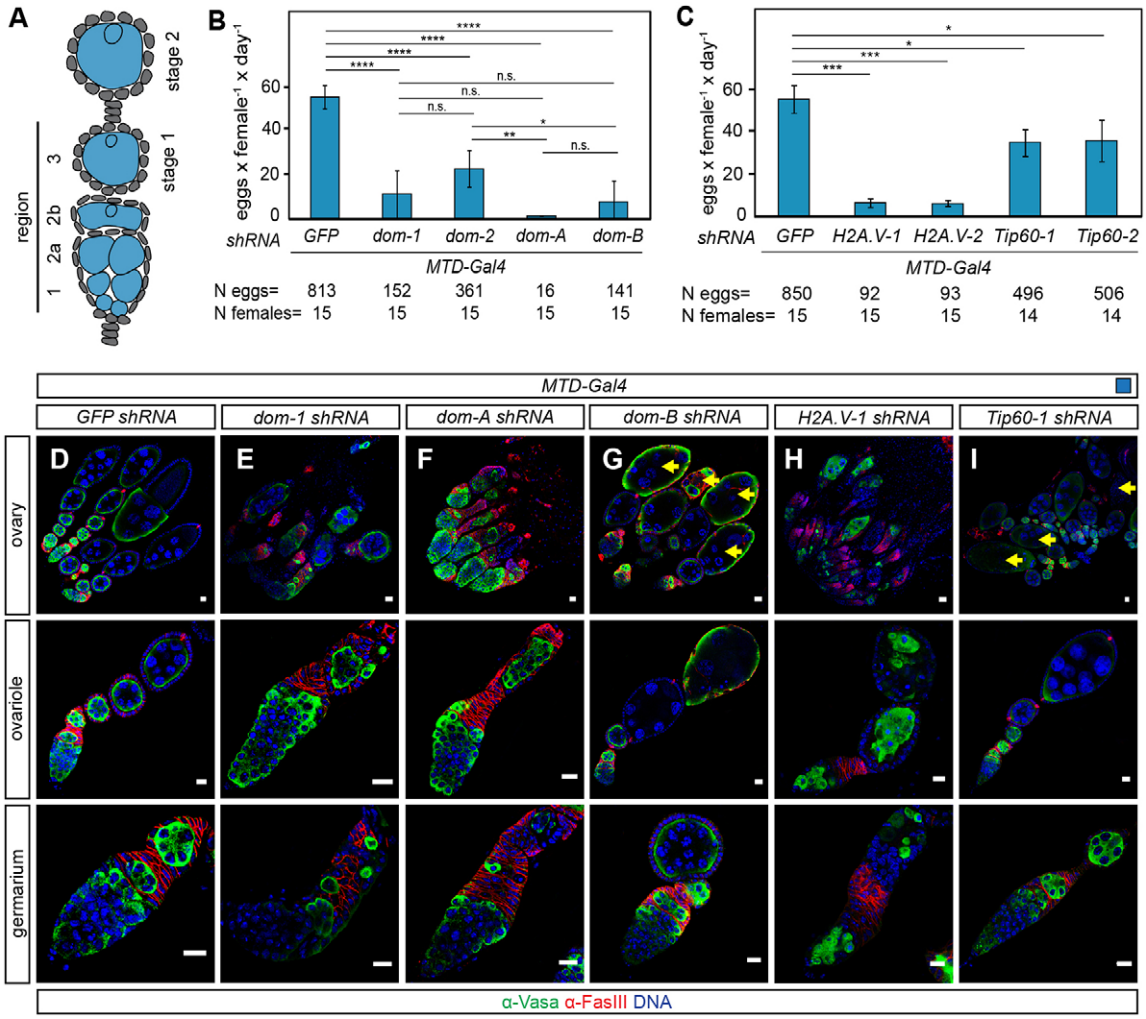

Fig. 3. Loss of DOM-A in germline cells leads to early cystoblast defects, while loss of DOM-B generates defective late egg chambers. (A) Diagram of the early stages of *D. melanogaster* oogenesis. The specific expression pattern of the *MTD-Gal4* driver in germline cells is highlighted in blue. (B,C) Quantification of egg laying capacity. The data show mean values of eggs laid per female per day with s.d. of three biological replicates. *N* eggs represents the total number of scored eggs and *N* females the total number of analyzed females. **P*<0.05, ***P*<0.01, ****P*<0.001, *****P*<0.0001; n.s., not significant. Two-tailed Student's *t*-test. (D-I) Immunofluorescence images of ovary, ovariole and germarium with staining of Vasa (green), Fasciclin III (red) and DNA (blue) for the following genotypes: *MTD-Gal4* with (D) *GFP*, (E) *dom-1*, (F) *dom-A*, (G) *dom-B*, (H) *H2A.V-1* and (I) *Tip60-1* shRNA. Arrows indicate defective late egg chambers. Scale bars: 10 µm.

Loss of DOM-A or DOM-B in somatic follicle cells leads to severe packaging defects

DOM function is not only required in the germline but is also essential for somatic follicle cell development (Xi and Xie, 2005). To address whether both DOM isoforms are also required for follicle cell function, we used the *traffic jam-Gal4* driver (Fig. 5G) in combination with different shRNAs. We scored severe packaging phenotypes upon DOM, DOM-A, DOM-B, TIP60 or H2A.V depletion, ranging from two cysts in a single egg chamber to complete ovariole fusions (Fig. 5A-F). Furthermore, many germaria showed additional stalk-like structures without germline cysts (Fig. 5H-K), indicating defects in the coordination of follicle cell proliferation with cyst differentiation. Remarkably, we observed egg chambers with abnormal cyst numbers ranging from one to more than 16 cells (Fig. 5A-F), suggesting a soma-dependent proliferation defect in the germline. Defective late egg chambers showed signals for activated Caspase 3 (Fig. 5L-O). As a result, egg laying capacity was drastically impaired (Fig. 5P). We validated packaging phenotypes and sterility with another somatic driver line, *c587-Gal4*, which is expressed in somatic escort cells and early follicle cells in the germarium (Fig. S5) (Eliazer et al., 2011; Kai and Spradling, 2003). We conclude that DOM-A and DOM-B function is crucial in somatic follicle cells for the proper packaging of egg chambers.

DOM-B promotes global H2A.V incorporation into germline chromatin of the germarium

In order to explore the roles of DOM isoforms in H2A.V incorporation into chromatin and in γH2A.V turnover *in vivo*, we raised a specific polyclonal antibody against an H2A.V peptide. We found H2A.V to be ubiquitously expressed in somatic and germline cells of the germarium with a notable enrichment in GSCs (Fig. 6A,B). Remarkably, H2A.V and γH2A.V signals were only detected in nurse cells up to stage 5 of oogenesis (Fig. 6C), and both signals were absent in later nurse cell nuclei (Fig. 6D). However, H2A.V was present in the surrounding follicle cells at all stages, providing convenient staining controls (Fig. 6A-D). These observations are in general agreement with previous studies (Joyce

Development (2016) 143, 3154-3167 doi:10.1242/dev.139634

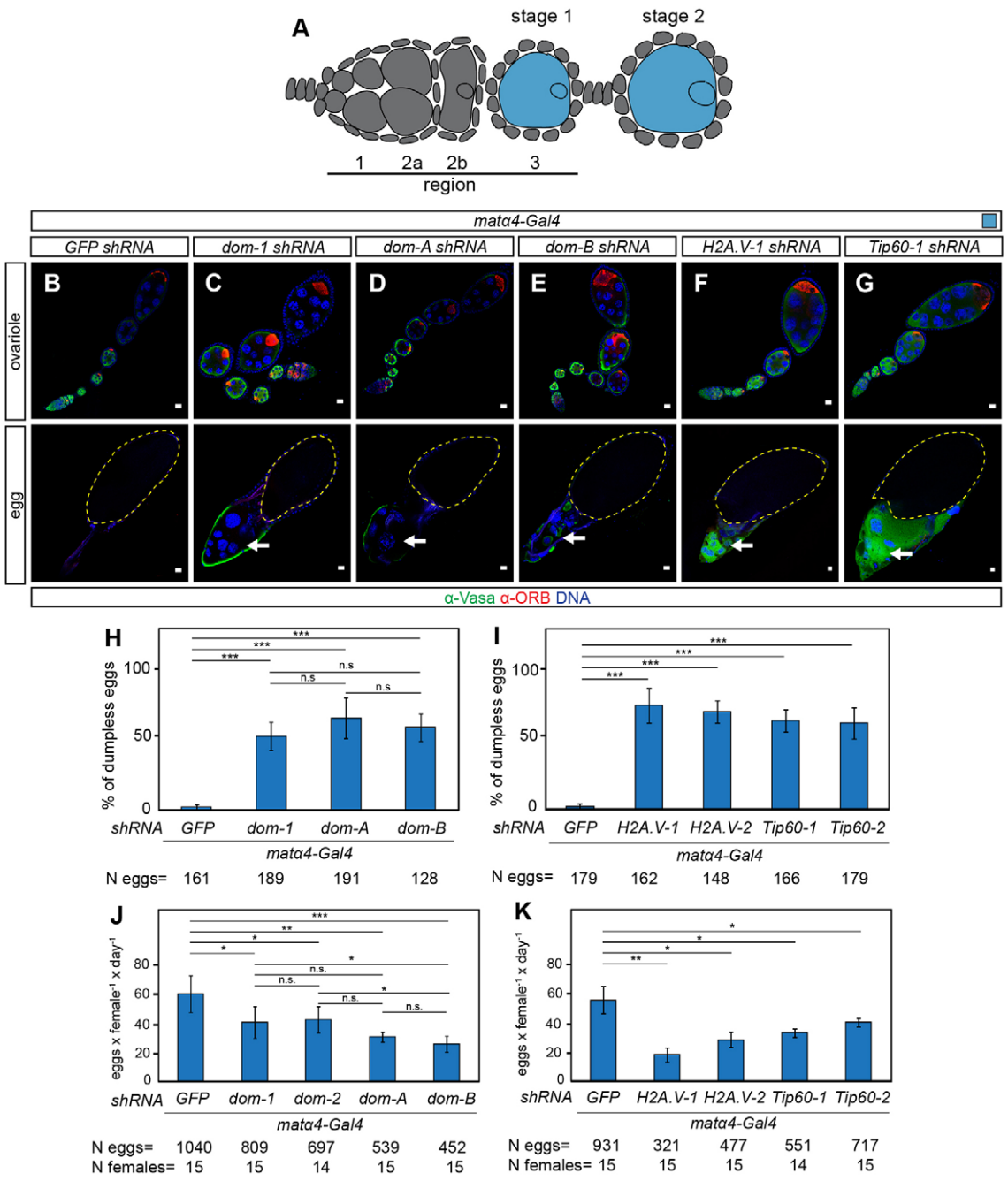

Fig. 4. Loss of DOM in germline cells outside the germarium leads to a 'dumpless' egg phenotype. (A) Diagram of the early stages of *D. melanogaster* oogenesis. The specific expression pattern of the *matα4-Gal4* driver in germline cells from stage 1 of oogenesis is highlighted in blue. (B-G) Immunofluorescence images of ovariole and egg with staining of Vasa (green), ORB (red) and DNA (blue) for the following genotypes: *matα4-Gal4* with (B) *GFP*, (C) *dom-1*, (D) *dom-A*, (E) *dom-B*, (F) *H2A.V-1* and (G) *Tip60-1* shRNA. Arrow indicates the anterior end of the egg chamber with non-fragmented nurse cells. Yellow dashed line indicates posterior egg. Scale bars: 10 µm. (H,I) Quantification of the 'dumpless' egg phenotype. The data show mean values in percentage with s.d. of three biological replicates. *N* eggs represents the total number of scored eggs. (J,K) Quantification of egg laying capacity. The data show mean values of eggs laid per female per day with s.d. of three biological replicates. *N* eggs represents the total number of scored eggs and *N* females the total number of analyzed females. **P*<0.05, ***P*<0.01, ****P*<0.001; n.s., not significant. Two-tailed Student's *t*-test.

et al., 2011), except that we did not detect signals for H2A.V in oocytes, possibly owing to differences in H2A.V epitope sequence.

Upon depletion of DOM and DOM-B with *MTD-Gal4* we found that H2A.V was lost specifically in germline cells of the germarium (Fig. 6F,H,L,M). H2A.V was essentially absent since the signals were comparable to those of *H2A.V* shRNA (Fig. 6I,L,M). As a control, levels of H2A.V were unaltered in somatic follicle cells, documenting the germline specificity of the effect (Fig. 6E-M). In remarkable contrast, loss of DOM-A or TIP60 did not affect levels of H2A.V (Fig. 6G,K-M). Likewise, depletion of ISWI ATPase, which causes similar germline phenotypes (Ables and Drummond-Barbosa, 2010; Xi and Xie, 2005; Yan et al., 2014), did not affect H2A.V levels (Fig. 6J,L,M). We conclude that DOM-B, but not DOM-A, is required for global incorporation of H2A.V into germline chromatin of the germarium.

Development (2016) 143, 3154-3167 doi:10.1242/dev.139634

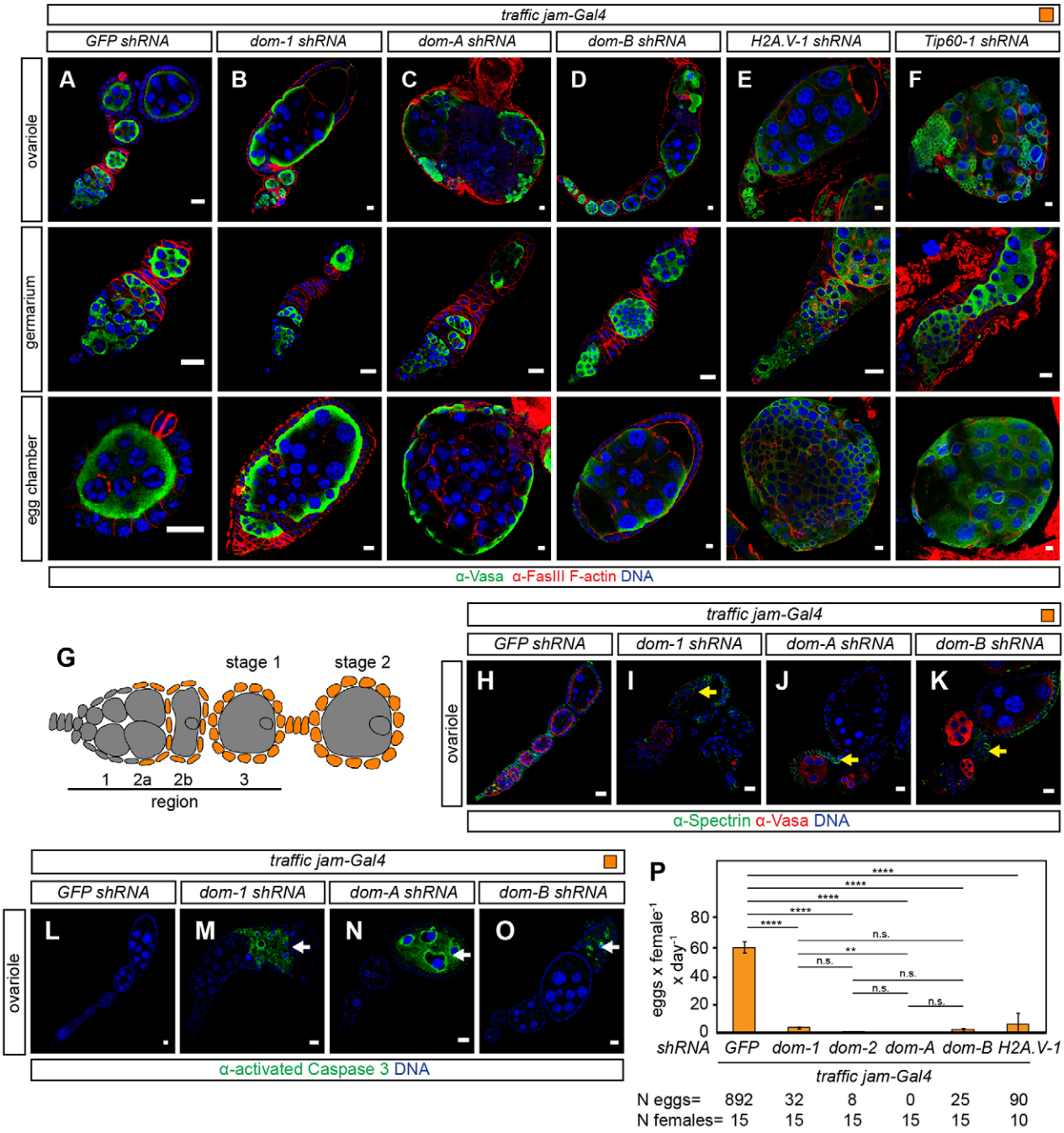

Fig. 5. Loss of DOM-A or DOM-B in somatic follicle cells leads to severe packaging defects. (A-F) Immunofluorescence images of ovariole, germarium and egg chamber with staining of Vasa (green), Fasciclin III and F-actin (red) and DNA (blue) for the following genotypes: *traffic jam-Gal4* with (A) *GFP*, (B) *dom-1*, (C) *dom-A*, (D) *dom-B*, (E) *H2A.V-1* and (F) *Tip60-1* shRNA. (G) Diagram of the early stages of *D. melanogaster* oogenesis. The specific expression pattern of the *traffic jam-Gal4* driver in somatic follicle cells is highlighted in orange. (H-K) Immunofluorescence images of ovarioles with staining of Spectrin (green), Vasa (red) and DNA (blue) for the following genotypes: *traffic jam-Gal4* with (H) *GFP*, (I) *dom-1*, (J) *dom-A* and (K) *dom-B* shRNA. Arrows indicate stalk-like structures. (L-O) Immunofluorescence images of ovarioles with staining of activated Caspase 3 (green) and DNA (blue) for the following genotypes: *traffic jam-Gal4* with (L) *GFP*, (M) *dom-1*, (N) *dom-A* and (O) *dom-B* shRNA. Arrows indicate apoptotic egg chambers. (P) Quantification of egg laying capacity. The data show mean values of eggs laid per female per day with s.d. of three biological replicates. *N* eggs represents the total number of scored eggs and *N* females the total number of analyzed females. ***P*<0.01, *****P*<0.0001; n.s., not significant. Two-tailed Student's *t*-test. Scale bars: 10 µm.

DOM-independent H2A.V incorporation in germline nurse cells

To monitor H2A.V levels in germline cells outside of the germarium we again employed the *matα4-Gal4* driver, which is specifically expressed from stage 1 of oogenesis onwards (Fig. 4A and Fig. S6) (Yan et al., 2014). As expected, *matα4-Gal4*-directed knockdown of DOM, DOM-A and DOM-B did not affect H2A.V levels in the germarium (Figs S7, S8). As a control, *H2A.V* shRNA knockdown specifically depleted H2A.V and γH2A.V in germline nurse cells of stage 3 egg chambers (Fig. 7A,E,G). Surprisingly, however, H2A.V and γH2A.V were unaltered in germline nurse cells up to stage 4 egg chambers upon DOM, DOM-A, DOM-B or TIP60 knockdown (Fig. 7B-D,F,G and Figs S7, S8). Notably,

Development (2016) 143, 3154-3167 doi:10.1242/dev.139634

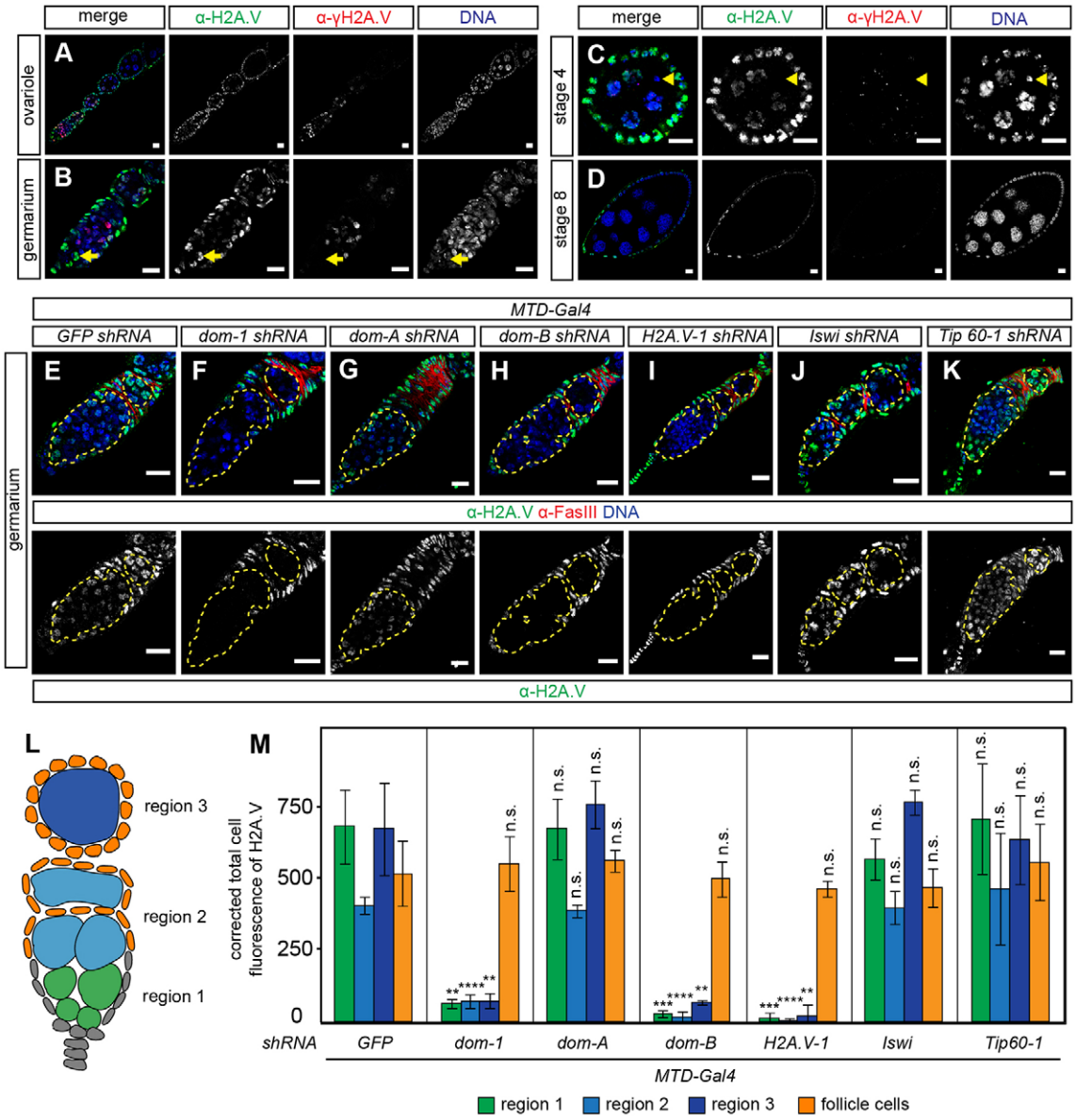

Fig. 6. DOM-B promotes global H2A.V incorporation into germline chromatin of the germarium. (A-D) Immunofluorescence images of ovariole, germarium, stage 4 and stage 8 egg chambers with staining of H2A.V (green), γH2A.V (red) and DNA (blue) for wild type. Arrows and arrowheads indicate GSCs and oocytes, respectively. (E-K) Immunofluorescence images of ovariole with staining of H2A.V (green), Fasciclin III (red) and DNA (blue) for the following genotypes: *MTD-Gal4* with (E) *GFP*, (F) *dom-1*, (G) *dom-A*, (H) *dom-B*, (I) *H2A.V-1*, (J) *Iswi* and (K) *Tip60-1* shRNA. Yellow dashed line indicates germline cells. (L) Diagram of *D. melanogaster* germarium. Green, light and dark blue indicate region 1, 2 and 3 of the germarium, respectively, as used for H2A.V signal quantification in M. (M) Quantification of H2A.V signals in germline and somatic cells of the germarium. Corrected total cell fluorescence of H2A.V was calculated for 30 germline cysts in different regions of the germarium and follicle cells, respectively. Mean values with s.d. of three biological replicates are shown. ***P*<0.01, ****P*<0.001, *****P*<0.0001; n.s., not significant. Two-tailed Student's *t*-test for comparison with *GFP* shRNA. Scale bars: 10 µm.

corresponding depletion of another SWI/SNF remodeler, INO80, with two different *Ino80* shRNAs (Bhatia et al., 2010; Yan et al., 2014) did not affect H2A.V localization in ovarioles (Fig. S9). This suggests that global H2A.V incorporation into germline chromatin at stage 3 might be independent of DOM.

Involvement of DOM-A/TIP60 in H2A.V eviction in germline cells from stage 5 onwards

We next assessed how depletion of individual DOM isoforms affects global H2A.V and γH2A.V in nurse cells of later egg chamber stages. Remarkably, H2A.V and γH2A.V signals persisted in stage 8 egg chambers upon DOM or DOM-A depletion (Fig. 8B,C,H,I,M and Figs S7, S8). Additionally, a moderate but significant increase of H2A.V as well as γH2A.V foci was detected upon TIP60 depletion (Fig. 8F,L,M). By contrast, H2A.V was removed in the absence of DOM-B as in wild-type ovarioles (Fig. 8A,D,G,J,M and Figs S7, S8). Evidently, DOM-A/TIP60 are specifically involved in removing H2A.V from germline cells by stage 5 of oogenesis, illustrating once more the functional diversification of the two splice variants.

DOM-B promotes global H2A.V incorporation into dividing follicle cell chromatin

To address whether other cell types also utilize DOM for H2A.V incorporation, we used the somatic driver *traffic jam-Gal4* for knockdown in follicle cells. As in germline cells of the germarium,

Development (2016) 143, 3154-3167 doi:10.1242/dev.139634

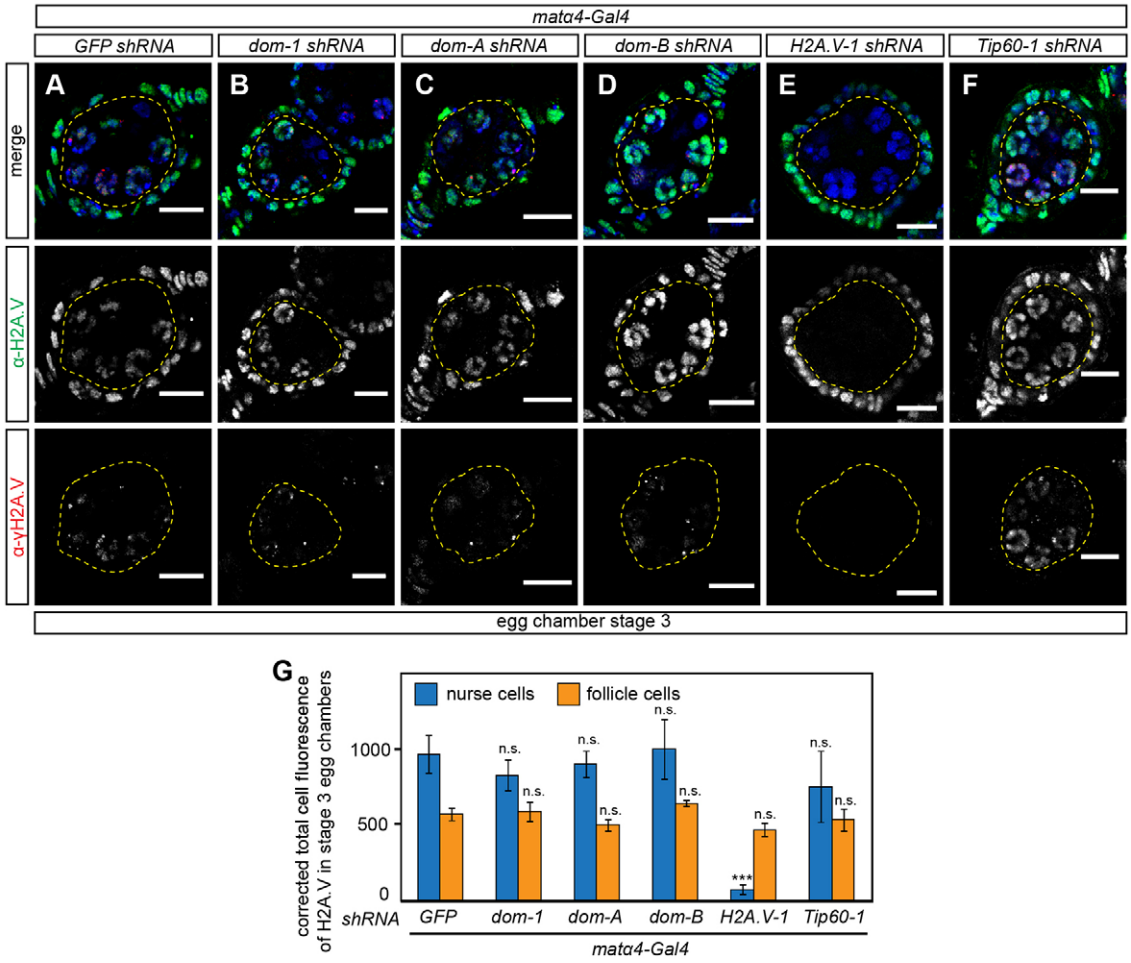

Fig. 7. DOM-independent H2A.V incorporation in germline nurse cells. (A-F) Immunofluorescence images of egg chambers with staining of H2A.V (green), γH2A.V (red) and DNA (blue) for the following genotypes: *matα4-Gal4* with (A) *GFP*, (B) *dom-1*, (C) *dom-A*, (D) *dom-B*, (E) *H2A.V-1* and (F) *Tip60-1* shRNA. Yellow dashed line indicates germline nurse cells. Scale bars: 10 µm. (G) Quantification of H2A.V signals in nurse and follicle cells of stage 3 egg chambers. Corrected total cell fluorescence of H2A.V was calculated for 50 germline nurse cells and 50 somatic follicle cells. Mean values with s.d. of three biological replicates are shown. ***P<0.001; n.s., not significant. Two-tailed Student's *t*-test for comparison with *GFP* shRNA.

we observed that depletion of DOM and DOM-B led to complete absence of H2A.V signals in follicle cell nuclei (Fig. 9A,B,D,H,I), when compared with the corresponding H2A.V knockdown (Fig. 9E,H,I). As before, *dom-A* and *Tip60* shRNAs did not affect H2A.V levels in follicle cells (Fig. 9C,G,H,I) and neither did depletion of ISWI (Fig. 9F,H,I), which causes similar packaging phenotypes (Börner et al., 2016). Furthermore, canonical histone H2A (Fig. 9J,K) and heterochromatin-associated HP1 protein (Fig. 9L,M) were unaltered upon DOM depletion, indicating a globally intact chromatin structure in the absence of H2A.V. This finding highlights the specific requirement of the DOM-B isoform for H2A.V incorporation not only in the germline but also in dividing somatic follicle cells.

In summary, our systematic analysis showed that the nucleosome remodeling factor isoforms DOM-A and DOM-B have non-redundant functions in germline and soma in the formation of egg chambers. We further demonstrated that the two DOM isoforms have distinct functions in H2A.V exchange during *D. melanogaster* oogenesis.

DISCUSSION

In *D. melanogaster* the properties of the two ancient, ubiquitous histone H2A variants H2A.X and H2A.Z are combined in a single molecule, H2A.V (Baldi and Becker, 2013; Talbert and Henikoff, 2010). Given that H2A.V carries out functions as a DNA damage sensor and architectural element of active promoters (Madigan et al., 2002; Mavrich et al., 2008), as well as having further roles in heterochromatin formation (Chioda et al., 2010; Hanai et al., 2008; Qi et al., 2006), this histone appears loaded with regulatory potential. Accordingly, placement of the variant, either randomly along with canonical H2A during replication or more specifically through nucleosome remodeling factors, becomes a crucial determinant in its function. Mechanistic detail for replacement of H2A-H2B dimers with variants comes from the analysis of the yeast SWR1 complex, which incorporates H2A.Z in a stepwise manner at strategic positions next to promoters (Luk et al., 2010; Mizuguchi et al., 2004; Ranjan et al., 2013).

So far, the published phenotypes associated with *dom* mutant alleles have not been systematically complemented (Braun et al., 1997; Eissenberg et al., 2005; Ruhf et al., 2001). Our comprehensive complementation analysis shows that *dom* mutant phenotypes are indeed due to defects in the *dom* gene. Remarkably, *dom* lethality and sterility can be partially rescued by complementation with the orthologous human *SRCAP* gene, providing an impressive example of functional conservation of SWR1-like remodelers (Eissenberg et al., 2005). The contributions of the two splice variants DOM-A

Development (2016) 143, 3154-3167 doi:10.1242/dev.139634

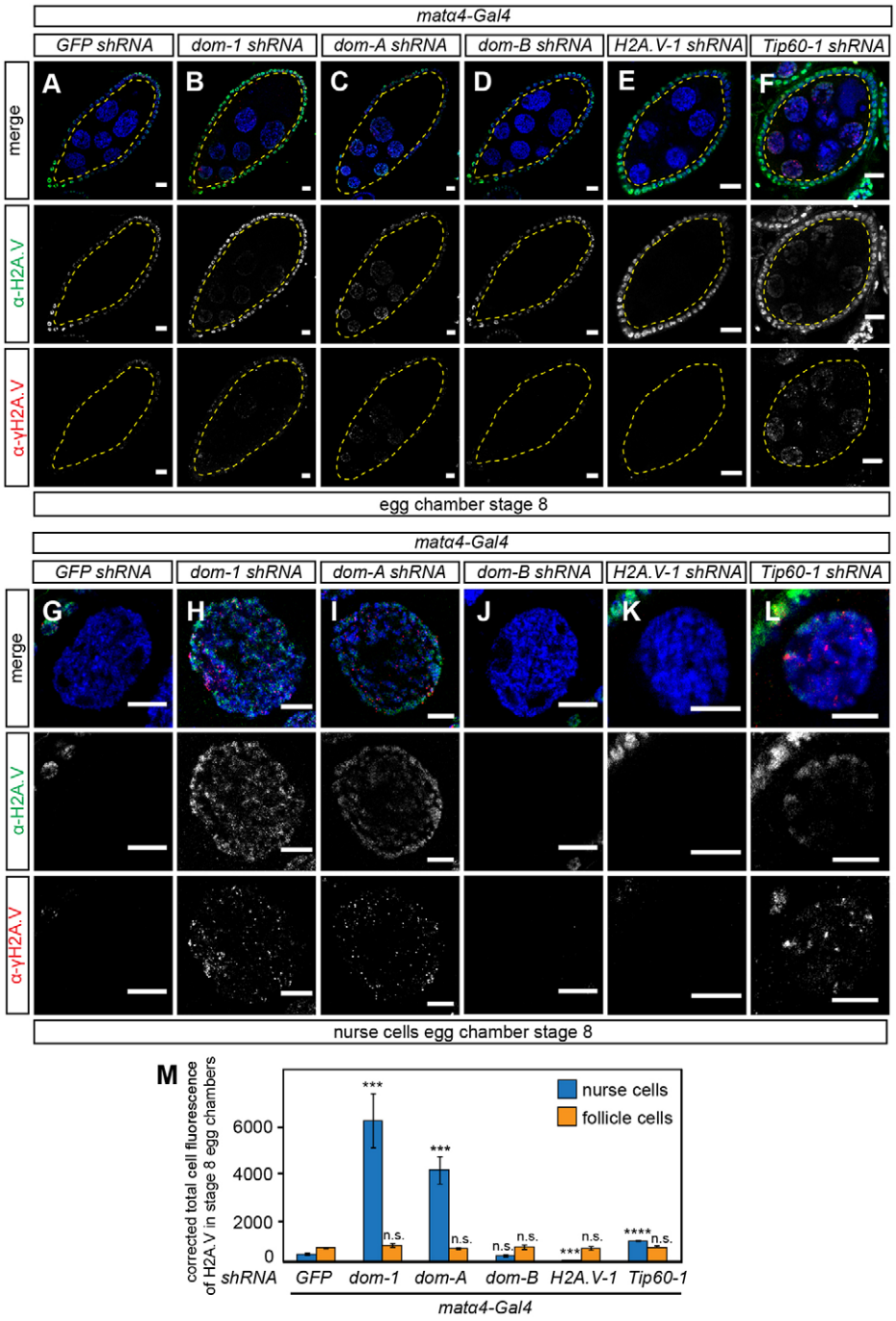

Fig. 8. Involvement of DOM-A/TIP60 in H2A.V eviction in germline cells from stage 5 onwards. (A-L) Immunofluorescence images of stage 8 egg chambers and nurse cells with staining of H2A.V (green), γH2A.V (red) and DNA (blue) for the following genotypes: *matα4-Gal4* with (A,G) *GFP*, (B,H) *dom-1*, (C,I) *dom-A*, (D,J) *dom-B*, (E,K) *H2A.V-1* and (F,L) *Tip60-1* shRNA. Yellow dashed line indicates germline nurse cells. Scale bars: 10 µm.
(M) Quantification of H2A.V persistence in germline nurse cells of stage 8 egg chambers. Corrected total cell fluorescence of H2A.V was calculated for 50 germline nurse cells and 50 somatic follicle cells. Mean values with s.d. of three biological replicates are shown. ***P<0.001, ****P<0.0001; n.s., not significant. Two-tailed Student's t-test for comparison with *GFP* shRNA.

and DOM-B had not been assessed. We now demonstrate that both isoforms are essential for development, suggesting non-redundant functions. The DOM-A isoform contains a SANT domain followed by several poly-Q stretches, which are widely found in transcriptional regulators, where they may modulate protein interactions (Gemayel et al., 2015). By contrast, SANT domains are thought to function as histone tail interaction modules that couple binding to enzyme catalysis (Boyer et al., 2004). Therefore, the SANT domain in DOM-A could mediate specificity towards H2A.V eviction depending on particular functional contexts. These features are also present in the C-terminus of p400 (EP400), the second human SWR1 ortholog, but are absent in either DOM-B or SRCAP (Eissenberg et al., 2005). Remarkably, p400 interacts directly with TIP60 (Jha et al., 2013) and the SANT domain of p400 inhibits TIP60 catalytic activity (Park et al., 2010), providing an interesting lead for further investigation of DOM isoforms and TIP60 interactions.

We speculate that distinct functions of p400 and SRCAP in humans might be accommodated to some extent by the two DOM isoforms in flies. Accordingly, it will be interesting to explore whether the two isoforms reside in distinct complexes. Previous affinity purification of a TIP60-containing complex using a tagged pontin subunit apparently only identified DOM-A, but not DOM-B (Kusch et al., 2004). Following up on the initial observation of early defects in GSCs and cyst differentiation upon loss of DOM (Yan et al., 2014), we now find that this phenotype is exclusively caused by loss of DOM-A. Interestingly, studies with human embryonic stem cells show that p400/TIP60 (KAT5) integrates pluripotency

Development (2016) 143, 3154-3167 doi:10.1242/dev.139634

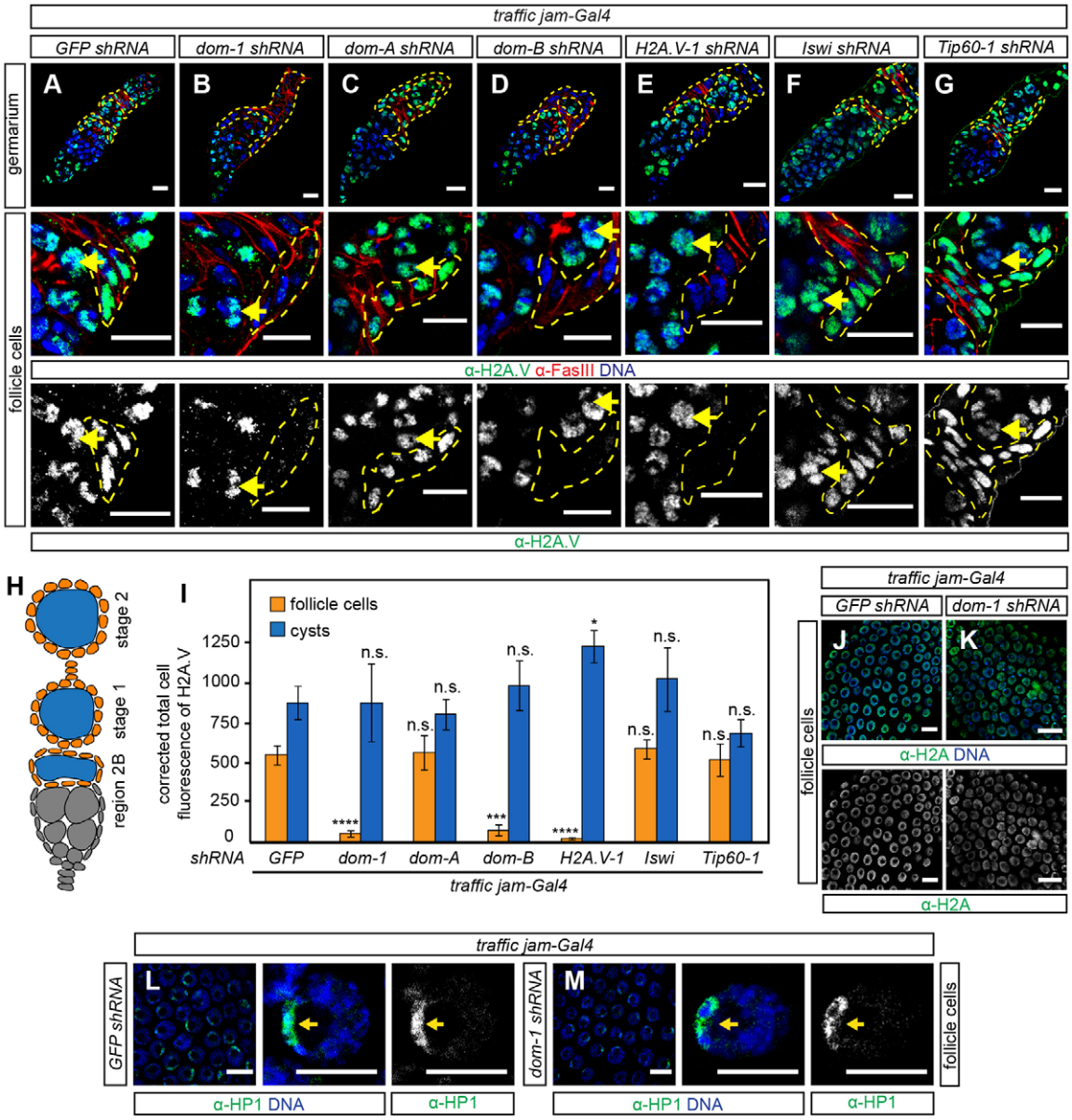

Fig. 9. DOM-B promotes global H2A.V incorporation into somatic follicle cell chromatin. (A-G) Immunofluorescence images of germarium with staining of H2A.V (green), Fasciclin III and F-actin (red) and DNA (blue) for the following genotypes: *traffic jam-Gal4* with (A) *GFP*, (B) *dom-1*, (C) *dom-A*, (D) *dom-B*, (E) *H2A.V-1*, (F) *Iswi* and (G) *Tip60-1* shRNA. Yellow dashed line indicates somatic follicle cells. Arrows indicate germline cysts. (H) Diagram of the early stages of *D. melanogaster* oogenesis. Orange and blue indicate follicle cells and cysts, respectively, as used for H2A.V signal quantification in I. (I) Quantification of H2A.V signals in somatic and germline cells. Corrected total cell fluorescence of H2A.V was calculated for 30 somatic follicle cells and 30 cysts. Mean values with s.d. of three biological replicates are shown. **P*<0.05, ****P*<0.001, *****P*<0.0001; n.s., not significant. Two-tailed Student's *t*-test for comparison with *GFP* shRNA. (J,K) Immunofluorescence images of follicle cells with staining of H2A (green) and DNA (blue) for the following genotypes: *traffic jam-Gal4* with (J) *GFP* and (K) *dom-1* shRNA. (L,M) Immunofluorescence images of follicle cells with staining of HP1 (green) and DNA (blue) for the following genotypes: *traffic jam-Gal4* with (L) *GFP* and (M) *dom-1* shRNA. Arrows indicate heterochromatic domain. Scale bars: 10 µm.

signals to regulate gene expression (Chen et al., 2013; Fazzio et al., 2008), suggesting similar roles for DOM-A in GSCs. This is in contrast to requirements for both isoforms for germline development outside of the germarium, highlighting a developmental specialization of the two DOM remodelers.

DOM is also involved in the differentiation and function of SSCs in the germarium (Xi and Xie, 2005). Our data now document non-redundant requirements of both DOM isoforms in somatic cells for proper coordination of follicle cell proliferation with cyst differentiation. Failure to adjust these two processes leads to 16-cell cyst packaging defects that manifest as compound egg chambers. These rare phenotypes had previously only been described upon perturbation of some signaling pathways, such as Notch, or Polycomb regulation (Jackson and Blochlinger, 1997; Narbonne et al., 2004).

Because the phenotypes of DOM depletions resemble those of H2A.V depletion we favor the idea that many of the cell-specification defects are due to compromised H2A.V incorporation, depriving key promoters of the H2A.Z-related architectural function. Alternatively, scaffolding activities might partially explain some roles of chromatin remodelers, as suggested for SRCAP (Bowman et al., 2011). So far, our knowledge of the

Development (2016) 143, 3154-3167 doi:10.1242/dev.139634

mechanisms of H2A.V incorporation has been anecdotal (Joyce et al., 2011; Kusch et al., 2014; Lu et al., 2007). Our comprehensive analysis revealed a specific involvement of DOM-B for the incorporation of H2A.V into chromatin at the global level. The N-termini of SWR1 and DOM-B harbor the HSA and ATPase spacer domains (Morrison and Shen, 2009), with interaction surfaces for further complex subunits (Billon and Côté, 2012; Gerhold and Gasser, 2014), and an additional H2A.Z-H2B dimer binding site (Wu et al., 2005, 2009). Given the requirement for both isoforms for cell specification during oogenesis, we speculate that DOM-B might serve to incorporate bulk H2A.V into chromatin similar to SWR1, whereas DOM-A would be more involved in the regulatory refinement of location.

Although the failures in cell specification and egg morphogenesis are likely to be explained by loss of the H2A.Z-related features of H2A.V, ablation of DOM might also compromise the DNA damage response, which involves phosphorylation of H2A.V (γH2A.V). Conceivably, the role of γH2A.V as a DNA damage sensor might be best fulfilled by a broad distribution of H2A.V throughout the chromatin (Baldi and Becker, 2013). Such an untargeted incorporation may be achieved by stochastic, chaperone-mediated incorporation during replication (Li et al., 2012) or by an untargeted activity of DOM-B. We observed DOM-independent incorporation in endoreplicating polyploid nurse cells of stage 3 egg chambers, where global H2A.V and γH2A.V signals did not depend on DOM. Immunofluorescence microscopy may lack the sensitivity to detect DOM-dependent incorporation of H2A.V at some specific sites. Nevertheless, DOM-independent incorporation of H2A.V might serve to cope with many naturally occurring DNA double-strand breaks during the massive endoreplication of nurse cells.

There is some evidence that nucleosome remodelers not only incorporate H2A variants but can also remove them. In yeast, the genome-wide distribution of H2A.Z appears to be established by the antagonistic functions of the SWR1 and Ino80 remodeling complexes, where Ino80 replaces stray H2A.Z-H2B with canonical H2A-H2B dimers (Papamichos-Chronakis et al., 2011). A recent study identified the vertebrate-specific histone chaperone ANP32E as part of a TIP60/p400 complex that facilitates the eviction of H2A.Z-H2B dimers from chromatin (Obri et al., 2014). Remarkably, in *D. melanogaster* a TIP60/DOM-A complex is involved in a similar reaction. The TIP60/DOM-A complex acetylates γH2A.V at lysine 5 to facilitate exchange of γH2A.V by unmodified H2A.V during the DNA damage response (Kusch et al., 2004). Furthermore, it has been speculated that H2A.V and γH2A.V could be actively removed from nurse cells, since corresponding signals are absent from stage 5 onwards (Jang et al., 2003; Joyce et al., 2011). We now demonstrate that depletion of DOM-A and TIP60 leads to the persistence of H2A.V and γH2A.V in nurse cells of late egg chambers, clearly documenting the ability of the remodeler to remove bulk H2A.V and variants modified during DNA damage induction.

Our findings highlight the specific requirements of DOM splice variants for the incorporation and removal of H2A.V during *D. melanogaster* oogenesis. It remains an interesting and challenging question how DOM-A and DOM-B complexes are targeted genome-wide and function *in vivo* to establish specific H2A.V patterns in different cell types during development.

MATERIALS AND METHODS

D. melanogaster strains and genetics

The genomic region of *dom* was modified by recombineering in *Escherichia coli* using pRedFLP4 recombination technology (Ejsmont et al., 2009). Details are provided in the supplementary Materials and Methods and in Tables S1 and S2. All fosmid, *UAS-shRNA* and *Gal4* driver lines are listed in the supplementary Materials and Methods. For ovary analysis, *UAS-shRNA* males were crossed with *Gal4* driver virgins at 29°C and 5- to 7-day-old F1 females were used, unless stated otherwise.

Complementation assays

Males and female virgins of dom^{1}/*bcg*; *dom* fosmid/+ or of dom^{9}/*bcg*; *dom* fosmid/+ genotype were crossed. F1 offspring were analyzed for *bcg* phenotype and rescue of pupal lethality was determined as percentage of observed to expected frequency of homozygous dom^{1} or dom^{9} offspring. Mean values in percentage with s.d. from three biological replicates were calculated.

Necrotic lymph glands were scored in third instar larvae of homozygous w^{1118}, dom^{1}, dom^{1};*GFP-dom*, dom^{1};*dom-A-GFP* and dom^{1};*dom-B-GFP*. Mean values in percentage with s.d. from three biological replicates were calculated.

Homozygous female virgins for w^{1118}, dom^{9}, dom^{9};*GFP-dom*, dom^{9};*dom-A-GFP*, dom^{9};*dom-B-GFP* and dom^{9};Δ*dom-GFP* were collected for 2-3 days at 25°C. Females of each genotype were mated with w^{1118} males in vials with yeast paste for 2 days. Females were placed in individual vials for 3 days without males and the egg laying capacity determined as the number of eggs laid per female per day. The data were averaged and mean values with s.d. from three biological replicates calculated.

Pupal hatching assay

UAS-shRNA males for *GFP*, *dom-1*, *dom-A* and *dom-B* were crossed with *actin-Gal4*/*CyO* driver virgins at 25°C. Pupae were transferred to new vials and numbered. A 1:1 ratio of *CyO* and *actin-Gal4* F1 siblings was expected. *CyO* phenotype was counted and pupal hatching was determined as the observed to expected frequency of *CyO* and *actin-Gal4* F1 siblings. Mean values in percentage with s.d. from three biological replicates were calculated.

Egg laying assay

Homozygous *UAS-shRNA* males for *GFP*, *dom-1*, *dom-2*, *dom-A* and *dom-B* were crossed with *MTD-*, *matα4-*, *c587-* or *traffic jam-Gal4* driver virgins at 29°C. F1 female virgins of each genotype (2-3 days old) were mated with w^{1118} males in vials with yeast paste for 2 days. Females were then placed in individual vials without males and the egg laying capacity determined as described above.

Analysis of wing phenotypes

UAS-shRNA males for *GFP*, *dom-1*, *dom-2*, *dom-A* and *dom-B* were crossed with *C96-Gal4* driver virgins at 29°C. Wing phenotypes were scored in F1 offspring and relative mean values in percentages with s.d. from three biological replicates were calculated.

Generation of DOA1, DOB2 and H2A.V antibodies

DOA1, DOB2 and H2A.V antibodies were made for this study as described in the supplementary Materials and Methods.

Immunological techniques and microscopy

Immunofluorescence microscopy was performed using standard procedures and a Leica TCS SP5 II confocal microscope. Images were processed using ImageJ (NIH) and Adobe Photoshop. For details, including the antibodies used, see the supplementary Materials and Methods.

Western blot

Twelve pairs of ovaries or 20 brains of third instar larvae were dissected, homogenized in Laemmli buffer and incubated at 95°C for 5 min. Western blot was performed using standard procedures; antibodies are listed in the supplementary Materials and Methods.

Statistical test

Two-tailed Student's *t*-test was used. *P*-values are given in the figure legends.

Acknowledgements
Some stocks were obtained from the Bloomington Drosophila Stock Center [NIH P40OD018537]. We thank the TRiP at Harvard Medical School [NIH/NIGMS R01-GM084947] for transgenic RNAi fly lines. The monoclonal antibodies ORB 4H8 and 6H4, 7G10 anti-Fasciclin III, Spectrin 3A9 (323 or M10-2), HP1 C1A9 and UNC93-5.2.1 were obtained from the Developmental Studies Hybridoma Bank. We thank A. Eberharter, J.-R. Huynh, J. Jiang, E. Kremmer, J. Müller, H. Saumweber, A. Spradling and P. Tomancak for providing reagents; and S. Baldi, D. Jain, N. Steffen and S. Vengadasalam for stimulating discussions.

Competing interests
The authors declare no competing or financial interests.

Author contributions
K.B. performed experiments; K.B. and P.B.B. developed concepts and approaches, analyzed data and prepared the manuscript.

Funding
This work was supported by the Deutsche Forschungsgemeinschaft [grants Be1140/7-1 and SFB1064/A01].

Supplementary information
Supplementary information available online at
http://dev.biologists.org/lookup/doi/10.1242/dev.139634.supplemental

References

Ables, E. T. and Drummond-Barbosa, D. (2010). The steroid hormone ecdysone functions with intrinsic chromatin remodeling factors to control female germline stem cells in Drosophila. *Cell Stem Cell* **7**, 581-592.
Baldi, S. and Becker, P. B. (2013). The variant histone H2A.V of Drosophila-three roles, two guises. *Chromosoma* **122**, 245-258.
Bhatia, S., Pawar, H., Dasari, V., Mishra, R. K., Chandrashekaran, S. and Brahmachari, V. (2010). Chromatin remodeling protein INO80 has a role in regulation of homeotic gene expression in Drosophila. *Genes Cells* **15**, 725-735.
Billon, P. and Côté, J. (2012). Precise deposition of histone H2A.Z in chromatin for genome expression and maintenance. *Biochim. Biophys. Acta-Gene Regul. Mech.* **1819**, 290-302.
Bönisch, C. and Hake, S. B. (2012). Histone H2A variants in nucleosomes and chromatin: more or less stable? *Nucleic Acids Res.* **40**, 10719-10741.
Börner, K., Jain, D., Vazquez-Pianzola, P., Vengadasalam, S., Steffen, N., Fyodorov, D. V., Tomancak, P., Konev, A., Suter, B. and Becker, P. B. (2016). A role for tuned levels of nucleosome remodeler subunit ACF1 during Drosophila oogenesis. *Dev. Biol.* **411**, 217-230.
Bowman, T. A., Wong, M. M., Cox, L. K., Baldassare, J. J. and Chrivia, J. C. (2011). Loss of H2A.Z is not sufficient to determine transcriptional activity of Snf2-related CBP activator protein or p400 complexes. *Int. J. Cell Biol.* **2011**, 715642.
Boyer, L. A., Latek, R. R. and Peterson, C. L. (2004). The SANT domain: a unique histone-tail-binding module? *Nat. Rev. Mol. Cell Biol.* **5**, 158-163.
Braun, A., Lemaitre, B., Lanot, R., Zachary, D. and Meister, M. (1997). Drosophila immunity: analysis of larval hemocytes by P-element-mediated enhancer trap. *Genetics* **147**, 623-634.
Braun, A., Hoffmann, J. A. and Meister, M. (1998). Analysis of the Drosophila host defense in domino mutant larvae, which are devoid of hemocytes. *Proc. Natl. Acad. Sci. USA* **95**, 14337-14342.
Cai, Y., Jin, J., Florens, L., Swanson, S. K., Kusch, T., Li, B., Workman, J. L., Washburn, M. P., Conaway, R. C. and Conaway, J. W. (2005). The mammalian YL1 protein is a shared subunit of the TRRAP/TIP60 histone acetyltransferase and SRCAP complexes. *J. Biol. Chem.* **280**, 13665-13670.
Chen, P. B., Hung, J.-H., Hickman, T. L., Coles, A. H., Carey, J. F., Weng, Z., Chu, F. and Fazzio, T. G. (2013). Hdac6 regulates Tip60-p400 function in stem cells. *Elife* **2**, e01557.
Chioda, M. and Becker, P. B. (2010). Soft skills turned into hard facts: nucleosome remodelling at developmental switches. *Heredity* **105**, 71-79.
Chioda, M., Vengadasalam, S., Kremmer, E., Eberharter, A. and Becker, P. B. (2010). Developmental role for ACF1-containing nucleosome remodellers in chromatin organisation. *Development* **137**, 3513-3522.
Eissenberg, J. C., Wong, M. and Chrivia, J. C. (2005). Human SRCAP and Drosophila melanogaster DOM are homologs that function in the notch signaling pathway. *Mol. Cell. Biol.* **25**, 6559-6569.
Eliazer, S., Shalaby, N. A. and Buszczak, M. (2011). Loss of lysine-specific demethylase 1 nonautonomously causes stem cell tumors in the Drosophila ovary. *Proc. Natl. Acad. Sci. USA* **108**, 7064-7069.
Ellis, K., Friedman, C. and Yedvobnick, B. (2015). Drosophila domino exhibits genetic interactions with a wide spectrum of chromatin protein-encoding loci. *PLoS ONE* **10**, e0142635.
Ejsmont, R. K., Sarov, M., Winkler, S., Lipinski, K. A. and Tomancak, P. (2009). A toolkit for high-throughput, cross-species gene engineering in Drosophila. *Nat. Methods* **6**, 435-437. .
Fazzio, T. G., Huff, J. T. and Panning, B. (2008). An RNAi screen of chromatin proteins identifies Tip60-p400 as a regulator of embryonic stem cell identity. *Cell* **134**, 162-174.
Gause, M., Eissenberg, J. C., Macrae, A. F., Dorsett, M., Misulovin, Z. and Dorsett, D. (2006). Nipped-A, the Tra1/TRRAP subunit of the Drosophila SAGA and Tip60 complexes, has multiple roles in notch signaling during wing development. *Mol. Cell. Biol.* **26**, 2347-2359.
Gemayel, R., Chavali, S., Pougach, K., Legendre, M., Zhu, B., Boeynaems, S., van der Zande, E., Gevaert, K., Rousseau, F., Schymkowitz, J. et al. (2015). Variable glutamine-rich repeats modulate transcription factor activity. *Mol. Cell* **59**, 615-627.
Gerhold, C. B. and Gasser, S. M. (2014). INO80 and SWR complexes: relating structure to function in chromatin remodeling. *Trends Cell Biol.* **24**, 1-13.
Hanai, K., Furuhashi, H., Yamamoto, T., Akasaka, K. and Hirose, S. (2008). RSF governs silent chromatin formation via histone H2Av replacement. *PLoS Genet.* **4**, e1000011.
Ho, L. and Crabtree, G. R. (2010). Chromatin remodelling during development. *Nature* **463**, 474-484.
Hudson, A. M. and Cooley, L. (2014). Methods for studying oogenesis. *Methods* **68**, 207-217.
Iovino, N. (2014). Drosophila epigenome reorganization during oocyte differentiation and early embryogenesis. *Brief. Funct. Genomics* **13**, 246-253.
Jackson, S. M. and Blochlinger, K. (1997). cut interacts with Notch and protein kinase A to regulate egg chamber formation and to maintain germline cyst integrity during Drosophila oogenesis. *Development* **124**, 3663-3672.
Jang, J. K., Sherizen, D. E., Bhagat, R., Manheim, E. A. and Mckim, K. S. (2003). Relationship of DNA double-strand breaks to synapsis in Drosophila. *J. Cell Sci.* **116**, 3069-3077.
Jha, S., Gupta, A., Dar, A. and Dutta, A. (2013). RVBs are required for assembling a functional TIP60 complex. *Mol. Cell. Biol.* **33**, 1164-1174.
Jin, J., Cai, Y., Li, B., Conaway, R. C., Workman, J. L., Conaway, J. W. and Kusch, T. (2005). In and out: histone variant exchange in chromatin. *Trends Biochem. Sci.* **30**, 680-687.
Joyce, E. F., Pedersen, M., Tiong, S., White-Brown, S. K., Paul, A., Campbell, S. D. and McKim, K. S. (2011). Drosophila ATM and ATR have distinct activities in the regulation of meiotic DNA damage and repair. *J. Cell Biol.* **195**, 359-367.
Kai, T. and Spradling, A. (2003). An empty Drosophila stem cell niche reactivates the proliferation of ectopic cells. *Proc. Natl. Acad. Sci. USA* **100**, 4633-4638.
Kusch, T., Florens, L., MacDonald, W. H., Swanson, S. K., Glaser, R. L., Yates, J. R., Abmayr, S. M., Washburn, M. P. and Workman, J. L. (2004). Acetylation by Tip60 is required for selective histone variant exchange at DNA lesions. *Science* **306**, 2084-2087.
Kusch, T., Mei, A. and Nguyen, C. (2014). Histone H3 lysine 4 trimethylation regulates cotranscriptional H2A variant exchange by Tip60 complexes to maximize gene expression. *Proc. Natl. Acad. Sci. USA* **111**, 4850-4855.
Kwon, M. H., Callaway, H., Zhong, J. and Yedvobnick, B. (2013). A targeted genetic modifier screen links the SWI2/SNF2 protein domino to growth and autophagy genes in Drosophila melanogaster. *G3* **3**, 815-825.
Li, Z., Thiel, K., Thul, P. J., Beller, M., Kühnlein, R. P. and Welte, M. A. (2012). Lipid droplets control the maternal histone supply of Drosophila embryos. *Curr. Biol.* **22**, 2104-2113.
Lu, J., Ruhf, M.-L., Perrimon, N. and Leder, P. (2007). A genome-wide RNA interference screen identifies putative chromatin regulators essential for E2F repression. *Proc. Natl. Acad. Sci. USA* **104**, 9381-9386.
Luk, E., Ranjan, A., FitzGerald, P. C., Mizuguchi, G., Huang, Y., Wei, D. and Wu, C. (2010). Stepwise histone replacement by SWR1 requires dual activation with histone H2A.Z and canonical nucleosome. *Cell* **143**, 725-736.
Madigan, J. P., Chotkowski, H. L. and Glaser, R. L. (2002). DNA double-strand break-induced phosphorylation of Drosophila histone variant H2Av helps prevent radiation-induced apoptosis. *Nucleic Acids Res.* **30**, 3698-3705.
Mavrich, T. N., Jiang, C., Ioshikhes, I. P., Li, X., Venters, B. J., Zanton, S. J., Tomsho, L. P., Qi, J., Glaser, R. L., Schuster, S. C. et al. (2008). Nucleosome organization in the Drosophila genome. *Nature* **453**, 358-362.
Messina, G., Damia, E., Fanti, L., Atterrato, M. T., Celauro, E., Mariotti, F. R., Accardo, M. C., Walther, M., Vernì, F., Picchioni, D. et al. (2014). Yeti, an essential Drosophila melanogaster gene, encodes a protein required for chromatin organization. *J. Cell Sci.* **127**, 2577-2588.
Mizuguchi, G., Shen, X., Landry, J., Wu, W.-H., Sen, S. and Wu, C. (2004). ATP-driven exchange of histone H2AZ variant catalyzed by SWR1 chromatin remodeling complex. *Science* **303**, 343-348.
Morillo Prado, J. R., Srinivasan, S. and Fuller, M. T. (2013). The histone variant His2Av is required for adult stem cell maintenance in the Drosophila testis. *PLoS Genet.* **9**, e1003903.
Morrison, A. J. and Shen, X. (2009). Chromatin remodelling beyond transcription: the INO80 and SWR1 complexes. *Nat. Rev. Mol. Cell Biol.* **10**, 373-384.

Narbonne, K., Besse, F., Brissard-Zahraoui, J., Pret, A.-M. and Busson, D. (2004). polyhomeotic is required for somatic cell proliferation and differentiation during ovarian follicle formation in Drosophila. *Development* **131**, 1389-1400.
Ni, J.-Q., Zhou, R., Czech, B., Liu, L.-P., Holderbaum, L., Yang-Zhou, D., Shim, H.-S., Tao, R., Handler, D., Karpowicz, P. et al. (2011). A genome-scale shRNA resource for transgenic RNAi in Drosophila. *Nat. Methods* **8**, 405-407.
Obri, A., Ouararhni, K., Papin, C., Diebold, M.-L., Padmanabhan, K., Marek, M., Stoll, I., Roy, L., Reilly, P. T., Mak, T. W. et al. (2014). ANP32E is a histone chaperone that removes H2A.Z from chromatin. *Nature* **505**, 648-653.
Olivieri, D., Sykora, M. M., Sachidanandam, R., Mechtler, K. and Brennecke, J. (2010). An in vivo RNAi assay identifies major genetic and cellular requirements for primary piRNA biogenesis in Drosophila. *EMBO J.* **29**, 3301-3317.
Papamichos-Chronakis, M., Watanabe, S., Rando, O. J. and Peterson, C. L. (2011). Global regulation of H2A.Z localization by the INO80 chromatin-remodeling enzyme is essential for genome integrity. *Cell* **144**, 200-213.
Park, J. H., Sun, X.-J. and Roeder, R. G. (2010). The SANT domain of p400 ATPase represses acetyltransferase activity and coactivator function of TIP60 in basal p21 gene expression. *Mol. Cell. Biol.* **30**, 2750-2761.
Qi, D., Jin, H., Lilja, T. and Mannervik, M. (2006). Drosophila Reptin and other TIP60 complex components promote generation of silent chromatin. *Genetics* **174**, 241-251.
Ranjan, A., Mizuguchi, G., FitzGerald, P. C., Wei, D., Wang, F., Huang, Y., Luk, E., Woodcock, C. L. and Wu, C. (2013). Nucleosome-free region dominates histone acetylation in targeting SWR1 to promoters for H2A.Z replacement. *Cell* **154**, 1232-1245.
Ruhf, M. L., Braun, A., Papoulas, O., Tamkun, J. W., Randsholt, N. and Meister, M. (2001). The domino gene of Drosophila encodes novel members of the SWI2/SNF2 family of DNA-dependent ATPases, which contribute to the silencing of homeotic genes. *Development* **128**, 1429-1441.
Ruhl, D. D., Jin, J., Cai, Y., Swanson, S., Florens, L., Washburn, M. P., Conaway, R. C., Conaway, J. W. and Chrivia, J. C. (2006). Purification of a human SRCAP complex that remodels chromatin by incorporating the histone variant H2A.Z into nucleosomes. *Biochemistry* **45**, 5671-5677.
Sadasivam, D. A. and Huang, D.-H. (2016). Maintenance of tissue pluripotency by epigenetic factors acting at multiple levels. *PLOS Genet.* **12**, e1005897.
Talbert, P. B. and Henikoff, S. (2010). Histone variants–ancient wrap artists of the epigenome. *Nat. Rev. Mol. Cell Biol.* **11**, 264-275.
Ting, X. (2013). Control of germline stem cell self-renewal and differentiation in the Drosophila ovary: concerted actions of niche signals and intrinsic factors. *Wiley Interdiscip. Rev. Dev. Biol.* **2**, 261-273.
Walker, J., Kwon, S. Y., Badenhorst, P., East, P., McNeill, H. and Svejstrup, J. Q. (2011). Role of elongator subunit Elp3 in Drosophila melanogaster larval development and immunity. *Genetics* **187**, 1067-1075.
Wu, W.-H., Alami, S., Luk, E., Wu, C.-H., Sen, S., Mizuguchi, G., Wei, D. and Wu, C. (2005). Swc2 is a widely conserved H2AZ-binding module essential for ATP-dependent histone exchange. *Nat. Struct. Mol. Biol.* **12**, 1064-1071.
Wu, W.-H., Wu, C.-H., Ladurner, A., Mizuguchi, G., Wei, D., Xiao, H., Luk, E., Ranjant, A. and Wu, C. (2009). N terminus of Swr1 binds to histone H2AZ and provides a platform for subunit assembly in the chromatin remodeling complex. *J. Biol. Chem.* **284**, 6200-6207.
Xi, R. and Xie, T. (2005). Stem cell self-renewal controlled by chromatin remodeling factors. *Science* **310**, 1487-1489.
Yan, D., Neumüller, R. A., Buckner, M., Ayers, K., Li, H., Hu, Y., Yang-Zhou, D., Pan, L., Wang, X., Kelley, C. et al. (2014). A regulatory network of drosophila germline stem cell self-renewal. *Dev. Cell* **28**, 459-473.

3.2.1 Supplementary information

Splice variants of the SWR1-type nucleosome remodeling factor Domino have distinct functions during *Drosophila melanogaster* oogenesis

Börner and Becker

Published in Development 143(17), Pages 3154-3167, 1 September 2016.

doi: 10.1242/dev.139634

Supplementary information

D. melanogaster strains and genetics

DOM-A and DOM-B protein sequences correspond to DOM-RA and DOM-RE transcripts, respectively (flybase.org, FB2016_03, released May 24, 2016). The *domino (dom)* fosmid derivatives are based on the fosmid library clone pflyfos016675 (kind gift of P. Tomancak, MPI-CPG, Germany). The *GFP-dom* fosmid codes for DOM with an N-terminal 2xTY1-sGFP-3xFLAG-tag which tags both isoforms DOM-A and DOM-B. The *dom-A-GFP* and *dom-B-GFP* fosmids code for DOM with a C-terminal 2xTY1-sGFP-3xFLAG-tag which tags DOM-A and DOM-B, respectively. The entire *dom* locus was replaced with 2xTY1-sGFP-3xFLAG-tag in the Δ*dom-GFP* fosmid. All oligonucleotide sequences and combinations are listed (Tabs. S1 and S2). All *dom* fosmid variants were verified by restriction enzyme digestion, PCR and sequencing before injection into *D. melanogaster*. Transgenic flies were made by phiC31 integrase-mediated site-specific integration into attP2 landing site on the 3rd chromosome (Genetic Services, Inc., USA). Fosmid constructs contain *dsRed* cassette driven by 3xP3 promoter to select for transformants.

The following homozygous fly lines containing fosmid constructs were obtained by appropriate crosses: *GFP-dom*, *dom-A-GFP*, *dom-B-GFP*, Δ*dom-GFP*, *dom*^{1};*GFP-dom*, *dom*^{1};*dom-A-GFP*, *dom*^{1};*dom-B-GFP*, *dom*^{9};*GFP-dom*, *dom*^{9};*dom-A-GFP*, *dom*^{9};*dom-B-GFP*, *dom*^{9};Δ*dom-GFP*, *traffic jam-Gal4*/*bcg*;*GFP-dom*, *traffic jam-Gal4*/*bcg*;*dom-A-GFP* and *traffic jam-Gal4*/*bcg*;*dom-B-GFP*.

UAS-shdom-A (HMC04451, attP2, Val20) and *UAS-shdom-B* (HMC04203, attP2, Val20) were made for this study by and *UAS-shdom-1* (HMS02612, attP2, Val20), *UAS-shdom-2* (HMS01855, attP2, Val20), *UAS-shH2A.V-1* (HM05177, attP2, Val10), *UAS-shH2A.V-2* (HMS00162, attP2, Val20), *UAS-shIno80.1* (HMS00586, attP2, Val20), *UAS-shIno80.2* (GL00616, attP2, Val22), *UAS-shIswi* (HMS00628, attP40, Val20), *UAS-shTip60-1* (HM05049, attP2, Val10) and *UAS-shTip60-2* (GL00130, attP2, Val22) were obtained from Transgenic RNAi Project (TRiP, Harvard Medical School, Boston, USA). *UAS-shEGFP* (#41557, attP40, Val22), *MTD-Gal4* (#31777), *matα4-Gal4* (#7063), *actin-Gal4*/*CyO* (#25708), *elav-Gal4* (#25750), *C96-Gal4* (#25757), *dom*^{1} (#10767) and *dom*^{9} (#9261) were obtained from Bloomington Drosophila Stock Center (BDSC, USA). *c587-Gal4* and *traffic jam-Gal4* were kind gifts of Allan C. Spradling (Carnegie Institution for Science, USA) and Jean-René Huynh (Institut Curie, France), respectively.

Generation of DOA1, DOB2 and H2A.V antibodies

DOA1 (KEHKRSRTDAGYDGSRRPNC) and DOB2 (TPKESQSEPRRKITQPKC) peptides with N-terminal PEG-Biotin and C-terminal coupled Ovalbumin were made by Peptide Specialty Laboratories (PSL, Germany). The monoclonal rat DOA1 17F4 and mouse DOB2 4H4 peptide antibodies were developed by E. Kremmer (Helmholtz Zentrum Munich, Germany). The specificity was confirmed in Western blot by RNAi (Fig. 2B) and with recombinantly expressed, C-terminally tagged DOM-A and

DOM-B (data not shown). Some lower-molecular weight bands were only detected with DOA1 but not with FLAG antibody suggesting limited degradation (data not shown).

H2A.V peptide (QPDQRKGNVIL) corresponding to aa 127-137 of H2A.V was coupled to KLH via C-terminal cysteine and used to raise polyclonal rabbit H2A.V antibody (Eurogentec, Netherlands). The specificity of H2A.V antibody was validated by loss of H2A.V immunofluorescence signal upon cell type-specific knockdown with H2A.V shRNA (Figs 6I,M; 7E,G; 8E,I and S6).

Antibodies used in Western blot

The following antibodies were used for Western blot: rat DOA1 17F4 (1:5), mouse DOB2 4H4 (1:5), mouse FLAG M2 (1:5000, F1804, Sigma-Aldrich, Germany), rabbit ISWI (1:1000, kind gift from J. Tamkun, University of California, Santa Cruz, USA) and mouse Lamin T40 (1:3000, kind gift H. Saumweber, Humboldt University Berlin, Germany). mouse (NA931V), rat (NA935V) or rabbit (NA934V) IgG secondary antibodies conjugated to HRP (1:20000, GE Healthcare, UK) and Immobilon Western HRP Substrate (Merck Millipore, Germany) were used for chemiluminescent detection with ChemiDoc Touch Imaging System (Bio-Rad Laboratories, Germany) or X-ray developer machine (AGFA curix 60, Belgium).

Antibodies used in immunofluorescence

The following primary antibodies were used in immunofluorescence: mouse Orb 6H4 (AB_528419) and 4H8 (AB_528418) [1:60, Developmental Studies Hybridoma Bank (DSHB), USA], mouse Fasciclin III 7G10 (1:100, AB_528238, DSHB), mouse UNC93-5.2.1 (γH2A.V, 1:1000, DSHB), mouse Spectrin 3A9 (1:10, AB_528473, DSHB), mouse HP1 C1A9 (1:10, AB_528276, DSHB), rabbit Vasa (1:100, sc-514249, Santa Cruz Biotechnology, USA), rabbit activated Caspase 3 (1:100, 9661, Cell Signaling Technology, USA), rabbit GFP (1:500, TP401, Acris Antibodies, Germany) and rabbit α-H2A (1:200, kind gift of J. Müller, MPI of Biochemistry, Martinsried, Germany). F-actin was visualized with Rhodamine-conjugated phalloidin (1:500, R415, Invitrogen). DAPI (0.1 mg/ml, 1:500) was used to stain DNA. The following secondary antibodies from Jackson Immuno Research Laboratories, INC. were used: Donkey mouse Cy3 (1:250, 715-165-150), Donkey mouse Alexa488 (1:300, 715-545-151), Donkey rat Alexa488 (1:300, 712-485-150) and Donkey rabbit Alexa488 (1:300, 711-545-152). Donkey rabbit Alexa555 (1:250, A-21429) was used from ThermoFisher Scientific, Germany.

Immunological techniques and microscopy

For signal quantification, 8-bit grayscale z-stack images were analyzed with ImageJ software. Area of DAPI-stained nuclei and mean signal intensity were measured for the following cell types: GFP signal in 10 follicle cells (Fig. 2I); H2A.V signal in 30 cysts in region 1, 2 and 3 of the germarium and follicle cells, respectively (Fig. 6E-K); H2A.V signal in 50 nurse and follicle cells of stage 3 egg

chambers, respectively (Fig. 7A-F); H2A.V signal in 50 nurse and follicle cells of stage 8 egg chambers, respectively (Fig. 8A-L) and H2A.V signal in 30 follicle and nurse cells of region 2B, stage 1 and 2, respectively (Fig. 9A-G). Integrated density values were calculated by multiplication of mean signal intensity with corresponding area. For background signal, mean signal intensity was measured and averaged in three adjacent DAPI-signal negative areas. Corrected total cell fluorescence was calculated by subtracting the product of area and average background signal from integrated density values. Mean CTCF values with SD were calculated from three biological replicates.

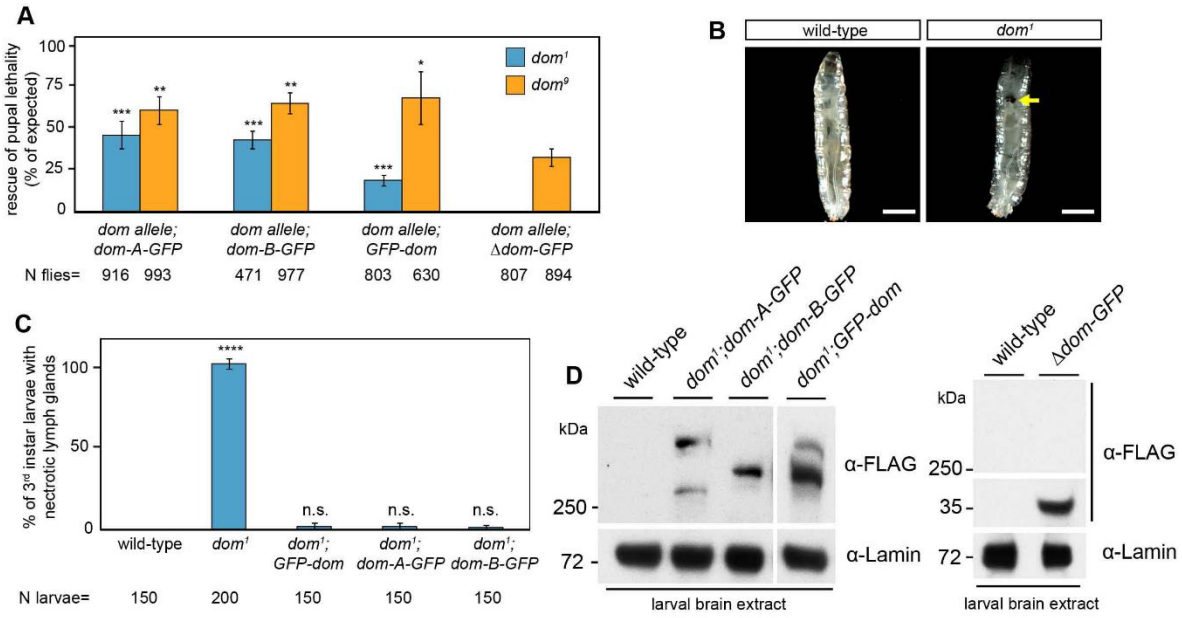

Fig. S1. Characterization of *domino* fosmids

(A) Complementation of *dom* alleles with *dom* fosmids partially rescues lethality phenotype. Rescue of pupal lethality was determined as percentage of observed to expected frequency of homozygous dom^1 or dom^9 offspring. The data show mean values in percentage with s.d. of three biological replicates. *N* represents the total number of scored flies. Two-tailed Student's *t*-test for comparison of dom^1 or dom^9 allele with Δ*dom-GFP*, respectively. **P*<0.05, ***P*<0.01 and ****P*<0.001. (B, C) Complementation of dom^1 allele with *dom* fosmids rescues necrotic lymph glands phenotype. (B) Representative images of 3rd instar larvae are shown for the following homozygous genotypes: wild-type and dom^1. Yellow arrow indicates necrotic lymph glands. Scale bars: 1 µm (C) Quantification of necrotic lymph glands phenotype. The data show mean values in percentage with s.d. of three biological replicates. Two-tailed Student's t-test for comparison with wild-type. *****P*<0.0001; n.s., not significant. (D) Western blot from brains of 3rd instar larvae probed with FLAG antibody is shown for the following homozygous genotypes: wild-type, dom^1;*dom-A-GFP*, dom^1;*dom-B-GFP* and dom^1;*GFP-dom*. Lamin signal provided controls.

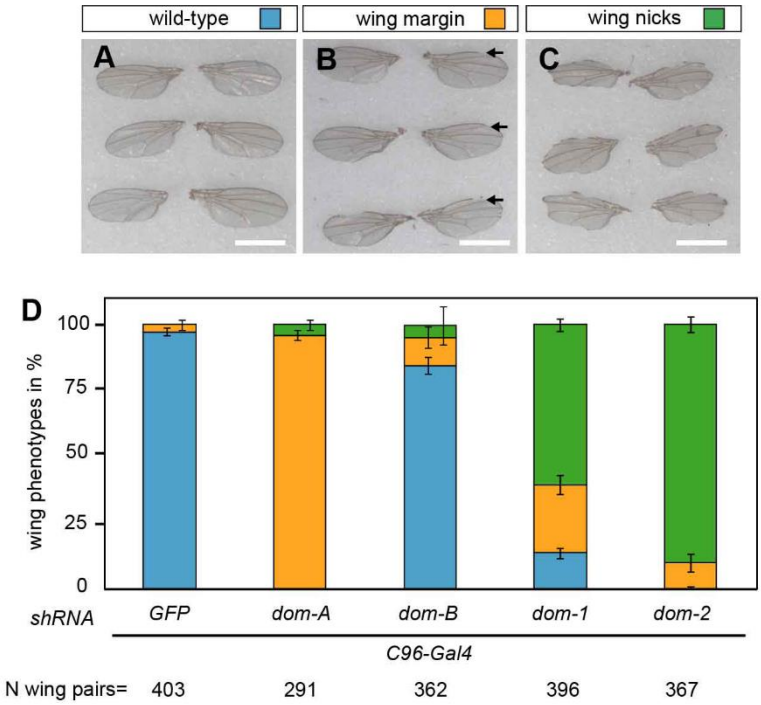

Fig. S2. Depletion of DOM isoforms causes Notch phenotypes in wing development

UAS-shRNA males for *GFP*, *dom-1*, *dom-2*, *dom-A* and *dom-B* were crossed with *C96-Gal4* driver females. (A-C) Wing margin and nick phenotypes were scored in F1 offspring. Black arrow indicates wing margin phenotype. Scale bars: 1 mm. (D) The data show mean percentage with s.d. from three biological replicates. Blue, yellow and green colors indicate wild-type, wing margin and wing nick phenotype, respectively.

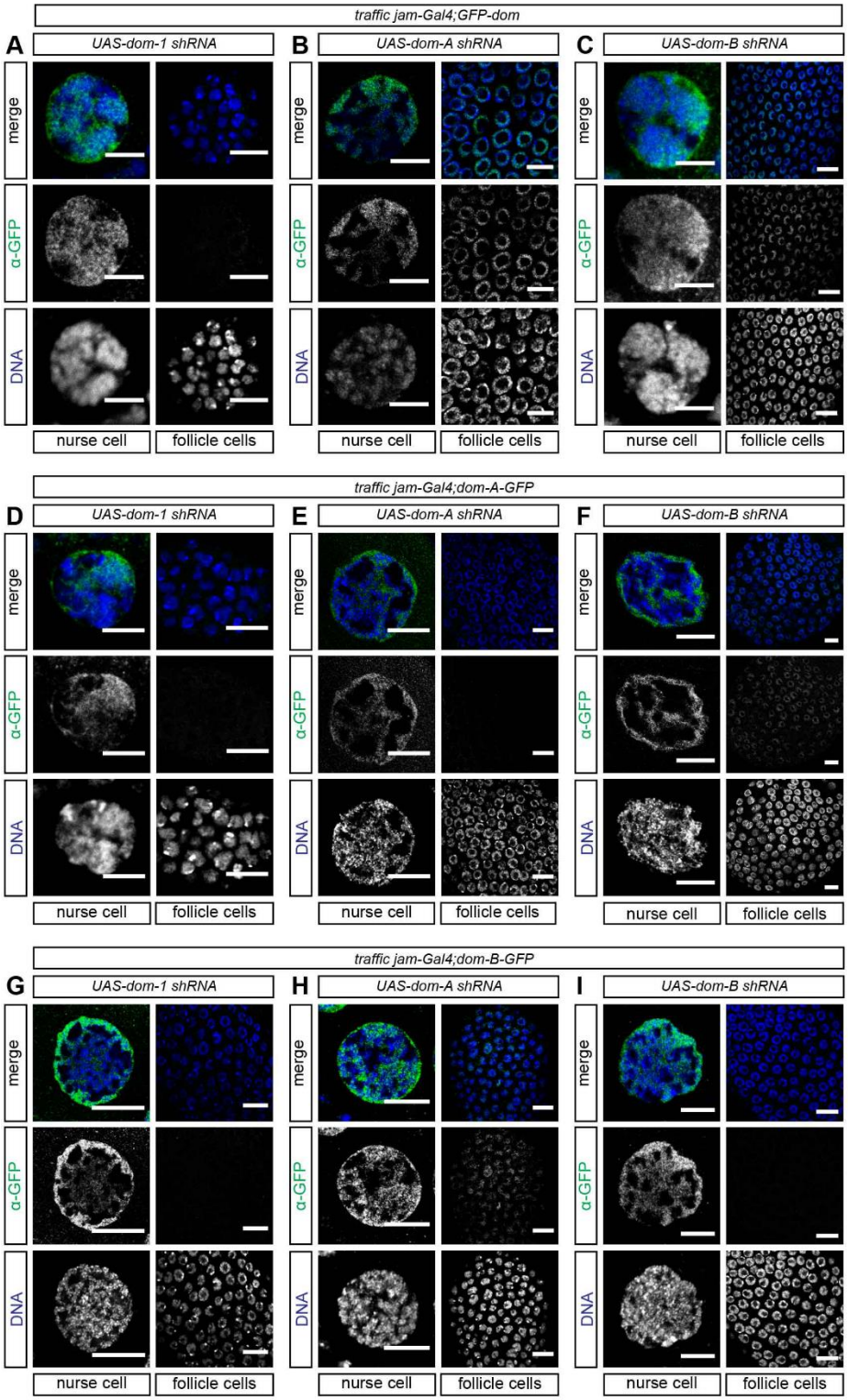

Fig. S3. Validation of cell-type specific knockdown with *dom-1*, *dom-A* and *dom-B shRNAs* and *dom* fosmids

(A-I) Immunofluorescence images of nurse and follicle cells in different stages of oogenesis with staining of GFP (green) and DNA (blue) are shown for the following genotypes: (A-C) *traffic jam-Gal4*;*GFP-dom* with (A) dom-1, (B) dom-A and (C) dom-B shRNA, (D-F) *traffic jam-Gal4*;*dom-A-GFP* with (D) dom-1, (E) dom-A and (F) dom-B *shRNA* and (G-I) *traffic jam-Gal4*;*dom-B-GFP* with (G) dom-1, (H) dom-A and (I) dom-B *shRNA*. Scale bars: 10 µm. Please also refer to Fig. 2 for additional information.

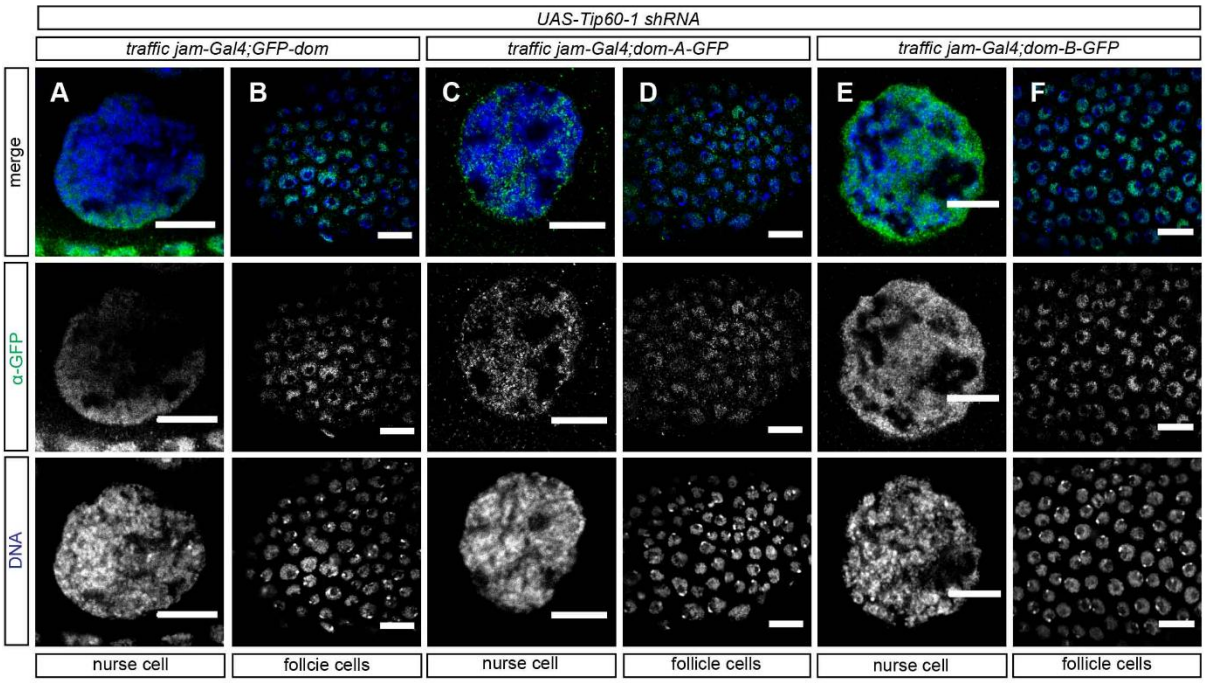

Fig. S4. TIP60 depletion does not affect DOM-A or DOM-B localization in follicle cells

(A-F) Immunofluorescence images of nurse and follicle cells in different stages of oogenesis with staining of GFP (green) and DNA (blue) are shown for the following genotypes: (A-F) UAS-Tip60-1 shRNA with (A,B) *traffic jam-Gal4*;*GFP-dom*, (C,D) *traffic jam-Gal4*;*dom-A-GFP* and (E,F) *traffic jam-Gal4*;*dom-B-GFP*. Scale bars: 10 µm. Please also refer to Fig. 2 for additional information.

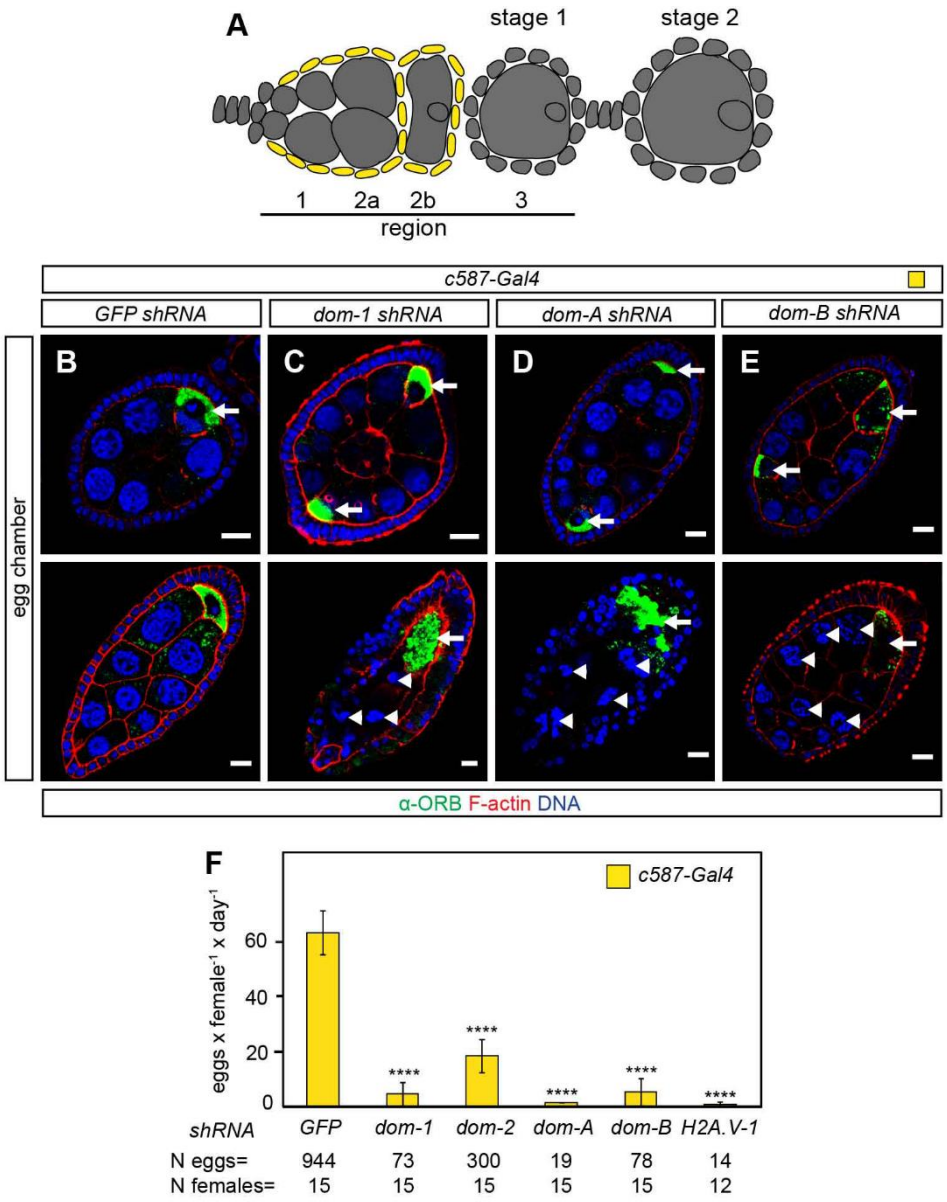

Fig. S5. Validation of packaging defects upon DOM-A or DOM-B depletion with somatic driver *c587-Gal4*

(A) Diagramm of early stages of *D. melanogaster* oogenesis. The specific expression pattern of *c587-Gal4* in somatic escort and follicle cells in the germarium is highlighted in yellow. (B-E) Immunofluorescence images of egg chambers with staining of ORB (green), F-actin (red) and DNA (blue) are shown for the following genotypes: *c587-Gal4* with (B) GFP, (C) dom-1, (D) dom-A and (E) dom-B shRNA. White arrows and arrowhead indicate oocyte and disintegrating nurse cell nuclei, respectively. Scale bars: 10 µm. Staining with the oocyte marker Orb revealed the nature of packaging defects as compound egg chambers with oocytes at opposite positions of an egg chamber and confirmed apoptotic phenotype. (G) Quantification of egg laying capacity. The data show mean values of laid eggs per female and day with s.d. of three biological replicates. *N* eggs represents the total number of scored eggs and *N* females the total number of analyzed females. Two-tailed Student's *t*-test for comparison with GFP shRNA. ****P<0.0001.

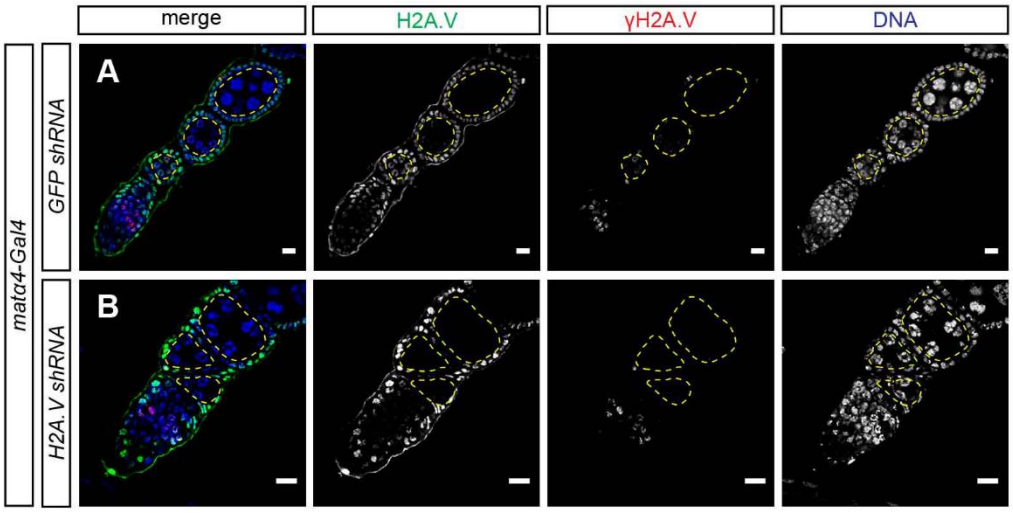

Fig. S6. Characterization of *matα4-Gal4 driver*

(A-B) Immunofluorescence images of ovarioles with staining of H2A.V (green), γH2A.V (red) and DNA (blue) are shown for the following genotypes: *matα4-Gal4* with (A) GFP and (B) H2A.V shRNA. Yellow dashed line indicates germline cells from stage 1 onwards. Scale bars: 10 μm.

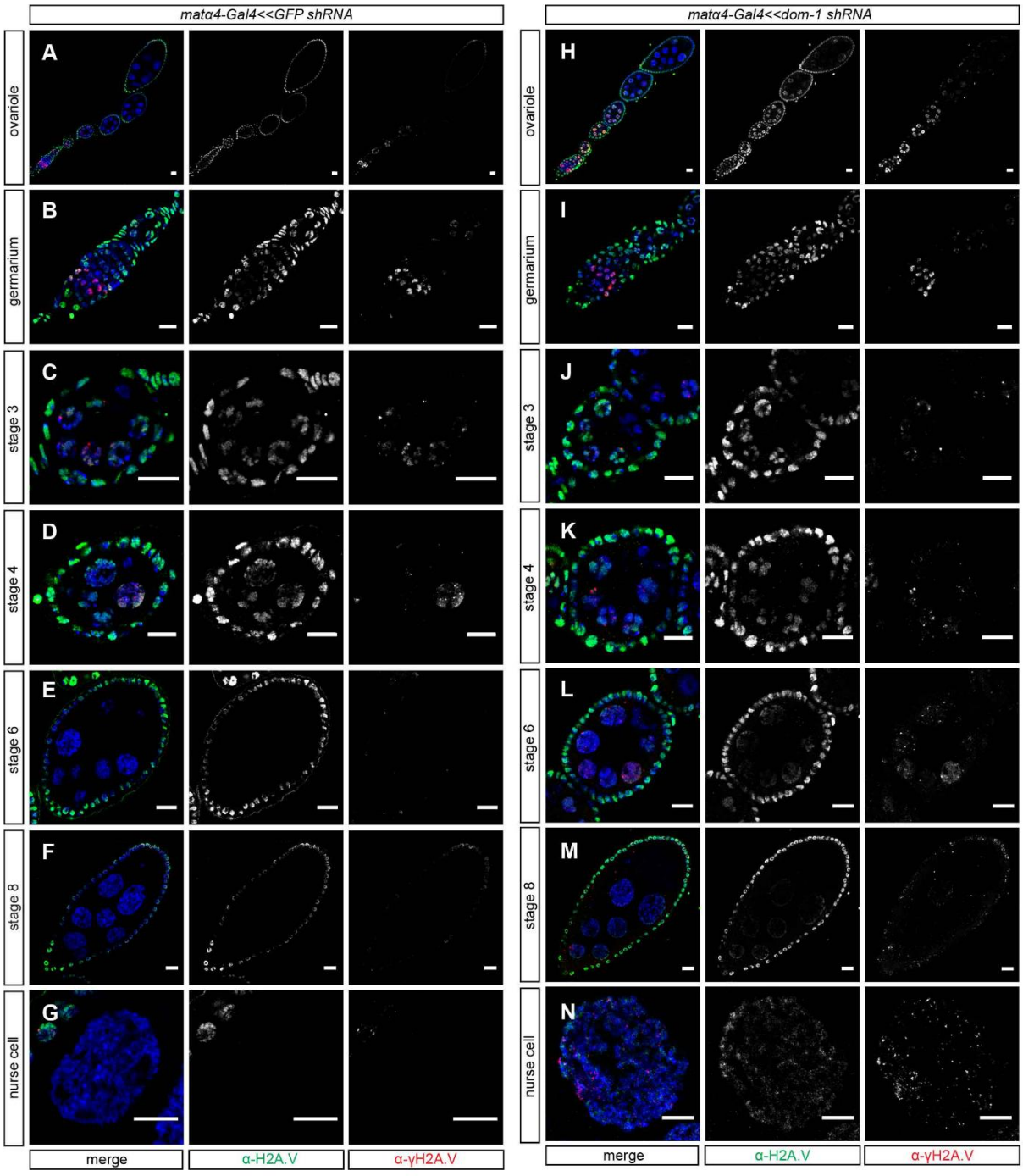

Fig. S7. Loss of DOM in germline cells leads to persistence of H2A.V/γH2A.V from stage 5 onwards

(A-N) Immunofluorescence images of ovariole, germarium, different stages of egg chambers and nurse cell nuclei with staining of H2A.V (green), γH2A.V (red) and DNA (blue) are shown for the following genotypes: *matα4-Gal4* with (A-G) GFP shRNA and (H-N) *d*om-1 shRNA. Scale bars: 10 µm. Please also refer to Fig. 7 and 8 for additional information.

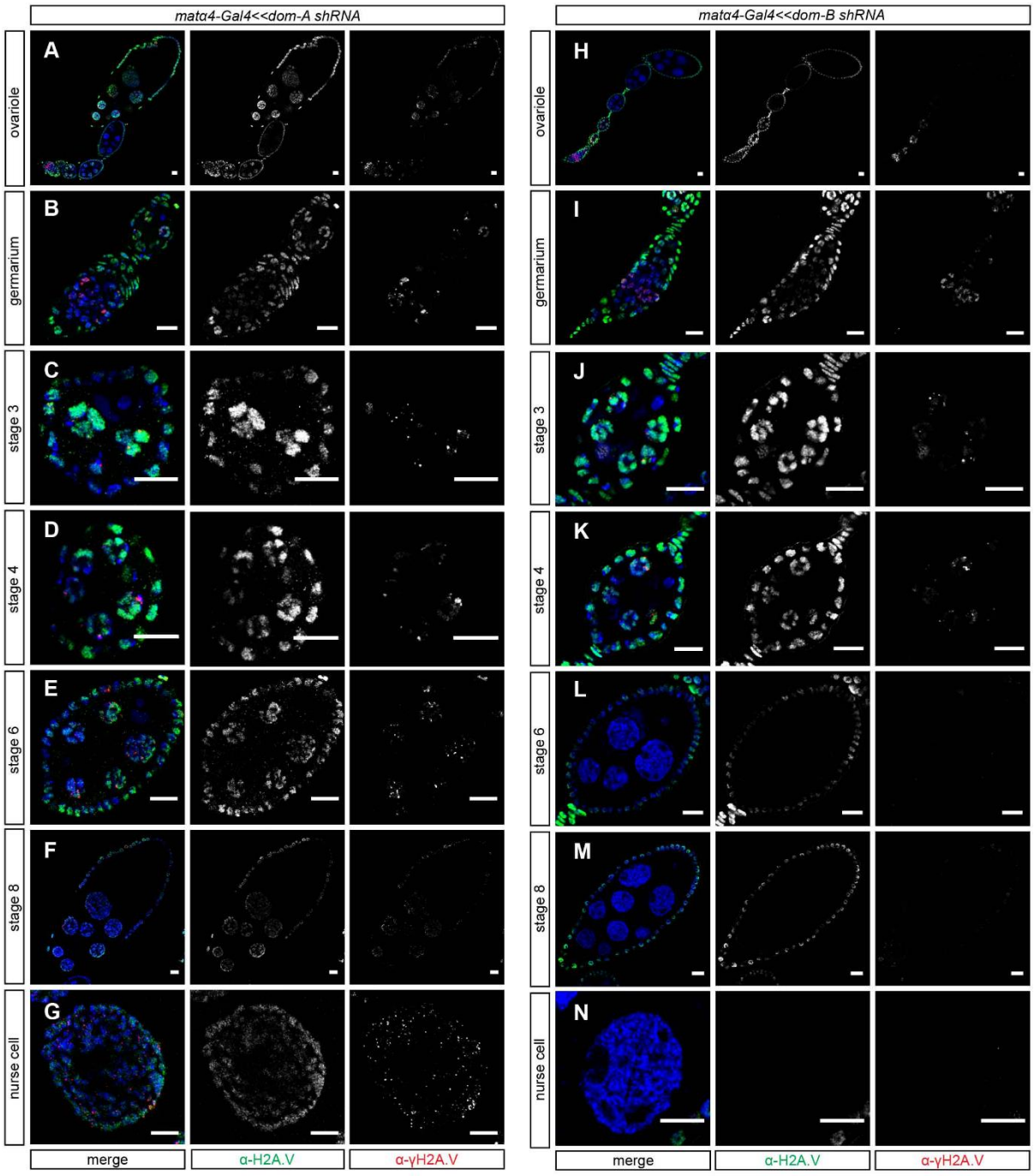

Fig. S8. Loss of DOM-A in germline cells leads to persistence of H2A.V/γH2A.V from stage 5 onwards

(A-N) Immunofluorescence images of ovariole, germarium, different stages of egg chamber and nurse cell nuclei with staining of H2A.V (green), γH2A.V (red) and DNA (blue) are shown for the following genotypes: *matα4-Gal4* with (A-G) dom-A shRNA and (H-N) dom-B shRNA. Scale bars: 10 µm. Please also refer to Fig. 7 and 8 for additional information.

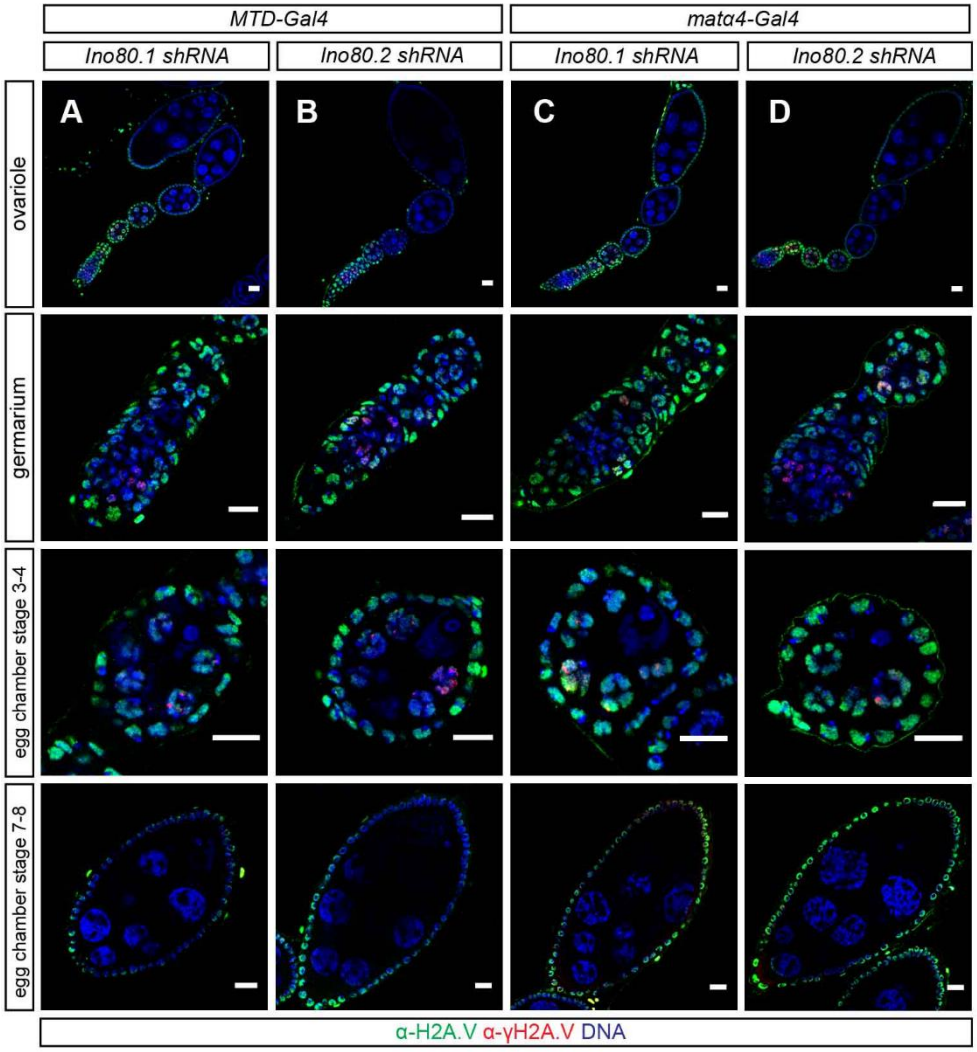

Fig. S9. Germline-specific knockdown of INO80 does not affect H2A.V/γH2A.V association to chromatin

(A-D) Immunofluorescence images of ovariole, germarium and different stages of egg chamber with staining of H2A.V (green), γH2A.V (red) and DNA (blue) are shown for the following genotypes: (A,B) *MTD-Gal4* with (A) Ino80.1 and (B) Ino80.2 shRNA and (C,D) *matα 4-Gal4* with (C) Ino80.1 and (D) *I*no80.2 shRNA. Scale bars: 10 µm.

Table S1. Oligonucleotide sequences used in this study. Please also refer to paragraph '*D. melanogaster* strains and genetics' in Supplementary information for additional information.

Oligonucleotide	Sequence
Dom-rec-N-F	actgtgaactcacacccttctatttttttttgcagatgtctcaaacatggaagtgcataccaatcaggac
Dom-rec-N-R	ggggccgggctgagcccttcatgccccctcctgctgaattaccttcattcttgtcgtcgtcatccttgta
DomA-rec-C-F	aggtacgcaagctggtgcagaaaaagatcctgatacgcagcgagaaagaagaagtgcataccaatcaggac
DomA-rec-C-R	ctcgtgatgctccgccgctgacgtggtctgacggctttagtcgagcgttacttgtcgtcgtcatccttgta
DomB-rec-C-F	cagtcagtggtgtttcgggaggaaatgcctcctcgagcggaacagccagggaagtgcataccaatcaggac
DomB-rec-C-R	aacacacacagctgataatactgactgaggtatgatagtgaacatcatcacttgtcgtcgtcatccttgta

Table S2. Oligonucleotide combinations used in this study. Please also refer to paragraph '*D. melanogaster* strains and genetics' in Supplementary information for additional information.

Transgenic fosmid	Forward Oligonucleotide	Reverse Oligonucleotide
GFP-dom	Dom-rec-N-F	Dom-rec-N-R
dom-A-GFP	DomA-rec-C-F	DomA-rec-C-R
dom-B-GFP	DomB-rec-C-F	DomB-rec-C-R
Δdom-GFP	Dom-rec-N-F	DomA-rec-C-R

3.3 Interplay of distinct nucleosome remodeling factors

It is widely appreciated that many DNA-dependent processes need the coordinated activity of distinct nucleosome remodeling factors with impressive examples coming from transcription initiation or dsDNA break repair (20,25,68,165–167). The outcome of the remodeling activity such as nucleosome sliding or histone variant replacement may be integrated by accessory subunits in a context-dependent manner (Fig. 1.5) (16). However, it remains largely unknown how the coordinated interplay of different nucleosome remodeling factors is achieved on a mechanistic level. Nucleosome remodeling factors are not only tightly controlled in their spatial and temporal expression (20,52), but also well regulated on the level of genome-wide targeting (168,169). At the target sites, the remodeling activity may be regulated by other proteins, PTMs, RNAs or chromatin structure (Fig. 1.5) (16,20,25,47). Yet, it is not well understood whether the concerted outcome of nucleosome remodeling requires the physical interaction of distinct nucleosome remodeling factors. Recent findings indicate an unexpected heterogeneity and tool sharing of nucleosome remodeling complexes challenging long-established paradigms of protein complexes (170).

In this context, recent unpublished data from our lab proposed a novel interplay between two distinct nucleosome remodeling complex subunits. According to this, the SWR1-type remodeling ATPase Domino and the signature subunit of nucleosome sliding factors ACF/CHRAC, ACF1, seem to be part of a previously uncharacterized complex (171,172). The physical combination of two nucleosome remodeling enzymes with different remodeling outcomes may turn out as a novel layer of regulating nucleosome remodeling reactions. Several lines of evidence indicated a direct physical interaction in a novel assembly called ACF1-Domino containing complex (ACDC) (171,172). Firstly, ACF1 co-fractionated with DOM over several chromatography columns and gel filtration in high-molecular weight fractions suggesting the formation of a stable complex. Moreover, immunoprecipitation experiments from nuclear extracts of preblastoderm embryos indicated an interaction between ACF1 and DOM *in vivo*. Remarkably, pull-down experiments with recombinant proteins further demonstrated a direct interaction of ACF1 with DOM-B *in vitro*, in particular to the characteristic ATPase domain of SWR1-type remodelers.

On the other hand, several technical restrictions in the experimental setup limited the conclusions from those experiments. Firstly, DOM antibodies used in this previous study did not distinguish between the two isoforms, DOM-A and DOM-B. Notably, DOM-A was identified as part of a TIP60 complex (79), but neither DOM-B nor any ACF subunit was

detected. Hence, it remained elusive whether ACF1 interaction is restricted to DOM-B. Systematic studies with recombinant DOM-A had not been performed since DOM-A tools such as cDNAs or antibodies were not available. Secondly, the recombinant proteins contained several sequence polymorphisms as compared to the most recent genome annotation, thus limiting the relevance of any result. Lastly, the identification of ISWI-independent ACF1 assemblies is unexpected, although it has been suggested that new complexes might be identified in future studies (20). Therefore, it was of general interest to investigate whether an ACDC complex may contain the ISWI ATPase as well.

3.3.1 Studying recombinant protein interactions of DOM/TIP60 with ACF

In this thesis, recombinantly expressed DOM-A and DOM-B were used to validate the direct interaction with ACF1 and ISWI-containing ACF complex. It is likely that ACF1 not only binds to DOM-B, but also to DOM-A since previous experiments suggest the 'split ATPase' domain of DOM as interaction surface for ACF1 (171,172). This remarkable observation may even indicate a direct interaction between the two remodeling ATPases: DOM and ISWI. Alternatively, ACF1 could be either part of ACF/CHRAC or ACDC suggesting a 'swap' of ATPases under particular circumstances yet to be defined. Interactions studies of ACF1 with other DOM complex subunits such as the histone acetyltransferase TIP60 could strengthen the idea of a novel ACDC assembly. A first mechanistic insight could come from the identification of domains that mediate interactions of ACF1 with DOM-B to direct future research on ACDCs nucleosome remodeling activity or outcome.

3.3.1.1 Expression of recombinant DOM-B proteins via Baculovirus expression system

To explore a potential direct interaction between DOM-B and ACF1, the baculovirus vectors were used to express recombinant protein in *Spodoptera frugiperda* Sf21 cells. Besides full-length DOM-B, constructs were made that lack either the N-terminus (DOM-B ΔNT 875-2498 aa) or C-terminus (DOM-B ΔCT 1-1825 aa) or both in case of the ATPase fragment (DOM-B ATPase 875-1825 aa) (Fig. 3.1A). Additionally, a point mutation was introduced into the conserved ATPase domain to produce a catalytically inactive DOM-B (DOM-B K945R) for future biochemical studies (Fig. 3.1A). All constructs were either untagged or contained an N- or C-terminal FLAG-tag. Recombinant proteins were purified via FLAG affinity chromatography and analyzed by Coomassie staining. Despite its molecular weight of approximately 275 kDa, full-length DOM-B and all derivatives were expressed and purified in sufficient amounts (Fig. 3.1B-D) for further interaction studies.

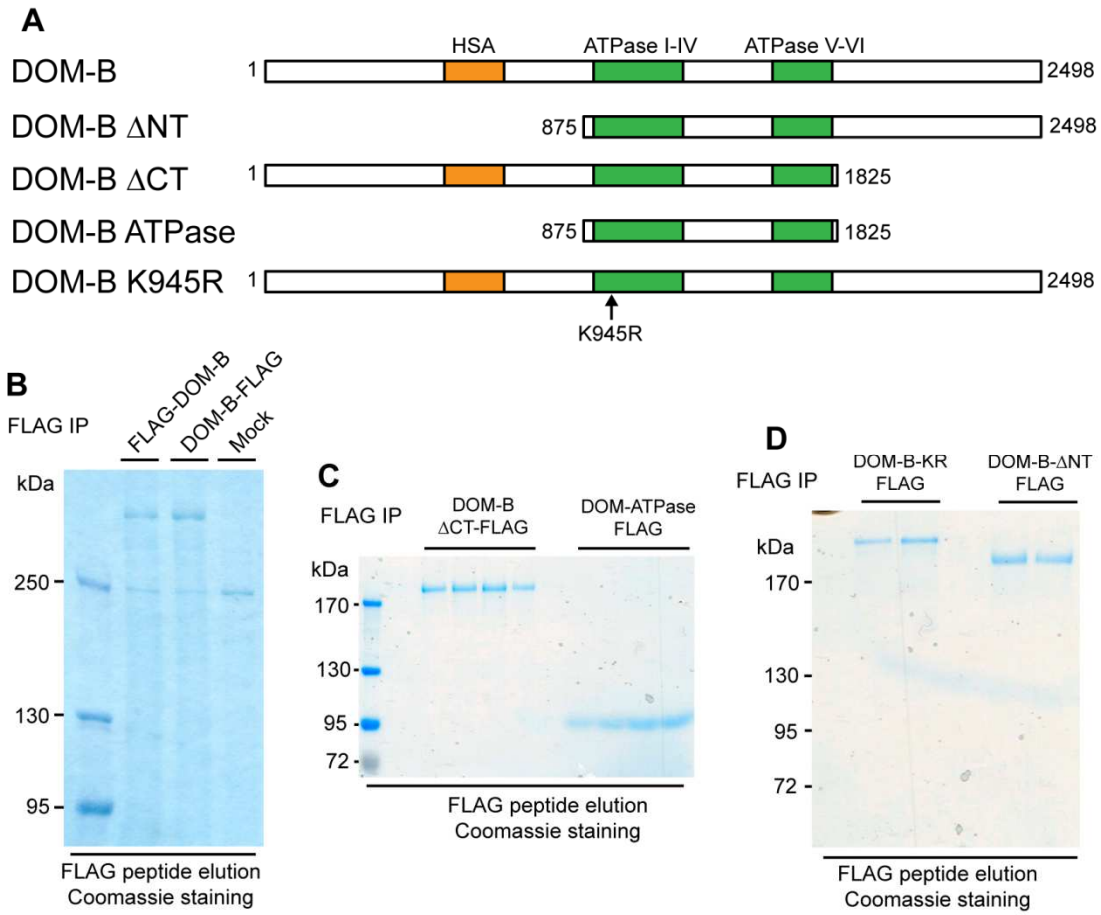

Figure 3.1. Recombinant expression of DOM-B proteins. **(A)** Schematic representation of DOM-B constructs. Orange and green rectangle represents HSA and ATPase domain, respectively. Numbers indicate length in amino acids. Arrow shows amino acid exchange of lysine in position 945 to arginine. Note characteristic 'spacer' region for SWR1-type remodeling enzymes between ATPase I-IV and V-VI domains. All constructs were either untagged or contained the FLAG-tag at N- or C-terminus. **(B-D)** Expression of recombinant full-length DOM-B and DOM-B deletion proteins. Constructs were expressed in *Spodoptera frugiperda* Sf21 cells via the Baculovirus expression system. Recombinant proteins were purified via FLAG affinity chromatography and FLAG peptide elution. Elutions (10-20%) were loaded on SDS-PAGE gel and analyzed by Coomassie staining. **(B)** Elutions of N- or C-terminal FLAG-tagged DOM-B in comparison to a untreated mock sample are shown. High-molecular weight band was only detected in DOM-B elutions but not in mock sample. Some degradation was detected in DOM-B elutions. Unspecific band (~250 kDa) was also detected in mock sample. **(C)** Four different elution samples of FLAG-tagged DOM-B-ΔCT and DOM-ATPase are shown. **(D)** Two different elution samples of FLAG-tagged DOM-B-K945R and DOM-B-ΔNT are shown.

3.3.1.2 Interaction studies of recombinant DOM-B with ACF1 and ISWI

Recombinantly coexpressed DOM-B-FLAG and untagged ACF1 from two different baculovirus stocks in Sf21 cells were employed to test for direct interactions with FLAG affinity chromatography. In brief, proteins were immunoprecipitated with FLAG antibody beads from cellular extracts, eluted with FLAG peptide and analyzed by Western blot. Signals

for DOM-B-FLAG were not detectable in input material due to low expression levels, but were enriched to detectable levels through FLAG affinity chromatography (Fig 3.2A). Remarkably, the ACF1 signal was only detected in FLAG peptide elution when coexpressed with DOM-B-FLAG (Fig. 3.2A). In contrast, the ACF1 signal was neither detected in elution of untreated mock nor single expression of DOM-B-FLAG (Fig. 3.2A). As a control, untagged ACF1 did not bind unspecifically to FLAG beads (Fig. 3.2A). This finding indicates a direct interaction of recombinant ACF1 with DOM-B.

Next, a direct interaction of the two nucleosome remodeling enzymes, DOM-B and ISWI, was studied *in vitro*. Towards this end, untagged ISWI was coexpressed with DOM-B-FLAG and FLAG affinity chromatography was analyzed by Western blot. As a positive control, ISWI was coexpressed with ACF1-FLAG to reconstitute the ACF complex (53,173). As expected, the ISWI signal was detected in FLAG peptide elution when coexpressed with ACF1-FLAG (Fig. 3.2B). However, no direct ISWI-DOM-B interaction was observed (Fig. 3.2B) suggesting that DOM-B interacts specifically with the signature subunit ACF1, but not with the ATPase ISWI *in vitro*.

It remained an interesting possibility that these three factors form a tertiary complex. On one hand, ACF1 might function as a link to mediate the interaction of two distinct ATPases in a ternary DOM-B-ACF1-ISWI complex. On the other hand, ACF1 could be exclusively associated with either ISWI or DOM-B depending on cellular environment or developmental stimuli. The second hypothesis rather argues for a swap of the ATPase ‘motor’ associated with ACF1, while the former idea favors the combination of distinct remodeling outcomes in a single ACDC complex. To test this more directly, two different *in vitro* reconstitution approaches were used. Firstly, ACF1, ISWI and DOM-B-FLAG were coexpressed in Sf21 cells and interactions analyzed by FLAG affinity chromatography (Fig. 3.2C). Secondly, coexpressed ACF1 and DOM-B-FLAG were coupled to FLAG beads and recombinant ISWI cell extract was added to test for interaction with a pre-assembled ACF1-DOM-B complex (Fig. 3.2D). In both experiments, ACF1 interaction with DOM-B-FLAG was confirmed (Fig. 3.2C, D). However, no ISWI interaction was detectable, neither upon coexpression of all three factors (Fig. 3.2C) nor on pre-assembled ACF1-DOM-B (Fig. 3.2D). These findings rather support the hypothesis of an ‘ATPase swap’, the exclusive binding of ACF1 to either ISWI or DOM-B depending on yet unknown physiological conditions.

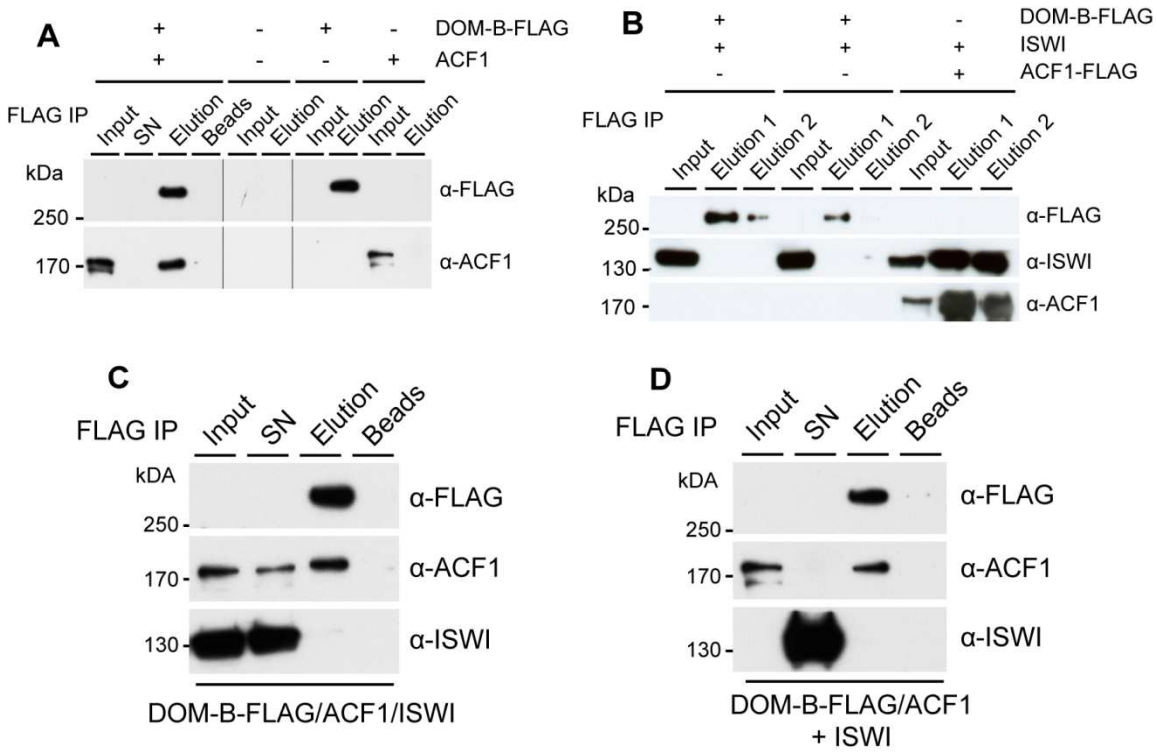

Figure 3.2. Interaction studies of recombinant DOM-B with ACF1 and ISWI. (A-D) Proteins were coexpressed in Sf21 cells via the Baculovirus expression system and purified via FLAG affinity chromatography and FLAG peptide elution. Input (2%), supernatant (SN 2%), FLAG peptide elution (20%) and FLAG beads (20%) were analyzed by Western blot with FLAG, ACF1 and ISWI antibody. **(A)** Recombinant ACF1 interacts with DOM-B. Signals for DOM-B-FLAG were not detectable in input due to low expression levels, but were enriched to detectable levels through FLAG affinity chromatography. ACF1 signal was only detected in elution when coexpressed with DOM-B-FLAG. As controls, no ACF1 signal was detected in elution of untreated mock sample or DOM-B-FLAG. Unspecific binding of ACF1 to FLAG beads was not observed. **(B)** Recombinant ISWI did not interact with DOM-B. ISWI signal was not detected in elution (Elution 1 = 90 min, Elution 2 = overnight) when coexpressed with DOM-B-FLAG. As a control, ISWI signals were detected in elution when coexpressed with ACF1-FLAG. **(C, D)** Recombinant ACF1-DOM-B did not interact with ISWI. **(C)** No ISWI signal was detected in elution when coexpressed with ACF1 and DOM-B-FLAG, while co-elution of ACF1with DOM-B was observed. **(D)** Recombinant ACF1-DOM-B-FLAG were bound to FLAG beads and cell extract with recombinantly expressed ISWI was added. No ISWI signal was detected in elution when coexpressed with ACF1 and DOM-B-FLAG, while co-elution of ACF1 with DOM-B was observed.

Future research might overcome some technical limitations of *in vitro* protein complex reconstitution. In brief, this approach does not reflect the physiological conditions of developmentally regulated complex assembly. For example, other subunits, PTMs, chromatin environment or developmental stimuli could facilitate complex assembly *in vivo*. Furthermore, limited amounts of purified proteins made it very challenging to perform biochemical experiments. It remains an interesting approach for future research to purify protein complexes from *in vivo* sources such as tagged flyfosmids embryos or tissue culture cells. Indeed, a functional DOM-A/TIP60 complex was purified from S2 cells which showed exchange activity towards phosphorylated H2A.V with unmodified H2A.V, but association of ACF1 or ISWI was not tested (79).

3.3.1.3 Delineation of interaction domains of DOM-B and ACF1

To further elucidate how ACF1 interacts with DOM-B the interaction domains of both proteins were dissected with ACF1 constructs lacking individual domains. In total, nine different FLAG-tagged ACF1 constructs were made (Fig. 3.3A). All constructs were expressed recombinantly in Sf21 cells as visualized by Coomassie staining (Fig. 3.3B) and purified by FLAG affinity chromatography (Fig. 3.3C). ISWI binds to the N-terminal part of ACF1, in particular to the DDT and BAZ1/2 domains (53). To validate the ACF1 constructs, we coexpressed untagged ISWI with ACF1-FLAG domain deletions in Sf21 cells and performed FLAG affinity chromatography. As expected, deletion of the WAC or PHD1/2-Bromodomain in ACF1 did not affect ISWI interaction (Fig. 3.3E). In contrast, association of ISWI with ACF1 was specifically lost upon deletion of the DDT, BAZ1 or BAZ2 domain (Fig. 3.3D) verifying previous observations that N-terminal domains of ACF1 contribute to ISWI interaction.

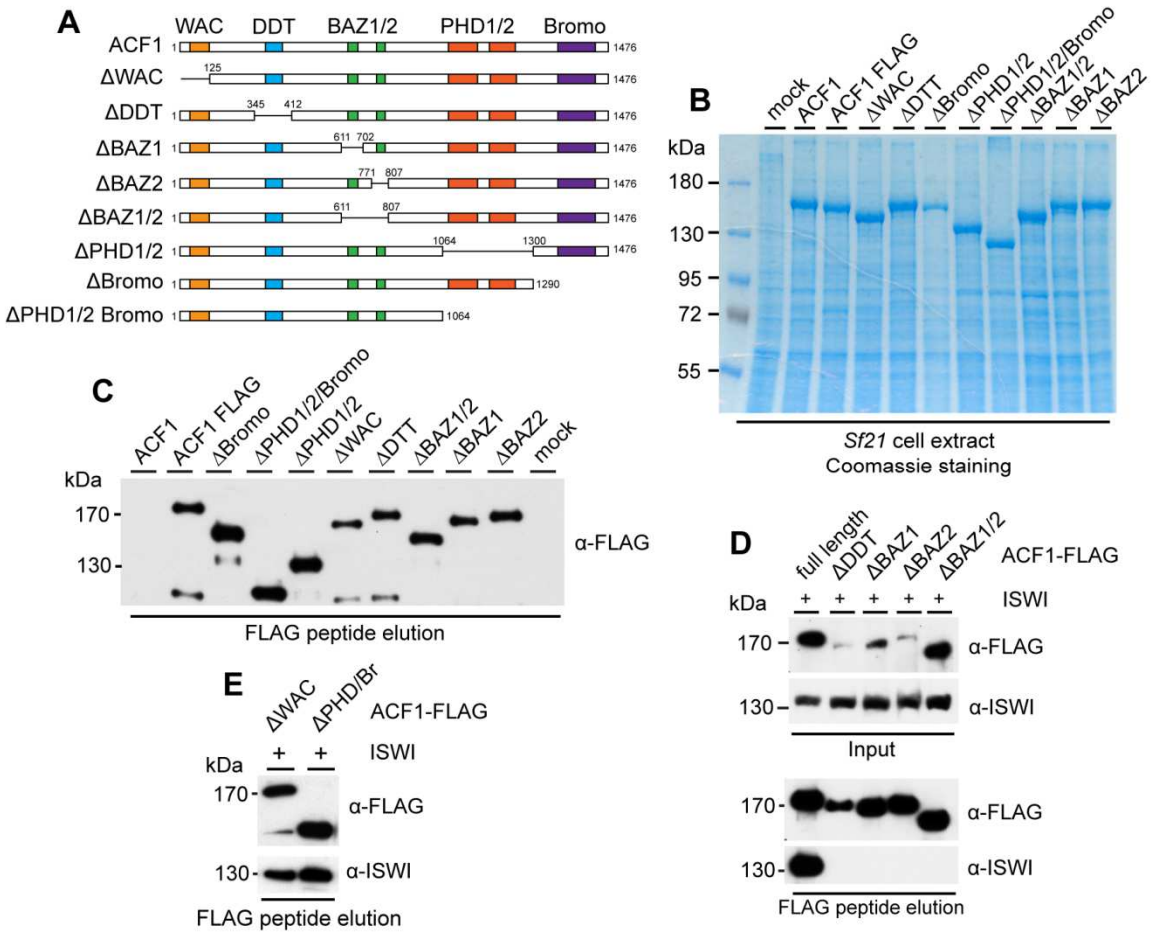

Figure 3.3. Recombinant expression of ACF1 domain deletion proteins. **(A)** Schematic representation of ACF1 constructs. Yellow, blue, green, red and violet rectangle represents WAC, DDT, BAZ, PHD and Bromo domain, respectively. Numbers indicate length in amino acids. ACF1 full-length construct was made with or without C-terminal FLAG-tag. All other constructs were tagged C-terminally with FLAG-tag. **(B, C)** Recombinant expression of ACF1-FLAG domain deletion proteins. **(B)** Constructs were expressed in Sf21 cells via the Baculovirus expression system and cell extracts were analyzed by Coomassie staining. Untreated cell extract was used as control (mock). **(C)** ACF1-FLAG proteins were purified via FLAG affinity chromatography and FLAG peptide elution. Elutions (10%) were analyzed by Western blot with FLAG antibody. **(D, E)** ISWI interacts with N-terminal DDT and BAZ domain of ACF1. ACF1-FLAG domain deletions and ISWI were coexpressed and purified via FLAG affinity chromatography and FLAG peptide elution. Input (2%) and FLAG peptide elution (10%) were analyzed by Western blot with FLAG and ISWI antibody. **(E)** ISWI signal was only detected in elution when coexpressed with ACF1, ACF1ΔWAC or ACF1ΔPHD/Bromo-FLAG, **(D)** but not with ACF1ΔDDT or ACF1ΔBAZ-FLAG.

Next, FLAG-tagged ACF1 domain deletions were coexpressed with DOM-B in Sf21 cells and the DOM-B specific antibody (DOB2 4H4, refer to results 3.2 and 3.3.2) was used for pull-down to identify ACF1 domains required for DOM-B interaction. As expected, full-length ACF1-FLAG was detected in the DOB2 IP fraction with FLAG antibody only when coexpressed with DOM-B, but not when expressed alone (Fig. 3.4A), confirming previous interactions with FLAG affinity chromatography (Fig. 3.2A, C and D). Surprisingly, all ACF1 deletion proteins coeluted with DOM-B (Fig. 3.4A). To rule out unspecific interactions with protein G beads, pull-downs were repeated with cell extracts of FLAG-tagged ACF1 deletion constructs without coexpressing DOM-B. Importantly, no FLAG signals were detectable in DOB2 IP fractions (Fig. 3.4B). These results might be explained by two different scenarios. Firstly, the ACF1 interaction domain might not be part of the different protein domains analyzed in this study, which covered only approximately 50% of the entire protein sequence. Otherwise, several redundant binding sites in ACF1 could contribute to binding of DOM-B. To demonstrate this, more quantitative approaches might be used in future studies with purified proteins and individual domains.

To delineate the interaction domain on DOM-B, untagged ACF1 was coexpressed with FLAG-tagged DOM-B domain deletion proteins for analyses via FLAG affinity chromatography and Western blot (Fig. 3.4C). Remarkably, the DOM ATPase fragment was sufficient to bind ACF1 (Fig. 3.4C). As controls, neither FLAG peptide elutions of the DOM ATPase fragment nor ACF1 alone showed detectable ACF1 signals (Fig. 3.4C). This finding validates previous results and strengthens the hypothesis of a direct interaction of ACF1 and DOM-B, in particular to the ATPase domain. It has been suggested that the spacer region of SWR1-type remodelers enables unique regulation mechanisms by binding of different factors that modulate the remodeling reaction or outcome (25). Besides, the ATPase domain is a common feature of both DOM isoforms. Is it likely, therefore, that ACF1 binds not only to DOM-B but also to DOM-A. Alternatively, the C-terminus of DOM-A could serve as regulatory element and compete with ACF1 for binding to the ATPase domain, a mechanism becoming more evident also in other nucleosome remodeling factors (19,46,47).

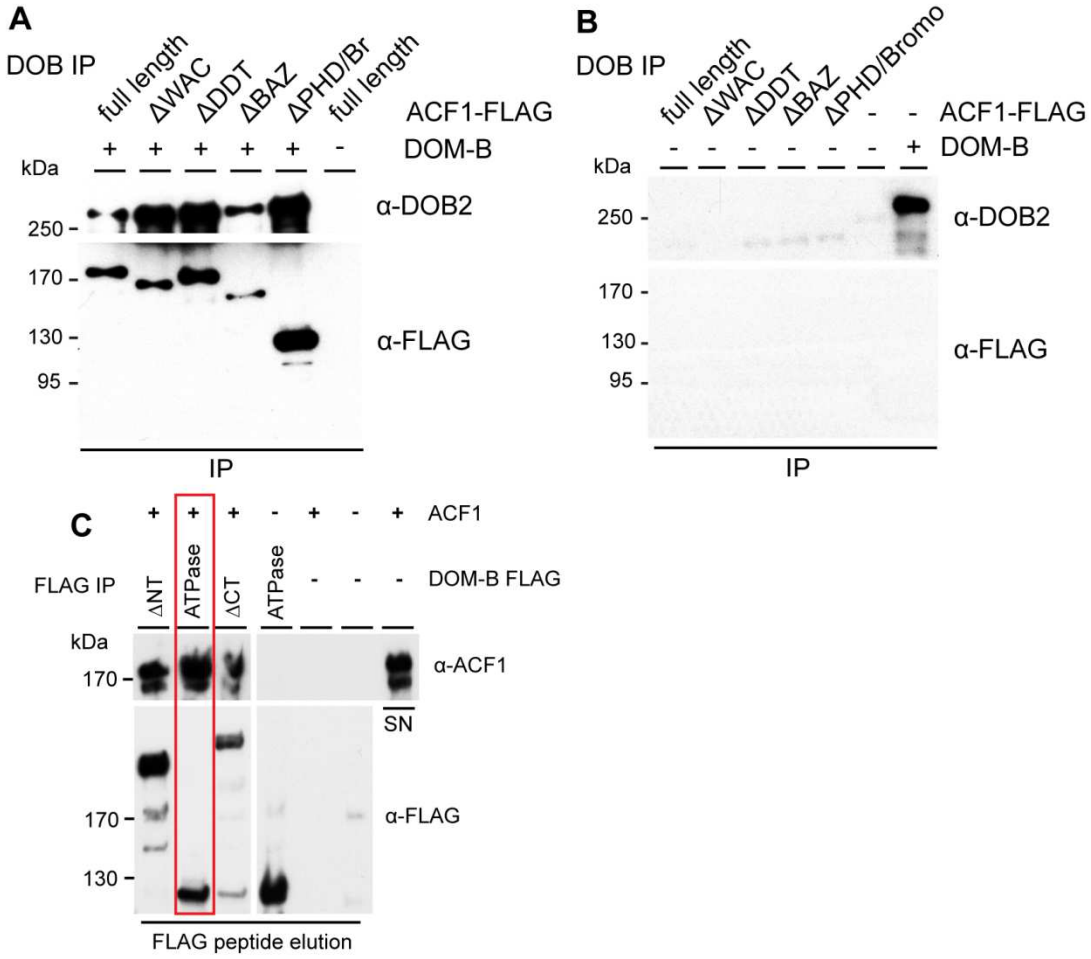

Figure 3.4. Delineation of interaction domains of DOM-B and ACF1. **(A)** Interaction with DOM-B is not mediated via ACF1 protein domains**.** ACF1-FLAG domain deletions and DOM-B were coexpressed in Sf21 cells via the Baculovirus expression system and purified via DOB2 4H4 antibody immunoprecipitation. IP fraction (20%) was analyzed by Western blot with FLAG and DOB2 4H4 antibody. FLAG signals were detected in all IP fractions of ACF1-FLAG domain deletions when coexpressed with DOM-B. As a control, no FLAG signal was detected in ACF1-FLAG IP fraction. **(B)** ACF1-FLAG domain deletions do not bind unspecifically to DOB2 antibody coupled agarose beads. ACF1-FLAG domain deletions were expressed in Sf21 cells via the Baculovirus expression system and purified via DOB2 4H4 antibody immunoprecipitation. IP fraction (20%) was analyzed by Western blot with FLAG and DOB2 4H4 antibody. FLAG signals were not detected in IP fractions of ACF1-FLAG domain deletions. As controls, no signals were detected in mock-treated and DOM-B IP fraction. **(C)** ACF1 interacts with the 'split' ATPase domain of DOM-B. ACF1 and DOM-B deletions were coexpressed in Sf21 cells via the Baculovirus expression system and purified via FLAG affinity chromatography and FLAG peptide elution. Elution (20%) was analyzed by Western blot with FLAG and ACF1 antibody. Signal for ACF1 was detected in elution when coexpressed with DOM-ATPase-FLAG (red rectangle). No ACF1 signal was detected in elution of ACF1, DOM-ATPase-FLAG or untreated mock sample. ACF1 signal was detected in supernatant (SN) of ACF1 sample.

3.3.1.4 Interaction studies of recombinant DOM-A with ACF1

To address whether ACF1 interacts with the other DOM isoform, untagged DOM-A or DOM-A-FLAG was recombinantly expressed via baculovirus in Sf21 cells (Fig. 3.5A). Remarkably, DOM-A-FLAG protein (350 kDa) was purified via FLAG affinity chromatography and detected with several antibodies in WB (Fig. 3.5B). Interestingly, ACF1 was specifically detected in FLAG peptide elution when coexpressed with DOM-A-FLAG (Fig. 3.5C). Conversely, no ACF1 signal was detectable in several control FLAG peptide elutions such as untreated mock , single expression of DOM-A-FLAG or ACF1 or coexpression of untagged DOM-A and ACF1 (Fig. 3.5C). In conclusion, ACF1 binds not only to DOM-B, but also to DOM-A. This can be explained by the fact that the common ATPase domain is sufficient to bind ACF1 *in vitro*. Since DOM-A has been characterized as an integral part of a TIP60 complex (79,96), it remains interesting whether other DOM-A/TIP60 complex subunits could interact with ACDC complex. So far, a direct interaction between DOM isoforms and TIP60 in *Drosophila* has not been addressed.

3.3.1.5 Interaction studies of recombinant DOM/TIP60 with ACF1

The orthologue of DOM-A in humans, p400, binds TIP60 via its SANT domain and through this represses its enzymatic activity (174). Therefore, it was interesting to test whether DOM isoforms and TIP60 from *D. melanogaster* interact with each other *in vitro*. To address this, DOM-A-FLAG and TIP60 (kind gift from Matthias Prestel, Ludwig-Maximilians-University Munich) were coexpressed in Sf21 cells to test for direct interaction via FLAG affinity chromatography. Remarkably, TIP60 signal was detected in FLAG peptide elution when coexpressed with DOM-A-FLAG (Fig. 3.6A). In contrast, no TIP60 signal was detectable in several control FLAG peptide elutions such as untreated mock, DOM-A-FLAG or TIP60 single expression (Fig. 3.6A). This finding further highlights the conserved interaction of TIP60 and DOM-A/p400 in different species. Furthermore, a preliminary experiment suggests an interaction with the other DOM isoform, DOM-B (Fig. 3.6B), similar to ACF1. Interestingly, ACF1 antibody does not only co-immunoprecipitate DOM but also TIP60 from nuclear extract of *D. melanogaster* embryos (172). Given this observation, FLAG affinity chromatography of TIP60 with ACF1-FLAG deletion constructs were performed to test for direct interaction *in vitro*. Remarkably, TIP60 was detected in FLAG peptide elution when coexpressed with ACF1-FLAG but not in untreated mock, single expression of DOM-A-FLAG or TIP60 (Fig. 3.6C). Further analysis with ACF1 deletions did not identify a particular domain for ACF1-TIP60 interaction (Fig. 3.6C).

Still, comprehensive *in vitro* interaction studies strengthen the hypothesis of an ACF1 interaction with DOM/TIP60 complexes.

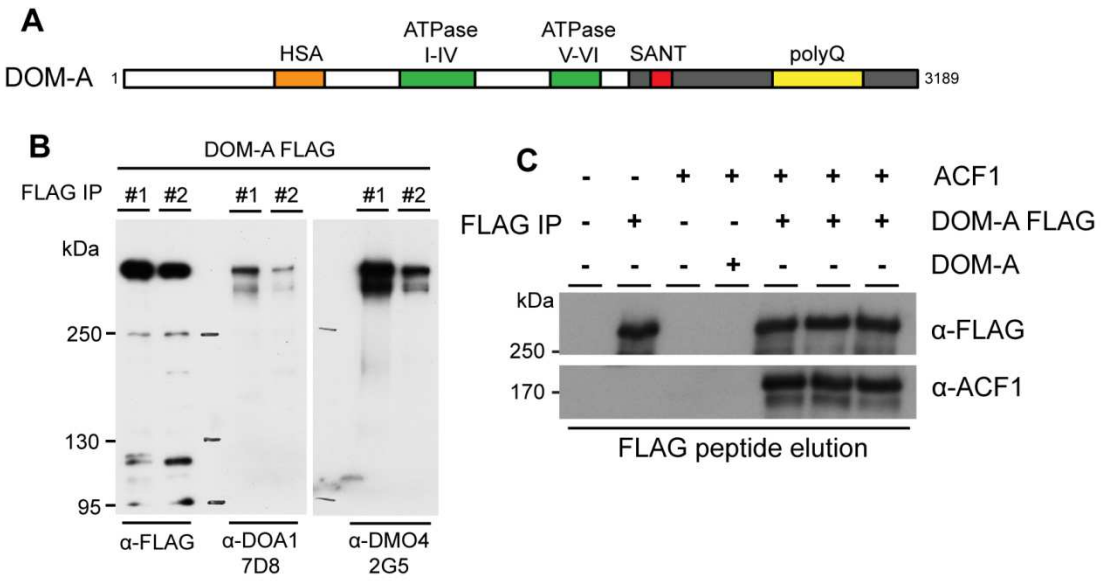

Figure 3.5. Interaction studies of recombinant DOM-A with ACF1. **(A)** Schematic representation of DOM-A construct. Orange, green, red and yellow rectangle represents HAS, ATPase, SANT and poly-Q domain, respectively. Numbers indicate length in amino acids. Note characteristic 'spacer' region for SWR1-type remodeling enzymes between ATPase I-IV and V-VI domains. DOM-A construct was either untagged or contained a C-terminal FLAG-tag. **(B)** Expression of recombinant full-length DOM-A. Construct was expressed in Sf21 cells via the Baculovirus expression system and proteins purified via FLAG affinity chromatography and FLAG peptide elution. Elution (20%) of two different samples was analyzed by Western blot with FLAG, DOA1 and DMO4 antibody. Some C-terminal degradation was detected with DOA1 and DMO4 antibody. Unspecific lower molecular weight bands were detected with FLAG antibody. **(C)** Recombinant ACF1 interacts with DOM-A. ACF1 and DOM-A-FLAG were coexpressed in Sf21 cells via the Baculovirus expression system and purified via FLAG affinity chromatography and FLAG peptide elution. Elution fraction (20%) was analyzed by Western blot with FLAG and ACF1 antibody. ACF1 signal was only detected in elution when coexpressed with DOM-A-FLAG in three different samples. As controls, no ACF1 signal was detected in elution of untreated mock sample or single expression of DOM-A-FLAG. Unspecific binding of ACF1 to FLAG beads was not observed.

In summary, FLAG affinity chromatography assays with recombinant proteins were used to assess the direct interaction of the two distinct nucleosome remodeling factors, ACF and DOM/TIP60, *in vitro*. Presented data in this thesis indicates a novel direct interaction of ACF1 with different subunits of DOM/TIP60 complexes.

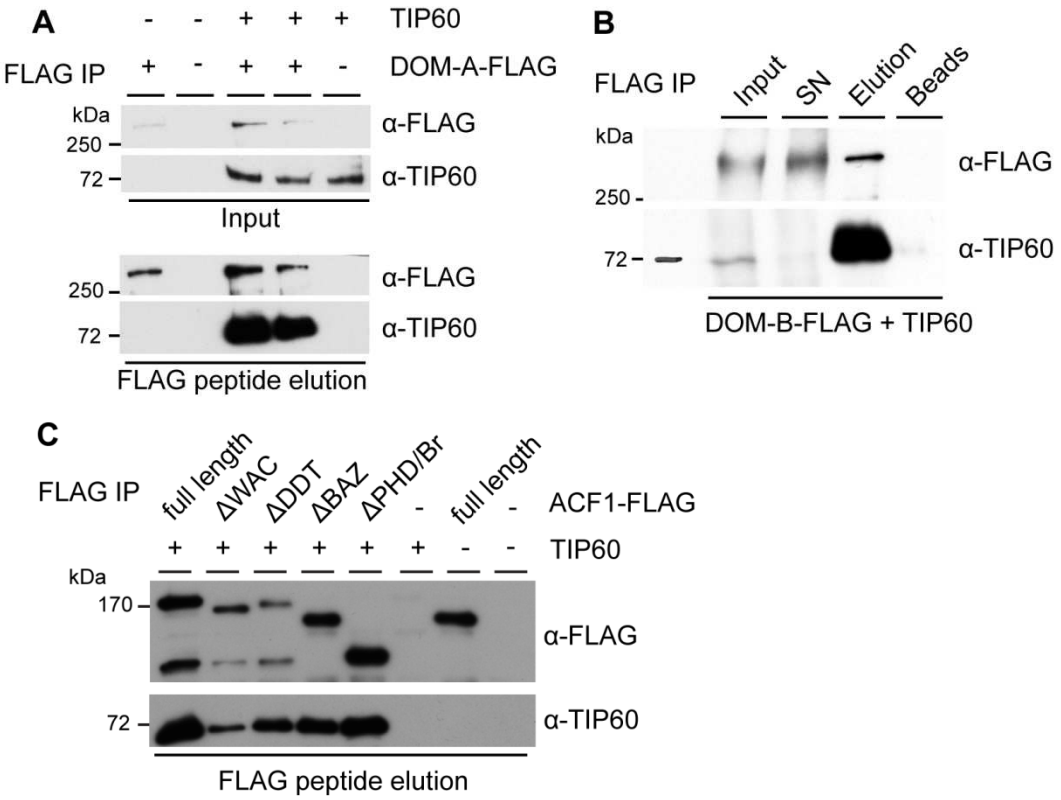

Figure 3.6. Interaction studies of recombinant DOM/TIP60 with ACF1. **(A)** Recombinant TIP60 interacts with DOM-A. TIP60 and DOM-A-FLAG were coexpressed in Sf21 cells via the Baculovirus expression system and purified via FLAG affinity chromatography and FLAG peptide elution. Input (2%) and elution fraction (20%) were analyzed by Western blot with FLAG and TIP60 antibody. TIP60 signal was only detected in elution when coexpressed with DOM-A-FLAG in two different samples. As controls, no TIP60 signal was detected in elution of untreated mock sample or single expression of DOM-A-FLAG. Unspecific binding of TIP60 to FLAG beads was not observed. **(B)** Preliminary result suggests interaction of recombinant TIP60 with DOM-B. TIP60 and DOM-B-FLAG were coexpressed in Sf21 cells via the Baculovirus expression system and purified via FLAG affinity chromatography and FLAG peptide elution. Input (2%), supernatant (SN 2%), FLAG peptide elution (20%) and FLAG beads (20%) were analyzed by Western blot with FLAG and TIP60 antibody. TIP60 signal was detected in elution when coexpressed with DOM-B-FLAG. TIP60 signal was strongly reduced in supernatant (SN) and only weakly detectable on FLAG beads. **(C)** Recombinant TIP60 interacts with ACF1 and its interaction is not mediated via ACF1 protein domains. ACF1-FLAG domain deletions and TIP60 were coexpressed in Sf21 cells via the Baculovirus expression system and purified via FLAG affinity chromatography and FLAG peptide elution. Elution fraction (20%) was analyzed by Western blot with FLAG and TIP60 antibody. Signal for TIP60 was detected in elution when coexpressed with ACF1-FLAG domain deletions. No TIP60 signal was detected in elution of TIP60, ACF1-FLAG or untreated mock sample.

3.3.2 Characterization of DOM-A and DOM-B antibodies

In order to directly visualize the two Domino splice variants, isoform-specific antibodies were raised for future studies as a valuable tool to dissect specific functions of DOM-A and DOM-B. In collaboration with Elisabeth Kremmer (Molecular Immunology, Helmholtz Zentrum Munich), two peptides each derived specifically from either DOM-A (DOA1 and DOA2) or DOM-B (DOB1 and DOB2) were used for immunization of rats and mice, respectively (Fig. 3.7A). In total, 134 primary tissue culture supernatants (TCS) of single hybridoma cell lines for DOA1, DOB1 and DOB2 were analyzed in an initial screening by Western blot, immunoprecipitation and immunofluorescence (Fig. 3.7B, C). A selection of hybridoma isolates was further subcloned as stable cell lines for antibody production (Fig. 3.7D).

Initially, primary TCSs for DOA and DOB were tested in Western blot with nuclear extract of 0-12 h old embryos (Figs. 3.7 and 3.8A-C). A prominent high-molecular weight band was detected with several DOA1, DOB1 and DOB2 antibodies (Fig. 3.8A-C). However, some lower molecular weight signals were also detected indicating some minor degradation or other DOM isoforms. Indeed, multiple DOM-A and DOM-B bands had been detected before (79,84). Latest modENCODE data shows several DOM-A transcripts, which differ only in a single exon, suggesting further DOM-A isoforms, not addressed in current work. DOB1 and DOB2 antibodies detected a single high molecular weight band when recombinant DOM-B protein was probed (Fig. 3.8D, E). In contrast, recombinant DOM-B protein lacking the C-terminus (DOM-B-ΔCT) did not show any high molecular weight band (Fig. 3.8D, E). As another control, untreated mock sample revealed only some unspecific band with lower molecular weight (Fig. 3.8D, E).

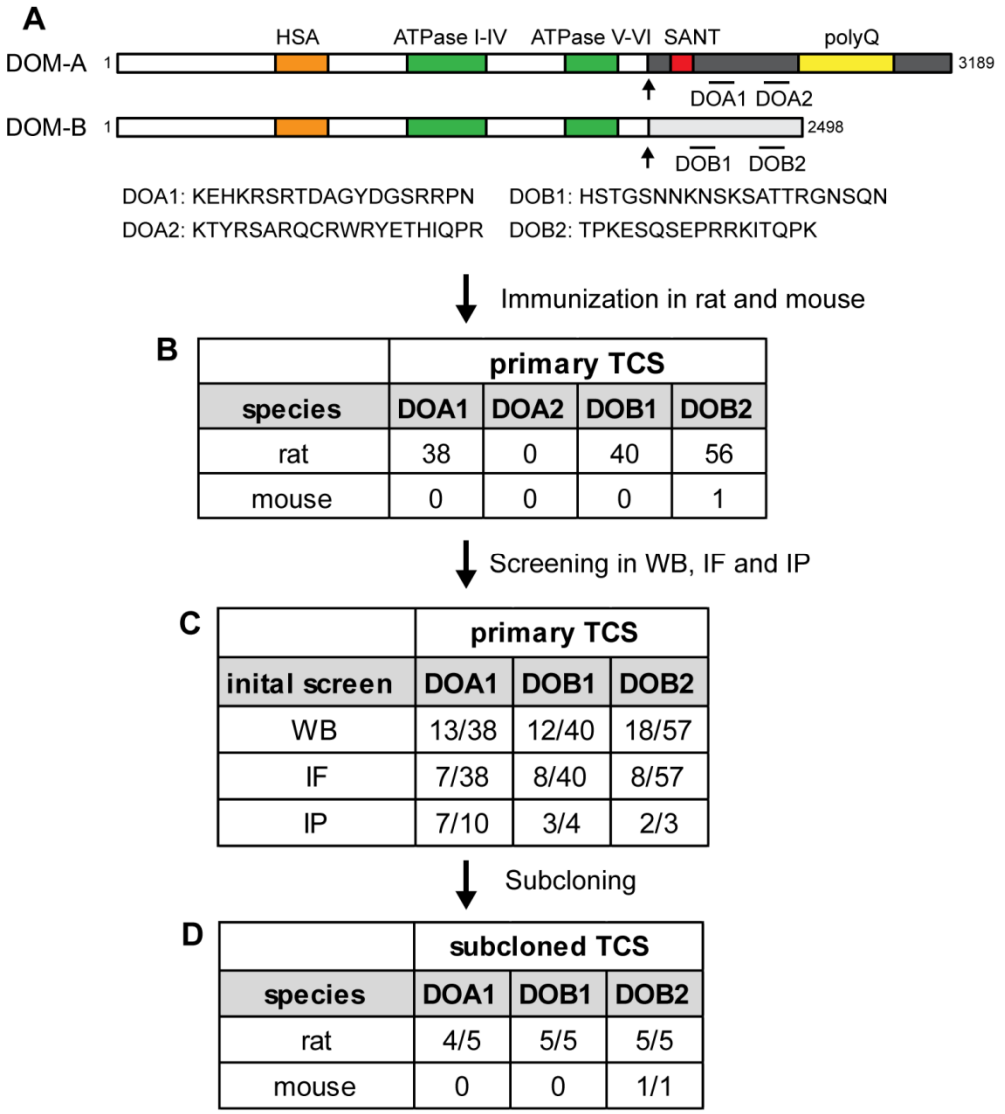

Figure 3.7. Generation and characterization of DOM-A and DOM-B antibodies. (A) Schematic representation of DOM-A and DOM-B protein structures. Orange, green, red and yellow rectangle represents HSA, ATPase, SANT and poly-Q domain, respectively. Arrow indicates specific C-termini of DOM-A (dark grey) and DOM-B (light grey). Numbers indicate length in amino acids. Regions for DOA and DOB peptides are indicated by black lines. **(B)** Summary of primary tissue culture supernatants (TCS) for DOA1, DOA2, DOB1 and DOB2 peptides. **(C)** Initial screening of primary TCSs for DOA1, DOB1 and DOB2 by Western blot (WB), immunoprecipitation (IP) and immunofluorescence (IF). Number of positively tested and total number of tested TCSs is shown. **(D)** Summary of stably subcloned TCSs for DOA1, DOB1 and DOB2. Number of successfully subcloned and total number of subcloned TCSs is shown.

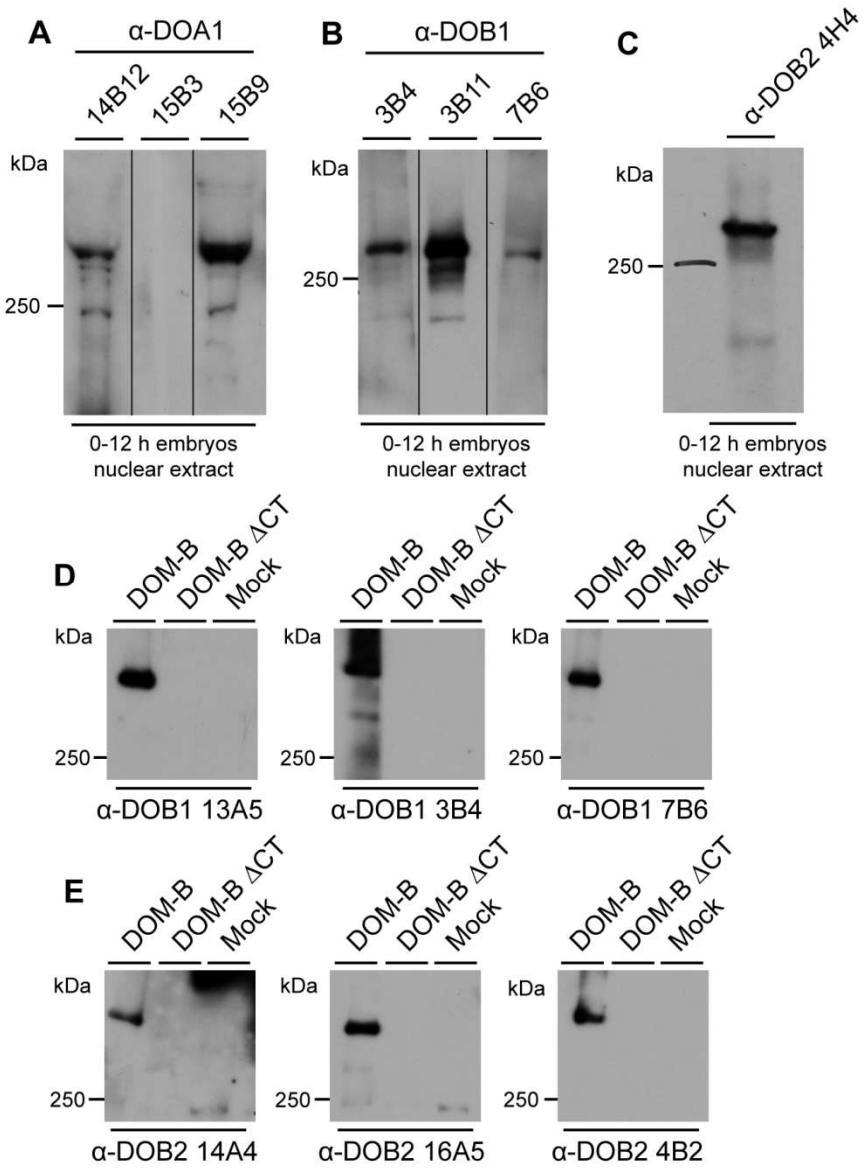

Figure 3.8. Western blot with DOA and DOB antibodies. (A-C) DOA and DOB antibodies were used for Western blot with nuclear extracts of 0-12 h old embryos. Nuclear extract (10 µl) was analyzed with 1:5 dilutions of primary TCSs. A selection of TCSs is shown. Please also refer to Fig. 3.7, Tab. 3 and 4. **(D, E)** DOA and DOB antibodies were used for Western blot with recombinant proteins. FLAG peptide elutions (10%) of recombinant DOM-B-FLAG, DOM-B-ΔCT-FLAG and untreated mock sample were used with 1:5 dilutions of primary TCSs.

Next, several subcloned TCSs for DOB1 and DOB2 were positively tested for immunoprecipitation with nuclear extract of 0-12 h old embryos (Fig. 3.9A). A promising candidate, the only mouse DOM-B antibody (DOB2 4H4), was also used for immunoprecipitation with extracts from different *D. melanogaster* cell lines (Fig. 3.9B). Recently, a study from our lab used a DOM antibody (DMO4 2G5), that recognizes both isoforms, to show an interaction of a DOM/TIP60 complex with ACF *in vivo* by immunoprecipitation from nuclear extract of 0-2 h old embryos (172). In agreement, the novel DOB1 3B4 antibody specifically immunoprecipitated TIP60, ACF1 and ISWI from extracts of early embryos (Fig. 3.9C), while signals were absent in a control using an unrelated antibody (Fig. 3.9C). In another approach, cell extracts with recombinant DOM-A-FLAG were used to identify DOA1 antibodies for immunoprecipitation (Fig. 3.9D, E). As a control, DOM-A-FLAG was immunoprecipitated by DMO4 2G5 antibody, but not by an unrelated antibody (Fig. 3.9D, E). In addition, DOA1 antibody did not react with recombinant DOM-B-FLAG (Fig. 3.9E). Finally, a cell type-specific knockdown approach in larval brains was used to confirm the specificity of DOA and DOB antibodies (refer to results 3.2).

To screen DOA and DOB antibodies for immunofluorescence, FLAG-HA-tagged DOM-A and DOM-B were transiently expressed in *D. melanogaster* L2-4 cells. Primary TCSs of DOA and DOB were used for co-staining with antibodies against FLAG or HA-tag. Several DOA1, DOB1 and DOB2 antibodies (species rat) gave positive nuclear signals in transiently transfected cells (Figs. 3.10A, B and 3.7). Despite all efforts, the FLAG antibody (species mouse) did not work in immunofluorescence for co-staining with DOA and DOB antibodies. Therefore, only DOB2 4H4 (species mouse) was used for co-staining with HA antibody (species rat) (Fig. 3.10C). Notably, overlapping signals with DOB2 4H4 and HA antibody were detected in nuclei of transiently transfected cells (Fig. 3.10C).

In summary, a combination of molecular, biochemical and immunofluorescence approaches identified and validated several monoclonal peptide antibodies against DOM-A and DOM-B. These antibodies will be valid tools for future studies aiming to dissect the functions of DOM-A and DOM-B *in vitro* and *in vivo*.

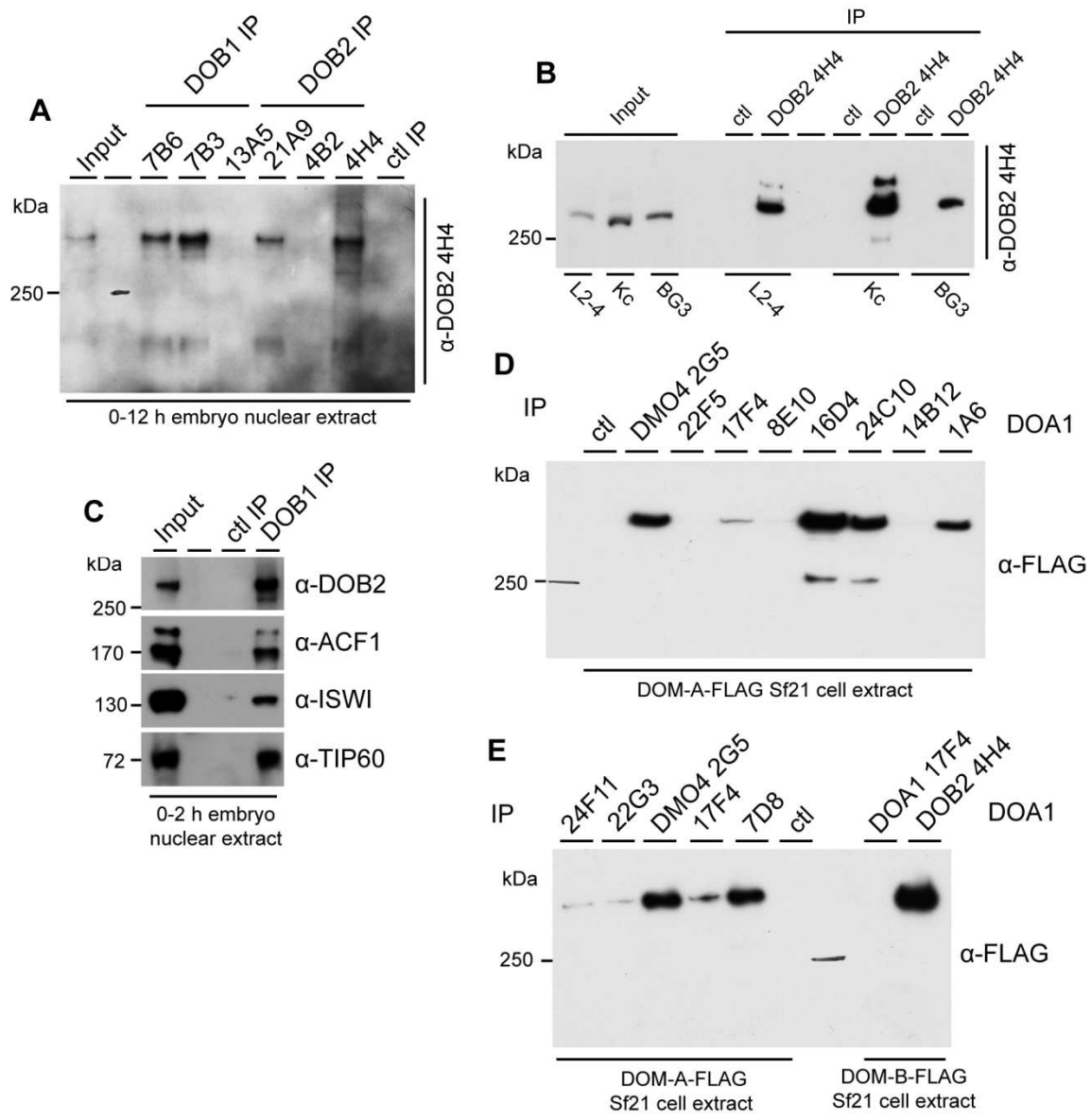

Figure 3.9. Immunoprecipitation with DOA and DOB antibodies. **(A)** DOB1 and DOB2 antibodies were used for immunoprecipitation with nuclear extracts of 0-12 h old embryos. Input (5%) and IP fraction (10%) were analyzed by Western blot with DOB2 4H4 antibody. An unrelated antibody (ctl IP) was used as negative control. Please also refer to Fig. 3.7, Tab. 3 and 4. **(B)** DOB2 4H4 antibody was used for immunoprecipitation with different extracts of L2-4, Kc and BG3 cells. Input (5%) and IP fraction (10%) were analyzed by Western blot with DOB2 4H4 antibody. An unrelated antibody (ctl) was used as negative control. **(C)** Co-immunoprecipitation of TIP60, ACF1 and ISWI with DOB1 3B4 antibody. Nuclear extracts of 0-2 h old embryos was used. Input (5%) and IP fraction (10%) were analyzed by Western blot with DOB2 4H4, ACF1 8E3, ISWI and TIP60 2C4 antibody. An unrelated antibody (ctl IP) was used as negative control. **(D, E)** DOA1 antibodies were used for immunoprecipitation with recombinant DOM-A. Sf21 cell extracts with recombinantly expressed DOM-A-FLAG were used. IP fraction (10%) was analyzed by Western blot with FLAG antibody. An unrelated antibody (ctl) was used as negative control. DMO4 2G5 antibody served as a positive control. DOM-B-FLAG was immunoprecipitated by DOB2 4H4, but not by DOA1 17F4.

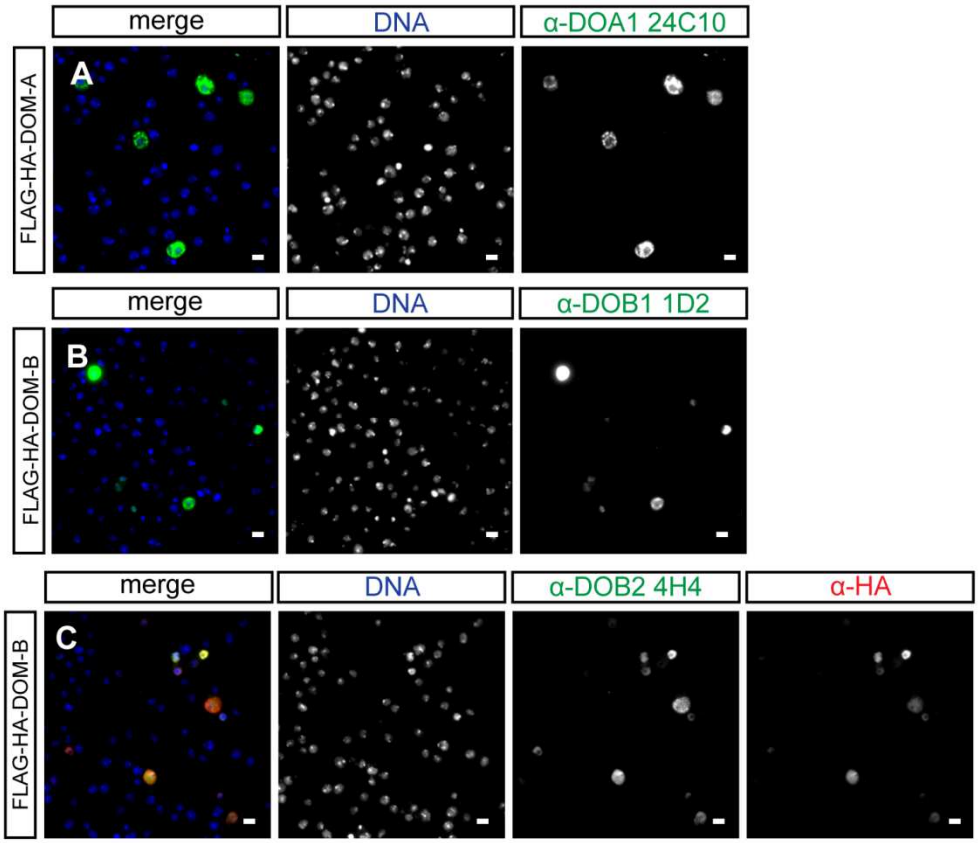

Figure 3.10. Immunofluorescence with DOA and DOB antibodies. **(A-C)** DOA and DOB antibodies were used for immunofluorescence with cells expressing tagged DOM proteins. L2-4 cells were transiently transfected with plasmids expressing N-terminally FLAG-HA-tagged DOM-A or DOM-B, respectively. All DOA1, DOB1 and DOB2 TCSs were screened for nuclear immunofluorescence signals. Please also refer to Fig. 3.7 and Tab. 4. A selection of representative immunofluorescence images of L2-4 cells is shown for: **(A)** FLAG-HA-DOM-A with DOA1 24C10 (green), **(B)** FLAG-HA-DOM-B with DOB1 1D2 (green) and **(C)** FLAG-HA-DOM-B with DOB2 4H4 (green) and HA (red). DAPI staining is shown in blue. Scale bar: 10 µm.

3.3.3 Materials and Methods

This section summarizes all materials and methods from results 3.3. For more details and information, please also refer to the Material and Methods sections of the research articles and supplementary information in results 3.1 and 3.2.

3.3.3.1 Cloning of *Domino* and *Acf1* constructs

Dom-A and *Dom-B* cDNAs were assembled into the pENTR 3c Dual Selection Vector (Gateway cloning system, ThermoFisher Scientific) via PCR-mediated In-Fusion HD Cloning Kit following the manufacturer's guidelines (Clonetech Laboratories). LD35056 and LD03212 or LD35056, LD03212 and LD32234 vectors (Drosophila Genomics Resource Center) were used as DNA templates for *Dom-A* and *Dom-B* cDNAs, respectively. Primers #26-31 and #1-8 (Tab. 1) were used for PCR amplification of *Dom-A* and *Dom-B* cDNAs, respectively. *Dom-A* and *Dom-B* constructs were analyzed with appropriate restriction enzyme digestions (New England Biolabs). *Dom-A* and *Dom-B* constructs were sequenced following the manufacturer's guidelines and services (GATC Biotech; MWG Biotech) with primers #9-16, 20-21 and 32-36 or #9-21 (Tab. 1), respectively. The *Dom-B* K945R construct was made via PCR-mediated QuikChange Site-Directed Mutagenesis Kit following the manufacturer's guidelines (Stratagene) with plasmid #5 (Tab. 2) and primers #24 and 25 (Tab. 1). The *Dom-B* K945R construct was analyzed with appropriate restriction enzyme digestions and sequenced with primers #9-21 (Tab. 1).

Dom-ΔCT, *Dom-B*-ΔNT and *Dom*-ATPase constructs were assembled into the pENTR 3c Dual Selection Vector via PCR-mediated In-Fusion HD Cloning Kit following the manufacturer's guidelines. Plasmid #5 (Tab. 2) was used as DNA template for PCR amplifications with primers #30, 31, 39 and 40 (*Dom*-ΔCT), #6, 8, 37 and 40 (*Dom-B*-ΔNT) and #37-40 (*Dom*-ATPase). Plasmid #8 was used as DNA template for PCR amplifications with primers #37-40 (*Dom*-ATPase K945R). The *Dom* deletion constructs were analyzed with appropriate restriction enzyme digestions and sequenced with primers #9-21 (Table 1).

Dom constructs were cloned into pDEST8 or pFASTBac1 vector (Tab. 2) using the Gateway cloning system following manufacturer's guidelines (ThermoFisher Scientific). Constructs were analyzed with appropriate restriction enzyme digestions and sequenced with primer #59 (Tab. 1).

Acf1 deletion constructs were made via PCR-mediated In-Fusion HD Cloning Kit following the manufacturer's guidelines using as DNA template pDEST_ACF1_FLAG_NT (175) and

primers #41-55 (Tab. 1). *Acf1* deletion constructs were analyzed with appropriate restriction enzyme digestions and sequenced as published (175). All plasmids are listed in Table 2.

pDEST8 or pFASTBac1 vector was transformed into DH10Bac *E. coli* cells to obtain recombinant bacmid DNA following the manufacturer's guidelines (Bac-to-Bac Baculovirus Expression System, Invitrogen). Bacmid DNAs were verified by PCR with primers #22 or 23 (Tab. 1) and appropriate internal primers and stored at 4°C.

3.3.3.2 Recombinant protein expression via baculovirus expression system in Sf21 cells

Recombinant bacmid DNA was used for transfection of *Spodoptera frugiperda* Sf21 cells following the manufacturer's guidelines (Bac-to-Bac Baculovirus Expression System, Invitrogen). P2 baculovirus stocks were obtained via two rounds of infection of Sf21 cells and amplification of baculovirus following the manufacturer's guidelines (Bac-to-Bac Baculovirus Expression System, Invitrogen). For protein expression, 20 ml or 200 ml Sf21 cells ($1x10^6$ cells/ml) were infected with appropriate amount of P2 virus for 3 days in a shaking incubator at 27°C following the manufacturer's guidelines (Bac-to-Bac Baculovirus Expression System, Invitrogen). Cells were harvested by centrifugation (5 min, 170 g) and pellet washed with ice-cold PBS. Cells were centrifuged (5 min, 170 g) and pellet was resuspended in 1 ml HEMG200 buffer (20 mM HEPES pH 7.6, 200 mM KCl, 0.5 mM EDTA, 1.5 mM $MgCl_2$, 10% Glycerol, 0.05% NP40, Roche Complete proteinase inhibitors), frozen in liquid nitrogen and stored at -80°C.

3.3.3.3 Purification of recombinant proteins via FLAG affinity chromatography

Sf21 cells in 1 ml HEMG200 buffer were thawed in a water bath at 37°C and put on ice for 10 min. Cells were sonicated using a Digital Sonifier (Branson) with 20% amplitude (4x 10 sec and 20 sec pause) and centrifuged (30.000 g, 4°C) for 30 min. 50 µl of the cellular supernatant was stored as input fraction (Input) at -80°C for further analysis. 950 µl of the cellular supernatant was used for FLAG affinity chromatography with 50 µl ANTI-FLAG M2 Affinity Gel (Sigma-Aldrich) for 3 h at 4°C on a rotating wheel. FLAG beads were centrifuged (2.000 rpm, 5 min, 4°C, Heraeus Pico17, Thermo Electron Corporation), supernatant removed and stored as supernatant fraction (SN) at -80°C for further analysis. FLAG beads were washed 3x with HEMG500 (20 mM HEPES pH 7.6, 500 mM KCl, 0.5 mM EDTA, 1.5 mM $MgCl_2$, 10% Glycerol, 0.05% NP40, Roche Complete proteinase inhibitors) and 2x HEMG200 for 10 min. Protein was eluted with 5 µl FLAG peptide (5 mg/1 ml, Sigma-Aldrich) in 100 µl HEMG200 for 90 min (Elution 1) or overnight (Elution 2) at 4°C on a rotating wheel and stored at -80°C. FLAG beads were boiled in

Laemmli buffer for 5 min and stored as bead fraction (Beads) for further analysis. FLAG IP fractions were analyzed by Western blot or Coomassie staining.

3.3.3.4 Interaction studies of recombinant proteins via FLAG affinity chromatography

For interaction studies, Sf21 cells were infected with appropriate amounts of P2 virus in two different ways. On the one hand, cells were infected with two or three P2 viruses for 3 days to facilitate coexpression of different proteins. Cell extracts were used for FLAG affinity chromatography to study the interaction of recombinant proteins that were assembled during cellular coexpression. On the other hand, cells were infected separately with single viruses for 3 days. Cells were mixed and lysed together to study potential interaction of recombinant proteins that were expected to assemble in cell lysates. For more details refer 3.3.3.2 and 3.3.3.3.

3.3.3.5 SDS-PAGE, Western blot and Coomassie staining

Samples were prepared in Laemmli buffer, incubated at 95°C for 5 min and loaded on to SDS polyacrylamide gel together with 5 µl of protein size marker (10-250 kDa; 10-170 kDa). In general, gels consisted of stacking (5% polyacrylamide) and separation gel (4-20% or 6% polyacrylamide). Samples were separated for 1-3 h at constant voltage (100V for stacking gel, 180V for separation gel). Gel was either analyzed by Coomassie staining following the manufacturer's guidelines (Colloidal Blue staining kit, NOVEX) or Western blot. For Western blot, proteins were transferred to PVDF membrane (Immobilon-P, Millipore) at 4°C for 90 min with constant power (400 mA) using a Mini Trans-Blot Electrophoretic Transfer Cell following the manufacturer's guidelines (Bio-Rad). Membrane was then blocked for 30 min in PBST (PBS 0,1% Tween) with 5% (w/v) milk powder on a shaking platform. Membrane was incubated overnight at 4°C with primary antibody solution (Tab. 4). Membrane was washed 3x for 10 min with PBST, incubated for 2 h at room temperature with secondary antibodies conjugated to horse radish peroxidase (1:20000 in PBST 5% milk, GE Healthcare) and washed again 3x for 10 min with PBST. Proteins were detected via chemiluminescence using the ECL detection system following the manufacturer's guidelines (GE Healthcare). Signals were exposed to X-ray films (Medical X-ray Super FX, Fuji) for 5 sec to 10 min and developed in X-ray developer machine (AGFA curix 60).

3.3.3.6 Design and generation of DOA and DOB antibodies

DOA1 (KEHKRSRTDAGYDGSRRPNC), DOA2 (KTYRSARQCRWRYETHIQPR), DOB1 (HSTGSNNKNSKSATTRGNSQN) and DOB2 (TPKESQSEPRRKITQPKC) peptides with

N-terminal PEG-Biotin and C-terminal coupled Ovalbumin were made by Peptide Specialty Laboratories (PSL, Heidelberg, Germany). Standard immunization of rats and mice with the individual peptides was done by the group of E. Kremmer (Molecular Immunology, Helmholtz Zentrum Munich).

3.3.3.7 Characterization of DOA and DOB antibodies

In total, 134 primary tissue culture supernatants of single hybridoma cell lines were analyzed in an initial screening by Western blot, immunoprecipitation and immunofluorescence. For Western blot analysis, nuclear extracts from 0-12 h old wild type embryos were used. Furthermore, FLAG IP elution fractions with recombinant DOM-A-FLAG, DOM-B-FLAG, DOM-B-ΔCT-FLAG or untreated mock sample were probed with monoclonal antibodies. DOA1 (17F4) and DOB2 (4H4) antibodies were validated by using a cell type-specific RNAi approach in larval brains (refer to results 3.2). Nuclear extracts from 0-12 h old wild type embryos were used for immunoprecipitation with DOB1 and DOB2 antibodies. Additionally, DOB2 (4H4) antibody was used for IP with RIPA (50 mM Tris pH 8.0, 0.1% SDS, 1% Triton X-100, 150 mM NaCl, 1% deoxycholic acid, 2 mM PMSF) extracts from *D. melanogaster* L2-4, Kc and BG3 cells. To test DOA1 antibodies in immunoprecipitation whole cell lysates from Sf21 cells were used with recombinant DOM-A-FLAG and DOM-B-FLAG in comparison to an untreated mock sample. An unrelated monoclonal antibody (Spt6-2 27C1, rat, Sarah Schunter, LMU Munich) served as a control in IP experiments. Lastly, L2-4 cells were transiently transfected with inducible plasmids expressing HA-FLAG-tagged DOM-A or DOM-B to screen monoclonal antibodies for immunofluorescence application.

A selection of hybridoma isolates was further subcloned as stable cell lines for antibody production (Molecular Immunology, Helmholtz Zentrum Munich). A detailed description of all subcloned monoclonal antibodies is listed (Tab. 3).

3.3.3.8 Nuclear extract preparation from *D. melanogaster* embryos

Embryo collection and nuclear extract preparation were done as published (176). In brief, 0-12h or 0-2 h collections of wild type embryos from large cage populations were washed with cold tap water using different sieves (0.71, 0.355, 0.125 mm diameters). Embryos were dechorinated with a 1:4 dilution of sodium hypochlorite for 3 min under constant stirring with a metal spatula. Embryos were washed in cold tap water for 5 min. Embryos were either directly used for nuclear extract preparation or frozen in liquid nitrogen and stored at -80°C. All subsequent steps were done at 4°C in the cold room. Embryos were resuspended in NX1 buffer (2 ml/g embryos, 15 mM HEPES pH 7.6, 10 mM KCl, 2 mM $MgCl_2$, 0.5 mM EGTA,

0.1 mM EDTA pH 8.0, 350 mM Sucrose, 1 mM DTT, 1 mM NaMBS and proteinase inhibitors) and homogenized with a Yamato LH-21 device (1.000 rpm, six passages). The homogenate was filtered through Miracloth filtration material, filled up to a final volume of 5ml/g embryos with NX1 buffer and centrifuged with the GSA rotor at 8.000 rpm for 15 min to pellet nuclei. Supernatant and white lipids were removed and the brown nuclei pellet was resuspended in NX2 buffer (1 ml/g embryo, 15 mM HEPES pH 7.6, 110 mM KCl, 2 mM $MgCl_2$, 0.1 mM EDTA pH 8.0, 1 mM DTT, 1 mM NaMBS and proteinase inhibitors). This process was aided with 20 strokes of glass douncer B and transferred to 45Ti tubes. Next, 10 volume percent of ammonium sulfate (4M, room temperature) were added and tubes mixed immediately. The solution was further mixed on a rotation wheel for 20 min followed by ultracentrifugation (Ti45 rotor, 35.000 rpm, 2 h, Beckman Coulter). The supernatant was precipitated under constant stirring with stepwise addition of ammonium sulfate (0.3 g of finely grounded powder per ml supernatant) for 5 min. The solution was centrifuged (SS34 rotor, 15.000 rpm, 20 min, Sorvall) and the pellet resuspended in NX3 buffer (0.2 ml/g embryos, 25 mM HEPES pH 7.6, 100 mM KCl, 2 mM $MgCl_2$, 0.1 mM EDTA pH 8.0, 1 mM DTT, 20% v/v Glycerol, 1 mM NaMBS and proteinase inhibitors). Afterwards, the solution was dialyzed for 4 h against 2 L of NX3 buffer subsequently pelleted by a last centrifugation step (SS34 rotor, 10.000 rpm, 5 min, Sorvall). Aliquots of nuclear extract were frozen in liquid nitrogen and stored at -80°C.

3.3.3.9 Immunoprecipitation with DOA and DOB antibodies

All incubation, washing and elution steps were done on a rotating wheel at 4°C. 50 µl protein G beads per reaction (E. Kremmer, Molecular Immunology, Helmholtz Zentrum Munich) were washed 3x with HEMG200 or PBST for 5 min. For antibody coupling, 0.2-5 ml TCS was added to protein G beads and incubated for 1 h. Beads were centrifuged (2.000 rpm, 5 min, 4°C, Heraeus Pico17, Thermo Electron Corporation) and further incubated in HEMG200 or PBST with 5% BSA for 1 h to block unspecific interactions. Beads were centrifuged (2.000 rpm, 5 min, 4°C, Heraeus Pico17, Thermo Electron Corporation) and used for IP experiments with different extracts. An unrelated monoclonal antibody (Spt6-2 27C1, refer also to 3.3.3.7) served as a control.

Different extracts were used as input for IP experiments such as 200 µl nuclear extract with 600 µl NX3 buffer, 500 µl Sf21 cell extract ($2x10^6$ cells/ml) in HEMG200 or 1 ml *Drosophila* cell extract ($1x10^6$ cells per ml of L2-4, Kc [Kc167] or BG3 [ML-DmBG3-c2]) in RIPA buffer. For cell extracts in RIPA buffer, cells were harvested by centrifugation (5 min, 170 g),

supernatant was discarded and pellet washed with ice-cold PBS. Cells were centrifuged (5 min, 170 g), pellet was resuspended in 1 ml RIPA buffer and incubated for 10 min on ice (3x mixing, 5 sec, Vortex Genie 2, Bachofer). Cell extracts were centrifuged (13.200 rpm, 30 min, 4°C, Centrifuge 5415R, Eppendorf), supernatants frozen in liquid nitrogen and stored at -80°C.

For pre-clearing of extracts, 50 µl of washed protein G beads were incubated for 1 h with different extracts and beads were collected by centrifugation (2.000 rpm, 5 min, 4°C, Heraeus Pico17, Thermo Electron Corporation). Next, precipitated material were removed by centrifugation (13.200 rpm, 30 min, 4°C, Centrifuge 5415R, Eppendorf) and pre-cleared supernatant of extracts were used for IP experiments. For co-IP experiments, 0.1 µl Benzonase endonuclease (100,000 Units, Merck Millipore) was added to 200 µl of nuclear extract (0-2 h old embryos) with 600 µl NX3 buffer (Fig. 3.9). Blocked protein G beads and pre-cleared extracts were incubated for 3 h and washed 3x with HEMG500 or PBST for 10 min. Proteins were eluted in 100 µl Laemmli buffer for 5 min at 95°C and stored at -20°C. Input and IP samples were analyzed by Western blot.

3.3.3.10 Screening of DOA and DOB antibodies for immunofluorescence application

Dom-A and *Dom-B* cDNAs were assembled into the pMK33-NFH-BD vector (Berkley *Drosophila* Genome Project) via PCR-mediated In-Fusion HD Cloning Kit following the manufacturer's guidelines (Clonetech Laboratories). The pMK33-NFH-BD vector contains a Hygromycin B selection marker, a Cu^{2+} inducible metallothionein promotor and an N-terminal FLAG-HA-tag. For *Dom-A* and *Dom-B* constructs, primers #56-58 (Tab. 1) were used for PCR amplification with plasmid #22 and #5 (Tab. 2), respectively. Next, *Dom-A* and *Dom-B* constructs were analyzed with appropriate restriction enzyme digestions and sequenced with primers #9-16, 20-21 and 32-36 or #9-21 (Tab. 2), respectively.

L2-4 cells ($3x10^6$) were attached in 6-well plates for 30 min and medium was replaced by 1.5 ml complete Schneider's *Drosophila* medium. Plasmids #34 or 35 (2 µg) were added to 100 µl Schneider's *Drosophila* medium without serum by pipetting. Next, 5 µl X-tremeGENE HP DNA Transfection Reagent (Sigma-Aldrich) was added to reaction by pipetting and incubated for 15 min. Complete Schneider's *Drosophila* medium (0,5 ml) was mixed with the reaction, added to L2-4 cells and incubated for 24 h at 26°C. 1 ml complete Schneider's *Drosophila* medium with CuSO4 solution (1:1000, 250 µM) was added and cells incubated for 24 h at 26°C.

Cells were attached on 10-well slides (Thermo Scientific) for 30 min and washed with PBS for 5 min. Next, cells were fixed with 3.7% PFA in PBS for 10 min and washed 2x with PBS for 5 min. Cells were permeabilized with ice-cold 0.25% Triton X-100 in PBS for 6 min and washed 2x with PBS for 5 min. For blocking, cells were incubated with Image-iT FX Signal Enhancer (ThermoFisher Scientific) for 1 h. Cells were incubated with primary antibody solutions (1:30 TCS and 1:50 α-HA rat in PBS with 5% NDS) for 3 h in a wet chamber and washed 2x with 0.1% Triton X-100 in PBS for 5 min. Cells were incubated with secondary antibody solution (1:300 Donkey α-rat Alexa488 and 1:250 Donkey α-mouse Cy3 in PBS with 5% NDS, Jackson ImmunoResearch) for 1 h and washed 2x with 0.1% Triton X-100 in PBS for 5 min. Lastly, cells were stained with DAPI solution (1:500, Life Technologies) for 10 min, washed with PBS for 5 min and mounted in Vectashield Mounting Medium (Enzo Life Sciences). Imaging was performed with the Axiovert 200 M microscope following the manufacturer's guidelines (Carl-Zeiss Light Microscopy) and images were processed using ImageJ (NIH, USA) and Adobe Photoshop. In ImageJ software, the region of interest was selected and cropped. Images were then split into channels and levels of individual channels were adjusted. Next, channels were merged and converted to RGB file. Image size and pixel number was set, scale bars were added and images saved as TIFF files. In Adobe Photoshop, image size was adjusted to reduce file size. Images were split again and individual channels were saved as TIFF files.

3.3.3.11 Table 1: List of primers used in this thesis.

	name	purpose	sequence
1	DomB1.Sal. ATG.fw	dom-B pENTR3c	AACCAATTCAGTCGACCAAAATGAATGAAGGTAATTCAGCAGGAGG
2	DomB1.rev	dom-B pENTR3c	ATCTTGGCACACTTCTTGGCCG
3	DomB2.fw	dom-B pENTR3c	GAAGTGTGCCAAGATGGTGCAG
4	DomB2.rev	dom-B pENTR3c	AAGCTCTTCAGCAAGTGGTTTAGGG
5	DomB3.fw	dom-B pENTR3c	CTTGCTGAAGAGCTTCGAGGAA
6	DomB3.EcoRV. Stop.rev	dom-B pENTR3c	AAGCTGGGTCTAGATGTCACCTGGCTGTTCCGCT
7	DomB1.Sal-ATG.for	dom-B pENTR3c	AACCAATTCAGTCGACCAATGAAGGTAATTCAGCAGGAGG
8	Dom3.EcoRV-Stop.rev	dom-B pENTR3c	AAGCTGGGTCTAGATGCCTGGCTGTTCCGCTCGA
9	DOM.1.fw	sequencing dom	AGTGAAGGGAATCGCCAGC
10	DOM.2.fw	sequencing dom	TTCACAGAATCAACGCCCG
11	DOM.3.fw	sequencing dom	AAGGCCCAAGAGCTGCAG
12	DOM.4.fw	sequencing dom	TAGTCCCAAGCGACGAAAG
13	DOM.5.fw	sequencing dom	ACCAAGCCAAATGCGTTCC
14	DOM.6.fw	sequencing dom	TACGTCTCGCACAAATCCC
15	DOM.7.fw	sequencing dom	ATTGGCAGCGCTTAAACG
16	DOM.8.fw	sequencing dom	TGGGCATCAATTTGACGG
17	DOM.9.fw	sequencing dom-B	AGCTGGAGGCCCAGAAAC
18	DOM.10.fw	sequencing dom-B	AGACAGTGTTGCAGCTGCC
19	DOM.11.fw	sequencing dom-B	AGCAAGGCGGAGGCTAAAG
20	pENTR3C.for	sequencing pENTR3C	GCCAGGCATCAAACTAAGC
21	pENTR3C.rev	sequencing pENTR3C	AGAGCTGCAGCTGGATGG
22	M13.fw(-40)	bacmid test	GTTTTCCCAGTCACGAC
23	M13.rev	bacmid test	CAGGAAACAGCTATGAC
24	DomB.K945R.fw	mutagenesis	GAGATGGGTCTGGGCCGAACCATCCAGACCATTGCG
25	DomB.K945R.rev	mutagenesis	CGCAATGGTCTGGATGGTTCGGCCCAGACCCATCTC

26	DominoA.rev2	dom-A pENTR3c	CCTTCCGCATTTGGATCTTCTG
27	DominoA.for3	dom-A pENTR3c	TCCAAATGCGGAAGGAGGTCC
28	DomA.EcoRV +STOP.rev3	dom-A pENTR3c	AAGCTGGGTCTAGATGTTATTCTTTCTCGCTGCGTATCAGGAT
29	DomA.EcoRV -STOP.rev3	dom-A pENTR3c	AAGCTGGGTCTAGATGTTCTTTCTCGCTGCGTATCAGGATCT
30	DomA.Dra1 +ATG.for1	dom-A pENTR3c	AAAAGCAGGCTCTTTCAAAATGAATGAAGGTAATTCAGCAGGAGGG
31	DomA.Dra1 -ATG.for2	dom-A pENTR3c	AAAAGCAGGCTCTTTCAATGAAGGTAATTCAGCAGGAGGGG
32	DomA.10.fw	sequencing dom-A	TACGAAACGCACATTCAGCC
33	DomA.11.fw	sequencing dom-A	GACCAGTTCCAATGTCTCGC
34	DomA.12.fw	sequencing dom-A	GAAGACGACAGTGATTCCCG
35	DomA.13.fw	sequencing dom-A	GATCAAGGTAACCATGCCCA
36	DomA.14.fw	sequencing dom-A	CAGCATAATCAGCGGCAGA
37	ATPase.Dra1 +ATG.fw	dom pENTR3c	AAAAGCAGGCTCTTTCAAAATGAACAAGGATGATATGCTGAACGAC
38	ATPase.EcoRV +Stop.rev	dom pENTR3c	AAGCTGGGTCTAGATGTTAAAAGAGATCCTTTATGGTGGAACTC
39	ATPase.EcoRV -Stop.rev	dom pENTR3c	AAGCTGGGTCTAGATGAAAGAGATCCTTTATGGTGGAACTC
40	ATPase.Dra1 -ATG.fw	dom pENTR3c	AAAAGCAGGCTCTTTCAACAAGGATGATATGCTGAACGAC
41	ACF1.Dra1 + ATG.for1	Acf1 pENTR3c	AAAAGCAGGCTCTTTCAAAATGCCCATTTGCAAGCGGG
42	ACF1.EcoRV -STOP.rev	Acf1 pENTR3c	AAGCTGGGTCTAGATGGCAAGCTTTGACTTCCCCGTTC
43	ACF1.EcoRV +STOP.rev	Acf1 pENTR3c	AAGCTGGGTCTAGATGTCAGCAAGCTTTGACTTCCCCG
44	ACF1.EcoRV dBr.rev	Acf1 pENTR3c	AAGCTGGGTCTAGATGTCGTTGTGGCATCGGCTTGC
45	ACF1.EcoRV dPHD1,2,Br.rev	Acf1 pENTR3c	AAGCTGGGTCTAGATGTAATGACTTATTGGTGGAACGCCTCC
46	ACF1.dPHD1,2 for	Acf pENTR3c	ACCAATAAGTCATTAGATCATGACCGCGATGAGGAGG
47	ACF1.dPHD1,2 rev	Acf1 pENTR3c	TAATGACTTATTGGTGGAACGCCTCC
48	ACF1.dWAC.for	Acf1 pENTR3c	AAAAGCAGGCTCTTTCAAAATGTCGGTGCAAGCTAAGAAGAACGC
49	ACF1.dDTT.for	Acf1 pENTR3c	GTCACATTGCTGCCTGAGGAGGAGGAATGCGCAGTGA
50	ACF1.dDTT.rev	Acf1 pENTR3c	AGGCAGCAATGTGACGATCTGTCT
51	ACF1.dBAZ1,2 for	Acf1 pENTR3c	AGTATTGCCGAGCTAGTTCTGCGTTCCTTAATCGAACAGC
52	ACF1.dBAZ1,2 rev	Acf1 pENTR3c	TAGCTCGGCAATACTCTTCTTTAATTTCTC

53	ACF1.dBAZ1.for	Acf1 pENTR3c	AGTATTGCCGAGCTACTCAAACTCTACGGAGACGACGAAAAG
54	ACF1.dBAZ2.for	Acf1 pENTR3c	TCAAGAAATGGGCAAGTTCTGCGTTCCTTAATCGAACAGC
55	ACF1.dBAZ	Acf1 pENTR3c	TTGCCCATTTCTTGAATCATGCAC
56	pHygro.DomA/B. fw	dom pHygro	ATTACGCCGGCGGCCGCAATGAAGGTAATTCAGCAGGAGGGG
57	pHygro.DomB. rev	dom-B pHygro	CACCGGATCCTCTAGATCACCTGGCTGTTCCGCTC
58	pHygro.DomA rev	dom-A pHygro	CACCGGATCCTCTAGATTATTCTTTCTCGCTGCGTATCAGGA
59	pBakPAC-FP	sequencing pDEST	TAAAATGATAACCATCTCGC

3.3.3.12 Table 2: List of plasmids made for this thesis.

	name	**purpose**
1	LD35056_DomB_cDNA1_pOT2	cDNA *Dom*
2	LD32012_DomB_cDNA2_pOT2	cDNA *Dom*
3	LD32234_DomB_cDNA3_pOT2	cDNA *Dom-B*
4	LD21920_DomA_cDNA _pOT2	cDNA *Dom-A*
5	pDEST8_DomB	Dom-B expression
6	pFASTBac1_DomB_FLAG_CT	Dom-B-FLAG-CT expression
7	pFASTBac1_DomB_FLAG_NT	Dom-B-FLAG-NT expression
8	pDEST8_DomB_K945R	Dom-B-K945R expression
9	pFASTBac1_DomB_FLAG_CT_K945R	Dom-B-K945R-FLAG-CT expression
10	pFASTBac1_DomB_FLAG_NT_K945R	Dom-B-K945R-FLAG-NT expression
11	pDEST8_ Dom_ATPase	Dom-ATPase expression
12	pDEST8_ Dom_ATPase_K945R	Dom-ATPase-K945R expression
13	pDEST8_ Dom_B_ΔNT	Dom-B-ΔNT expression
14	pFASTBac1_Dom_ATPase_FLAG_CT	Dom-ATPase-FLAG-CT expression
15	pFASTBac1_Dom_ATPase_K945R_FLAG_CT	Dom-ATPase-K945R-FLAG-CT expression
16	pFASTBac1_ Dom_ΔCT_FLAG_CT	Dom-ΔCT expression
17	pFASTBac1_ Dom_ΔNT_FLAG_CT	Dom-ΔNT-FLAG-CT expression
18	pFASTBac1_ Dom_ΔNT_FLAG_NT	Dom-ΔNT-FLAG-NT expression
19	pFASTBac1_Dom_ATPase_FLAG_NT	Dom-ATPase-FLAG-NT expression
20	pFASTBac1_Dom_ATPase_K945R_FLAG_NT	Dom-ATPase-K945R-FLAG-NT expression
21	pDEST8_DomA	Dom-A expression
22	pFASTBac1_DomA_FLAG_CT	Dom-A-FLAG-CT expression
23	pFASTBac1_ACF1_FLAG_CT	ACF1-FLAG-CT expression
24	pDEST8_ACF1	ACF1 expression
25	pFASTBac1_ACF1_ΔBromo_FLAG_CT	ACF1-ΔBromo-FLAG-CT expression

26	pFASTBac1_ACF1_ΔPHD_Bromo_FLAG_CT	ACF1-ΔPHD-Bromo-FLAG-CT expression
27	pFASTBac1_ACF1_ΔPHD_FLAG_CT	ACF1-ΔPHD-FLAG-CT expression
28	pFASTBac1_ACF1_ΔWAC_FLAG_CT	ACF1-ΔWAC-FLAG-CT expression
29	pFASTBac1_ACF1_ΔDDT_FLAG_CT	ACF1-ΔDDT-FLAG-CT expression
30	pFASTBac1_ACF1_ΔBAZ1_2_FLAG_CT	ACF1-ΔBAZ1-2-FLAG-CT expression
31	pFASTBac1_ACF1_ΔBAZ1_FLAG_CT	ACF1-ΔBAZ1-FLAG-CT expression
32	pFASTBac1_ACF1_ΔBAZ2_FLAG_CT	ACF1-ΔBAZ2-FLAG-CT expression
33	pMK33-NFH-BD _DomA_FLAG_HA_NT	transient transfection of *Drosophila* cells
34	pMK33-NFH-BD _DomB_FLAG_HA_NT	transient transfection of *Drosophila* cells

3.3.3.13 Table 3: List of antibodies generated in this thesis.

name	species	WB	IF	IP
DOA1 24C10	rat G1	✓	✓	✓
DOA1 7D8	rat 2c	✓	-	✓
DOA1 16D4	rat 2c	-	✓	✓
DOA1 17F4	rat 2a	✓	-	✓
DOB1 4A8	rat 2a	-	✓	-
DOB1 13A5	rat G1	✓	-	✓
DOB1 21A9	rat 2c	✓	-	✓
DOB1 3B4	rat 2c	✓	-	✓
DOB1 7B6	rat 2c	✓	-	✓
DOB1 12D2	rat 2c	-	✓	-
DOB2 14A4	rat 2b	✓	-	-
DOB2 16A5	rat 2b	✓	-	-
DOB2 4B2	rat 2b	✓	-	-
DOB2 7D5	rat 2a	✓	✓	✓
DOB2 13E3	rat 2a	✓	✓	✓
DOB2 4H4	mouse 2a	✓	✓	✓

Please refer also to Material and Methods (3.3.3) for more information.

3.3.3.14 Table 4: List of antibodies used for Western blot.

Primary antibody	species	WB dilution
DOA1 7D8	rat	1:5
DOA1 17F4	rat	1:5
DOB1 13A5	rat	1:5
DOB1 3B4	rat	1:5
DOB1 7B6	rat	1:5
DOB2 14A4	rat	1:5
DOB2 16A5	rat	1:5
DOB2 4B2	rat	1:5
DOB2 4H4	mouse	1:5
DMO 2G5	rat	1:5
ACF1 8E3	rat	1:20
ISWI (Tamkun)	rabbit	1:2000
TIP60 2C4	mouse	1:5
FLAG M2	mouse	1:5000

4 References

1. Luger K, Mäder AW, Richmond RK, Sargent DF, Richmond TJ. Crystal structure of the nucleosome core particle at 2.8 A resolution. Nature. 1997;389(6648):251–60.
2. Andrews AJ, Luger K. Nucleosome Structure(s) and Stability: Variations on a Theme. Annu Rev Biophys. 2011;40(1):99–117.
3. Pepenella S, Murphy KJ, Hayes JJ. Intra- and Inter-nucleosome interactions of the core histone tail domains in higher-order chromatin structure. Chromosoma. 2014;123:3–13.
4. Davey CA, Sargent DF, Luger K, Maeder AW, Richmond TJ. Solvent mediated interactions in the structure of the nucleosome core particle at 1.9 A resolution. J Mol Biol. 2002;319(5):1097–113.
5. Luger K. Structure and dynamic behavior of nucleosomes. Curr Opin Genet Dev. 2003;13(2):127–35.
6. Grigoryev SA, Woodcock CL. Chromatin organization - The 30nm fiber. Exp Cell Res. Elsevier Inc.; 2012;318(12):1448–55.
7. Fussner E, Ching RW, Bazett-Jones DP. Living without 30nm chromatin fibers. Trends Biochem Sci. Elsevier Ltd; 2011;36(1):1–6.
8. Fussner E, Strauss M, Djuric U, Li R, Ahmed K, Hart M, et al. Open and closed domains in the mouse genome are configured as 10-nm chromatin fibres. EMBO Rep. Nature Publishing Group; 2012;13(11):992–6.
9. Maeshima K, Hihara S, Eltsov M. Chromatin structure: does the 30-nm fibre exist in vivo? Curr Opin Cell Biol. 2010 Jul;22(3):291–7.
10. Hansen JC. Human mitotic chromosome structure: what happened to the 30-nm fibre? EMBO J. Nature Publishing Group; 2012;31(7):1621–3.
11. Maeshima K, Imai R, Tamura S, Nozaki T. Chromatin as dynamic 10-nm fibers. Chromosoma. 2014;123(3):225–37.
12. Bergmann JH, Spector DL. Long non-coding RNAs: Modulators of nuclear structure and function. Curr Opin Cell Biol. 2014;10–8.
13. McBryant SJ, Adams VH, Hansen JC. Chromatin architectural proteins. Chromosom Res. 2006;14(1):39–51.
14. Smith ZD, Meissner A. DNA methylation: roles in mammalian development. Nat Rev Genet. Nature Publishing Group; 2013;14(3):204–20.
15. Swygert SG, Peterson CL. Chromatin dynamics: Interplay between remodeling enzymes and histone modifications. Biochim Biophys Acta. 2014;1839(8):728–36.
16. Clapier CR, Cairns BR. The biology of chromatin remodeling complexes. Annu Rev Biochem. 2009 Jan;78:273–304.
17. Flaus A, Martin DMA, Barton GJ, Owen-Hughes T. Identification of multiple distinct Snf2 subfamilies with conserved structural motifs. Nucleic Acids Res. 2006

Jan;34(10):2887–905.

18. Flaus A, Owen-Hughes T. Mechanisms for ATP-dependent chromatin remodelling : the means to the end. FEBS J. 2011;278:3579–95.

19. Mueller-Planitz F, Klinker H, Becker PB. Nucleosome sliding mechanisms: new twists in a looped history. Nat Struct Mol Biol. Nature Publishing Group; 2013 Sep 5;20(9):1026–32.

20. Becker PB, Workman JL. Nucleosome remodeling and epigenetics. Cold Spring Harb Perspect Biol. 2013;5(9).

21. Bao Y, Shen X. SnapShot: Chromatin remodeling: INO80 and SWR1. Cell. Elsevier; 2011 Jan 7;144(1):158–158.e2.

22. Korber P, Becker PB. Nucleosome dynamics and epigenetic stability. Essays Biochem. 2010 Sep 20;48(1):63–74.

23. Hargreaves DC, Crabtree GR. ATP-dependent chromatin remodeling: genetics, genomics and mechanisms. Cell Res. Nature Publishing Group; 2011 Mar;21(3):396–420.

24. Längst G, Manelyte L. Chromatin remodelers: From function to dysfunction. Genes (Basel). 2015;6(2):299–324.

25. Morrison AJ, Shen X. Chromatin remodelling beyond transcription: the INO80 and SWR1 complexes. Nat Rev Mol Cell Biol. 2009 Jun;10(6):373–84.

26. Corona DF V, Tamkun JW. Multiple roles for ISWI in transcription, chromosome organization and DNA replication. Biochim Biophys Acta. 2004 Mar 15;1677(1-3):113–9.

27. Deuring R, Fanti L, Armstrong JA, Sarte M, Papoulas O, Prestel M, et al. The ISWI Chromatin-Remodeling Protein Is Required for Gene Expression and the Maintenance of Higher Order Chromatin Structure In Vivo. Mol Cell. 2000;5:355–65.

28. Baldi S, Becker PB. The variant histone H2A.V of Drosophila-three roles, two guises. Chromosoma. 2013 Apr 4;122(4):245–58.

29. Yadon AN, Tsukiyama T. SnapShot: Chromatin remodeling: ISWI. Cell. Elsevier; 2011 Feb 4;144(3):453–453.e1.

30. Corona DF, Eberharter A, Budde A, Deuring R, Ferrari S, Varga-Weisz P, et al. Two histone fold proteins, CHRAC-14 and CHRAC-16, are developmentally regulated subunits of chromatin accessibility complex (CHRAC). EMBO J. 2000;19(12):3049–59.

31. Ito T, Levenstein ME, Fyodorov D V, Kutach AK, Kobayashi R, Kadonaga JT. ACF consists of two subunits, Acf1 and ISWI, that function cooperatively in the ATP-dependent catalysis of chromatin assembly. Genes Dev. 1999;13:1529–39.

32. Hartlepp KF, Fernández-Tornero C, Eberharter A, Grüne T, Müller CW, Becker PB. The histone fold subunits of Drosophila CHRAC facilitate nucleosome sliding through dynamic DNA interactions. Mol Cell Biol. American Society for Microbiology;

2005;25(22):9886–96.

33. Fyodorov D V, Blower MD, Karpen GH, Kadonaga JT. Acf1 confers unique activities to ACF/CHRAC and promotes the formation rather than disruption of chromatin in vivo. Genes Dev. 2004 Jan 15;18(2):170–83.

34. Hanai K, Furuhashi H, Yamamoto T, Akasaka K, Hirose S. RSF governs silent chromatin formation via histone H2Av replacement. PLoS Genet. 2008 Feb;4(2):e1000011.

35. Racki LR, Yang JG, Naber N, Partensky PD, Acevedo A, Purcell TJ, et al. The chromatin remodeller ACF acts as a dimeric motor to space nucleosomes. Nature. Nature Publishing Group; 2009;462(7276):1016–21.

36. Varga-Weisz PD, Wilm M, Bonte E, Dumas K, Mann M, Becker PB. Chromatin-remodelling factor CHRAC contains the ATPases ISWI and topoisomerase II. Nature. 1997;388(6642):598–602.

37. Alkhatib SG, Landry JW. The nucleosome remodeling factor. FEBS Lett. Federation of European Biochemical Societies; 2011;585(20):3197–207.

38. Emelyanov A V., Vershilova E, Ignatyeva MA, Pokrovsky DK, Lu X, Konev AY, et al. Identification and characterization of ToRC, a novel ISWI-containing ATP-dependent chromatin assembly complex. Genes Dev. 2012;26:603–14.

39. Vanolst L, Fromental-Ramain C, Ramain P. Toutatis, a TIP5-related protein, positively regulates Pannier function during Drosophila neural development. Development. 2005;132:4327–38.

40. Grüne T, Brzeski J, Eberharter A, Clapier CR, Corona DF V, Becker PB, et al. Crystal structure and functional analysis of a nucleosome recognition module of the remodeling factor ISWI. Mol Cell. 2003;12(2):449–60.

41. Corona DF V, Längst G, Clapier CR, Bonte EJ, Ferrari S, Tamkun JW, et al. ISWI is an ATP-dependent nucleosome remodeling factor. Mol Cell. 1999;3(2):239–45.

42. Mueller-Planitz F, Klinker H, Ludwigsen J, Becker PB. The ATPase domain of ISWI is an autonomous nucleosome remodeling machine. Nat Struct Mol Biol. 2013 Jan;20(1):82–9.

43. Becker PB, Hörz W. ATP-dependent nucleosome remodeling. Annu Rev Biochem. 2002 Jan;71:247–73.

44. Dang W, Kagalwala MN, Bartholomew B. Regulation of ISW2 by concerted action of histone H4 tail and extranucleosomal DNA. Mol Cell Biol. 2006;26(20):7388–96.

45. Yang JG, Madrid TS, Sevastopoulos E, Narlikar GJ. The chromatin-remodeling enzyme ACF is an ATP-dependent DNA length sensor that regulates nucleosome spacing. Nat Struct Mol Biol. 2006;13(12):1078–83.

46. Clapier CR, Cairns BR. Regulation of ISWI involves inhibitory modules antagonized by nucleosomal epitopes. Nature. Nature Publishing Group; 2012;492(7428):280–4.

47. Toto M, D'Angelo G, Corona DF V. Regulation of ISWI chromatin remodelling

activity. Chromosoma. 2014 Jan 12;(1).

48. Goldman JA, Garlick JD, Kingston RE. Chromatin remodeling by imitation switch (ISWI) class ATP-dependent remodelers is stimulated by histone variant H2A.Z. J Biol Chem. 2010;285(7):4645–51.

49. Torigoe SE, Urwin DL, Ishii H, Smith DE, Kadonaga JT. Identification of a Rapidly Formed Nonnucleosomal Histone-DNA Intermediate that Is Converted into Chromatin by ACF. Mol Cell. Elsevier Inc.; 2011;43(4):638–48.

50. Fei J, Torigoe SE, Brown CR, Khuong MT, Kassavetis GA, Boeger H, et al. The prenucleosome, a stable conformational isomer of the nucleosome. Genes Dev. 2015;29(24):2563–75.

51. Maier VK, Chioda M, Rhodes D, Becker PB. ACF catalyses chromatosome movements in chromatin fibres. EMBO J. 2008 Mar 19;27(6):817–26.

52. Chioda M, Becker PB. Soft skills turned into hard facts: nucleosome remodelling at developmental switches. Heredity (Edinb). Nature Publishing Group; 2010 Jul;105(1):71–9.

53. Eberharter A, Vetter I, Ferreira R, Becker PB. ACF1 improves the effectiveness of nucleosome mobilization by ISWI through PHD-histone contacts. EMBO J. 2004 Oct 13;23(20):4029–39.

54. Jain D, Baldi S, Zabel A, Straub T, Becker PB. Active promoters give rise to false positive “Phantom Peaks” in ChIP-seq experiments. Nucleic Acids Res. 2015;1–10.

55. Hwang WL, Deindl S, Harada BT, Zhuang X. Histone H4 tail mediates allosteric regulation of nucleosome remodelling by linker DNA. Nature. Nature Publishing Group; 2014;512(7513):213–7.

56. Chioda M, Vengadasalam S, Kremmer E, Eberharter A, Becker PB. Developmental role for ACF1-containing nucleosome remodellers in chromatin organisation. Development. 2010 Oct;137(20):3513–22.

57. Collins N, Poot RA, Kukimoto I, García-Jiménez C, Dellaire G, Varga-Weisz PD. An ACF1-ISWI chromatin-remodeling complex is required for DNA replication through heterochromatin. Nat Genet. 2002 Dec;32(4):627–32.

58. Lan L, Ui A, Nakajima S, Hatakeyama K, Hoshi M, Watanabe R, et al. The ACF1 Complex Is Required for DNA Double-Strand Break Repair in Human Cells. Mol Cell. Elsevier Inc.; 2010;40(6):976–87.

59. Sánchez-Molina S, Mortusewicz O, Bieber B, Auer S, Eckey M, Leonhardt H, et al. Role for hACF1 in the G2/M damage checkpoint. Nucleic Acids Res. 2011;39(19):8445–56.

60. Ho L, Crabtree GR. Chromatin remodelling during development. Nature. 2010;463(7280):474–84.

61. Iovino N. Drosophila epigenome reorganization during oocyte differentiation and early embryogenesis. Brief Funct Genomics. 2014;13(3):246–53.

62. Xi R, Xie T. Stem cell self-renewal controlled by chromatin remodeling factors. Science. 2005 Dec 2;310(5753):1487–9.

63. Ables ET, Drummond-Barbosa D. The steroid hormone ecdysone functions with intrinsic chromatin remodeling factors to control female germline stem cells in drosophila. Cell Stem Cell. Elsevier Inc.; 2010;7(5):581–92.

64. Yan D, Neumüller RA, Buckner M, Ayers K, Li H, Hu Y, et al. A Regulatory Network of Drosophila Germline Stem Cell Self-Renewal. Dev Cell. 2014 Feb;28(4):459–73.

65. Meshorer E, Misteli T. Chromatin in pluripotent embryonic stem cells and differentiation. 2006;7(July):540–6.

66. Mattout A, Meshorer E. Chromatin plasticity and genome organization in pluripotent embryonic stem cells. Curr Opin Cell Biol. Elsevier Ltd; 2010;22(3):334–41.

67. Gerhold CB, Gasser SM. INO80 and SWR complexes: relating structure to function in chromatin remodeling. Trends Cell Biol. Elsevier Ltd; 2014;24(11):619–31.

68. van Attikum H, Gasser SM. The histone code at DNA breaks: a guide to repair? Nat Rev Mol Cell Biol. 2005 Oct;6(10):757–65.

69. Wu W-H, Alami S, Luk E, Wu C-H, Sen S, Mizuguchi G, et al. Swc2 is a widely conserved H2AZ-binding module essential for ATP-dependent histone exchange. Nat Struct Mol Biol. 2005;12(12):1064–71.

70. Chen L, Cai Y, Jin G, Florens L, Swanson SK, Washburn MP, et al. Subunit organization of the human INO80 chromatin remodeling complex: An evolutionarily conserved core complex catalyzes ATP-dependent nucleosome remodeling. J Biol Chem. 2011;286(13):11283–9.

71. Jha S, Dutta A. RVB1/RVB2: Running Rings around Molecular Biology. Mol Cell. Elsevier; 2009;34(5):521–33.

72. Szerlong H, Hinata K, Viswanathan R, Erdjument-Bromage H, Tempst P, Cairns BR. The HSA domain binds nuclear actin-related proteins to regulate chromatin-remodeling ATPases. Nat Struct Mol Biol. 2008;15(5):469–76.

73. Shen X, Ranallo R, Choi E, Wu C. Involvement of actin-related proteins in ATP-dependent chromatin remodeling. Mol Cell. 2003;12(1):147–55.

74. Ruhl DD, Jin J, Cai Y, Swanson S, Florens L, Washburn MP, et al. Purification of a human SRCAP complex that remodels chromatin by incorporating the histone variant H2A.Z into nucleosomes. Biochemistry. 2006;45(17):5671–7.

75. Luk E, Ranjan A, FitzGerald PC, Mizuguchi G, Huang Y, Wei D, et al. Stepwise histone replacement by SWR1 requires dual activation with histone H2A.Z and canonical nucleosome. Cell. Elsevier Inc.; 2010;143(5):725–36.

76. Mizuguchi G, Shen X, Landry J, Wu W-H, Sen S, Wu C. ATP-Driven Exchange of Histone H2AZ Variant Catalyzed by SWR1 Chromatin Remodeling Complex. Science (80-). 2004;303:343–8.

77. Ranjan A, Mizuguchi G, Fitzgerald PC, Wei D, Wang F, Huang Y, et al. Nucleosome-

free Region Dominates Histone Acetylation in Targeting SWR1 to Promoters for H2A.Z Replacement. Cell. Elsevier; 2013 Sep 12;154(6):1232–45.

78. Wong MM, Cox LK, Chrivia JC. The chromatin remodeling protein, SRCAP, is critical for deposition of the histone variant H2A.Z at promoters. J Biol Chem. 2007;282(36):26132–9.

79. Kusch T, Florens L, Macdonald WH, Swanson SK, Glaser RL, Yates JR, et al. Acetylation by Tip60 is required for selective histone variant exchange at DNA lesions. Science. 2004 Dec 17;306(5704):2084–7.

80. Cai Y, Jin J, Florens L, Swanson SK, Kusch T, Li B, et al. The mammalian YL1 protein is a shared subunit of the TRRAP/TIP60 histone acetyltransferase and SRCAP complexes. J Biol Chem. 2005 Apr 8;280(14):13665–70.

81. Papamichos-Chronakis M, Watanabe S, Rando OJ, Peterson CL. Global regulation of H2A.Z localization by the INO80 chromatin-remodeling enzyme is essential for genome integrity. Cell. Elsevier Inc.; 2011;144(2):200–13.

82. Conaway RC, Conaway JW. The INO80 chromatin remodeling complex in transcription, replication and repair. Trends Biochem Sci. Elsevier Ltd; 2009 Feb;34(2):71–7.

83. Obri A, Ouararhni K, Papin C, Diebold M-L, Padmanabhan K, Marek M, et al. ANP32E is a histone chaperone that removes H2A.Z from chromatin. Nature. Nature Publishing Group; 2014 Jan 22;505:648–53.

84. Ruhf ML, Braun A, Papoulas O, Tamkun JW, Randsholt N, Meister M. The domino gene of Drosophila encodes novel members of the SWI2/SNF2 family of DNA-dependent ATPases, which contribute to the silencing of homeotic genes. Dev Cambridge Engl. 2001;128(8):1429–41.

85. Eissenberg JC, Wong M, Chrivia JC. Human SRCAP and Drosophila melanogaster DOM Are Homologs That Function in the Notch Signaling Pathway. Mol Cell Biol. 2005;25(15):6559–69.

86. Gause M, Eissenberg JC, Macrae AF, Dorsett M, Misulovin Z, Dorsett D. Nipped-A, the Tra1/TRRAP Subunit of the Drosophila SAGA and Tip60 Complexes, Has Multiple Roles in Notch Signaling during Wing Development. Mol Cell Biol. 2006;26(6):2347–59.

87. Lu J, Ruhf M-L, Perrimon N, Leder P. A genome-wide RNA interference screen identifies putative chromatin regulators essential for E2F repression. Proc Natl Acad Sci U S A. 2007 May 29;104(22):9381–6.

88. Kwon MH, Callaway H, Zhong J, Yedvobnick B. A Targeted Genetic Modifier Screen Links the SWI2/SNF2 Protein Domino to Growth and Autophagy Genes in Drosophila melanogaster. G3 (Bethesda). 2013 Jan;3(5):815–25.

89. Sadasivam DA, Huang D-H. Maintenance of Tissue Pluripotency by Epigenetic Factors Acting at Multiple Levels. PLOS Genet. 2016;12(2):e1005897.

90. Ellis K, Friedman C, Yedvobnick B. Drosophila domino Exhibits Genetic Interactions

with a Wide Spectrum of Chromatin Protein-Encoding Loci. PLoS One. 2015;10(11):e0142635.

91. Walker J, Kwon SY, Badenhorst P, East P, McNeill H, Svejstrup JQ. Role of elongator subunit Elp3 in Drosophila melanogaster larval development and immunity. Genetics. 2011 Apr;187(4):1067–75.

92. Braun A, Hoffmann JA, Meister M. Analysis of the Drosophila host defense in domino mutant larvae, which are devoid of hemocytes. Proc Natl Acad Sci U S A. 1998 Nov 24;95(24):14337–42.

93. Boyer LA, Latek RR, Peterson CL. The SANT domain: a unique histone-tail-binding module? Nat Rev Mol Cell Biol. 2004;5(2):158–63.

94. Gemayel R, Chavali S, Pougach K, Legendre M, Zhu B, Boeynaems S, et al. Variable Glutamine-Rich Repeats Modulate Transcription Factor Activity. Mol Cell. 2015;59(4):615–27.

95. Messina G, Damia E, Fanti L, Atterrato MT, Celauro E, Mariotti FR, et al. Yeti, an essential Drosophila melanogaster gene, encodes a protein required for chromatin organization. J Cell Sci. 2014 Jun 1;127(Pt 11):2577–88.

96. Kusch T, Mei A, Nguyen C. Histone H3 lysine 4 trimethylation regulates cotranscriptional H2A variant exchange by Tip60 complexes to maximize gene expression. Proc Natl Acad Sci U S A. 2014 Apr 1;111(13):4850–5.

97. Talbert PB, Henikoff S. Histone variants - ancient wrap artists of the epigenome. Nat Rev Mol cell Biol. 2010 Apr;11(4):264–75.

98. Marzluff WF, Wagner EJ, Duronio RJ. Metabolism and regulation of canonical histone mRNAs: life without a poly(A) tail. Nat Rev Genet. 2008;9(11):843–54.

99. Bönisch C, Hake SB. Histone H2A variants in nucleosomes and chromatin: More or less stable? Nucleic Acids Res. 2012;40(21):10719–41.

100. Malik HS, Henikoff S. Phylogenomics of the nucleosome. Nat Struct Biol. 2003;10(11):882–91.

101. Zlatanova J, Thakar A. H2A.Z: View from the Top. Structure. 2008;16(2):166–79.

102. Faast R, Thonglairoam V, Schulz TC, Beall J, Wells JRE, Taylor H, et al. Histone variant H2A.Z is required for early mammalian development. Curr Biol. 2001;11(15):1183–7.

103. van Daal A, Elgin SC. A histone variant, H2AvD, is essential in Drosophila melanogaster. Mol Biol Cell. 1992;3(6):593–602.

104. Iouzalen N, Moreau J, Méchali M. H2A.ZI, a new variant histone expressed during Xenopus early development exhibits several distinct features from the core histone H2A. Nucleic Acids Res. 1996;24(20):3947–52.

105. Clarkson MJ, Wells JR, Gibson F, Saint R, Tremethick DJ. Regions of variant histone His2AvD required for Drosophila development. Nature. 1999;399(6737):694–7.

106. Suto RK, Clarkson MJ, Tremethick DJ, Luger K. Crystal structure of a nucleosome

core particle containing the variant histone H2A.Z. Nat Struct Biol. 2000;7(12):1121–4.

107. Zhang H, Roberts DN, Cairns BR. Genome-wide dynamics of Htz1, a histone H2A variant that poises repressed/basal promoters for activation through histone loss. Cell. 2005;123(2):219–31.

108. Guillemette B, Bataille AR, Gevry N, Adam M, Blanchette M, Robert F, et al. Variant histone H2A.z is globally localized to the promoters of inactive yeast genes and regulates nucleosome positioning. PLoS Biol. 2005;3(12):1–11.

109. Barski A, Cuddapah S, Cui K, Roh TY, Schones DE, Wang Z, et al. High-Resolution Profiling of Histone Methylations in the Human Genome. Cell. 2007;129(4):823–37.

110. Zilberman D, Coleman-Derr D, Ballinger T, Henikoff S. Histone H2A.Z and DNA methylation are mutually antagonistic chromatin marks. Nature. 2008;456(7218):125–9.

111. Weber CM, Henikoff JG, Henikoff S. H2A.Z nucleosomes enriched over active genes are homotypic. Nat Struct Mol Biol. Nature Publishing Group; 2010;17(12):1500–7.

112. Adam M, Robert F, Larochelle M, Gaudreau L. H2A.Z is required for global chromatin integrity and for recruitment of RNA polymerase II under specific conditions. Mol Cell Biol. 2001;21(18):6270–9.

113. Hardy S, Jacques PE, Gevry N, Forest A, Fortin ME, Laflamme L, et al. The euchromatic and heterochromatic landscapes are shaped by antagonizing effects of transcription on H2A.Z deposition. PLoS Genet. 2009;5(10).

114. Ishibashi T, Dryhurst D, Rose KL, Shabanowitz J, Hunt DF, Ausio J. Acetylation of vertebrate H2A.Z and its effect on the structure of the nucleosome. Biochemistry. 2009;48(22):5007–17.

115. Thakar A, Gupta P, Ishibashi T, Finn R, Silva-Moreno B, Uchiyama S, et al. H2A.Z and H3.3 histone variants affect nucleosome structure: Biochemical and biophysical studies. Biochemistry. 2009;48(46):10852–7.

116. Fan JY, Rangasamy D, Luger K, Tremethick DJ. H2A.Z alters the nucleosome surface to promote HP1α-mediated chromatin fiber folding. Mol Cell. 2004;16(4):655–61.

117. Creyghton MP, Markoulaki S, Levine SS, Hanna J, Lodato MA, Sha K, et al. H2AZ Is Enriched at Polycomb Complex Target Genes in ES Cells and Is Necessary for Lineage Commitment. Cell. 2008;135(4):649–61.

118. Pengelly AR, Kalb R, Finkl K, Müller J. Transcriptional repression by PRC1 in the absence of H2A monoubiquitylation. Genes Dev. 2015;29(14):1487–92.

119. Chakravarthy S, Bao Y, Roberts VA. Structural Characterization of Histone H2A Variants Structural Characterization of Histone H2A Variants. 2004;LXIX:227–34.

120. Viens A, Mechold U, Brouillard F, Gilbert C, Leclerc P, Ogryzko V. Analysis of human histone H2AZ deposition in vivo argues against its direct role in epigenetic templating mechanisms. Mol Cell Biol. 2006;26(14):5325–35.

121. Jin C, Zang C, Wei G, Cui K, Peng W, Zhao K, et al. H3.3/H2A.Z double variant-containing nucleosomes mark “nucleosome-free regions” of active promoters and other regulatory regions. Nat Genet. Nature Publishing Group; 2009;41(8):941–5.

122. Jin C, Felsenfeld G. Nucleosome stability mediated by histone variants H3.3 and H2A.Z. Genes Dev. 2007;21(12):1519–29.

123. Rogakou EP, Pilch DR, Orr AH, Ivanova VS, Bonner WM. DNA Double-stranded Breaks Induce Histone H2AX Phosphorylation on Serine 139. J Biol Chem. 1998;-5868.

124. Rogakou EP, Boon C, Redon C, Bonner WM. Megabase chromatin domains involved in DNA double-strand breaks in vivo. J Cell Biol. 1999;146(5):905–15.

125. Burma S, Chen BP, Murphy M, Kurimasa A, Chen DJ. ATM Phosphorylates Histone H2AX in Response to DNA Double-strand Breaks. J Biol Chem. 2001;276(45):42462–7.

126. Stiff T, O’Driscoll M, Rief N, Iwabuchi K, Löbrich M, Jeggo PA. ATM and DNA-PK Function Redundantly to Phosphorylate H2AX after Exposure to Ionizing Radiation. Cancer Res. 2004;64(7):2390–6.

127. Ismail HI, Hendzel MJ. The y-H2A.X: Is It Just a Surrogate Marker of Double-Strand Breaks or Much More? Environ Mol. 2008;49:73–82.

128. Mannironi C, Bonner WM, Hatch CL. H2A.X. a histone isoprotein with a conserved C-terminal sequence, is encoded by a novel mRNA with both DNA replication type and polyA 3’ processing signals. 1989;17(22):9113–26.

129. Nagata T, Kato T, Morita T, Nozaki M, Kubota H, Yagi H, et al. Polyadenylated and 3’ processed mRNAs are transcribed from the mouse histone H2A.X gene. Nucleic Acids Res. 1991;19(9):2441–7.

130. Shroff R, Arbel-Eden A, Pilch D, Ira G, Bonner WM, Petrini JH, et al. Distribution and Dynamics of Chromatin Modification Induced by a Defined DNA Double-Strand Break. Curr Biol. 2004;14:1703–11.

131. Celeste A, Petersen S, Romanienko PJ, Fernandez-Capetillo O, Chen HT, Sedelnikova OA, et al. Genomic Instability in Mice Lacking Histone H2AX. Science (80-). 2002;296:922–7.

132. van Attikum H, Gasser SM. Crosstalk between histone modifications during the DNA damage response. Trends Cell Biol. 2009;19(5):207–17.

133. Tsukuda T, Fleming AB, Nickoloff JA, Osley MA. Chromatin remodelling at a DNA double-strand break site in Saccharomyces cerevisiae. Nature. 2005;438(7066):379–83.

134. Keogh M-C, Kim J-A, Downey M, Fillingham J, Chowdhury D, Harrison JC, et al. A phosphatase complex that dephosphorylates gammaH2AX regulates DNA damage checkpoint recovery. Nature. 2006;439(7075):497–501.

135. van der Heijden GW, Derijck AA, Posfai E, Giele M, Pelczar P, Ramos L, et al. Chromosome-wide nucleosome replacement and H3.3 incorporation during

mammalian meiotic sex chromosome inactivation. Nat Genet. 2007;39(2):251–8.

136. Turner JM, Mahadevaiah SK, Fernandez-Capetillo O, Nussenzweig A, Xu X, Deng CX, et al. Silencing of unsynapsed meiotic chromosomes in the mouse. Nat Genet. 2005;37(1):41–7.

137. Joyce EF, Pedersen M, Tiong S, White-Brown SK, Paul A, Campbell SD, et al. Drosophila ATM and ATR have distinct activities in the regulation of meiotic DNA damage and repair. J Cell Biol. 2011 Oct 31;195(3):359–67.

138. Mavrich TN, Jiang C, Ioshikhes IP, Li X, Venters BJ, Zanton SJ, et al. Nucleosome organization in the Drosophila genome. Nature. 2008;453(7193):358–62.

139. Swaminathan J, Baxter EM, Corces VG. The role of histone H2Av variant replacement and histone H4 acetylation in the establishment of Drosophila heterochromatin. 2005;65–76.

140. Madigan JP, Chotkowski HL, Glaser RL. DNA double-strand break-induced phosphorylation of Drosophila histone variant H2Av helps prevent radiation-induced apoptosis. Nucleic Acids Res. Oxford University Press; 2002;30(17):3698–705.

141. Ting X. Control of germline stem cell self-renewal and differentiation in the Drosophila ovary: Concerted actions of niche signals and intrinsic factors. Wiley Interdiscip Rev Dev Biol. 2013;2(2):261–73.

142. Hudson AM, Cooley L. Methods for studying oogenesis. Methods. Elsevier Inc.; 2014;68(1):207–17.

143. Kirilly D, Xie T. The Drosophila ovary: an active stem cell community. Cell Res. 2007 Jan;17(1):15–25.

144. Huynh JR, St Johnston D. The origin of asymmetry: Early polarisation of the Drosophila germline cyst and oocyte. Curr Biol. 2004;14(11):438–49.

145. Roth S, Lynch JA. Symmetry Breaking During Drosophila Oogenesis. 2009;1:21.

146. Claußen M, Suter B. BicD-dependent localization processes: From Drosophilia development to human cell biology. Ann Anat. 2005;187:539–53.

147. Vazquez-Pianzola P, Suter B. Conservation of the RNA transport machineries and their coupling to translation control across eukaryotes. Comp Funct Genomics. 2012;2012.

148. Mehrotra S, McKim KS. Temporal analysis of meiotic DNA double-strand break formation and repair in Drosophila females. PLoS Genet. 2006;2(11):1883–97.

149. Fuller MT, Spradling AC. Germline Stem Cells : Two Versions of Immortality. Science (80-). 2007;(April):402–4.

150. Liu JL, Buszczak M, Gall JG. Nuclear bodies in the Drosophila germinal vesicle. Chromosom Res. 2006;14:465–75.

151. McCall K. Eggs over easy: Cell death in the Drosophila ovary. Dev Biol. 2004;274:3–14.

152. Thomson TC, Fitzpatrick KE, Johnson J. Intrinsic and extrinsic mechanisms of oocyte

loss. Mol Hum Reprod. 2010;16(12):916–27.

153. Jenkins VK, Timmons AK, McCall K. Diversity of cell death pathways: Insight from the fly ovary. Trends Cell Biol. Elsevier Ltd; 2013;23(11):567–74.

154. Yoon J, Lee KS, Park JS, Yu K, Paik SG, Kang YK. dSETDB1 and SU(VAR)3-9 sequentially function during germline-stem cell differentiation in Drosophila melanogaster. PLoS One. 2008;3(5):3–9.

155. Wang X, Pan L, Wang S, Zhou J, McDowell W, Park J, et al. Histone H3K9 trimethylase eggless controls germline stem cell maintenance and differentiation. PLoS Genet. 2011;7(12).

156. Koch CM, Honemann-Capito M, Egger-Adam D, Wodarz A. Windei, the Drosophila homolog of mAM/MCAF1, is an essential cofactor of the H3K9 methyl transferase dSETDB1/eggless in germ line development. PLoS Genet. 2009;5(9):1–15.

157. Di Stefano L, Ji JY, Moon NS, Herr A, Dyson N. Mutation of Drosophila Lsd1 Disrupts H3-K4 Methylation, Resulting in Tissue-Specific Defects during Development. Curr Biol. 2007;17(9):808–12.

158. Eliazer S, Shalaby NA, Buszczak M. Loss of lysine-specific demethylase 1 nonautonomously causes stem cell tumors in the Drosophila ovary. PNAS. 2011;108(17):7064–9.

159. Iovino N, Ciabrelli F, Cavalli G. PRC2 Controls Drosophila Oocyte Cell Fate by Repressing Cell Cycle Genes. Dev Cell. Elsevier Inc.; 2013 Aug 26;26(4):431–9.

160. Ables ET, Drummond-Barbosa D. The steroid hormone ecdysone functions with intrinsic chromatin remodeling factors to control female germline stem cells in drosophila. Cell Stem Cell. 2010;7:581–92.

161. He J, Xuan T, Xin T, An H, Wang J, Zhao G, et al. Evidence for Chromatin-Remodeling Complex PBAP-Controlled Maintenance of the Drosophila Ovarian Germline Stem Cells. PLoS One. 2014;9(7).

162. Liu YI, Chang M V., Li HE, Barolo S, Chang JL, Blauwkamp TA, et al. The chromatin remodelers ISWI and ACF1 directly repress Wingless transcriptional targets. Dev Biol. Elsevier Inc.; 2008;323(1):41–52.

163. Song H, Spichiger-Haeusermann C, Basler K. The ISWI-containing NURF complex regulates the output of the canonical Wingless pathway. EMBO Rep. Nature Publishing Group; 2009;10(10):1140–6.

164. Morillo Prado JR, Srinivasan S, Fuller MT. The Histone Variant His2Av is Required for Adult Stem Cell Maintenance in the Drosophila Testis. PLoS Genet. 2013 Nov;9(11):e1003903.

165. Petty E, Pillus L. Balancing chromatin remodeling and histone modifications in transcription. Trends Genet. 2013;

166. Venkatesh S, Workman JL. Histone exchange, chromatin structure and the regulation of transcription. Nat Rev Mol Cell Biol. Nature Publishing Group; 2015;16(3):178–89.

167. Gerhold C-B, Hauer MH, Gasser SM. INO80-C and SWR-C: Guardians of the Genome. J Mol Biol. Elsevier Ltd; 2015;427(3):637–51.

168. Erdel F, Krug J, Längst G, Rippe K. Targeting chromatin remodelers: signals and search mechanisms. Biochim Biophys Acta. Elsevier B.V.; 2011 Sep;1809(9):497–508.

169. Erdel F, Rippe K. Chromatin remodelling in mammalian cells by ISWI-type complexes – where , when and why ? 2011;278:3608–18.

170. Meier K, Brehm A. Chromatin regulation: How complex does it get? Epigenetics. 2014;9(11):1485–95.

171. Vengadasalam S. Physical and Functional Interaction between DOM-B and ACF1. Dr thesis, Ludwig-Maximilians-University Munich. 2011;

172. Vengadasalam S, Chioda M, Steffen N, Kremmer E, Eberharter A, Becker PB. Physical and functional interaction between Drosophila nucleosome remodellers ACF and Domino. Unpubl data.

173. Eberharter A, Ferrari S, La G, Straub T, Imhof A, Varga-weisz P, et al. Acf1, the largest subunit of CHRAC, regulates ISWI-induced nucleosome remodelling. 2001;20(14):3781–8.

174. Park JH, Sun X-J, Roeder RG. The SANT domain of p400 ATPase represses acetyltransferase activity and coactivator function of TIP60 in basal p21 gene expression. Mol Cell Biol. 2010 Jun;30(11):2750–61.

175. Jain D. Effects of nucleosome remodeling factor ACF1 on in vivo chromatin organization. Dr thesis Ludwig-Maximilians-University Munich. 2015;

176. Kunert N, Brehm A. Mass Production of Drosophila Embryos and Chromatographic Purification of Native Protein Complexes. Drosoph Methods Protoc. 2008;420:359–71.

5 Acknowledgements

I would like to express my deepest gratitude to all the people who went on this journey with me and without whom it would have not been possible to achieve this doctoral thesis.

First of all, I would like to show my greatest appreciation to my mentor Prof. Dr. Peter B. Becker, for his continuous support and guidance, inspiring ideas and discussions and freedom to pursue my own paths. You have shaped my scientific and personal development and made this an incredibly valuable time in my life. Thank you again.

Secondly, I am deeply grateful to my direct supervisors Dr. Natascha Steffen and Dr. Sandra Vengadasalam. From day one, you made me an equivalent member of the 'ACDC' team and taught me all essential genetic, molecular and biochemical techniques. Even more valuable was all your support in difficult phases of the project. You made it fun coming to the lab.

I would like to thank all my collaborators who made this a fruitful collaboration, in particular Prof. Dr. Beat Suter and Dr. Paula Vazquez-Pianzola (RNA *in situ* analysis), Dr. Pavel Tomancak (pflyfosmids), Dr. Alexander Konev and Dr. Dmitry V. Fyodorov (*Acf1*^{7} allele) and Dr. Dhawal Jain (*Acf1* and *Chrac-16* transgenic fly lines). Thank you again Dhawal for teaching me flyfosmid recombineering and being always very supportive. I want to thank Prof. Dr. Gunter Reuter, Dr. Sandy Mietzsch, Dr. Jean-René Huynh and Dr. Neuza Matias for their support in early phases of this project.

I have greatly benefited from past and present members of the Becker lab. In particular, I am in debt to Dr. Sandro Baldi and Angelika Zabel for their very helpful support in genome-wide sequencing analyses. I am also thankful to Dr. Mathias Prestel and Dr. Henrike Klinker for TIP60 reagents and advices in ATPase assays, respectively. I want to thank Heike Fensterseifer, Silke Krause, Andrea Schmid and Daisy Schwarzlose for so much support with flies, antibodies, cells and cloning. I would like to particularly thank Dr. Andreas Thomae for introducing me to the world of microscopy.

I appreciated the feedback, support and discussions offered by Christian Albig, Dr. Manuel Arteaga, Lisa Harpprecht, Nadine Harrer, Dr. Christian Feller, Johanna Ludwigsen, Dr. Marisa Müller, Dr. Felix Müller-Planitz, Nadia Prayitno, Dr. Catherine Regnard, Alessandro Scacchetti, Dr. Tamas Schauer, Dr. Tobias Straub and Dr. Raffaella Villa. Special thanks to my long-term desk neighbor Sarah Schunter who made the most difficult parts of this doctoral thesis bearable with all the fun we had.

I also want to thank all past and present members and staff of the Molecular Biology Unit at the Adolf-Butenandt-Institute and Biomedical Center of the LMU Munich. I have had generous support of Dr. Jörn Böke and Dr. Elizabeth Schroeder-Reiter who coordinated the IRTG Graduate Program 1064 Chromatin Dynamics.

Abschließend möchte ich mich von ganzem Herzen bei meinen Eltern und meinem Bruder sowie meinen Großeltern und der gesamten Familie für eure unablässige Unterstützung bedanken! Ihr habt einen unermesslichen Anteil zu dieser Arbeit beigetragen - dafür bin ich euch für immer dankbar.

Liebe Linda, deine herzerwärmende Liebe, deine bedingungslose Unterstützung und dein felsenfestes Vertrauen haben mich auf unserem gesamten Weg begleitet. Das möchte ich nie wieder missen! Dir wird für immer meine aufrichtige Liebe gelten.